DEVELOPMENT AND CHARACTERIZATION OF HIGH ENERGY CATHODE MATERIALS FOR LITHIUM-ION BATTERIES

A THESIS SUBMITTED TO
THE GRADUATE SCHOOL OF NATURAL AND APPLIED SCIENCES
OF
MIDDLE EAST TECHNICAL UNIVERSITY

BY

ATIL BÜYÜKBURÇ

IN PARTIAL FULFILLMENT OF THE REQUIREMENTS FOR
THE DEGREE OF DOCTOR OF PHILOSOPHY
IN
METALLURGICAL AND MATERIALS ENGINEERING

AUGUST 2013

Approval of the thesis:

DEVELOPMENT AND CHARACTERIZATION OF HIGH ENERGY CATHODE MATERIALS FOR LITHIUM-ION BATTERIES

submitted by **ATIL BÜYÜKBURÇ** in partial fulfillment of the requirements for the degree of **Doctor of Philosophy in Metallurgical and Materials Engineering Department, Middle East Technical University** by,

Prof. Dr. Canan Özgen
Dean, Graduate School of **Natural and Applied Sciences** ________

Prof. Dr. C. Hakan Gür
Head of Department, **Metallurgical and Materials Engineering** ________

Prof. Dr. M. Kadri Aydınol
Supervisor, **Metallurgical and Materials Engineering Dept., METU** ________

Examining Committee Members:

Prof. Dr. Tayfur Öztürk
Metallurgical and Materials Engineering Dept., METU _________

Prof. Dr. M. Kadri Aydınol
Metallurgical and Materials Engineering Dept., METU _________

Prof. Dr. Şakir Bor
Metallurgical and Materials Engineering Dept., METU _________

Assoc. Prof. Dr. Zafer Evis
Engineering Sciences Dept., METU _________

Assist. Prof. Dr. Ziya Esen
Materials Science and Engineering Dept., Çankaya University _________

Date: 02.08.2013

I hereby declare that all information in this document has been obtained and presented in accordance with academic rules and ethical conduct. I also declare that, as required by these rules and conduct, I have fully cited and referenced all material and results that are not original to this work.

Name, Last name : ATIL, BÜYÜKBURÇ

Signature :

ABSTRACT

DEVELOPMENT AND CHARACTERIZATION OF HIGH ENERGY CATHODE MATERIALS FOR LITHIUM-ION BATTERIES

Büyükburç, Atıl
Ph. D., Department of Metallurgical and Materials Engineering
Supervisor: Prof. Dr. M. Kadri Aydınol

August 2013, 148 pages

The aim of this thesis is to produce high energy cathode materials based on $LiCoO_2$ materials with the general formula $LiCo_{1-x}M_xO_2$ and $LiCo_{1-y-x}M_xN_yO_2$. In order to achieve this formula, less exploited doping elements such as Mo, Cr and W will be used as well as Mn. During the study, the parameters of the processes which are solution preparation, freeze drying and calcination are optimized. According to the results, 24 hours of freeze drying is enough for drying the samples. Calcination at lower (< 700°C) temperatures as well as higher temperatures (> 800°C) do not yield single phase $LiCoO_2$. It is also determined that, holding pH around 10.75 and Li:Co ratio are very important for having single phase $LiCoO_2$. XRD, SEM and SEM-EDX are used for structural analyses. ICP and XPS are used for chemical analysis. For electrochemical characterization, galvanostatic charge-discharge tests, CV and EIS are applied. The results have shown that the sample containing 1 mole% W and 1 mole% Mn has the best electrochemical performance among the other samples. The reason for the electrochemical superiority of this sample is due to the different surface chemistry.

Keywords: $LiCoO_2$, Doping, Freeze Drying, Electrochemical Performance, Surface Chemistry.

ÖZ

LİTYUM İYON PİLLER İÇİN YÜKSEK KAPASİTELİ VE ENERJİLİ KATOT MALZEMELERİNİN GELİŞTİRİLMESİ, ÜRETİLMESİ VE KARAKTERİZASYONU

Büyükburç, Atıl
Doktora, Metalurji ve Malzeme Mühendisliği Bölümü
Tez Yöneticisi: Prof. Dr. M. Kadri Aydınol

Ağustos 2013, 148 sayfa

Bu tezin amacı pillerde kullanılan katot malzemelerinden $LiCoO_2$ malzemesi temeline dayanan ve genel formülü $LiCo_{1-x}M_xO_2$ veya $LiCo_{1-y-x}M_xN_yO_2$ olan yüksek enerjili katot malzemesi üretmektir. Bunu sağlamak için, literatürde daha az çalışılmış olan Mo, Cr ve W gibi alaşım elementleri ile daha sıklıkla kullanılan Mn elementi kullanılmıştır. Tez çalışmaları boyunca, çözelti hazırlama, dondurarak kurutma ve kalsinasyon gibi işlemlerin eniyilemesi çalışılmıştır. Elde edilen sonuçlara göre dondurarak kurutma işleminin 24 saat uygulanması, etkili bir kuruma için yeterlidir. 700°C'nin altında veya 800°C'nin üstünde uygulanan kalsinasyon işlemi sonucunda tek faz tabakalı $LiCoO_2$ elde edilememiştir. Ayrıca pH'ın 10.75 değerine yakın bir yerde tutulması ve Li:Co oranının tek faz tabakalı $LiCoO_2$ elde edilmesi için önemli olduğu tespit edilmiştir. Yapısal analiz için XRD, SEM ve SEM-EDX kullanılmıştır. Kimyasal analiz için ICP ve XPS kullanılmıştır. Elektrokimyasal karakterizasyon için şarj-deşarj testleri, CV ve EIS yöntemi kullanılmıştır. Elde edilen sonuçlar, mol yüzdesi olarak %1 W ve %1 Mn içeren numunenin en iyi elektrokimyasal davranış gösterdiğini ortaya koymuştur. Bu numunenin elektrokimyasal özellikler açısından üstünlüğünün yüzey kimyasının farklı olmasından kaynaklandığı tespit edilmiştir.

Anahtar Kelimeler: $LiCoO_2$, Alaşımlama, Dondurarak Kurutma, Elektrokimyasal Özellik, Yüzey Kimyası.

,

To Derya, Berin and Uğur

BÜYÜKBURÇ

ACKNOWLEDGEMENTS

First of all but not for tradition, I would like to express my deepest gratitude to my supervisor, Prof. Dr. Kadri Aydınol for his encouragement, guidance and friendship throughout the study. His valuable comments and discussions not only increased my motivation about the thesis but also improved the findings and results of the thesis. Besides these, his efforts during electrochemical characterization tests were memorable. Studying with him is a great honour for me.

I would also convey my heartfelt thanks to Berke Pişkin and Esin Camcı for their support during SEM and XRD analyses, respectively. Thanks to other friends, especially Şafak Halıcı, Afşin Izanlou, Fatih Pişkin, Orkun Muğan, Şafak Doğu and Burcu Kayıplar, in Metallurgical and Materials Department of METU. İlker Yıldız from METU Central Lab is acknowledged for his support during XPS analysis. Thanks to retired Necmi Avcı for his effort for conducting XRD analyses on time at the beginning of the study.

I would like to express my sincere thanks to Mustafa Ay, my director in the Scientific and Technological Research Council of Turkey (TÜBİTAK), for his tolerances.

I would like to appreciate TÜBİTAK for permitting me doing this study. Financial support from METU Scientific Research Projects (BAP) and Ministry of Development was acknowledged.

Thanks to Berin and Uğur Büyükburç for teaching me about the importance of research and questioning.

Although she does not really know what is happening around, I would like to thank my 5 years old daughter Ceylan. I hope, with the outcomes of the thesis, I will not regret for the times which should have belonged to her but must be reserved for the thesis. Also I would like to thank to Neşe Gazioğlu, my mother-in-law, for supporting me, my wife and our daughter during my late home comings.

Finally, I am so much obliged to my wife, Derya Büyükburç. Although, this time period was not easily handled by her, she always supported and encouraged me instead of complaining. I believe this thesis could not be completed without her patience.

Definitely, I carry all the responsibility for the mistakes and deficiencies in the thesis.

TABLE OF CONTENTS

CHAPTERS

LIST OF TABLES

TABLES

LIST OF FIGURES

FIGURES

LIST OF ABBREVIATIONS

LiN	Lithium Nitrate
LiA	Lithium Acetate
LiH	Lithium Hydroxide
CoN	Cobalt Nitrate
CoA	Cobalt Acetate
CoH	Cobalt Hydroxide
HT	High Temperature
LT	Low Temperature
FD	Freeze Drying or Freeze Dried
CV	Cyclic Voltammetry or Cyclic Voltammogram
EIS	Electrochemical Impedance Spectroscopy
XRD	X-ray Diffraction
EDX	Energy Dispersive X-Ray Spectroscopy
AMoT	Amonium Heptamolybdate Tetrahydrate
MnAT	Manganese Acetate Tetrahydrate
AWOH	Amonium Tungsten Oxide Hydrate
METU	Middle East Technical University
E_{pa}	Peak potential at the anodic scan
E_{pc}	Peak potential at the cathodic scan
i_{pa}	Peak current at the anodic scan
i_{pc}	Peak current at the cathodic scan
ν	Scan rate
D	Diffusion coefficient

CHAPTER 1

INTRODUCTION

1.1. Battery Technology

The increasing demand for cheap, safe and renewable energy forces companies, governments and institutions as well as investors into finding alternative sources to fossil based fuels. Finding an alternative is obligatory not only for energy considerations but also for environmental legislations which are becoming stricter and vital day by day. Although there are many competitors for this alternative, the energy obtained by electrochemical methods governs an important place. The batteries are the most known electrochemical energy sources.

In the recent years, R&D studies concentrate mainly on the storing higher energy in batteries in order to use them as an energy source in the electricity dependent vehicles. Electric vehicles (EV), hybrid electric vehicles (HEV) and plug-in hybrid electric vehicles (PHEV) are the types of these vehicles. In addition to these, recently range extended electric vehicles (ReEV) came to stage. ReEVs can be thought as an improved version of PHEVs. It seems that battery operated vehicles will be on roads in foreseeable future. However; for the time being, the technological level of batteries are far away from meeting the current needs of the automotive industry.

The most important problem preventing the batteries from widespread application in cars lies in the fact that they have very low gravimetric (Wh/kg) and volumetric energy density (Wh/l) when compared with other automotive fuels. The comparison of energy densities of various fuels and batteries is given in Figure 1.1.

Despite this drawback, the energy dissipated from the batteries can be increased by using several cells. However; this requires significant number of cells which increase the weight and cost of the car. Pollet et al. [1] estimated the manufacture cost of a 35 kWh battery as 30000$ which is unaffordable for individuals. However; battery driven cars have the advantage of carbon free transportation, lower maintenance requirements and lower operating cost due to the low cost of electricity [2]. Moreover; Unnasch and Browning [3] estimated the well-to-wheel efficiency of batteries about 2.6 times more than that of internal combustion engines (ICE). These important advantages of EVs make them very attractive alternative for automotive industry.

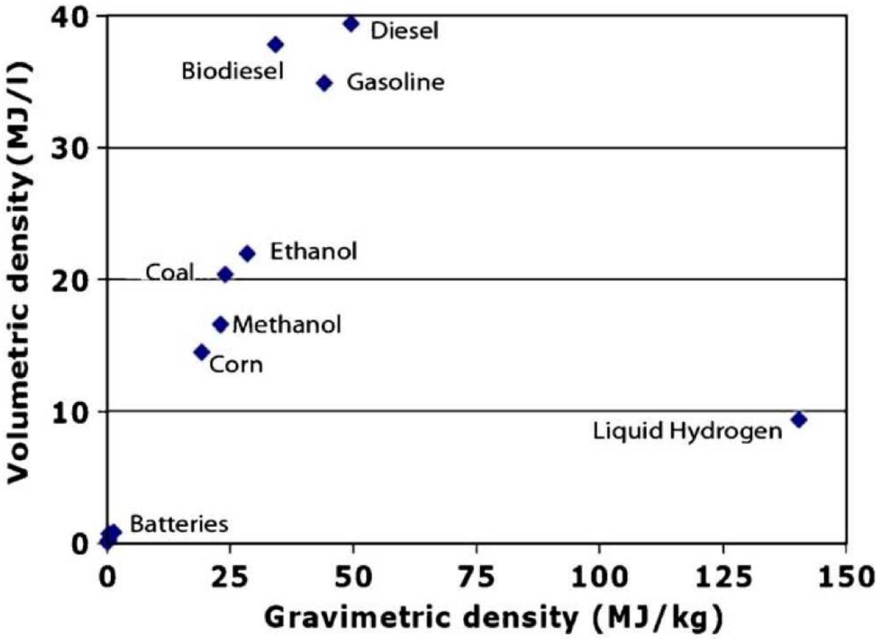

Figure 1.1. Energy densities of various fuels and batteries [4].

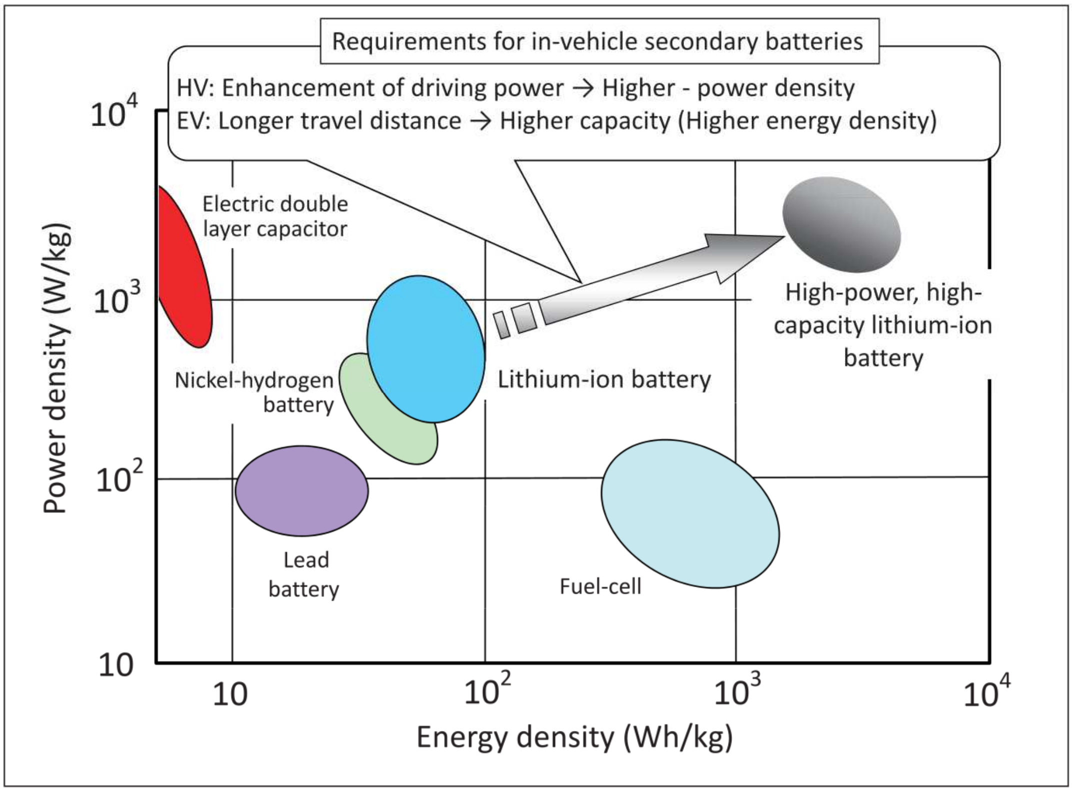

Figure 1.2. Power and energy density requirements for EV [5].

As stated above, R&D studies on the batteries focus on increasing the energy density without sacrificing safety, economy and other electrochemical properties such as cycle life and high rate capability. Kawamoto [5] illustrated the relation between energy density and power density of batteries which is given in Figure 1.2. From the figure it is seen that Li-ion batteries are the most promising chemistry to be used in EVs. Kawamoto [5] also claimed that CO_2 emissions from EVs are ¼ of that of ICEs.

Zu and Li [6] prepared a figure that illustrated the increase of energy densities of various chemistries through years by using data of Kawamoto [5]. From this figure (Figure 1.3) it is seen that the increase in the energy density of the batteries has accelerated in the last three decades. The energy density of Li-ion batteries has doubled in only 15 years (solid line in Figure 1.3) and these batteries have shown the steepest increase. New Energy and Industrial Technology Development Organization (NEDO) in Japan aim to reach the energy density of 500 Wh/kg by 2030 [6]. This value is more than 2 fold of the current value of the energy density of Li-ion batteries. It is certain that increasing the energy density from 100 Wh/kg to 200 Wh/kg is easier than increasing from 250 Wh/kg to 500 Wh/kg. However; to reach this target is beyond being wish, instead it must be achieved when environmental benefits and depletion of fossil fuels are considered. Therefore to reach this target, enormous studies of R&D must be done.

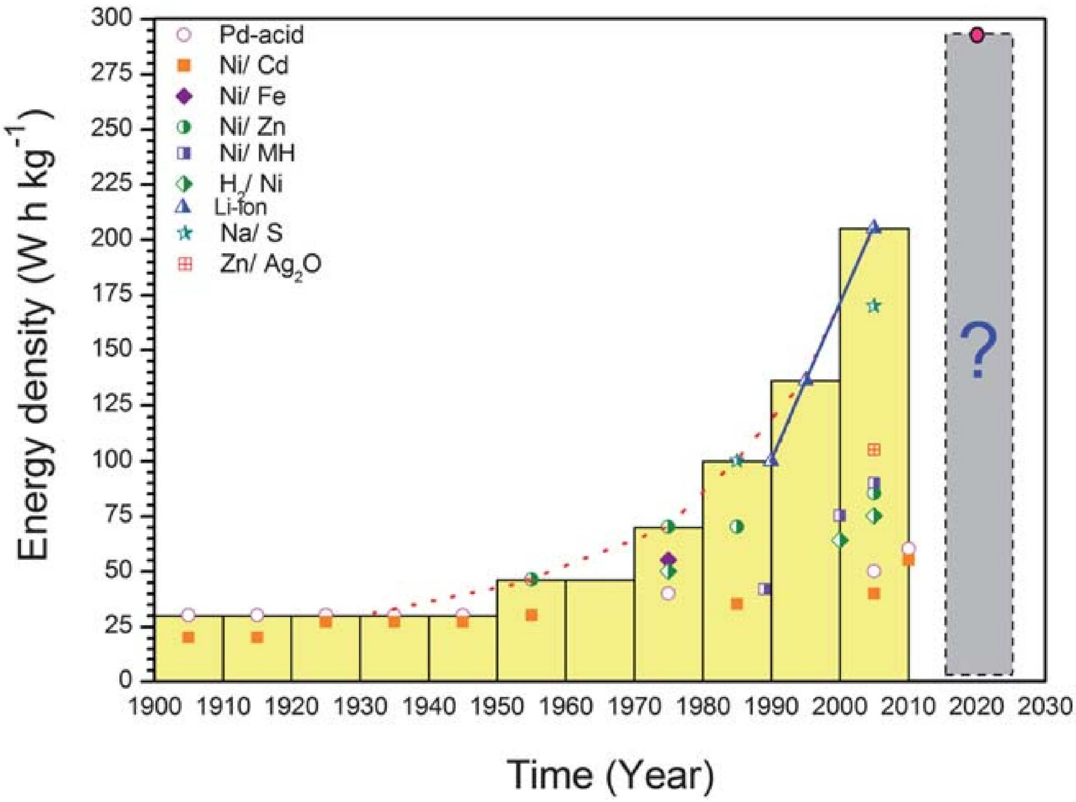

Figure 1.3. The increase in energy density of various battery chemistries through years [6].

The studies for decreasing the cost of the battery go parallel with the studies for increasing energy density. Hill and Mjos [7] posted in their report that 2-3 years ago the cost of lithium battery pack was \$700-\$1000/kWh but this reduced to \$400-\$700/kWh in year 2012.

1.2. Battery Terminology, Science and Types

Batteries use the chemical energy which is stored in its active materials for converting into electric energy by means of an electrochemical oxidation-reduction (redox) reactions. As the battery electrochemically converts chemical energy into electric energy, it is not subject to the limitations of the Carnot cycle like heat engines. Therefore, batteries are capable of having higher energy conversion efficiencies [8].

While the term “battery” is often used, the basic unit is the “cell”. A battery consists of one or more of these cells, connected in series or parallel or both, depending on the desired output voltage and capacity.

Cell voltage is related with the chemistry of the batteries meaning that the voltage depends on the materials used in the cell. For example, NiCd batteries produce 1.2V per cell while lead-acid batteries produce 2.0V per cell. This increases to 3.6V/cell for Li ion batteries having $LiCoO_2$ as cathode material. Battery voltages must be multiples of the basic unit. For example, with Li-ion battery having $LiCoO_2$ as cathode material, only batteries of voltage 3.6V, 7.2V and 10.8 V can be produced but not 5V or 6V with this cathode material [9].

Cell capacity is actually infinite meaning that it depends on the amount of active materials in the battery. Increasing the amount of active electrode material increases the capacity. Moreover, amount of electrode material corresponds to the amount of electrons taking part in the electrochemical reactions. Therefore active material in a cell means that it loses or gains electrons when power is applied. Cell capacity is measured by ampere-hours.

Batteries technological performance is mainly defined by energy (current * voltage integrated over time) or power (current * voltage).

When an application needs more voltage than a cell can provide, than several cells are connected in series to achieve the desired voltage. Series connection means that positive terminal of one cell is connected to the negative terminal of the next cell. This sequence is followed until the desired number of cells is connected. For example, in order to achieve 6 V of output, 3 lead-acid batteries must be connected in series.

Similarly, when an application needs more capacity than a cell can provide, than several cells are connected in parallel to achieve the desired capacity. Parallel connection means that positive terminal of one cell is connected to the positive terminal of the next cell.

C-rate is an important parameter defining the performance of charge and discharge rates of cells. C-rate is basically current flow rate equal to the cell rated capacity. For example, for 1

Ah capacity cell, C-rate is 1 A, while for 5 Ah capacity cell, C-rate is 5 A. Therefore, for 5 Ah cell, charging with 0.5C means that charging is applied with rate of 2.5 A. Same terminology is used for describing discharge rates.

A battery mainly consists of three components; anode, cathode and electrolyte :

The anode or negative electrode: The reducing electrode—which gives up electrons to the external circuit and is oxidized during the electrochemical reaction.

The cathode or positive electrode: The oxidizing electrode—which accepts electrons from the external circuit and is reduced during the electrochemical reaction.

The electrolyte: The ionic conductor—which provides the medium for transfer of charge by the movement of ions inside the cell between the anode and cathode.

1.2.1. The Thermodynamics of Batteries

In a cell, reactions essentially take place at two areas or sites in the device. These reaction sites are the electrode interfaces. In generalized terms, the reaction at one electrode (reduction in forward direction) can be represented by

$$aA + ne^- \rightleftharpoons cC \tag{2.1}$$

where, a moles of A take up n moles of electrons, e^-, to form c moles of C. At the other electrode, the reaction (oxidation in forward direction) can be represented by

$$bB - ne^- \rightleftharpoons dD \tag{2.2}$$

The overall reaction in the cell is given by addition of these two half-cell reactions

$$aA + bB \rightleftharpoons cC + dD \tag{2.3}$$

The change in the standard free energy of this reaction is expressed as;

$$\Delta G^0 = -nFE^0 \tag{2.4}$$

where, F = constant known as the Faraday constant (96487 coulombs)

E^0 = standard electromotive force (with reference to $H^+ + e^- \rightleftharpoons \frac{1}{2}H_2$, $E^0 =$ 0 V)

When conditions are other than in the standard state, the voltage E of a cell is given by the Nernst equation;

$$E = E^0 - \frac{RT}{nF}\ln\frac{a_C^c a_D^d}{a_A^a a_B^b} \tag{2.5}$$

where,

a_i = activity of relevant species

n = number of electrons involved in stoichiometric reaction

R = gas constant

T = absolute temperature

The change in the standard free energy ΔG^0 of a cell reaction is the driving force which enables a battery to deliver electrical energy to an external circuit.

1.2.2. The classification of batteries

The batteries are classified in two categories, primary batteries and secondary batteries. Primary batteries are the ones that are discarded after usage so they are discharged only once. Secondary batteries are the ones that can be recharged to their original condition by passing current in the opposite direction of the discharge current. Primary batteries are still in use especially for portable applications, representing about 80% of the total number batteries sold [10]. The advantages of primary batteries are better for the following properties when compared with secondary batteries, ease of producing in various sizes, shelf-life, safety level, reliability and sometimes cost.

Secondary batteries are basically storage devices for electric energy and are known as “storage batteries” or “accumulators”. They are characterized and distinguished by high power density, high discharge rate, flat discharge curves, and good low-temperature performance. Their energy densities are generally lower than those of primary batteries. Their charge retention also is poorer than that of most primary batteries, although the capacity of the secondary battery can be restored by recharging. The application areas of secondary batteries fall in two categories;

- The battery is used as an energy storage device. It is constantly connected to an energy source and charged by it. It can then release the stored energy whenever needed. Some application areas are; car accumulators, aircraft systems, standby power resources,

- The battery is used as a primary battery but it is recharged instead of being disposed of. Some application areas are; electric vehicles, mobile phones, cameras, power tools, toys.

1.3. Secondary Batteries

They are mainly five chemistries used in secondary batteries. These are Pb-acid, NiCd, NiMH, Li-ion and alkaline batteries. The cost, cell voltage, discharge capacity, cycle life, environmental factors, safety vs. are important parameters that are considered for choosing the right battery chemistry. A detailed comparison of these batteries is given in Table 1.1 [11].

Due to the severe competing market, the manufacturers must produce batteries with high capacity, light weight and high cycle life. From Table 1.1, it can be inferred that Li-ion batteries are the most promising batteries to meet these requirements. As the cell voltage of Li-ion batteries is the highest, fewer cells are needed for a given voltage requirements.

Table 1.1. Battery Chemistry Characteristics [11].

Parameter	Sealed Pb-acid	NiCd	NiMH	Li-ion	Alkaline
Cell Voltage, V	2.0	1.2	1.2	3.6	1.5
Relative Cost, NiCd=1	0.6	1.0	1.6	2.0	0.5
Self-Discharge, %/month	2 – 4	15-30	18-20	6-10	0.3
Cycle Life, reaching of 80% capacity	500-2000	500-1000	500-800	1000-1200	<25
Overcharge Tolerance	High	Medium	Low	Very Low	Medium
Energy by Volume, Wh/l	70-110	100-120	135-180	230	220
Energy by weight, Wh/kg	30-45	45-50	55-65	90	80

1.4. Lithium-Ion Batteries (Anode, Cathode and Electrolyte Materials)

Although, the primary lithium batteries were in the market for a long time, the commercialization of secondary lithium batteries dates back to 1990s. They were introduced by Sony Corporation to be used in portable phones. In that battery, the anode material is carbon, the cathode material is $LiCoO_2$ and the electrolyte is $LiPF_6$ containing propylene carbonate/diethyl carbonate (PC/DEC). This battery configuration is still in use although there are many competitor materials in terms of voltage, capacity, cycle life, safety and cost.

Vaughey et al. [12] list the required properties of an anode material for Li-ion battery as low potential versus metallic lithium, a specific capacity greater than 300 mAh/g, high cycling efficiency, low irreversible capacity, high levels of safety and low cost.

Although the best anode material to be used in lithium ion batteries is the lithium metal with anode potential of –3.045 V (vs. standard hydrogen electrode) and high specific capacity (3860 mAh/g), prolonged deposition/dissolution cycling causes dendrite formation of the lithium metal, which in turn results in serious problems in safety and cycleability [13].

The problems associated with the usage of lithium metal as anode material are summarized by [14]. Freshly deposited Li is more reactive than bulk Li and tends to be encapsulated by electrolyte decomposition products, and becomes inactive. This inactivity results in loss of active Li so the charge/discharge efficiency decreases which necessitates the usage of excess Li (3-4 times) with respect to the cathode capacity. Li can only deposit on the remaining active Li sites and grows in a dendritic form. With repeated cycling, dendrites can perforate the separator and reach the positive electrode thus shorting the cell. Dendrite formation of lithium at the electrodes is illustrated in Figure 1.4 [15].

Due to these reasons, there is no any commercial production of batteries having lithium metal as the anode material. Therefore, researches are concentrated on finding new anode materials. There are many candidate materials but graphitic carbon seems to be the best when compared with other materials. By using carbon materials as an anode for lithium ion rechargeable batteries, carbon can be lithium doped/undoped during charging/discharging without a morphology change at the surface. The reaction of Li-CIC (Carbon Intercalation Compound) during charge-discharge can be expressed as the following equation:

$$\mathrm{Li_xC} \underset{\text{charge}}{\overset{\text{discharge}}{\rightleftharpoons}} \mathrm{Li_{x-y}C} + \mathrm{yLi^+} + \mathrm{ye^-} \qquad (2.6)$$

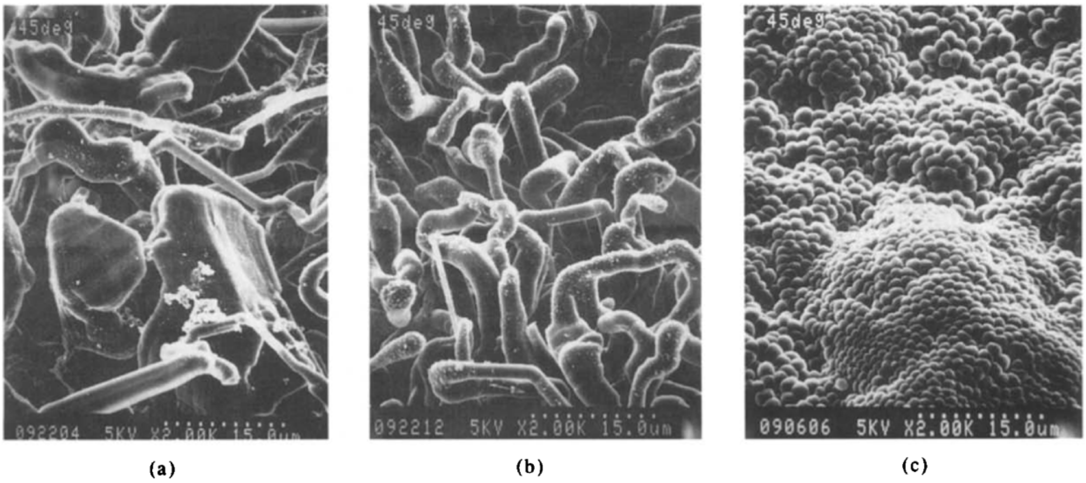

(a) (b) (c)

Figure 1.4. The morphological forms of lithium on anode material, a) dendritic + spherical, b) dendritic, c) spherical [15].

Since this reaction is reversible and the cathode containing $LiCoO_2$ is also a lithium intercalation compound which can be lithium doped/undoped without a morphology change, long cycle life can be attained.

Graphite is distinguished from carbon materials because of its high crystallinity. It is well known to react with lithium to form lithium graphite intercalation compounds (Li-GIC). Carbon materials are classified into two categories according to the structure characteristics: graphitizable carbon and nongraphitizable carbon. Compared with graphitizable carbon, non-graphitizable carbon generally has low density, porous surface, small crystallites, relatively random orientation of crystallites and long interplanar spacing (d002). Since graphitizable carbon is similar to graphite with respect to crystallinity, lithium intercalation into the graphitizable carbon seems to be preferable to that of non-graphitizable carbon [15]. The structure of graphitizable carbon and nongraphitizable carbon are given in Figure 1.5.

There are a lot of anode materials that can be alternative for carbon materials. For example, those based on: (a) elemental aluminium, silicon or tin (b) composite structures formed in situ by electrochemical reduction of metal oxides and (c) host structures in which there is a strong structural relationship between the parent structure and its lithiated product, for example Cu_6Sn_5 and MnSb [12]. However; none of these materials has the desired anode properties like carbon.

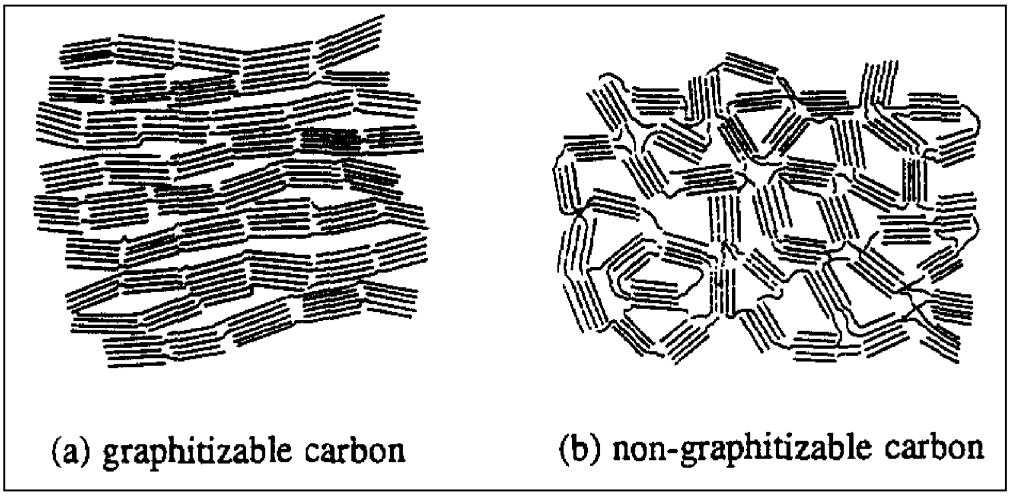

(a) graphitizable carbon

(b) non-graphitizable carbon

Figure 1.5. The structure models of carbon materials [16].

The most commonly used electrolytes for lithium batteries are liquid solutions of lithium salts in aprotic organic solvents. The main parameters which govern the choice of the electrolyte are:

For solvent:

- stability towards both the positive and negative electrodes;
- high solubility for lithium salts;
- safety and non-toxicity.

For lithium salt:

- high ionic mobility for the lithium ion;
- thermal, electrochemical and chemical stability;
- Compatibility with the environment.

Solvents were initially selected primarily on the basis of the conductivity of their salt solutions, the most common example is propylene carbonate (PC). However, solutions based on PC on its own were soon found to cause poor cycleability of the lithium electrode, due to uncontrolled passivation. Solvent mixtures were therefore developed for the combination of high dielectric solvents (e.g. ethylene carbonate, EC) with an alkyl carbonate (e.g. dimethylcarbonate, DMC), to stabilize the protective passivation film on the lithium electrode.

The choice of salt is also important. The major considerations are related to thermal and electrochemical stability, toxicity and cost. Although lithium perchlorate ($LiClO_4$) is moderately conductive, may be subject to violent decomposition, particularly in ether solutions. Lithium hexafluoroarsenate ($LiAsF_6$) suffers from thermal and electrochemical instability, which leads to formation of AsF_5 and insoluble LiF. Lithium hexafluorophosphate ($LiPF_6$) undergoes thermal decomposition at around 30ºC in the solid state and 130ºC in solution [17].

Whittingham [18] lists the key requirements for a material to be successfully used as a cathode in a rechargeable lithium battery as follows:

(i) The material contains a readily reducible/oxidizable ion, for example a transition metal, in the case of $LiCoO_2$, this is the reaction of Co^{3+}/Co^{4+},

(ii) The material reacts with lithium as fast as possible in a reversible manner. Therefore host structure should not be changed with the addition or removal of lithium ions. Fast reaction means high power density.

(iii) The material reacts with lithium with a high free energy of reaction.

(a) High capacity, preferably at least one lithium per transition metal.

(b) High voltage, preferably around 4 V (as limited by stability of electrolyte).

(c) This leads to a high-energy storage.

(iv) The material is a good electric conductor, preferably a metal.

(a) This allows for the easy addition or removal of electrons during the electrochemical reaction.

(b) This allows for reaction at all contact points between the cathode active material and the electrolyte rather than at ternary contact points between the cathode active material, the electrolyte, and the electronic conductor (such as carbon black).

(c) This minimizes the need for inactive conductive additions, which reduce the overall energy density.

(v) The material is stable, with overdischarge and overcharge, it does not change structure or degrade.

(vi) The material has low cost.

(vii) The material is environmentally benign.

The cathode materials that can fulfill the above requirements are mainly oxides of transition metals, which can undergo oxidation to higher valences when lithium is removed. This structural stability is a particular challenge during charging when most (ideally all) of the lithium is removed from the cathode. During discharge lithium is inserted into the cathode material and electrons from the anode reduce the transition metal ions in the cathode to a lower valence. The rates of these two processes, as well as access of the lithium ions in the electrolyte to the electrode surface, control the maximum discharge current [19].

The crystal structure of cathode materials used in lithium ion batteries can be classified and discussed in 3 categories. These are;

- α-$NaFeO_2$ structure (layered oxides, typical examples are $LiCoO_2$ and $LiNiO_2$)
- spinel structure ($LiMn_2O_4$)
- olivine structure ($LiMPO_4$, most commonly $LiFePO_4$)

The layered oxides have a rock salt structure where lithium and transition metal cations occupy alternate layers of octahedral sites in a cubic close-packed oxygen ion lattice. The lattice is depicted in Figure 1.6.

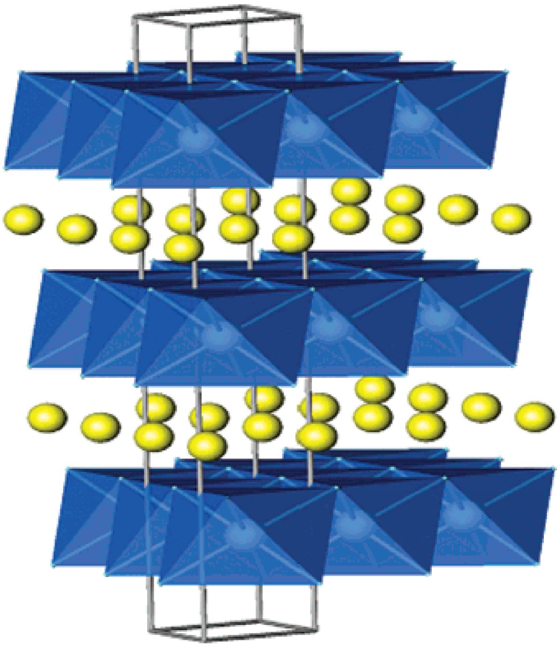

Figure 1.6. Layered structure (light spheres are Li, sheets are transition metal oxides) [18].

The cathode material most commonly used in lithium ion batteries is $LiCoO_2$. It has a rock-salt structure where the cations order in alternating (111) planes. This ordering results in a trigonal structure ($R\bar{3}m$) and planes of lithium ions through which lithiation and delithiation can occur. Although $LiCoO_2$ is a successful cathode material, alternatives are being developed to lower cost and improve stability. Cost reduction studies focus on decreasing or fully discarding the use of cobalt which is less available and more toxic than other transition metals, such as manganese, nickel and iron. In addition, $LiCoO_2$ is not as stable as other potential electrode materials and can undergo performance degradation or failure when overcharged. The increase in charging voltage can increase the cell capacity, but can also lead to more rapid decrease in capacity as the cell is cycled during recharging. Several reasons have been given for the degradation during cycling. One is that, during delithiation, Co^{3+} is oxidized to Co^{4+} with CoO_2 in the structure. Cobalt (Co^{4+}) is dissolved in the electrolyte resulting in intercalation of less lithium during discharge. Another is that the CoO_2 layer formed after full delithiation shears from the electrode surface, which also results in less capacity for lithium intercalation. In addition to these, the lattice parameters of $LiCoO_2$ change sharply with Li intercalation/deintercalation which can lead to stresses and micro-cracking of the cathode particles.

Fergus [19] listed some alternative cathode materials to $LiCoO_2$ as $LiNiO_2$, V_2O_5, $LiMn_2O_4$ and $LiMPO_4$. $LiNiO_2$ also has the α-$NaFeO_2$ structure, is lower in cost and has a higher energy density (15% higher by volume, 20% higher by weight) but is less stable and less ordered as compared to $LiCoO_2$. As occupation of Ni ions in the Li site is seen in this material, $LiNi_{1-x}Co_xO_2$, typically containing mostly nickel (x~0.2), has been used. Moreover production of $LiNiO_2$ is not as easy as $LiCoO_2$. Although vanadium oxide containing electrodes have high capacities, they have relatively low voltages (typically 3V or less) as compared to the other alternative cathode compounds. $LiMn_2O_4$ has a spinel structure ($Fd\bar{3}m$), in which manganese occupies the octahedral sites and lithium predominantly occupies the tetrahedral sites. $LiMn_2O_4$ has lower cost and is safer than $LiCoO_2$, but has a lower capacity as compared to other cathode materials. One of the challenges in the use of $LiMn_2O_4$ as a cathode material is that phase changes can occur during cycling. Capacity loss has also been observed during storage due to dissolution of manganese in the electrolyte or due to changes in particle morphology or crystallinity. Other transition metals, including iron and cobalt have been added to $LiMn_2O_4$.

Another promising class of cathode materials are phosphates ($LiMPO_4$) with the olivine structure (Pnma). The phosphate most commonly used for the cathode is $LiFePO_4$, which delithiates to $FePO_4$ as the Fe^{2+} is oxidized to Fe^{3+}. Some iron ions occupy lithium sites, which results in the formation of lithium ion vacancies to maintain charge neutrality. The largest drawback of $LiFePO_4$ is its low conductivity. Studies concentrate on some additions and coatings with carbon, however, the amount of the additions is critical as larger amount results in decrease of the capacity by blocking lithium diffusion paths.

The above discussed batteries operate at about 3.5-4.0 V. However; researches are also concentrated on finding cathode materials having higher operating voltage (4.5-5.5 V).

Kawai et al. [20] discussed these materials from various studies. Although voltage profiles at about 4.5-5.0 V can be achieved, the capacities of these materials are relatively low. The largest capacity is achieved with $LiCoMnO_4$ (95 mAh/g) at 4.5 V [20].

The most widely used electrode couple (anode-cathode) in Li-ion batteries are $LiCoO_2$ and carbon. So the electrode and cell reactions in this configuration are as follows and it is depicted in Figure 1.7 [8];

$$\text{Positive} \quad : \ LiMO_2 \underset{\text{discharge}}{\overset{\text{charge}}{\rightleftharpoons}} Li_{1-x}MO_2 + xLi^+ + xe^- \tag{2.7}$$

$$\text{Negative} \quad : \ C + xLi^+ + xe^- \underset{\text{discharge}}{\overset{\text{charge}}{\rightleftharpoons}} Li_xC \tag{2.8}$$

$$\text{Cell} \quad : \ LiMO_2 + C \underset{\text{discharge}}{\overset{\text{charge}}{\rightleftharpoons}} Li_{1-x}MO_2 + Li_xC \tag{2.9}$$

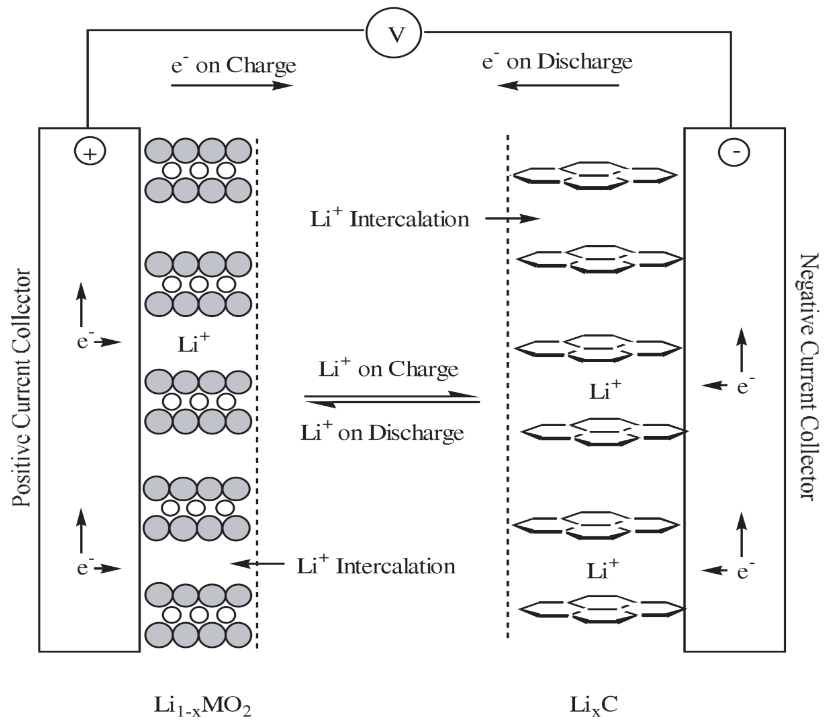

Figure 1.7. The electrochemical process in a typical Li-ion battery [8].

CHAPTER 2

LITERATURE SURVEY

2.1. Formation and Production of $LiCoO_2$

$LiCoO_2$ has two different crystal structures: high temperature (HT) with ideal layered bidimensional α-$NaFeO_2$ structure (space group $R\bar{3}m$) and low temperature (LT) with a spinel-like structure ($Fd\bar{3}m$) in which about 6% of Co^{3+} ions are located in lithium sites. As names imply LT-$LiCoO_2$ is synthesized at relatively low temperatures such as 350-400ºC whereas HT-$LiCoO_2$ is synthesized at higher temperatures as 800-900ºC. The electrochemical performance of LT-$LiCoO_2$ is not as satisfactory as that of HT-$LiCoO_2$ due to different structural arrangement and occurrence of phase changes during Li intercalation/deintercalation reactions [21]. To prove this phase changes, Gummow et. al [22] applied detailed structural refinement of LT-$LiCoO_2$ and LT-$Li_{0.4}CoO_2$. They concluded that phase transition between rock-salt structure to spinel-type structure during Li deintercalation/intercalation reactions was responsible for poor cycleability. Production of LT-$LiCoO_2$ with stable spinel structure might lead to better cycleability according to them.

$LiCoO_2$ was firstly synthesized by Ellestad and Babbitt [23] in 1951 and they patented their study. They have produced $LiCoO_2$ by the reaction of various Co oxides (Co_3O_4, Co_2O_3 and CoO) with lithium carbonate (Li_2CO_3) at 900-1000ºC. They ensured that the product was $LiCoO_2$ by making some calculations on the available oxygen content. Obviously, they did not apply any phase determining technique.

The structural analysis of $LiCoO_2$ was firstly done by Johnston et al. [24] in 1958. They studied the system of $Li_xCo_{1-x}O_2$. They produced various forms of $Li_xCo_{1-x}O_2$ by heating CoO and Li_2O_2 at 900ºC. They investigated that the lattice parameter of the cubic system decreased with the increase in lithium content. When x=0.5, $LiCoO_2$ was produced and a rhombohedral structure was formed.

The invention that $LiCoO_2$ can be used as a cathode material was made by Mizushima et al. [25] in 1980. It was found that the measured open circuit voltage of $LiCoO_2$ is twice higher than that of $LiTiS_2$ which was the cathode material in 1980s. $LiCoO_2$ was prepared by mixing Li_2CO_3 and $CoCO_3$ in air at 900ºC for 20 hours. This preparation method is referred as traditional or conventional. High temperature is needed for this method as starting materials have low reactivity and mixing is insufficient. This prolonged calcination causes the grain coarsening as well as lithium evaporation which in turn impair the electrochemical properties of the product. So to overcome this drawback, different synthesis methods have been conducted. Antolini [26] listed some of these synthesis methods as sol-gel, spray-drying, combustion synthesis, hydrothermal synthesis and mechanical activation with other less known methods such as microwave synthesis and freeze drying.

Sol-gel is a widely applied method for producing $LiCoO_2$. Kang et al. [27] produced both HT-$LiCoO_2$ and LT-$LiCoO_2$ by citrate sol-gel method. Li_2CO_3, $Co(NO_3)_2.6H_2O$ and $C_6H_8O_7$(citric acid) were dissolved in the mole ratio of 1:1:2 in distilled water. The solution was adjusted to pH 3–4 with aqueous NH_4OH by considering the solubility diagram. The solution was evaporated at 80ºC under vacuum and subsequent organometallic complexes were decomposed into organic compounds and metal oxide precursor at 300ºC. The metal oxide precursor was pre-heated at 600ºC for 6 hours and annealed at 850ºC for 20 hours in air to obtain HT-$LiCoO_2$. LT-$LiCoO_2$ was synthesized by heating the metal oxide precursor at 400ºC for 120 hours. They found the first discharge capacity of LT-$LiCoO_2$ as ~80 mAh/g (at 100 $\mu A/cm^2$) and that of HT-$LiCoO_2$ as 130 mAh/g (at 200 $\mu A/cm^2$). The cell polarization of HT-$LiCoO_2$ is very small but that of LT-$LiCoO_2$ is very large.

Jeong and Lee [28] produced HT-$LiCoO_2$ by mechanical activation (alloying). They used $LiOH.H_2O$ and $Co(OH)_2$ as the starting materials and the molar ratio of Li:Co is 1:1 in the ball mill. They applied milling for 6 hours. After milling, subsequent heat treatment was applied at 600ºC for 2 hours under air. They also produced $LiCoO_2$ in a traditional way and compared the electrochemical properties of their samples with that of conventional $LiCoO_2$. The discharge capacity of $LiCoO_2$ produced by various methods are in the range of 120-140 mAh/g but the discharge capacity of $LiCoO_2$ produced by mechanical alloying (MA) is 152 mAh/g. They have claimed that in comparison with conventional solid state reactions, this method of production has less expensive firing conditions so it saves energy. However; the cycleability was about 72% of the maximum value after 30 cycles which is inferior to that of conventional process. This was due to low crystallinity according to them.

Burukhin et al. [29] studied to produce $LiCoO_2$ with hydrothermal synthesis. In this method, the reagent grade cobalt (II) nitrate hexahydrate, lithium hydroxide monohydrate and hydrogen peroxide (50%) were used as starting materials. Firstly the suspension was produced with the addition of solution of cobalt nitrate to the lithium hydroxide solution. After that, the suspension of cobalt (II) hydroxide was oxidized by hydrogen peroxide solution. The Li/Co ratio was varied from 4:1 to 8:1 for 3 and 6M LiOH solution, respectively. Reactant mixtures with different Co/Li ratios were hydrothermally treated at 150–250ºC for 0.5–24 hours in a Teflon-lined autoclave The heating rate to desired temperature was 2.5 ºC/min. They have studied the properties of both as prepared sample and annealed (550ºC for 72 hours) sample. They have seen that they could not produce single phase $LiCoO_2$ at 120ºC. They have reached a very interesting conclusion that at high discharge rate (C/2) cycleability was worse with the annealed sample. They claimed that this was due to the smaller particle size and higher surface area of the as-prepared sample when compared to annealed sample.

Li et al. [30] produced $LiCoO_2$ by spray-drying process. The process was simply as follows: Equivalent molar compositions of lithium acetate and cobalt acetate were dissolved in de-ionized water and then a quantity of polyethylene glycol (PEG) was added. The solution was dried by using spray-drying apparatus. Inlet air temperature was 300ºC, and exit air temperature was 100ºC. Finally, the ultrafine $LiCoO_2$ powder was synthesized by calcining the mixed precursor in air at 800ºC for 4 h. The obtained powder was homogeneous and was HT-$LiCoO_2$ having the α-$NaFeO_2$ structure type. An electrochemical test with constant-current charge–discharge confirmed that the electrochemical property of the powder in a laboratory coin cell was good with an initial charge capacity of 148 mAh/g, a discharge capacity of 135 mAh/g, and capacity did not change after 10 cycles. The authors thought that this behaviour was due to the particle size (200-700 nm) of $LiCoO_2$ although they did not make extensive discussion.

Santiago et al. [31] produced $LiCoO_2$ by combustion synthesis method. For this synthesis, cobalt nitrate hexahydrate and lithium nitrate were used as oxidant reactants and metal sources, while urea was used as fuel. The reactants were mixed in a glassy crucible able to withstand a high thermal gradient. The mixture was homogenized with pure water and heated on a hot plate at 350ºC in contact with the room atmosphere. The first step of the combustion reaction was the evaporation of the water and the production of the gases, such as NO_x and NH_3. The amount of gases and the heat generated during the combustion reaction could be modulated by the nitrate/urea ratio. All samples have been heat treated at various temperatures (400, 500, 600, 700ºC) for 12 hours. For $LiCoO_2$ obtained at 700ºC, the first discharge capacity was 136 mAh/g, which was a comparable value to that of $LiCoO_2$ obtained by the conventional solid-state method. They believed that at lower temperatures, spinel phase of $LiCoO_2$ was left in the structure hence the capacity was decreased.

Yan et al. [32] produced $LiCoO_2$ by microwave synthesis. In this method, $LiCH_3COO.2H_2O$ and $Co(CH_3COO)_2.4H_2O$ were used as the starting materials and the starting Li:Co atomic ratio was 1:1. They were dissolved in de-ionized water and milled at 60°C for 24 h. After drying at 120°C for 24 h, the powder was calcined at 400°C for 5 h to burn out the organic substances. Then pellets were pressed and submitted to microwave calcination. The microwave calcination was conducted in air with a 2.45 GHz microwave. The pellets were further heated at temperatures ranging from 600 to 900°C for 10 min. A single-mode microwave heating device was used in this experiment. The precursor precalcined at 400°C, displayed two charge and discharge plateaus and the discharge capacity was only 60 mAh/g. Through microwave calcination, the capacity of $LiCoO_2$ increased greatly and reached a maximum of 140 mAh/g when the synthesizing temperature was 800°C. The microwave synthesized $LiCoO_2$ had a good cycleability. After 40 cycles, the capacity was still greater than 130 mAh/g, which was a rather good result for a Li/$LiCoO_2$ cell. They claimed that the capacity increase was due to the smaller particle size (100-500 nm) obtained. They also observed lithium loss of 4% which was a very low value when compared with the lithium loss (20-30%) during the conventional method.

Choi et al. [33] produced $LiCoO_2$ by spray pyrolysis. They began by mixing the nitrate solutions of lithium and cobalt. This solution was fed to an apparatus containing a pump, nebulizer and electric furnace. Nebulizer was used to generate droplets of the solution and carrier gas took the droplets to the furnace. The temperature of the furnace was 800-900°C and droplets were subjected to this temperature for only 1.5 seconds. The dried and decomposed powder were heat treated at about 700-900°C for 1-12 hours. They achieved a specific capacity of 171 mAh/g and the voltage plateau at 3.9 V for the sample synthesized at 840°C and heat treated at 890°C for 10 hours. The particle size was around 5 µm.

Chiang et al. [34] were the first to use freeze drying for production of $LiCoO_2$. They prepared a suspension by dissolving a mixture of LiOH and cobalt nitrate solutions. With pH value of around 11, $Co(OH)_2$ was precipitated. Precipitate was washed and centrifuged for 4-5 times in order to get rid of the nitrate ions. Then LiOH solution and the $Co(OH)_2$ precipitate were again mixed at a Li:Co ratio of 1:1. The suspension was freeze dried. The precursors after the freeze drying process were heat treated between 100-800ºC for 2 hours. They saw that the sample heat treated at 100°C had shown relatively good electrochemical behaviour although the best behaviour was seen in the sample heat treated at 800°C. However; the sample heat treated at 100°C had Li_2CO_3 as an impurity phase and this phase disappeared with increasing of the temperature. They conducted charge-discharge tests between 2.5-4.25 V and the discharge capacity was 120 mAh/g at a charge rate of 0.2C. In addition to that the charge-discharge voltage plateau occurred at about 4V. The capacity loss of the powder after 30 cycles was very low. Therefore they have concluded that freeze drying was useful for producing cathode materials for Li-ion batteries.

Brylev et al. [35] applied freeze drying for producing $LiCoO_2$ with different starting materials. The following combinations of salts were used for preparing starting solution for the freeze drying:

a) $HCOOLi.H_2O + Co(HCOO)_2.2H_2O$ (formate precursor),
b) $CH_3COOLi.2H_2O + Co(CH_3COO)_2.4H_2O$ (acetate precursor),
c) $LiNO_3.3H_2O + Co(CH_3COO)_2.4H_2O$ (nitrate–acetate precursor),
d) $CH_3COOLi.2H_2O + Co(NO_3)_2.6H_2O$ (acetate–nitrate precursor)

Initial aqueous solutions containing Li and Co salts in a molar ratio of 1.2:1 (in order to prevent Li loss during heat treatment) were sprayed into liquid nitrogen by pneumatic nozzle. After this, freeze drying was applied at a pressure of $5x10^{-2}$ mbar for 48 hours. Freeze dryer cooled down to 210 K (-63°C) and then samples were subjected to freeze drying while temperature rose to 315 K (42°C). Heat treatment was applied in air between 300 and 850 ºC.

As can be seen from Table 2.1, all materials possessed completely different electrochemical behaviour. As can be expected, better properties in terms of capacity retention were observed in materials with HT-$LiCoO_2$. Although the highest initial capacity was attained for materials containing LT-$LiCoO_2$, capacity dropped rapidly with cycling. They explained the difference in the electrochemical behaviour by the help of TG curves and impurity phases. The appearance of cubic spinel Co_3O_4 led to the formation of cubic spinel $LiCoO_2$ (LT-$LiCoO_2$). Moreover, Co_3O_4 retarded the transformation of LT-$LiCoO_2$ to HT-$LiCoO_2$. TG curves proved that acetate precursors had no impurity phase of Co_3O_4 hence the production of HT-$LiCoO_2$ could be achieved after heat treatment at 850°C.

Table 2.1. Electrochemical properties and phase composition of $LiCoO_2$ obtained from different precursors after heat treatment at 850ºC [35].

Precursor	Initial Discharge Capacity (mAh/g)	Discharge Capacity of 4th Cycle (mAh/g)	Phase composition
Formate	142	100	Mostly LT-$LiCoO_2$
Acetate	98	92	Only HT-$LiCoO_2$
Nitrate-Acetate	145	80	Mostly LT-$LiCoO_2$
Acetate-Nitrate	135	77	HT- and LT-$LiCoO_2$

2.2. Structure and Ordering Characteristics of HT-$LiCoO_2$

HT-$LiCoO_2$ belongs to the oxide groups having the general formula AMO_2. Here A is an alkali metal and M can be one or more elements having different oxidation states. A^+ ions reside between the O_2 sheets formed by edge-shared MO_6 octahedra. Layered AMO_2 is termed due to the coordination of the alkali metal (octahedral, prismatic, tetrahedral) and the number of MO_2 sheets per unit cell. Therefore the layered oxides can have the structures such as O3, T1, P2, P3. [36]. Considering this classification, HT-$LiCoO_2$ belongs the O3 group in which Li ions reside in octahedral positions and there are three MO_2 sheets. The oxygen stacking sequence is ABCABCABC along the lattice parameter *c*. From Figure 2.1, the 2D view and 3D view of the O3 group as well as the structure of HT-$LiCoO_2$ with the ions positioned to their sites can be seen.

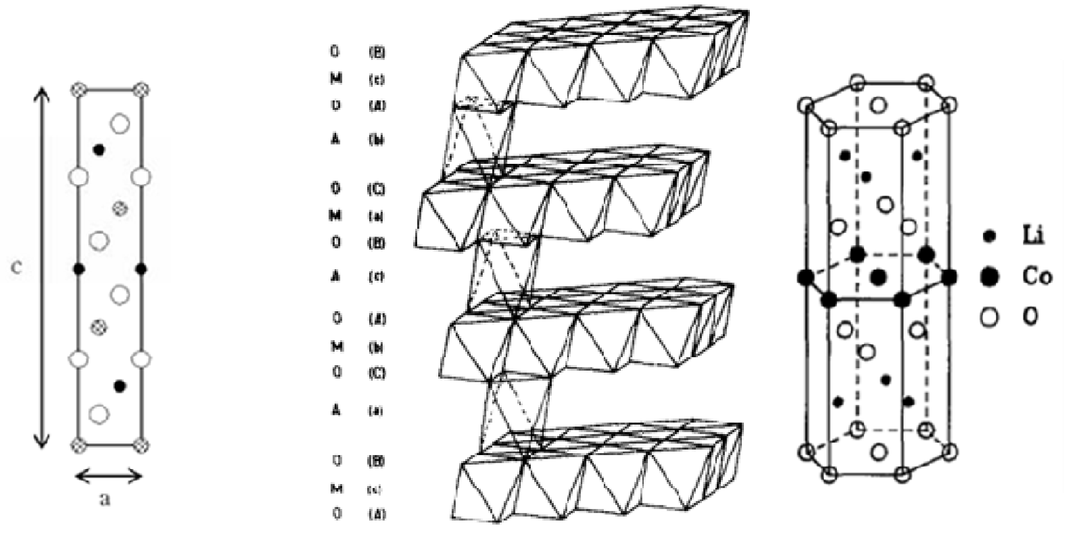

(a

(b

(c

Figure 2.1. 2D view (a) [36] and 3D view (b) [37] of the O3 group. The hexagonal structure of HT-$LiCoO_2$ and position of the ions, (c) [38].

There is a great relation between the structure and electrochemical behavior of HT-$LiCoO_2$. In XRD, HT-$LiCoO_2$ is differed from its low temperature structure with the splitting of

[006]/[102] peaks and [108]/[110] peaks. A typical XRD of both types was given by Gummow et al. [21] which is shown in Figure 2.2. As it is seen from Figure 2.2, [006]/[102] and [108]/[110] peaks are overlapped for LT-$LiCoO_2$ whereas they are clearly distinguishable for HT-$LiCoO_2$. Gummow et al. [21] explained this difference as a parameter related with the cation ordering of these two types. It was mentioned that cobalt ions adopt a different arrangement in these two structures. In other words, occupation of Co ions in Li-sites and occupation of Li-ions in Co-sites are different for LT-$LiCoO_2$ and HT-$LiCoO_2$.

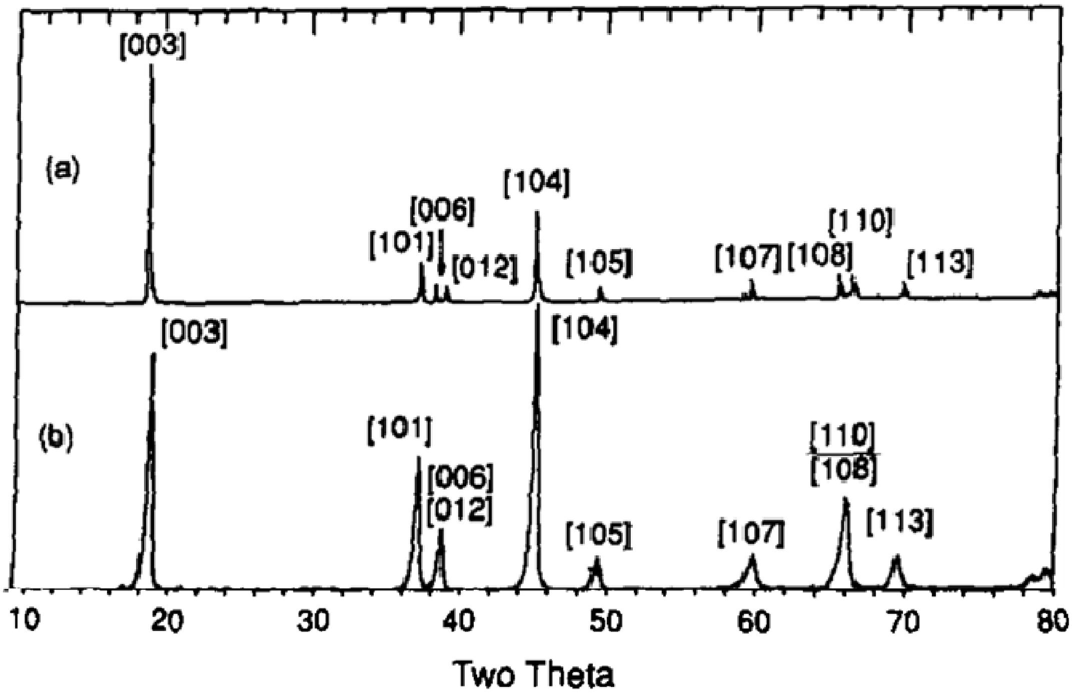

Figure 2.2. Typical XRD patterns for a) HT-$LiCoO_2$ and b) LT-$LiCoO_2$ [21].

The lattice parameters for HT-Li_xCoO_2 change with lithium amount, x. Gummow et al. [21], Honders et al. [39], and Mizushima et al. [25] have shown that with increasing x, decrease in lattice parameter *c* and slight increase in lattice parameter *a* are observed (Table 2.2). With these results, it can be easily inferred that *c/a* ratio increases when x in Li_xCoO_2 decreases.

The ratio of the peak intensities of [003] and [104] ($I_{[003]}/I_{[104]}$, will be shown as [003]/[104] hereafter) is important for determining the ordering characteristics of the HT-$LiCoO_2$ apart from distinguishing it from LT-$LiCoO_2$. Shlyakhtin et al. [40] claimed that high ratio of [003]/[104] for a nanocrystalline powder (particle size: 50-60 nm) was an indication of anomalies of element distribution in Co sublattice. The authors referred to the study of Kanamura et al. [41] who claimed that the high ratio of [003]/[104] showed that there are some crystal structure defects in the structure such as substitution of Co^{3+} ions by Li^+ ions. The ratio of the said peaks was about 3.5 for both of these studies.

Table 2.2. Change of lattice parameters when Li is less than the stoichiometric amount.

Formula	*c* (Å)	*a* (Å)	Reference
HT-$LiCoO_2$	14.060	2.818	Gummow et al. [21]
HT-$Li_{0.86}CoO_2$	14.124	2.816	
HT-$LiCoO_2$	14.060	2.815	Honders et al. [39]
HT-$Li_{0.75}CoO_2$	14.200	2.811	
HT-$Li_{0.50}CoO_2$	14.420	2.808	
HT-$Li_{0.34}CoO_2$	14.400	2.807	
HT-$LiCoO_2$	14.080	2.816	Mizushima et al. [25]
HT-$Li_{0.74}Co_{1.01}O_2$	14.220	2.812	
HT-$Li_{0.49}Co_{1.01}O_2$	14.420	2.807	

In contrast to that, many studies thought that the higher the ratio of [003]/[104], the better the ordering is. One of these researchers was Arof. He [42] claimed that the high ratio of [003]/[104] shows that there is an hexagonal ordering in the structure which will potentially lead to good electrochemical behaviour. He also had given a formula for estimating measure of degree of lattice disorder, by using R. The formula for R is as follows:

$$R = \frac{I[102] + I106]}{I[101]} \tag{2.10}$$

and y gives the lattice ordering;

$$y = 1.073 - 0.228R + 0.039R^2 \tag{2.11}$$

However; the researchers in this field do not refer to this approach for determining the ordering of the structure. Most of the researchers use [003]/[104] ratio for ordering determination.

Jeong et al. [43] thought in a similar manner with Arof. They have thought that the intensity of [003] peak decreases when an atom occupies octahedral Li sites in $LiMO_2$ (M = Co, Ni, V, Cr). As they achieved high [003] peak in their study, they have concluded that Li and Co layers are well spaced in the structure. Jeong and Lee [44] produced $LiCoO_2$ with mechanical alloying and they claimed that decreasing the [003]/[104] ratio led to an increase in cation mixing in the structure. They saw that [003]/[104] ratio decreased after sintering at 850°C for 24 hours due to the loss of lithium. Therefore some Co ions must occupy Li sites in the structure due to their argument. Support to the idea of relating the increase of [003]/[104] ratio to the ordering property came from Sathiya et al. [45]. They concluded that when the aforesaid ratio increases to a value higher than 1.2, then this is the indication of the absence of cation mixing, the ratio below 1.2 indicates a considerable extent of cation mixing.

$LiCoO_2$ and $LiNiO_2$ are similar in crystal structure. They have both layered structures. Larcher et al. [46] claimed that for $LiNiO_2$, if the ratio of [003]/[104] is higher than 1.3, then it can be thought that the structure is well-ordered.

There are a lot of studies in the literature discussing the production of HT-$LiCoO_2$ as well as its microstructure. Many of the authors are on the side that increase of the [003]/[104] ratio is an evidence of more ordered structure, although Shlyakhtin et. al. [40] and Kanamura et al. [41] are on the opposite side. The details of the Rietveld analysis as well as the importance of [003]/[104] ratio will be discussed in the following chapters.

As it was previously discussed, occupation of Li-sites with Co ions in LT-$LiCoO_2$ is higher than that of HT-$LiCoO_2$. Lithium ions reside in 3a positions at (0 0 0), cobalts ions reside in 3b positions at (0 0 0.5) and oxygen ions occupy 6c position at (0 0 z) for HT-$LiCoO_2$. However; for LT-$LiCoO_2$, 6 mole% of cobalt ions occupy Li sites and 4 mole% of lithium ions occupy Co sites [21]. This mixing is responsible for the differences of electrochemical performances of two structures leading to phase transition during Li insertion and extraction.

2.3. Doping of $LiCoO_2$

There are huge numbers of publications in literature that dope elements to $LiCoO_2$ in order to enhance the electrochemical properties. Almost all studies denote doping with a formula of $LiCo_{1-x}M_xO_2$. Moreover there are a lot of studies that incorporates more than one doping elements to $LiCoO_2$ denoted by $LiCo_{1-x-y}M_xN_yO_2$. However; there are relatively more studies that use Ni, Mn (transition metals) or Al (non-transition metals) as the doping elements. Although, there is no strict general rule for the effect of alloying additions, Venkatraman et al. [47] and Ceder et al. [48] came through a conclusion as “The doping of $LiCoO_2$ with non-transition metals results in higher voltage with a reduced capacity, whereas transition metal ions doping yields a higher capacity with a lower voltage profile”.

The literature about doping of HT-$LiCoO_2$ will be divided in three sections, first the effect of common doping elements such as Al, Ni and Mn will be discussed, second section will cover the literature about the dopants relating with the subject of this thesis (Cr, Mo and W), last section will be devoted to the discussion of the elements having the oxidation states larger than that of Co ion (3^+).

2.3.1. Doping with Al, Ni and Mn

Aluminium is the mostly used element for doping of $LiCoO_2$. As usual, it is alloyed instead of Co. Aydinol et al. [49] show by ab initio calculations that theoretical intercalation voltage of $LiAlO_2$ is about 5V. However; $LiAlO_2$ is electrochemically inactive. Therefore, doping of $LiAlO_2$ with transition metals and/or doping $LiCoO_2$ with Al may result in better electrochemical property. The advantage of Al doping is that Al is lighter and less toxic than Co.

Jang et al. [50] doped $LiCoO_2$ with Al for the aim of getting the formula $LiAl_yCo_{1-y}O_2$ (y=0, 0.25 and 0.5). They applied freeze drying prior to calcination at 700-800°C for 2 hours. The

XRD yielded a peak of a phase of $LiAlO_2$ at y=0.5 therefore solid solubility could not be attained at a value between y=0.25 and 0.5. Although OCV increased with doping of Al, capacity fade with cycling decreased. Al doping caused broadening of the XRD peaks. They explained the increase in the voltage as a result of more electron exchange of Al^{3+} with oxygen than that of Co^{3+}.

Huang et al. [51] applied conventional solid state synthesis for obtaining $LiAl_yCo_{1-y}O_2$ ($0 \leq y \leq 0.3$). They got similar results with [50] in terms of intercalation voltage and capacity but the best electrochemical behaviour in their study belonged to $LiAl_{0.15}Co_{0.85}O_2$. It is interesting that after a significant loss of capacity after first cycle, capacity retention could be attained for the following 10 cycles without losing the hexagonal settings cycled between 2.5 and 4.5 V. They did not observe hexagonal to monoclinic phase transformation in $LiAl_{0.15}Co_{0.85}O_2$. The absence of the two phase region at high voltages (~4.5 V) was also observed by [52].

Myung et al. [53] produced $LiAl_yCo_{1-y}O_2$ (y=0, 0.1, 0.2 and 0.3) by applying emulsion drying method. They also applied structural analysis as a function of intercalated lithium. They concluded that doping with Al prevented the Co dissolution during charge/discharge cycles therefore it stabilized the $LiCoO_2$ structure. They calculated that the dissolution decreased with the addition of Al, Co dissolution in electrolyte (10 ml volume) was 20 ppm for undoped $LiCoO_2$ and 3.6 ppm for $LiAl_{0.3}Co_{0.7}O_2$. They constructed a triangle (Figure 2.3) showing the effect of Al addition to the properties of $LiCoO_2$.

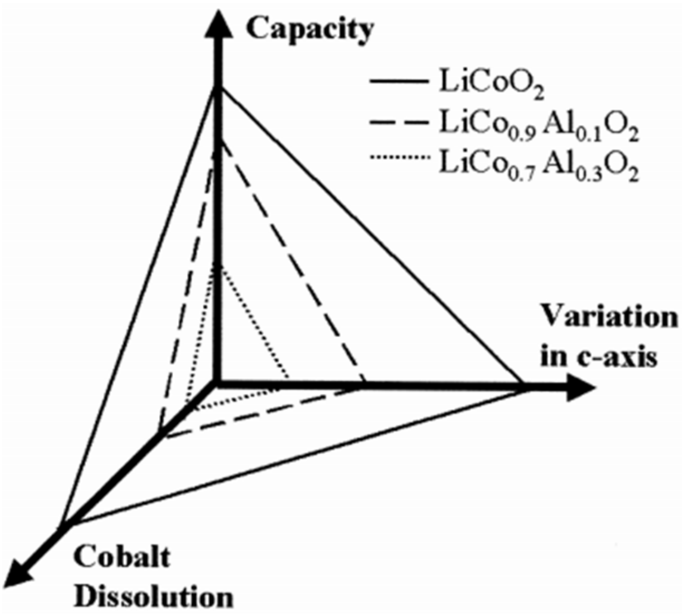

Figure 2.3. Effect of Al doping on discharge capacity, cobalt dissolution and variation in the lattice parameter *c* [53].

The most recent study for producing Al doped $LiCoO_2$ was done by Khan and Bashir [54]. They applied detailed structural analysis and they achieved a single phase up to 70 mole% Al doping which means they got a single phase of $LiAl_{0.7}Co_{0.3}O_2$. They applied sol-gel and heat treated the samples for 24 hours at 800°C. The observation of the shrinkage of interatomic distance (lattice parameter *a*) within a CoO_2 layer and the expansion of the interplanar distance between CoO_2 layer (lattice parameter *c*) was observed, also.

As Ni is cheaper than Co, $LiNiO_2$ becomes advantageous towards $LiCoO_2$. Also higher discharge capacity makes the former material be a promising cathode material for Li-ion batteries [55]. However; synthesis is so difficult that it cannot find widespread application in aforesaid batteries. Generally a formula of $Li_{1-y}Ni_{1+y}O_2$ $(0 \leq y \leq 0.2)$ [56] is achieved which will eventually lead to less capacity than the stoichiometric phase. In this manner, doping of $LiCoO_2$ with Ni becomes important.

Kinoshita et al. [55] doped Ni to $LiCoO_2$ in an extensive range of 10 to 90 mole% Ni instead of Co. They produced the desired material by mixing hydroxides of the metals at 850°C for 20 hours. The structure is entirely α-$NaFeO_2$ for all doping amounts. With addition of Ni, lattice parameters *a* and *c* increase due the differences of the ionic radius between Ni and Co, Ni is slightly larger than Co. They found the largest discharge capacity for $LiNi_{0.7}Co_{0.3}O_2$ with a value of 159 mAh/g. However; this material cannot be termed as Ni doped $LiCoO_2$, it is better to define it as Co doped $LiNiO_2$. There are more studies in the literature that dope Co to $LiNiO_2$ than that of Ni to $LiCoO_2$. They will not be discussed here.

Julien [57] studied the extensive range of Ni doping to $LiCoO_2$. Although he got satisfactory electrochemical behaviour with $LiCo_{0.7}Ni_{0.3}O_2$, the initial capacity of it was smaller than that of $LiCo_{0.4}Ni_{0.6}O_2$.

Alcantara et al. [58] produced a cathode material with a formula $Li_{1-x}(Ni_{0.13}Co_{0.87})_{1+x}O_2$ and $Li_{1-x}(Ni_{0.88}Co_{0.12})_{1+x}O_2$. They observed that Ni rich composition had better reversibility with respect to Co rich composition. Worse reversibility of Co was due to the presence of the Co^{4+} ions according to them.

Fergus [19] claimed that the mostly used material containing Ni and Co is $LiNi_{0.8}Co_{0.2}O_2$. Ni ions occupy the Li sites in $LiNiO_2$ so that the structure is less stable and less ordered when compared to $LiCoO_2$. Co addition to $LiNiO_2$ makes it more ordered by decreasing the amount of Ni in the Li sites.

Mn is another element which is widely doped to $LiCoO_2$. There are different cathode materials to be used in Li-ion batteries such as $LiMnO_2$, $LiMn_2O_4$, $Li_2Mn_4O_9$ and $Li_4Mn_5O_{12}$. Among these; $LiMn_2O_4$ is more promising cathode material than $LiMnO_2$.

Stoyanova et. al. [59] studied the effect of Mn doping to $LiCoO_2$ over the whole Co-Mn range, in other words they added Mn in the amounts ranging from 4 to 100 mole%. They observed that with the addition of Mn, lattice parameters *a* and *c* were increased, *a* increased less than c so that c/a value increased. Due to the authors, as ionic radius of Mn^{3+} is larger than that of Co^{3+}, this is an expected result. However; ratio of [003]/[104] decreased with Mn addition. This was an indication of cation mixing in the structure in which Li^{+}, Mn^{3+} and Co^{3+} ions were disordered in the lattice. So it was inferred that when Mn is added to $LiCoO_2$, ordering diminished. The authors revealed that incorporation of 20 mole% Mn into the layered $LiCoO_2$ caused a structural change from trigonal to cubic.

Numata and Yamanaka [60] doped Mn and Li instead of Co and they produced a solid solution having a formula of $Li_{1.033}Mn_{0.067}Co_{0.9}O_{2.}$ However; the charge-discharge tests yielded worse results than that of $LiCoO_2$. It was believed that replacement of Co ions with Li and Mn resulted in a material having higher oxidation voltage. Moreover; it was observed that discharge capacity decreased with the addition of Mn ions.

Waki et al. [61] doped Mn to $LiCoO_2$ in the amounts ranging from 1 to 50 mole%. They found that the ratio of [003]/[104] did not change with the addition of Mn which contradicted with [59]. They saw a shift of the [003] peak to the left which indicated a change in lattice parameter *c*. They have observed nearly the same behavior for the lattice parameter *c* with the study of [59] but they added that for a significant change, Mn addition should be at least 20 mole%. The addition of Mn yielded a lower particle size. They concluded that addition of 20 mole% Mn increased the cycle life of $LiCoO_2$ due to lower particle size and/or expansion of lattice parameter *c*.

Zou et. al. [62] doped Mn to $LiCoO_2$ at an amount of 5 mole%. They observed increase in lattice parameter *c* and *c/a* as with the other authors. They saw the ratio of [003]/[104] was higher than unity indicating a perfect hexagonal ordering. They observed particle size reduction and they claimed that this reduction led to easy intercalation/deintercalation of lithium. The authors concluded that the cycle life of $LiMn_{0.05}Co_{0.95}O_2$ was increased so that this material could be a candidate cathode material in Li-ion batteries at high voltages (3.5-4.5 V). This material delivered a capacity of 158 mAh/gr between 3.5 and 4.5 V.

Lu et al. [63] used three different Mn content for doping. The formulas were $LiMn_{0.33}Co_{0.67}O_2$, $LiMn_{0.25}Co_{0.75}O_2$ and $LiMn_{0.20}Co_{0.80}O_2$. The best electrochemical behaviour was achieved by the sample containing 20 mole% Mn. This was due to the inactive impurity phase especially for $LiMn_{0.33}Co_{0.67}O_2$. When ICP was applied to the materials, it was seen that the sample containing 20 mole% Mn had the highest Li content which led to better cycling efficiency.

Recently, Zheng et al. [64] tried to produce $LiMnCoO_2$ by using different ratios of Mn/Co. They saw that increasing Mn/Co ratio to a value larger than 1 resulted in $LiMnO_2$ phases. XRD peaks are given in Figure 2.4. Also they saw that when Mn/Co ratio was 4/6, ratio of [003]/[104] was the highest indicating the best ordering was achieved with Mn/Co ratio of 4/6 hence the formula obtained was $LiMn_{0.40}Co_{0.60}O_2$.

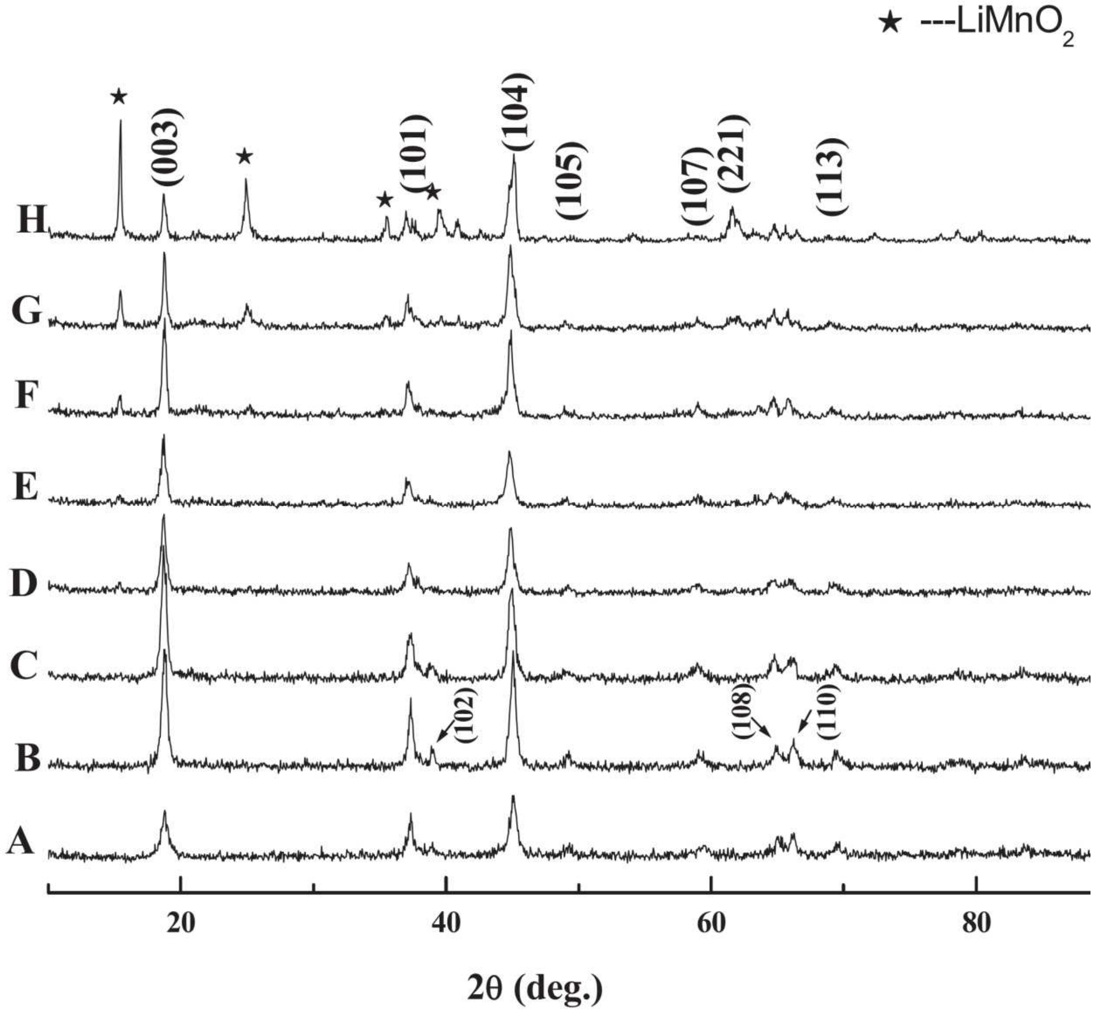

Figure 2.4. XRD results of $LiMnCoO_2$ samples with the Mn/Co ratios of A, B, C, D, E, F, G, H as 2/8, 3/7, 4/6, 5/5, 6/4, 7/3, 8/2, 9/1, respectively [64].

2.3.2. Doping with Cr, Mo and W

Although there occurs a material with the formula $LiCrO_2$, it is electrochemically inactive since trivalent Cr cannot be oxidized to tetravalent Cr. Interestingly reduction of tetravalent state to trivalent state is possible. This drawback makes this material unsuitable for it to be used in Li-ion batteries [65].

Jones et al. [38] studied the doping of $LiCoO_2$ with chromium (Cr). They added Cr instead of Co at an amount of minimum 20 mole%. They applied a process where $Li_xCr_yCo_{1-y}O_2$ was achieved by mixing $LiCoO_2$ and $LiCrO_2$ in stoichiometric amounts under argon gas at 950°C. Other methods, as well as other gases or lower temperatures did not yield a unique solid solution $Li_xCr_yCo_{1-y}O_2$. Increasing the Cr content resulted in increase of both lattice parameters as well as *c/a* value. However; *c/a* was the lowest for $LiCrO_2$. They did not focus on the ordering characteristics but the ratio of [003]/[104] was near 2 for the sample

$LiCr_{0.4}Co_{0.6}O_2$. They did not see any improvement in the electrochemical property, instead they observed that the cycle life was decreased. They concluded that Cr doped $LiCoO_2$ was not a good candidate as a cathode material in Li-ion batteries.

Madhavi et al. [66] also studied doping of Cr to $LiCoO_2$ and they claimed that an effective doping was the one that the Cr content was below 25 mole%. They saw the increase of both lattice parameters *c*, *a* and *c/a* for the Cr additions between 3 and 20 mole%. Their results with lattice parameters *c*, *a* and *c/a* were similar to the Jones et al. [38]. Although [003]/[104] ratio was near 3 for Cr doping levels of 10 mole%, it decreased to 1 for doping with 20 mole%. This might be an indication of the cation mixing in which Cr ions were located in the Li sites. Impurity phases like LiOH and CoO were seen in all their samples containing Cr, but Cr containing impurity was not formed. The electrochemical behaviour in terms of capacity and voltage was not satisfactory.

Another study that focused on Cr doping of $LiCoO_2$ was performed by Pan et al. [67]. They studied the Li-MAS NMR (magic-angle spinning nuclear magnetic resonance) of the local structure of the Cr doped $LiCoO_2$ and concluded that as the resonances in the Li NMR increased with the addition of Cr, this was an indication of Cr appearance in the local Li cation coordinates.

Zou et al. [68] claimed that splitting of [006]-[102] and [108]-[110] peaks were an indication of uniform ordering of lithium and other metals in the structure. They also claimed that abnormal height of [003] ([003]/[104] ratio was higher than 10) meant a deviation from perfect ordering which was an interesting statement. Although they did not compare their results with pristine $LiCoO_2$, the electrochemical behaviour of the Cr doped sample had the highest first capacity, but lowest reversibility hence lowest cycle life when compared with the other dopants (Zr, Sn, Bi). After the first cycle, the capacity of Cr doped sample decreased about 40%.

Needham et al. [69] studied doping of 2 mole% Mo to $LiCoO_2$, to produce $LiMo_{0.02}Co_{0.98}O_2$. According to their findings lattice parameters *a* and *c* were increased when compared to HT-$LiCoO_2$. Interestingly, they claimed that as *c/a* value was larger than 4.899, there was no significant cation mixing in the structure. They also came into a conclusion that the structure was ordered by the ratio of [003]/[104] which was larger than 1 as well as the splitting of peaks [006]-[012] and [108]-[110] were occured. Although, they indicated that there were minor amount of secondary phases in Mo-doped sample due to the synchrotron radiation XRD, they discussed the electrochemical properties as if single phase $LiMo_{0.02}Co_{0.98}O_2$ could be produced. They observed a little decrease of cycle life with Mo doping when compared to pristine $LiCoO_2$. They claimed that occurrence of secondary (impurity) phases led to a decrease of Li content in $LiCoO_2$ resulting in higher Co than the stoichiometric value. This eventually caused more Co^{4+} ions in the structure which degraded during cycling.

Although it is believed that comprehensive literature search was conducted, there is only one more study focusing on the doping of Mo to $LiCoO_2$. Tukamoto and West [70] conducted a study that investigated the electronic conductivity change of $LiCoO_2$ when it was doped with several elements such as Cr, Mn, Mo, W, Mg, Ti, Zr, Al, Si, B, Al etc. They only gave information of the secondary and/or impurity phases occurring during doping. With 5 mole% Mo doping instead of Co, they saw that there occurred an impurity phase which could not be identified. They also doped 5 mole% W to $LiCoO_2$ for the same purpose. With this amount of W doping, they determined that there occurred impurity phases as Li_2WO_4 and Li_4WO_5. With 5 mole% Mn, impurity phases of $LiMn_2O_3$ and Co_3O_4 were seen. They did not display any impurity phase when doped with 5 mole% Cr. The highest increase in the conductivity of $LiCoO_2$ was seen when it was doped with 5 mole% Mg.

2.3.3. Doping with Ti, Si and Zr

The doping studies in the literature mainly focus on doping with an element having the same oxidation state with Co or they always assume that the oxidation state of the dopant is 3. However; this may lead to wrong discussion of the results especially the electrochemical results as charge compensation mechanisms such as reduction of Co^{3+} ions to Co^{2+}, generation of vacancies and oxidation of O^{-2} ions may occur during doping. Therefore, discussion of the effect of doping elements having higher oxidation state can be useful in order to understand the electrochemical and structural behaviours better.

Jin et al. [71] studied the doping of Si to $LiCoO_2$ in the range of 1 to 35 mole%. The motivation of their study was the strength of the Si-O bonds which was expected to increase the structure stability during charge-discharge tests. Doping of 35 mole% Si resulted in impurity phase. In contrast to that; 1 mole% doping which was a material with the formula of $LiSi_{0.01}Co_{0.99}O_2$ yielded the best cycling efficiency. They attributed this behaviour to the change of Co^{3+} to Co^{2+} when doped with Si^{4+} in order to compensate charge. Iodometric titration showed that this approach was valid since the oxidation state of Co decreased from 2.94 for undoped sample to about 2.85 with doping of 10 mole% Si and to 2.54 with doping of 35 mole% Si. Moreover; with Si doping, the particle size was lowered. The voltage profiles of Si doped samples were better than that of undoped $LiCoO_2$.

Needham et al. [69] doped $LiCoO_2$ with Zr but they claimed that they observed secondary phase in their structure which was inactive and decreased capacity retention. They did not see any improvement in the electrochemical performance of the Zr doped sample.

Kim et al. [72] studied the doping of Zr in the range of 1 to 10 mole%. Impurity phase of ZrO_2 was seen when $LiCoO_2$ was doped with 10 mole% Zr. They obtained better electrochemical results especially in reversibility for the sample $LiZr_{0.01}Co_{0.99}O_2$ which they attributed this to enhancing the structure stability of $LiCoO_2$ with Zr doping. They thought that Zr ions moved to the surface and formed a coating that prevented the dissolution of Co^{4+} ions into the electrolyte. According to them another reason for structure stability lied in the fact that when Li^+ deintercalated, Co moved to the inter-slab space because of the vacant ordering. As Co^{3+} ions have smaller ionic radius than Li^+ ions, this space was narrowed and the intercalation of Li ions became difficult. Zr ions moved to this inter-slab space during deintercalation and as the ionic radii of Zr and Li are nearly same, narrowing of the space was not seen. This led to stabilization of $LiCoO_2$ structure. This is schematically illustrated in Figure 2.5.

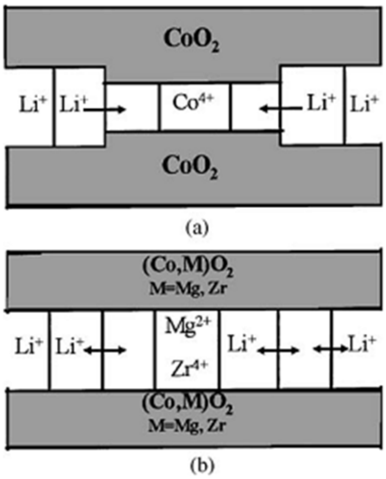

Figure 2.5. Schematic represantation of inter-slab space; (a) $LiCoO_2$ b) Zr or Mg doped $LiCoO_2$ [72].

Gopukumar et al. [73] doped Ti to $LiCoO_2$. They saw secondary phases beyond the doping levels of 10 mole%. With X-Ray Absorption Near Edge Structure (XANES), they confirmed the presence of Co^{2+} ions in 1 mole% doped sample. They did not observe similar behavior for 5 mole% doped sample and they claimed that this was due to the inhomogeneous mixing of Ti ions. Although the first charge-discharge loss of $LiTi_{0.01}Co_{0.99}O_2$ was larger than $LiCoO_2$, it showed better cycling performance thereafter. According to the authors, this loss was due to the inactive Ti^{4+} ions in the structure, however they believed that the structure became more stable due to the charge compensation of Co^{2+} ion.

2.4. Freeze Drying Synthesizing of Battery Materials

As it was previously stated in section 2.1 of this chapter, freeze drying was firstly applied by Chiang et al. [34] for producing layered $LiCoO_2$. Later, Brylev et al. [35] also used this process for the same aim. Jang et al. [50] doped Al to $LiCoO_2$ with freeze drying. These studies were discussed in relevant sections of the literature survey. Therefore this section is devoted to the application of freeze drying to the battery materials (especially cathode materials) other than $LiCoO_2$.

The most widely synthesized cathode material by freeze drying is $LiFePO_4$. Palomares et al. [74] applied freeze drying for producing $LiFePO_4$ for the first time. In order to increase the conductivity of $LiFePO_4$, carbon was added during synthesis. They dissolved the source of Li, Fe, P and C in water and freeze dried the solution for 48 hours. They did not give the details of freeze drying (temperature and vacuum values). According to them, the choice of freeze drying would be beneficial to get homogeneous distribution of reactants. They also thought that they need lower annealing temperatures for producing desired product. At the end of the process, they heat treated the precursors at 350°C and 600°C under nitrogen atmosphere. As a result, they obtained the product having similar discharge performance with those prepared by other methods although they did not receive perfect homogeneous morphology. Even if their product contained 16.1 mole% C, it had low conductivity value. Therefore they could lower the C content. By this was they could increase the active material in their product. From Palomares et al. [74], it was inferred that freeze drying could be used for synthesizing $LiFePO_4$.

Koleva et al. [75] incorporated freeze drying in their study for controlling particle size and carbon content. By changing the concentration of the solution concentration, they could control both the particle size of the precursors and the end-product $LiFePO_4$, as well as the carbon content. The ratio between the components in the resulting solution was Li^+: Fe^{2+}:PO_4^{3-}:$HCOO^-$ = 1:1:1:2 and the concentrations was used as 0.05M, 0.1M and 0.2M (with respect to metal ions). The solution was frozen instantly with liquid nitrogen and dried in vacuum (20-30 mbars) at -20°C for 17 hours. They applied heat treatment at temperature of 400, 500 and 600°C. At the end of their study, they achieved the best result with the experiment having the lowest molarity (0.05M) and moderate annealing temperature (500°C). This sample had particle size of about 85 nm, narrow particle size distribution (about 40 nm) and carbon content of about 2.3 weight%.

Shlyakhtin et al. [40] synthesized $LiNi_{0.5}Mn_{0.5}O_2$ and Xu and Yang [76] synthesized MnO_2 as the cathode materials in lithium batteries by using freeze drying of 48 hours and 24 hours, respectively. Moreover, Schlörb et al. [77] doped $LiMn_2O_4$ and MnO_2 with Bi by using freeze drying but they gave no further information other than remarking of usage of freeze drying.

With above pioneering studies, recent years witnessed widespread application of freeze drying for producing $LiFePO_4$. Freeze drying is preferred as it can provide uniform particle size distribution which seems very important for cathode materials. It can be anticipated that freeze drying will be used for producing cathode materials in batteries technology in the future.

CHAPTER 3

BACKGROUND of the METHODS USED IN THE STUDY

3.1. Freeze Drying (FD)

Freeze drying is a name of a process applied during cryochemical synthesis of materials. Synonyms for freeze drying are lyophilisation and cryodesiccation. The industrial application of freeze drying dates back to World War II due to the increase need for human blood [78]. Freeze drying is widely used in pharmaceutical industry since the products in this industry are heat sensitive and freeze drying operates at lower temperatures. According to Baresi et al. [79], this process is used for valuable products as it deals with very low temperatures, it needs vacuum and drying is very slow. These requirements inevitably make the process expensive so valuable products can be used. Tretyakov and Shlyakhtin [80] listed the application areas of freeze drying as ferrites, composites, catalysts, resistive materials, phosphors, superionics, high temperature and magnetic superconductors. The use of freeze drying for synthesizing battery materials have increased in the last few years.

In cryochemical synthesis, the first stage is preparation of the single or multi component solution containing the components of the target material in a stoichiometric ratio. In most cases, aqueous solutions are used, though it is possible to use other solvents such as tert-butanol, acetic acid, benzene, toluene, etc. The prepared solution is then subjected to freezing. Unlike biomedical studies, where slow cooling is used, freezing of aqueous solutions in cryochemical synthesis was performed by fast cooling. This process is usually realized by spraying the solution into liquid nitrogen via a pneumatic nozzle or ultrasonic nebulizer under intense mechanical stirring.

The next important stage of synthesis is the freeze-drying process. Low temperatures and reduced pressures are selected such that the drying time is minimized, while preventing the formation of liquid phase. Temperature should be lower than 0°C and as low as possible when freezing of solutions are applied, however, it must be gradually increased and most of the time of drying should be spent at temperatures between -5°C and -15°C in order to increase the driving force hence rate for solid to gas phase transformation. Trays are used for pouring the solutions and freeze-drying is applied in devices containing temperature-controlled shelves. Working pressures of 5×10^{-2} mbar or less are used during operation. The main drawback of the freeze-drying process is its long duration. Depending on the amount and type of product and the geometry of the freeze drying machine, the process takes from several hours to several days. After freeze drying it can be thought that the product is completely dried but two more processes are needed to finish freeze drying. Unfrozen water may remain in the product and it is removed by careful raise of the temperature of the shelves under vacuum. This process is called secondary drying. Lastly, the condenser is heated for the melting of the ice collected on it.

In most cases, freeze-drying is not the final stage of the synthesis process. Its product needs further processing in order to be converted to the final oxide or metal powder. These subsequent thermal decomposition and powder processing techniques are the same or similar to other chemical methods. Essential features of multi component freeze-drying products are their high chemical homogeneity, often leading to the formation of complex oxides just in the course of thermal decomposition, and the low bulk density of the powders. From Figure 3.1, the processes in cryochemical synthesis can be seen [81].

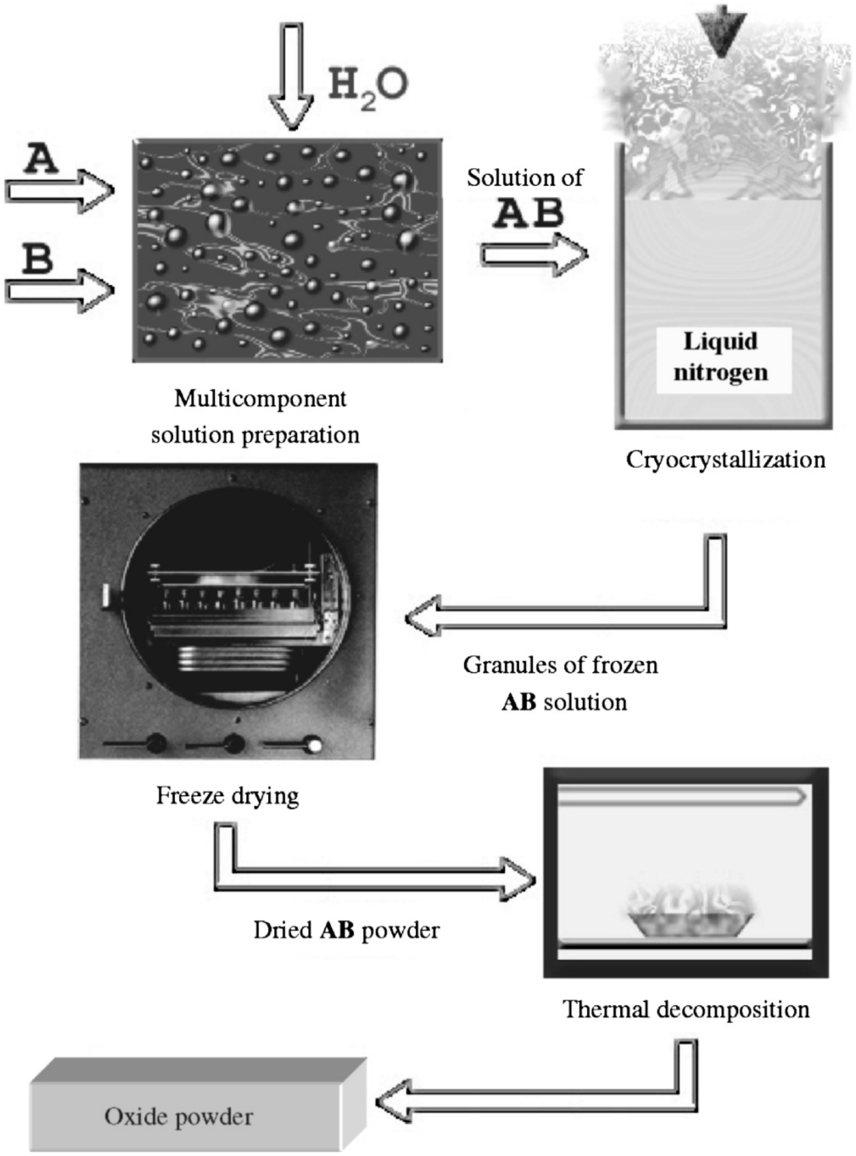

Figure 3.1. The process of cryochemical synthesis [81].

3.2. Cyclic Voltammetry (CV)

Cyclic voltammetry (CV) is a widely used electrochemical characterization technique in which the working electrode is subjected to linearly ramped potential. The difference from linear sweep voltammetry is that at a defined cut-off potential, the potential is reversed. This cycle can be applied many times. While the electrode is subjected to potential, the correspondent current is measured. At the end of the test, a plot of current versus potential is constructed which is called cyclic voltammogram. From this plot, wealth of electrochemical data is gained which contains kinetic and thermodynamic details of the working electrode. The potential cycle and a typical cyclic voltammogram are given in Figure 3.2.

E_1 and E_2 in the upper part of Figure 3.2 must be chosen at the voltages that reduction and oxidation will occur in between. In the lower part of Figure 3.2, E_{pa} and E_{pc} belong to anodic and cathodic peak potentials. Similarly i_{pa} and i_{pc} belong to anodic and cathodic peak currents.

Considering that there occurs a redox reaction between A and B, it is likely that a plot of CV for this redox reaction will depend on [82];

- Electrochemical rate constant and formal potential of A/B couple,
- The diffusion coefficients of A and B,
- The voltage sweep rate, ν (V/s) as well as E_1 and E_2.

From the peak voltages and peak currents obtained during CV, some indicators for determining reversibility of the process can be found. For a process to be reversible three conditions must be met. These conditions are as follows:

a. $\Delta Ep = 0.059/n$,
b. $i_{pa}/i_{pc} = 1$
c. i_p (i_{pa} and/or i_{pc}) is linearly proportional to $\nu^{1/2}$

where;
n; number of electrons involved in the redox process,
$\Delta E_p = (E_{pa} - E_{pc})$, in V,
i_{pa} and i_{pc}, anodic and cathodic peak currents in mA, respectively,
ν, voltage sweep rate or scan rate in V/s.

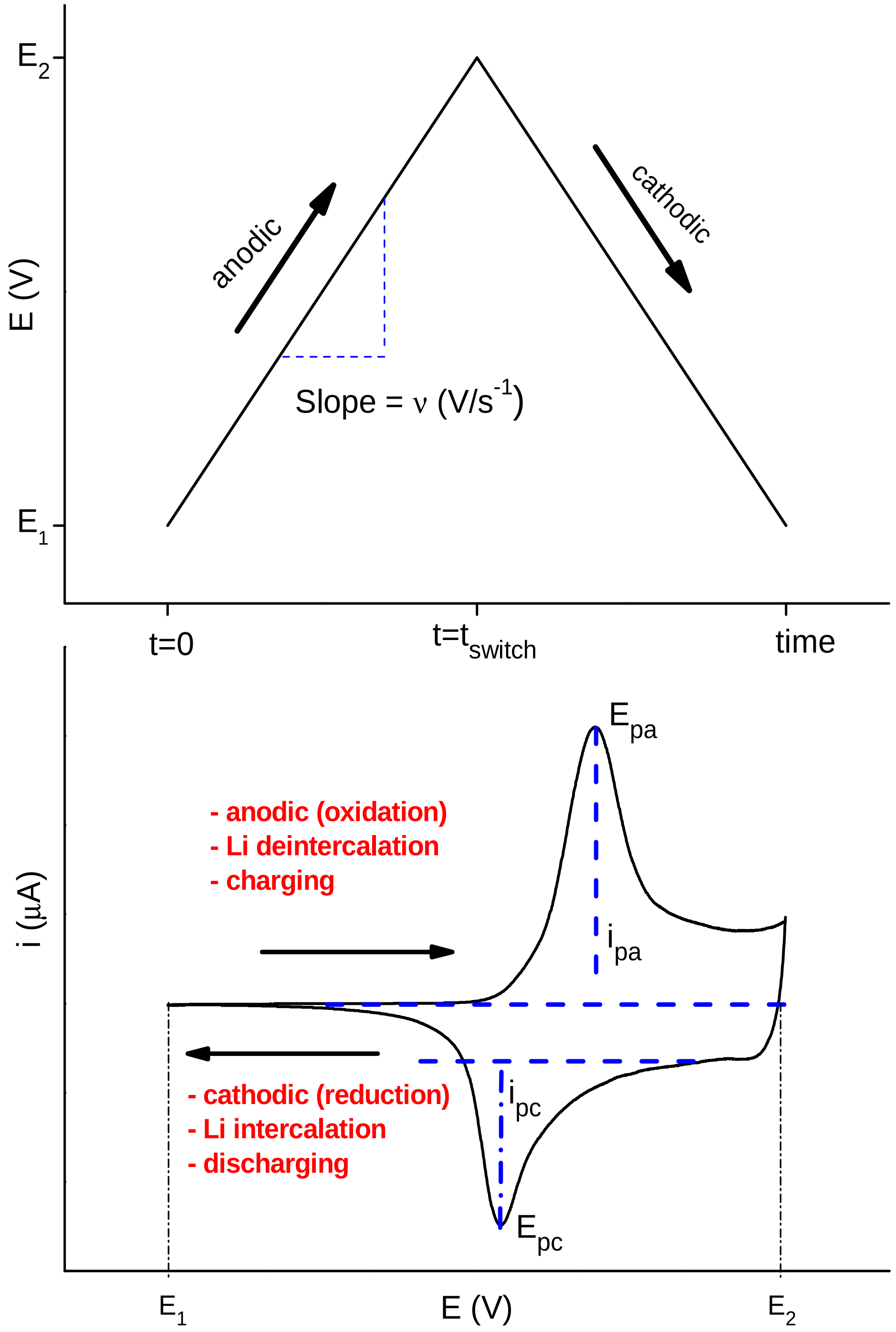

Figure 3.2. The potential cycle (upper curve) and a typical voltammogram during CV.

The first condition can be estimated easily by looking at CV for peak potentials. Although the estimation of second condition seems as easy as the first condition, estimation of cathodic peak current is complicated since the location of the proper baseline for this scan is important. Some approaches were offered for this problem. The first one is directly reading the peak cathodic current. The second one is to draw a tangent line (extrapolating the cathodic line) to the cathodic scan as done in Figure 3.2. If CV is much more complicated, then the method offered by Nicholson [83] can be used.

The last condition is relating the peak current ratios to scan rate by using Randles-Sevcik equation. At 298 K, this equation is given as;

$$i_p = 2.69 \times 10^5 \times n^{3/2} \times A \times D^{1/2} \times C \times \nu^{1/2} \tag{3.1}$$

where;

A, electrode area, cm^2
D, diffusion coefficient of electroactive species (Li^+ ion in $LiCoO_2$ material), cm^2/s
C, bulk concentration of electroactive species, $moles/cm^3$

Linear increasing of the peak currents as a function of the square root of scan rate is an indication for the kinetics of the redox reaction. In order to find the linear dependence of peak current and scan rate, plot of i_p versus ν is drawn. Perfect linear relationship is an indication of better reversibility provided that other two conditions are met. If perfect match cannot be achieved, then a best line can be drawn. The slope of this best line (i_p/ν) can be used to estimate the anodic and cathodic diffusion coefficients of the redox reactions as values of A, C and n in Equation 3.1 are known for an electrochemical process. Figure 3.3a shows the change of peak potentials and currents with scan rate. Figure 3.3b is helpful for understanding the importance of relation between the peak currents and scan rate. In this figure, as the gap between the anodic and cathodic current peaks is increasing then the difference between the anodic and cathodic reaction rates with scan rate is increasing. Moreover, as the cathodic slope is larger than anodic slope, than the diffusion coefficient of cathodic reaction is larger than anodic reaction.

In addition to data acquired from current versus scan rate plots, the difference between the anodic and cathodic potentials can be found with respect to scan rate from CVs. Plot of potential versus scan rate gives important data about the polarization (overpotential) resistance of the working electrodes. It is desired that the gap between anodic and cathodic peak voltages is small. This gap is directly related with the polarization resistance of the electrodes. In other words, the smaller the gap is, the smaller the polarization resistance. From Figure 3.3c, a typical plot of potential versus scan rate can be seen.

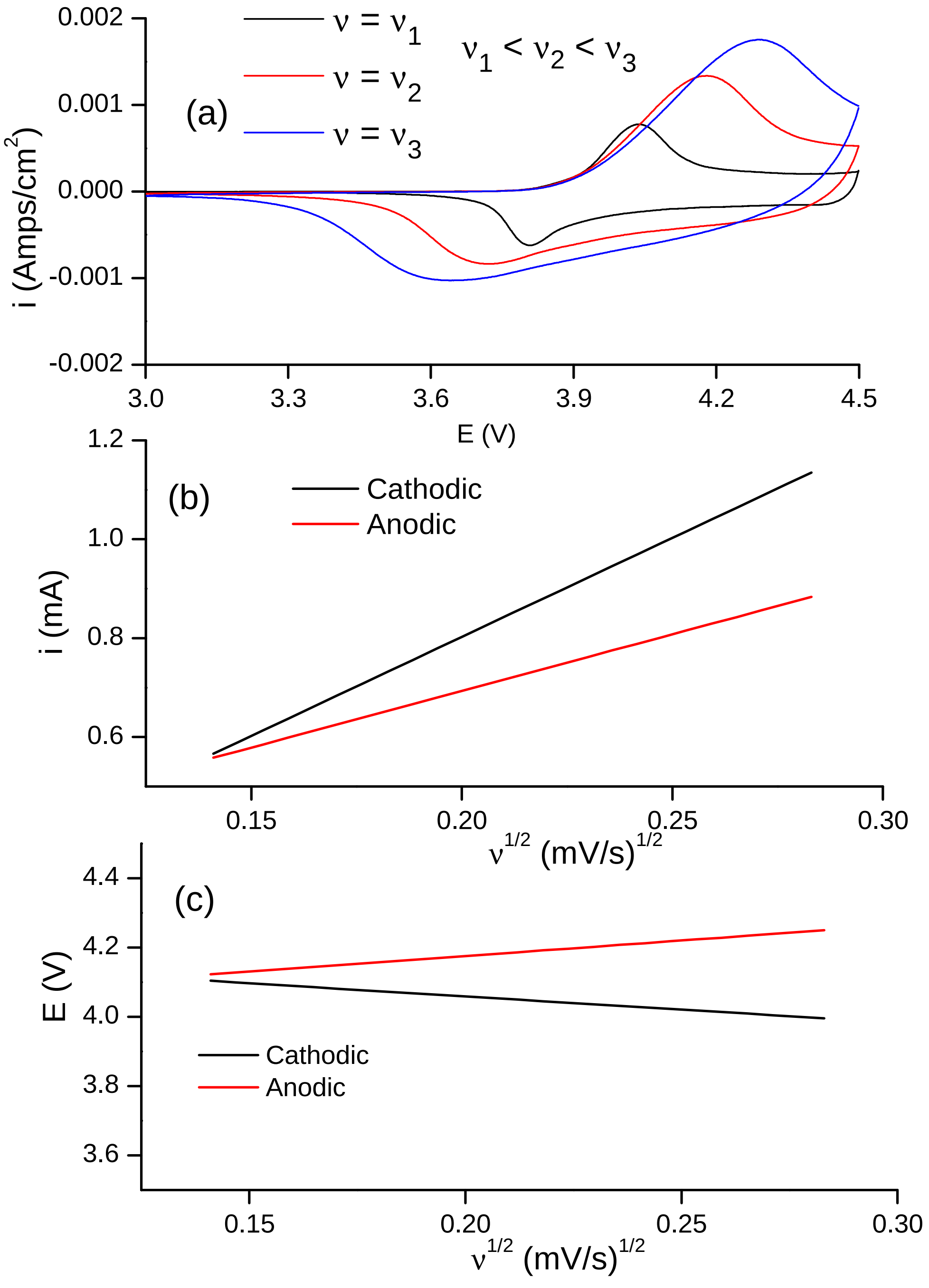

Figure 3.3. a) change of peak positions with increasing ν b) plot of i_p vs. $\nu^{1/2}$, c) plot of E_p vs. $\nu^{1/2}$.

3.3. Electrochemical Impedance Spectroscopy (EIS)

The concept of electrical resistance is very well known. It is simply the resistance to the flow of electrical current. This term is formulated by Ohm's Law as;

$$R = \frac{V}{I} \tag{3.2}$$

The use of this relationship is limited to only one circuit element, ideal resistor. While mentioning ideal resistor, three simplifications are considered [84];

a. It follows Ohm's law at all voltages and currents
b. The resistance is independent of frequency
c. Alternating current (AC) and voltage are in phase with each other

These statements are true under direct current (DC) conditions. However; when there is a circuit under alternating current conditions, the change of resistance with voltage and current is not as easy as in Equation 3.2. There are more complex relations between circuit elements as well as voltage, current and so on. So another term is defined called impedance which is also a measure of resistance but does not have the restrictions above.

Electrochemical impedance is conducted by applying AC voltage to the electrochemical cell and the current through this cell is measured. Therefore impedance spectroscopy is a powerful tool for examining complex electrochemical reactions and processes. This is an important advantage for EIS but there are more advantages as time-dependent and quantitative data can be collected. Moreover, during application, no destruction or any similar degradation of the cell is seen as the test is non-invasive. The largest disadvantage is the need for extensive and complex analysis for interpreting the collected data.

The principle of EIS is mainly related with the perturbations which shift the electrochemical system from steady state to non-steady state. The rate at which it reaches to new steady state depends on the reaction rate constants, diffusion coefficients, charge transfer resistance and double layer capacitance. In order not to move away from linearity, small perturbations must be applied so that limiting forms of mathematical expressions can be used [85].

The perturbations applied to electrochemical system are usually sinusoidal [86]. For applied voltage and current;

$$V(t) = V_0 \sin(\omega t) \tag{3.3}$$

$$I(t) = I_0 \sin(\omega t + \phi) \tag{3.4}$$

where;

V(t) and I(t) are the voltage and current at time t, V_0 and I_0 are voltage and current amplitude, ω is the radial frequency (in rad.s^{-1}) which is equal to $\omega = 2\pi f$ where f is the frequency in Hertz (Hz.). Φ is the phase shift by which voltage lags the current. Schematic representation of this lag is given in Figure 3.4.

While applying EIS, the frequencies ranging from 0.01 Hz to 10^6 Hz can be used according to the device used. This wide range allows the complete analysis of the circuit elements.

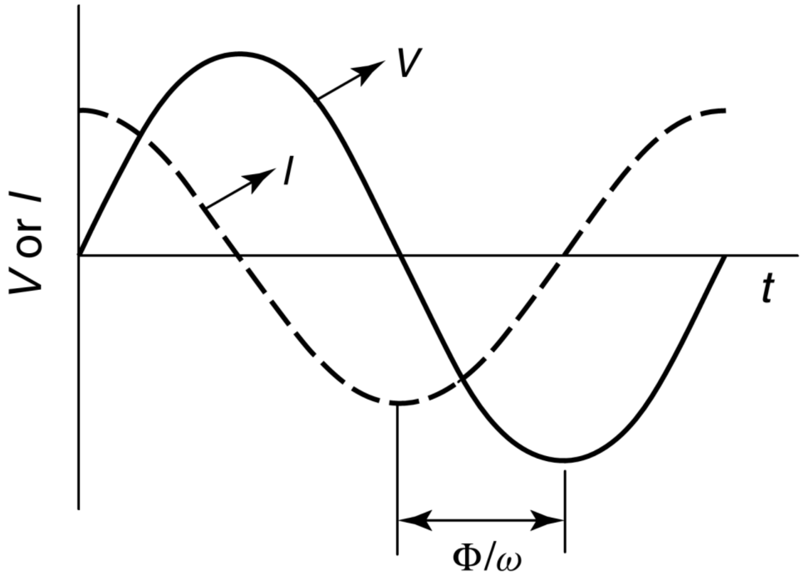

Figure 3.4. The perturbation of voltage and response of current [86].

As it was stated before, impedance is analogous to resistance, therefore impedance is estimated with below formula;

$$Z = \frac{V(t)}{I(t)} = Z_0 e^{j\Phi} \qquad (3.5)$$

$$Z = Z' + jZ'' \qquad (3.6)$$

Z has a magnitude of Z_0 (V_0/I_0) and a phase of Φ. In Equation 3.6, $j=(-1)^2$ and Z' and Z'' are the real and imaginary part of Z, respectively. Equation 3.5 is the value of impedance in polar form and Equation 3.6 is the value in Cartesian coordinates (standard form). The equivalence of polar form and standard form is proved by Euler relationship and they are shown in Figure 3.5.

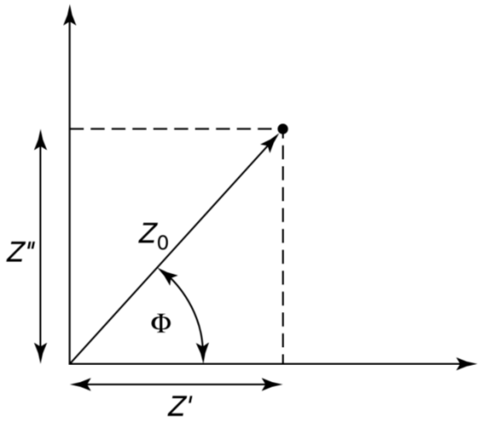

Figure 3.5. Illustration of real and imaginary parts of impedance in both polar and Cartesian forms [86].

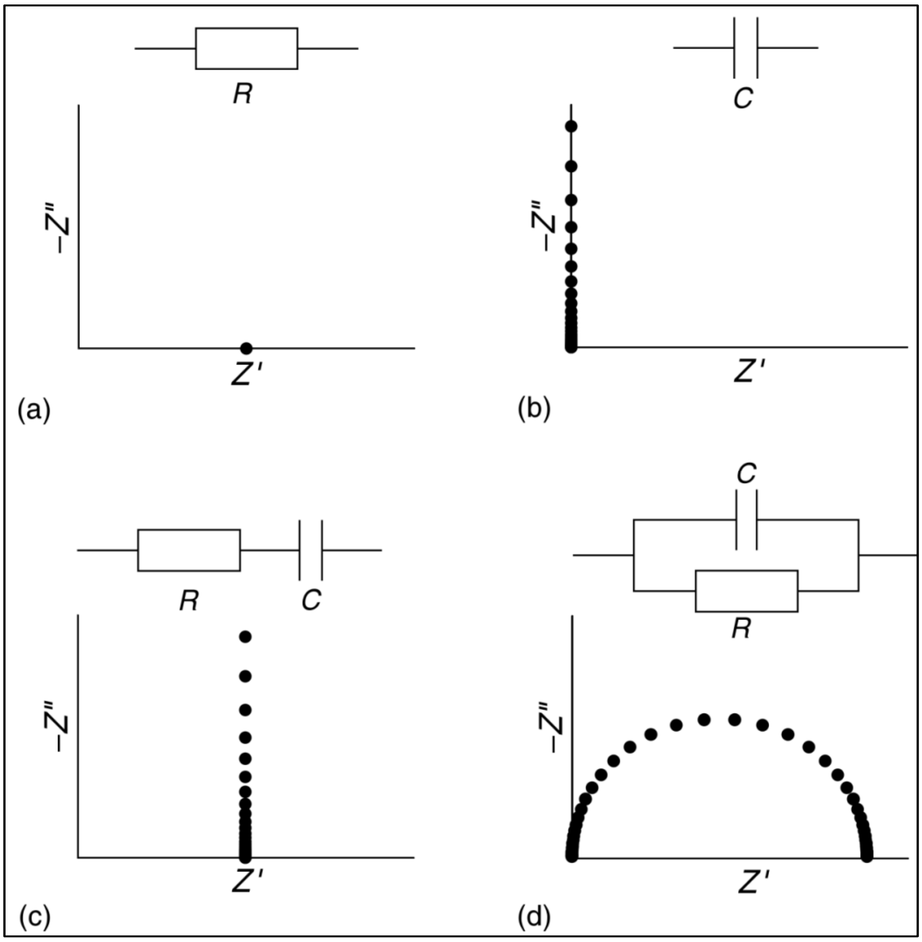

Figure 3.6. Nyquist plots for different circuit elements [86].

As implied before, direct reading of EIS data is not possible so the data must be fitted to circuit elements such as resistors, capacitance and constant phase elements. The plot of imaginary versus real part of impedance is called Nyquist plot. This plot can be seen in Figure 3.6a through 3.6d for circuit elements containing only resistance (3.6a), only capacitance (3.6b), resistance and capacitance in series (3.6c) and resistance and capacitance in parallel (3.6d).

Nyquist plots have the disadvantage that it is not possible to see the values of frequency and phase shift. However; with Bode plots this drawback is overcome. From Figure 3.7, Bode plot and Nyquist plot can be seen for the same circuit having resistance and capacitance (Figure 3.6d) parallel to each other.

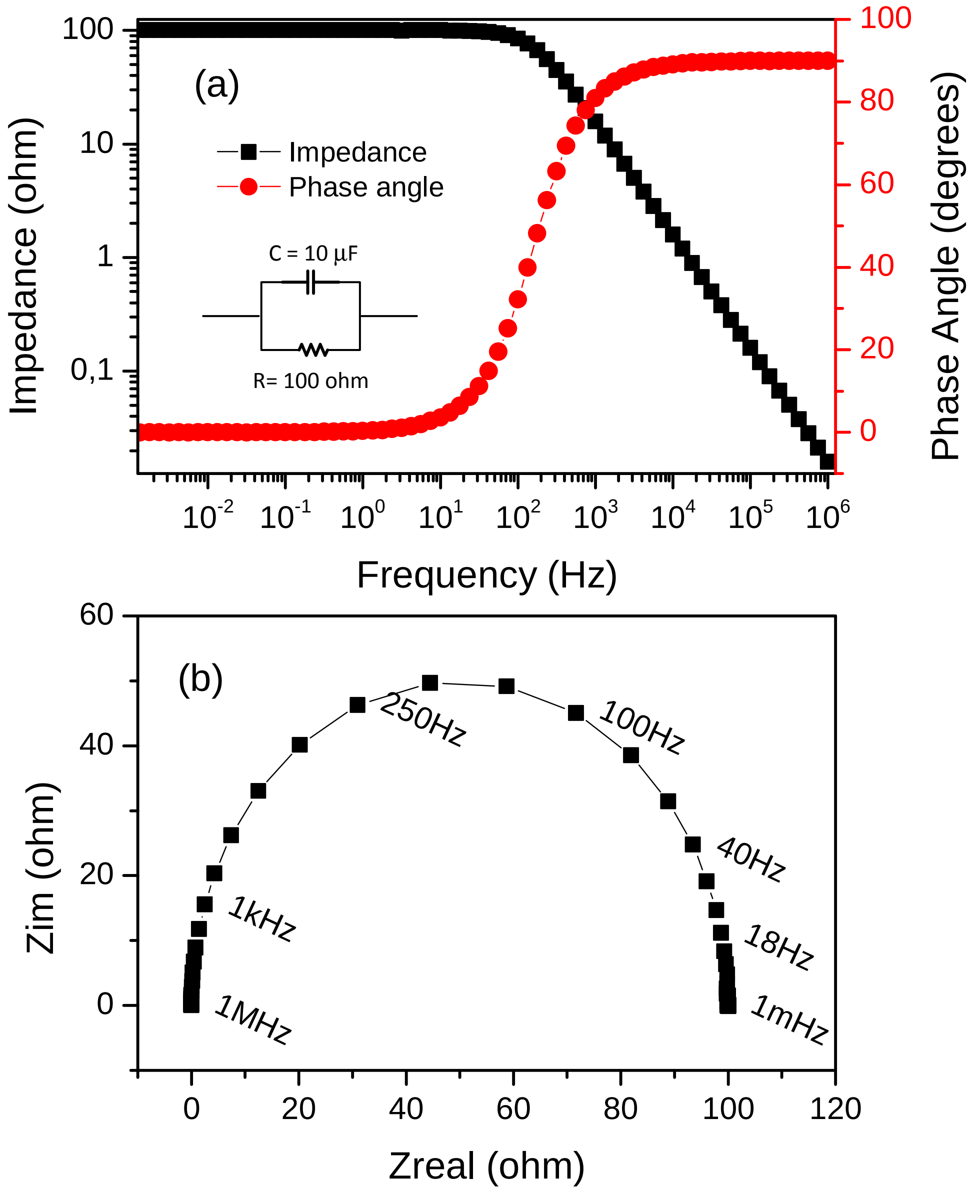

Figure 3.7. a) Bode plot and b) Nyquist plot of a circuit having resistance and capacitance in parallel.

Alternative parameters can be used as the vertical axis of Bode plot like Z_0, Z' and Z''.

3.3.1. Equivalent Circuit Elements in Electrochemical Cell

It is usually common practice to express the electrochemical cell with fitting it to an equivalent circuit. At least three parameters must be considered for this purpose. These parameters are electrolyte resistance (R_e), double layer capacitance (C_{dl}) and impedance of the charge transfer which is called faradaic impedance. In this circuit faradaic impedance and double layer capacitance are parallel with each other while electrolyte resistance is series to both. When electroactive species are present in the process then faradaic impedance will become simply charge-transfer resistance, R_{ct}.

In every electrolytic solution, the electrolyte shows ohmic resistance to ionic movement between the electrodes which is called electrolyte resistance (R_e or R_{el}). This resistance depends on ionic concentration, type of ions, temperature and the geometry of the area in which current is carried. For batteries, this term is simply related with the resistance of movement of electrochemically active species (Li^+ in Li-ion batteries).

Double layer capacitance (C_{dl}) is an important electrochemical circuit element which forms through the interface of all electrodes in electrolytic solutions. This double layer is formed as ions from the solution "stick on" the electrode surface. Charges in the electrode are separated from the charges of these ions. Therefore ordering of positive and negative charges occurs at the interface. This ordering is depicted in Figure 3.8. The separated charges form a capacitor. Double layer capacitance is influenced by the chemical content of electrode, the potential of the electrode, roughness of the surface of the electrode, types of ions etc.

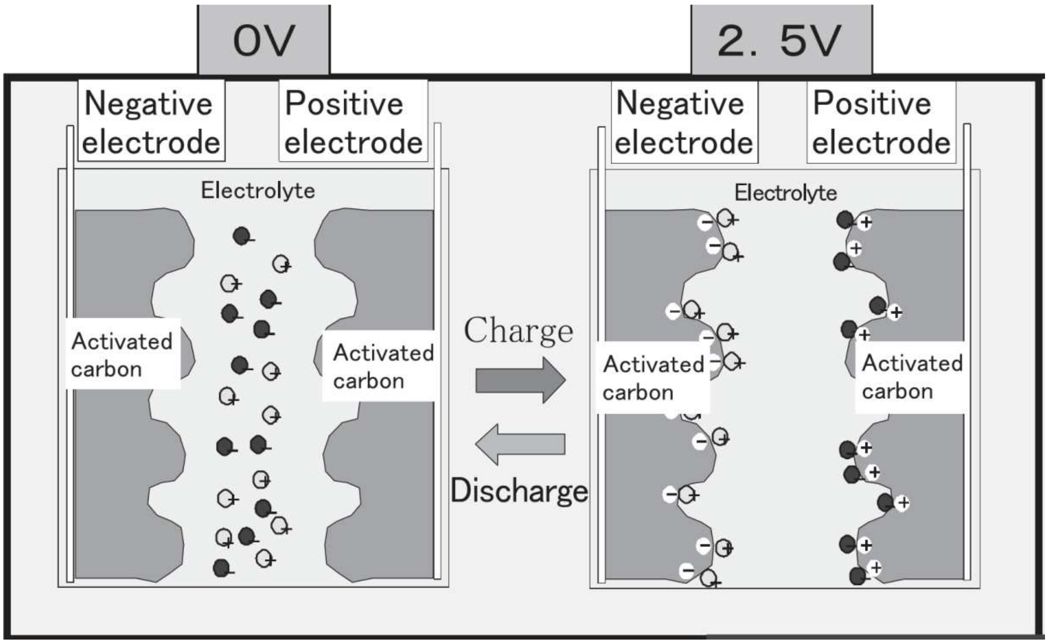

Figure 3.8. Schematic illustration of double layer on carbon electrodes [87].

Charge-transfer resistance (R_{ct}) occurs when a single kinetically controlled reaction is considered. When a metal electrode is immersed in an electrolytic solution, the metal will dissolve into the electrolyte according to the reaction [84];

$$M \rightleftarrows M^{n+} + ne^{-} \tag{3.7}$$

With above reaction, metal moves in electrolyte while electrons enter in the metal. Consequently charge is transferred. This transfer has a certain speed which depends on the kind of reaction, the temperature, the concentration of the reaction products and the potential. Expectedly, charge-transfer resistance (R_{ct}) decreases the speed of charge transfer. The equation for charge-transfer resistance is found by using Butler-Volmer Equation which can be used when bulk and surface concentrations of electrodes are same and polarization (overpotential which means the deviation of potential from the value at open circuit, $\eta = E_{app} - E_{OCV}$) depends only on charge-transfer kinetics;

Butler-Volmer Equation; $$i = i_0 \left[\exp\left(\alpha \frac{nF}{RT} \eta \right) - \exp\left(-(1-\alpha) \frac{nF}{RT} \eta \right) \right] \tag{3.8}$$

where;

i_0 is exchange current density,
α is symmetry factor

when overpotential η is very small then e^x is equal to 1+x [88] and Equation 3.8 becomes to;

$$i = i_0 \frac{Fn}{RT} \eta \tag{3.9}$$

η / i has units of resistance [88] so charge-transfer resistance is;

$$R_{ct} = \frac{RT}{nFi_0} \tag{3.10}$$

At high frequencies, impedances of double layer capacitance and charge transfer are small. So, intercept of the semicircle at the real axis gives the electrolyte resistance. In contrast to that, at lower frequencies, the impedance of the double layer capacitance becomes significantly larger than charge transfer resistance, and the impedance spectrum is dominated by electrolyte and charge transfer resistance (low frequency intercept of the real axis). Hence the diameter of the semicircle gives the magnitude of charge transfer resistance. Figure 3.9 illustrates electrolyte resistance and charge-transfer resistance on Nyquist plot.

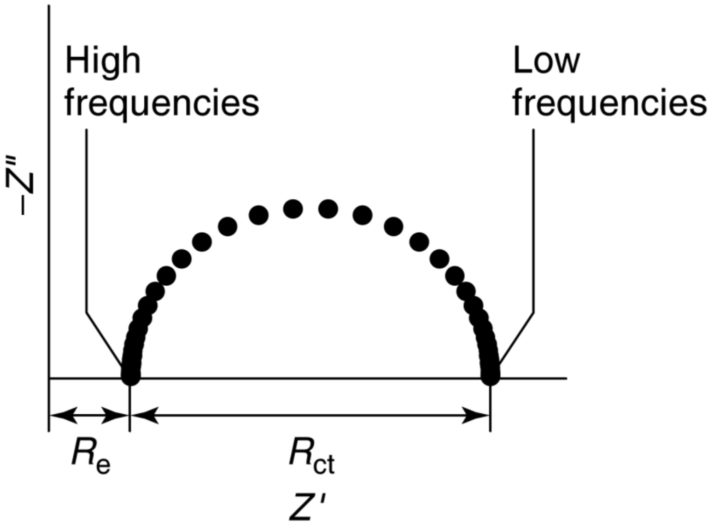

Figure 3.9. Nyquist plot for a simple electrochemical cell [86].

The Nyquist plot in Figure 3.9 does not contain diffusion effects. In the presence of diffusion, faradaic impedance is subdivided into two circuit elements; charge-transfer resistance and mass-transfer impedance which is also called Warburg impedance (Z_w). By using some mathematics, an equation for the real and imaginary parts of Warburg impedance is achieved.

$$Z_W = \frac{\sigma}{\omega^{1/2}} - j\frac{\sigma}{\omega^{1/2}} \tag{3.11}$$

where;

$$\sigma = \frac{RT}{n^2F^2A\sqrt{2}}\left(\frac{1}{D_O^{1/2}c_O^*} + \frac{1}{D_R^{1/2}c_R^*}\right) \tag{3.12}$$

where;

D_O and D_R are diffusion coefficients of oxidized and reduced species, respectively. Similarly, c_O^* and c_R^* are surface concentrations of oxidized and reduced species, respectively.

From equation 3.10, it is seen that real and imaginary parts of Warburg impedance are equal so it must be shown as an inclined line with making 45° with real and imaginary axes. An equivalent circuit called Randles circuit is given in Figure 3.10 where faradaic impedance is expressed as charge-transfer resistance and Warburg impedance.

Warburg impedance is simply the resistance to bulk diffusion as Equation 3.12 implies and during EIS low frequencies are needed to estimate this impedance.

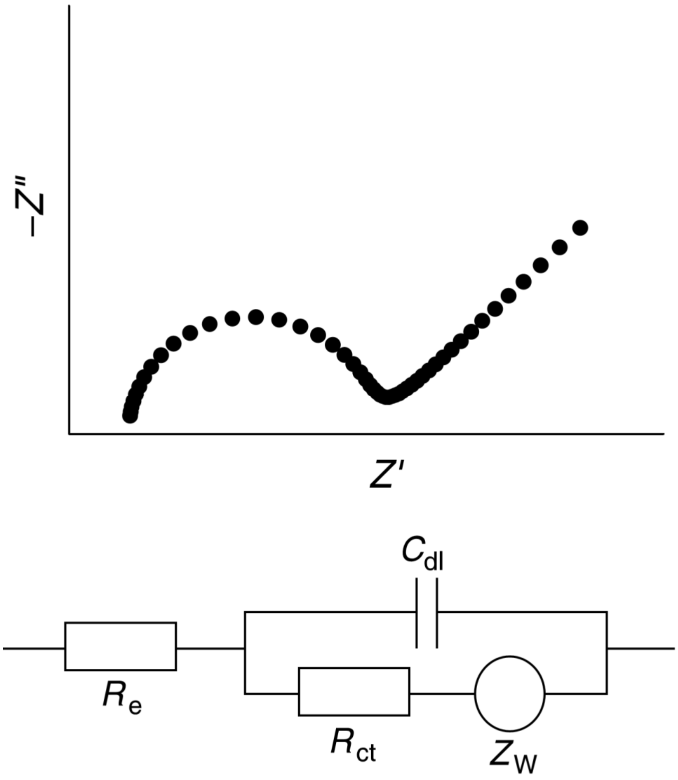

Figure 3.10. Randles circuit with Warburg impedance and the associated Nyquist plot [86].

Another parameter used in electrical circuits for modelling electrochemical cells is constant phase element (CPE). It is a capacitor which is used to model the non-ideal electrochemical cells. In fact, electrochemical cells always behave non-ideally. Replacing of the capacitance by CPE results in better fit of the proposed electrical circuit model to elements in electrochemical cell. Lvovich [89] listed some of the electrode properties where CPE results in better fit than capacitance. Some of them are electrode inhomogeneity, surface roughness, electrode porosity, nonuniform potential and current distribution at the surface as well as slow and uneven adsorption to the surface [89]. The equation for the impedance of CPE is given as;

$$Z_{CPE} = \frac{1}{(j\omega)^{\alpha} Y_0} \tag{3.13}$$

where;

Y_o = capacitance
ω = angular frequency

and α takes a value between 0 and 1, generally 0.9. When α is 1, it describes an ideal capacitor and when it is 0, it describes an ideal resistor. During fitting, CPE makes the semicircles more depressed. Andre et al. [90] defined α as depression factor. As the model cannot satisfactorily fit to data without depression factor, CPE lets the model be fitted to the experimental data more closely. Nyquist plot showing the change of the semicircle with α values is given in Figure 3.11.

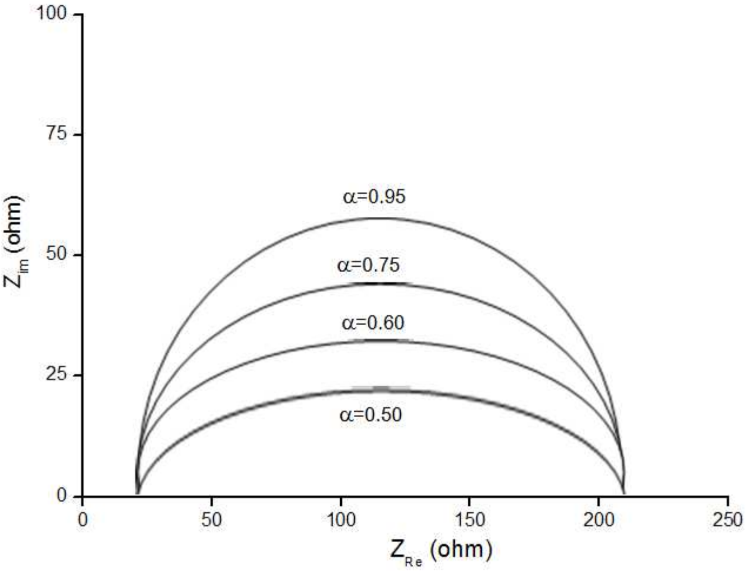

Figure 3.11. Nyquist plot showing the effect of α value to the shape of semicircles.

For estimation of capacitance from CPE, different approaches are used. Hsu and Mansfeld [91] offered an equation 3.14 for parallel connection of CPE and resistance (R) whereas Brug et al. [92] offered equation 3.15 for this type of connection;

$$C = Y_0 \left(\omega_{max}\right)^{\alpha-1} \tag{3.14}$$

where ω_{max} is the frequency of the maximum of Z''.

$$C = \frac{(Y_0 \times R)^{1/\alpha}}{R}. \tag{3.15}$$

The validity and comparison of these equations are discussed in section 6.5 of this study.

Apart from the above discussed circuit elements and models, in order to see the behaviour of battery materials during operation, many models have been proposed. The most widely used model for Li-ion batteries is the one that has additional impedance of surface film. These models were discussed by many authors, some examples are the studies of Bruce and Saidi [93], Levi et al. [94] and Zhang and Wang [95] .

Bruce and Saidi [93], in their study with Li_xTiS_2 electrode, showed that an ionically conducting film could form on the surface layer of intercalation electrodes when they are in contact with liquid electrolytes. To represent these layers, series connection of electrolyte resistance with resistor and capacitor in parallel with each other is added to the equivalent circuit of simple electrode which is shown in Figure 3.10. Bruce and Saidi [93] claimed that, the resistor and capacitor represent ion transport and polarization, respectively. With these additional circuit elements Nyquist plot contains one more semi-circle at higher frequencies. An illustration of Nyquist plot having surface layer elements is given in Figure 3.12. In the figure, inlet is the enlargement of the semicircle belonging to surface layer resistance.

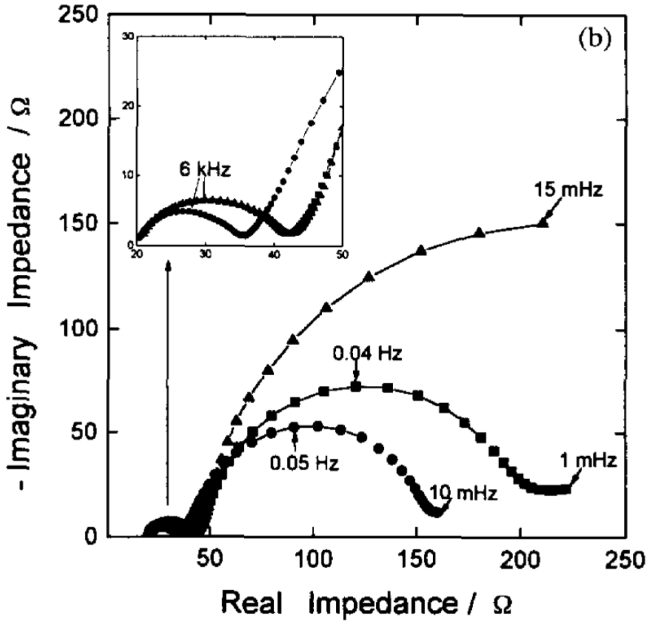

Figure 3.12. A Nyquist plot having two semicircles, numbers belong to frequency values [96].

With addition of resistor and capacitor, equivalent circuit of an electrode contains electrolyte resistance (R_{el}), surface layer (film) resistance (R_{sf}), charge transfer resistance (R_{ct}), constant phase element for surface layer (Φ_{sei} or Φ_s or Φ_{sl}) and double layer (Φ_{dl}), respectively. This circuit is depicted in Figure 3.13a and defined as surface layer (SL) model.

In an electrochemical cell, when a surface layer is identified, this layer grows outwards with passage of time on open circuit. With the growing of this layer, increase in R_{sf} and decrease in Φ_{sl} are expected. This phenomenon can be observed by storing the cathode materials for a relatively long time in an air-tight cell. The results of this application are discussed in section 6.5. Zhang and Wang [95] claimed that growth of surface layer hence increasing of resistance with decreasing temperature and increasing cycles was seen.

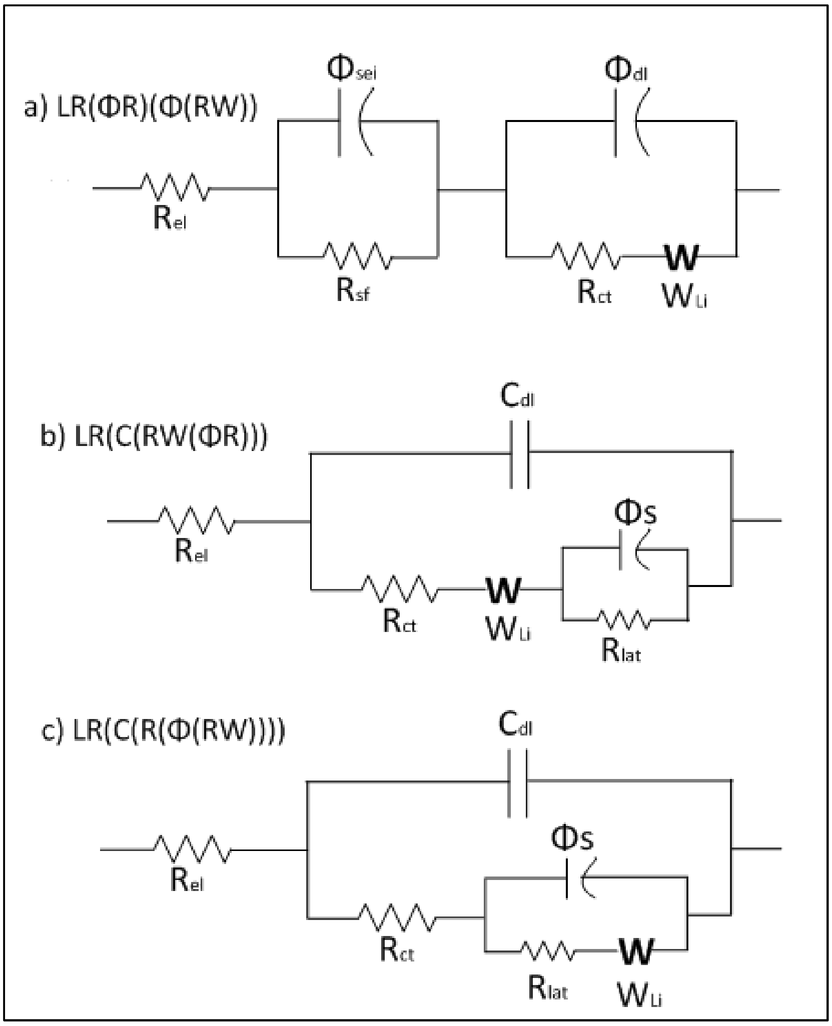

Figure 3.13. Electrical circuit models used in this study, a) SL, b) AD, c) mAD models

Bruce and Saidi [93] proposed another model which they called as adatom (AD) model. The associated electrical circuit can be seen in Figure 3.13b. A pictorial representation of this model is given in Figure 3.14 by Zhuang et al [97]. In this model, instead of formation of surface layer, they claimed that solvated ions in the electrolyte just near the electrode have partially desolvated and form an atom adsorbed on the metal surface by transferring electron from the electrode. This atom was defined as adion. According to them [93], this adion diffused across the surface and at a suitable crystal site, it lost its remaining solvent molecules and became incorporated into the lattice. Therefore, in this circuit (Figure 3.13b), R_{lat} shows resistance to lattice incorporation, W_{Li} represents Warburg diffusional impedance (W_{Li}) and Φ_s shows constant phase element of surface which depends on the surface concentration of adatoms. In Figure 3.13b, Φ_s involves C_s (surface capacitance) and Z_{cpa} (an impedance term introduced by Bruce and Saidi [93] for compensating rough nature of electrode surface. Figure 3.13c is the modified version of adatom model (mAD).

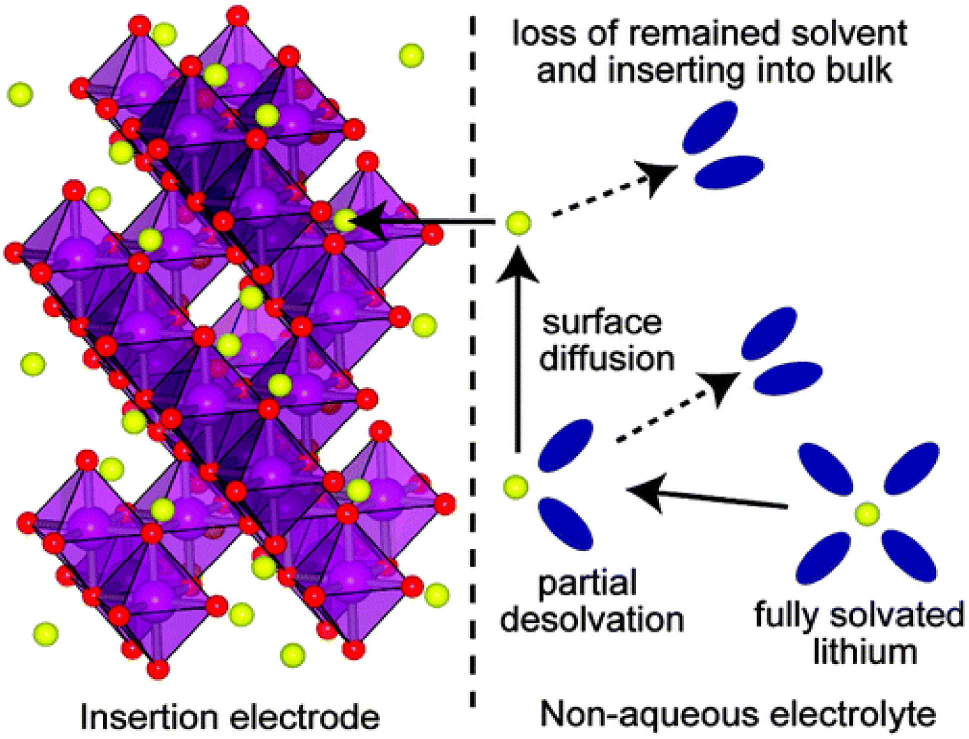

Figure 3.14. Pictorial representation of adatom model [97].

Zhuang et al. [97] remarked that the origin of high frequency semicircle which belongs to surface film resistance is debatable issue for Li-ion cells. For surface layer model, this means the migration of Li ions through the surface film while it is considered as solvated or lost solvated of Li ions for adatom model. In other words, the semicircle gives the resistance of cation losing part of its solvent molecules.

According to them [97], for adatom model second semicircle represents the ion losing its remaining solvent molecules and enters the host lattice. Therefore, both models ascribe second semicircle as charge transfer resistance.

Many authors studying impedances in Li-ion batteries were on the side of surface layer model as solid electrolyte interphase (SEI) occurs in these batteries. It is certain that the main and important difference between surface layer and adatom models lies in occurrence of surface film. Difference in charge transfer resistance is not dominant to explain the differences of these models.

Throughout this study, the three models depicted in Figure 3.13 were used for fitting the EIS data. The results were discussed in detail in section 6.5. Constant phase elements were introduced in order to better fit the model to real life although Bruce and Saidi [93] used capacitances in their models.

CHAPTER 4

EXPERIMENTAL PROCEDURE

4.1. Powder Preparation

During the study, the chemicals used for producing HT-$LiCoO_2$ are listed below:

- Lithium Nitrate (LiN); $LiNO_3$.
- Lithium Acetate (LiA); $CH_3COOLi.2H_2O$
- Lithium Hydroxide (LiH); LiOH
- Cobalt Nitrate (CoN); $Co(NO_3)_2.6H_2O$
- Cobalt Acetate (CoA); $(CH_3COO)_2Co.4H_2O$
- Chromic Acid; CrO_3
- Amonium Chromate (AmC); $(NH4)_2CrO_4$
- Amonium Heptamolybdate Tetrahydrate (AMoT); $(NH_4)_6.Mo_7O_{24}.4H_2O$
- Manganese Acetate Tetrahydrate (MnAT); $(CH_3CO_2)2Mn.4H_2O$
- Amonium Tungsten Oxide Hydrate (AWOH); $(NH_4)_6.W_{12}O_{39}.xH_2O$, x=4.8

Two different methods were used in this study to prepare HT-$LiCoO_2$ powders. The first method was termed as acetate-nitrate method and LiA, LiN, CoN and CoA were used as starting chemicals in this method. The second method was hydroxide method and LiH and CoN were used as starting chemicals in this method.

4.1.1. Acetate-Nitrate Method

As previously stated acetates and nitrates of lithium and cobalt were used in this method. Li and Co acetate or nitrate as well as doping element (will be abbreviated with M, corresponding to Cr, Mo, Mn and W dopants) containing chemical was dissolved in distilled water separately until clear solutions were achieved. Then Li, Co and M containing solutions were mixed and stirred for further 10-15 minutes. Mixed solution was quenched to liquid nitrogen in metal trays. After the solution was completely poured, metal trays were put into freeze dryer which was cooled down to -40°C before operation. The vacuum is about 30 mtorr during freeze drying.

After freeze drying process, the dried powders were subjected to pre-calcination at lower temperatures like 250-400°C for 1 or 2 hours. Pre-calcined powders were divided to the number of different calcination temperatures and were further subjected to calcination at higher temperatures between 400-850°C for 1-24 hours. Calcined samples were immediately taken out from the furnace and characterization techniques were applied. From Figure 4.1, flowchart of acetate-nitrate method can be seen.

4.1.2. Hydroxide Method

As previously stated, lithium hydroxide and cobalt nitrate were used in this method. Solution containing LiH and CoN were prepared separately and CoN solution was slowly added to LiH solution under control of pH around 11. With this pH, cobalt hydroxide, $Co(OH)_2$, was precipitated. Then the solution was hold at room temperature for least 12 hours in order to complete the precipitation of $Co(OH)_2$. Then the precipitate was washed for 4-5 times with LiOH solution (pH ~ 11) for getting rid of nitrate species by applying decantation and centrifuging. After having rinsed the precipitate thoroughly, stoichiometric amounts of LiH and M containing solution were added to the precipitate and stirred until the precipitate was dispersed in the solution, a suspension was achieved. This suspension was quenched to liquid nitrogen in metal trays. After the solution was completely poured, metal trays were put into freeze dryer which was cooled down to -40°C before operation. The vacuum is about 30 mtorr during freeze drying.

After freeze drying process, calcination was applied with the same procedure of acetate-nitrate method. From Figure 4.2, flowchart of hydroxide method can be seen.

4.2. Applied Characterization Techniques

4.2.1. X-Ray Diffraction and Rietveld Analysis

The obtained samples were subjected to XRD analysis by using the XRD apparatus of Metallurgical and Materials Engineering Department (Rigaku DMAX 2200). XRD was applied between 10-70° with step size of 0.5°/min. The quantity of phases as well as the values of structural parameters (lattice parameters *a* and *c*, oxygen position) were determined after Rietveld refinements of the diffraction patterns using the software MAUD [98] were applied. The XRD patterns of the samples in this study were fitted by using the structural parameters obtained by Orman and Wiseman [99].

During Rietveld analysis, Li_2CO_3, Co_3O_4, LT-$LiCoO_2$, a Co-Mo containing spinel like phase, Li_2CrO_4, Li_4WO_5 were identified and added to the analysis as impurity phases. When the amount of any phase was lower than 1 mole%, then this is shown by the term “minor” throughout this study. The results were discussed on the value of R value (difference between the fitted value and the experiment pattern) as well as compliance of the content of HT-$LiCoO_2$. Occupation ratio of M dopants in Li-site and/or Co-site was also altered. When it was decided that single phase HT-$LiCoO_2$ was produced, Rietveld analyses were again applied to the same XRD patterns of the samples for the aim of determining the occupation ratio of lithium and cobalt sites. Moreover, the structural parameters were more precisely refined by this method. During applying these precise Rietveld analyses, GSAS software [100] was also used.

4.2.2. Chemical Analysis

Inductively Coupled Plasma (ICP) was applied to the samples by using Perkin Elmer DRC II model ICP-MS in Central Laboratory of METU. Li, Co and M contents of the samples were determined and the averages of 5 tests were calculated for each sample.

X-ray Photoelectron Spectroscopy was applied to the samples by using PHI 5000 VersaProbe in Central Laboratory of METU. Elements of O, C, Li, Co, Mn and W were scanned in the binding energy range of 0-1 keV. The convolution of the main spectra was applied in order to analyse each element separately and carefully. The depth of the chemical analysis was about 6-10 nm. Moreover; Ar etching was applied for investigating the inner content of the samples. Ar etching was applied twice at 3000 eV/min for 5 minutes.

Energy Dispersive X-Ray Spectroscopy (EDX) was applied by using SEM of Metallurgical and Materials Engineering Department (FEI Nova Nano 430). For every sample, EDX was applied in 2 or 3 different regions and with different magnifications. Elements of Co, W, Mn, Cr and Mo were scanned. The samples that were characterized electrochemically were subject to mapping by using the same device. Mapping was applied to powder samples or electrodes for 30 minutes.

4.2.3. Scanning Electron Microscope

The photos of the samples were taken by using SEM of Metallurgical and Materials Engineering Department (FEI Nova Nano 430). The particle size and morphology were determined. For each sample, photos were taken at different magnifications but mostly at magnifications of x20000 and x40000.

4.2.4. Electrochemical Characterization

Galvanostatic Tests, Cyclic Voltammetry (CV) and Electrochemical Impedance Spectroscopy (EIS) were applied by using the cell having the produced HT-$LiCoO_2$ as cathode material. As anode, graphite is used in galvanostatic cycles whereas metallic lithium is used in CV and EIS measurements.

All sample powders were vacuum dried at 120°C for 24 hours and then stored in glove box after calcination. For cathode preparation, powders were mixed with polyvinylidene difluoride (PVDF) and C black with the ratio of 90:5:5. PVDF was used as a solution after dissolved in N-methyl pyrrolidinone (NMP). This solution was mixed with HT-$LiCoO_2$ and C-black and a slurry of these was prepared. For anode, graphite was mixed with PVDF and C black with the ratio of 88:6:6 with the same procedure applied for cathode. These slurries were stirred vigorously in order to get uniform distribution of active materials. Cathode slurry was coated on aluminium foil and anode slurry was coated on copper foil by using Doctor Blade technique. The coated material were dried at 120° for 3 hours and then were further dried in vacuum at again 120°C for another 1 day. Discs having diameter of 18 mm were cut from the prepared electrodes. Then they were put in a glove box (having 0.1 ppm O_2 and 0.1 ppm H_2O) and hold there until cell assembly. For cell assembly, a glass fibre sheet with the density of 52 g/m^2 was used as separator. The electrolyte was 1 M LiPF6 in a 50:50 EC:DEC solution. Air tight cells were used and assemblage was applied in glove box.

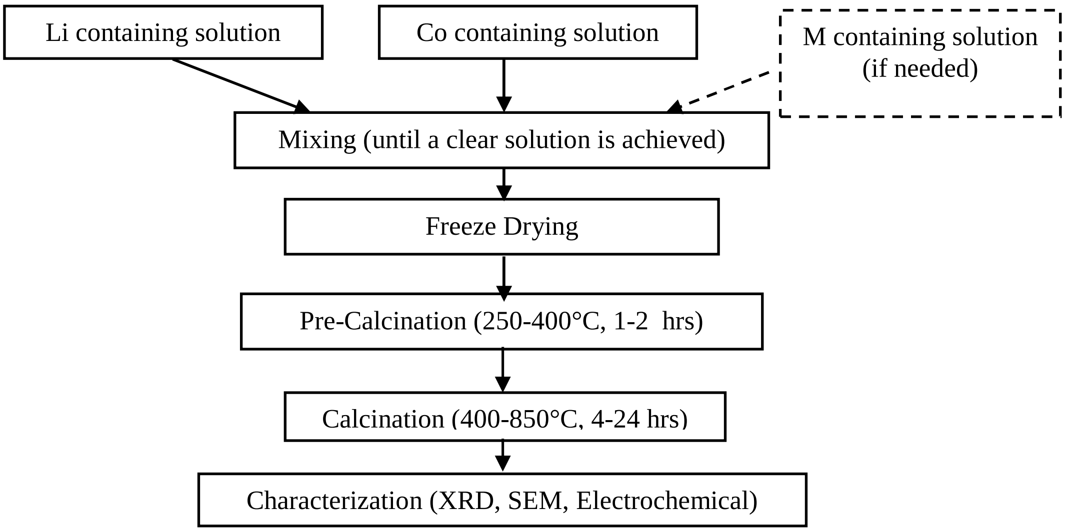

Figure 4.1. The process flowchart of acetate-nitrate method.

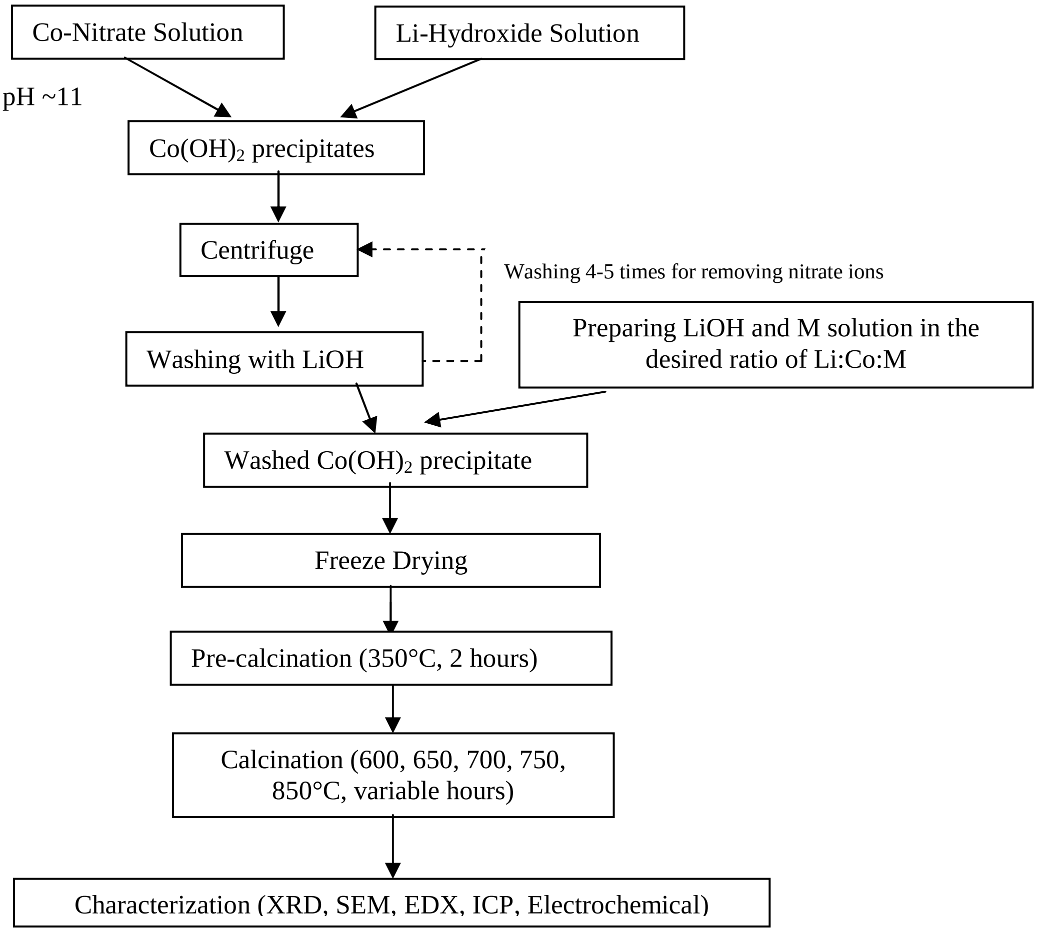

Figure 4.2. The process flowchart of hydroxide method.

The device used for galvanostatic tests and cyclic voltammetry was Solartron 1470 potentiostat and Versastat III was used for electrochemical impedance spectroscopy.

4.2.4.1 Galvanostatic (Charge-Discharge) Tests

During charge-discharge cycles, charge rates of 0.3C and 1C and discharge rates of 0.3C, 0.75C, 1.5C and 3C were used. The cells were cycled 20 times at each discharge rate and 5 more cycles were applied at the slowest discharge rate (0.3C) at the end. 1C corresponded to a rate of about 140 mAh/g. The charge-discharge tests were conducted between 2.75 and 4.25 V. For all samples, a cycle with charge and discharge rates of 0.3C was applied at the beginning.

4.2.4.2 Cyclic Voltammetry (CV)

CV was applied at the first and second cycles at scan rates of 0.02 mV/s, 0.05 mV/s and 0.08 mV/s between 3 and 4.5 V. The cells were charged to 4.5 V first and CVs were begun at the charged state. The initial scan was applied towards the cathodic direction which was from higher potential to lower potential. During CV, two-electrode assembly was used.

4.2.4.3 Electrochemical Impedance Spectroscopy (EIS)

Potentiostatic EIS was applied between the frequency range of 100 mHz and 300 kHz at the open circuit potential (OCV) of the cells. The AC amplitude was ±10 mV. EIS was carried out at different state of charge values of the cell as can be inferred from the OCV values of the cell. Highest OCV corresponds to fully charged state and lowest OCV to fully discharged state.

CHAPTER 5

SYNTHESIS of SINGLE PHASE and ORDERED HT-$LiCoO_2$

5.1. Preliminary Tests of Freeze Drying and Calcination

The study began with using LiN, CoN and CoA. Solutions of Li and Co chemicals were prepared at Li:Co ratio of 1.1:1 and 1.2:1 in order to compensate for the Li loss during high temperature treatment. After all the chemicals dissolved, the solutions were mixed and freeze drying was applied. Riley [101] suggested the increase of solution temperature for evaporating some water to an extent that some crystals in the solution were seen before freeze drying. However; in our study, we did not see any crystals at lower molarities. Although some crystals were seen at higher molarities (5 M), no difference was seen in the XRD patterns applied after the calcination process. After the preparation of Li and Co containing solution, cooling under liquid nitrogen was applied prior to freeze drying. The duration for freeze drying was altered between 12 and 48 hours and the vacuum was held at about 30 mtorr. It was not achieved to produce completely dried powders even after 48 hours of freeze drying. Increasing soaking time to about 54 hours did not yield complete drying also. When the reason for this abnormality was investigated, it was seen that the duration at lower temperatures such as -40°C was very high that the sublimation could not be completed. From water phase diagram (Figure 5.1) it is seen that applying freeze drying starting from the point ā will lead to more driving force for freezing. It is needed to get down to a temperature in the vicinity of ā in order to completely freeze the solution. However; staying at that temperature more than needed will eventually result in longer time for drying hence drying could not be completed. Therefore, after complete freezing, the temperature should gradually increase to a value around -10°C (point ē in Figure 5.1) and the sample should be soaked there for enough time. However; it was seen that very long durations (about 20 hours) were spent in the vicinity of point ā (in the range between -40 and -30°C). This was unnecessary, instead more time must be allocated at the temperatures around point ē. Inherently, samples were soaked for longer times such as 40 hours at temperatures of -20°C and -10°C and this led to better drying performances. Eventually the receipt for freeze drying was set as follows;

a. 10 minutes hold at -40°C
b. Ramp to -30°C from -40°C in 20 minutes
c. 150 minutes hold at -30°C
d. Ramp to -25°C from -30°C in 10 minutes
e. 890 minutes hold at -25°C
f. Ramp to -20°C from -25°C in 10 minutes
g. 710 minutes hold at -20°C
h. Ramp to -10°C from -20°C in 20 minutes
i. 1060 minutes hold at -10°C
j. Ramp to -10°C from 2°C in 15 minutes
k. 60 minutes hold at 45°C

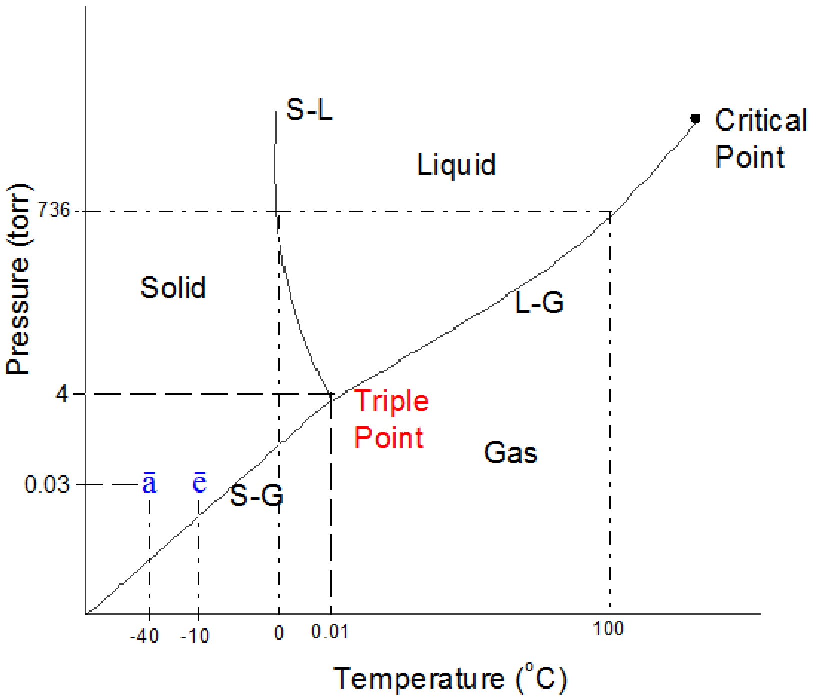

Figure 5.1. The schematic display of phase diagram of water.

Freeze dried products were subjected to calcination at temperature of 450°C with different soaking time. With increasing time, it was seen that the amount of $LiCoO_2$ was increased regardless of the structure. However; 450°C was not enough for producing HT-$LiCoO_2$. The sample contained at most 50 mole% HT-$LiCoO_2$ with *c/a* values lower than 4.99, near 4.90. Therefore, the calcination temperature was increased to 720°C. It was seen that all the fingerprints of HT-$LiCoO_2$ could be found. These were the location of [003] peak, *c/a* ratio and splitting of [006]-[102] and [108]-[110] peaks. According to [35], the position of [003] might be another indication of formation of layered $LiCoO_2$. The 2θ value of HT-$LiCoO_2$ was lower than LT-$LiCoO_2$. When both structures are present in the material two humps in the vicinity of $2\theta \sim 19°$ are seen which are depicted in Figure 5.2. This figure belongs to a sample containing 26 and 50 mole% HT-$LiCoO_2$ and LT-$LiCoO_2$, respectively. If there is single phase in the sample, no humps can be seen in XRD pattern independent of the type of the structure (layered or spinel). When compared with spinel structure, [003] peak of layered structure is at lower 2θ values hence shifting of this peak to left is occurred. This can be seen from Figure 5.3. In this figure the upper XRD (green points) belongs to a structure containing only HT-$LiCoO_2$ and the lower one (red points) belongs to a structure containing about 95 mole% LT-$LiCoO_2$. From Figure 5.3a, the difference in the positions of [003] peaks can be seen, from Figure 5.3b and Figure 5.3c, the differences in the splitting of [006]-[102] and [108]-[110] peaks can be seen, respectively. For HT-$LiCoO_2$, splitting of aforesaid peaks is seen whereas no splitting of these peaks is seen for LT-$LiCoO_2$.

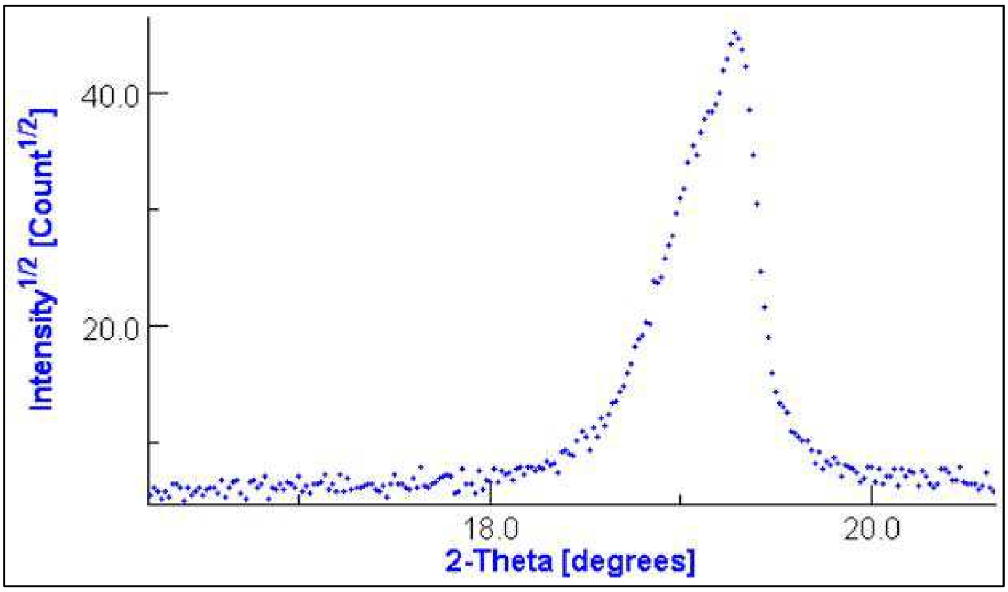

Figure 5.2. The enlarged display of [003] peak belonging to a mixed structure.

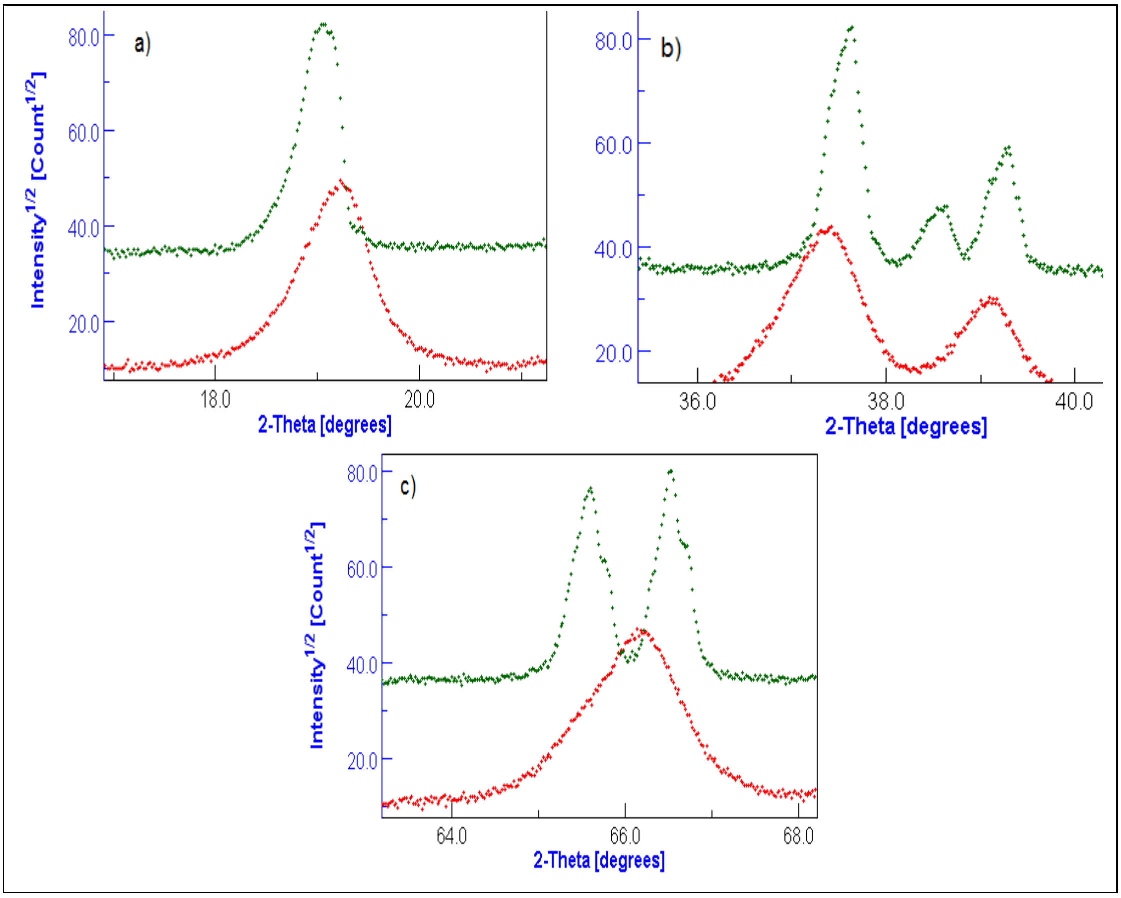

Figure 5.3. Portion of XRD patterns of HT-$LiCoO_2$ (green points) and LT-$LiCoO_2$ (red points) which show the differences between peaks of a) [003] b) [006]-[102] c) [108]-[110].

To sum up; freeze drying of 48 hours under 0°C which most of the drying time is reserved for temperatures around -10°C is needed for relatively effective drying. For achieving single phase HT-$LiCoO_2$, calcination at temperatures higher than 700°C are needed. Besides these, the freeze dried precursors are melted during calcination which is strictly undesired. With melting, the importance and advantage of freeze drying are lost.

5.2. Studies with Acetate-Nitrate Method

During the preliminary studies, melting occurred as it was stated in the previous section. In addition to melting, bursting of the sample was seen so the samples were dispersed in the furnace. In order to prevent these two undesired situations, pre-calcination was applied at various temperatures like 200, 250, 300 and 350°C for 1 or 2 hours. After some tests, it was decided to apply calcination at 350°C for 2 hours and this was continued throughout the study.

Deciding on the optimum parameters for obtaining HT-$LiCoO_2$, experiments were conducted with different chemicals, such as LiA, LiN, CoA, CoN. All 4 combinations of these chemicals were applied. Moreover; the temperature range of calcination was between 400°C and 850°C. The soaking time was 24 hours. Li:Co ratio was kept as 1.2:1. Li was used 20 mole% excess for compensating Li losses at higher temperatures. The flowchart applied during this section was given in Figure 4.1. The hint for the notation used in this chapter is as follows;

First and second letters belong to Li and Co containing chemicals, respectively and A stands for acetate, N stands for nitrate and H stands for hydroxide. If doping is applied, then doped element is shown by its elemental formula and the doping content is shown just near this formula. The three digit number shows the calcination temperature and last number shows the calcination time. If there occurs no number after the three digit number, it means that calcination was applied for 24 hours. As an example, the notation of ANCr5-850-12 means that the starting chemicals are LiA and CoN, the sample is doped with 5 mole% Cr and calcination was applied at 850°C for 12 hours.

5.2.1. Production of undoped $LiCoO_2$

The results of the experiments are given in Table 5.1. From this table, it is seen that at least 700°C is needed for obtaining nearly single phase HT-$LiCoO_2$. The impurity is mainly Li_2CO_3 which comes almost from air. Although acetate containing experiments contain more carbon than that of nitrate containing samples, at the end of experiments the amount of Li_2CO_3 in the structure does not differ.

When the lattice parameters are considered, it is seen than lattice parameter *c* expands with temperature while lattice parameter *a* more or less stays same. Therefore *c/a* value increases with temperature.

It is seen that the ratio of [003]/[104] is far from being 1, it is at most 0.818 implying that there is a problem with the ordering of HT-$LiCoO_2$

Table 5.1. The results of the experiments to produce undoped $LiCoO_2$.

Sample Name	Li_2CO_3 (%)	Spinel (%)	Layered (%)	*a* (Å)	*c* (Å)	*c/a*	Peak separation	[003]/ [104]
NA-400	5.50	92.12	-----	-----	-----	-----	No	0.780
NA-550	12.29	45.86	41.20	2.820	14.063	4.989	No	0.687
NA-700	1.26	-----	98.74	2.818	14.061	4.990	Yes	0.673
NA-850	Minor	-----	99.16	2.817	14.071	4.995	Yes	0.656
AN-400	8.30	51.54	39.38	2.818	14.058	4.989	No	0.818
AN-550	34.80	37.89	27.32	2.819	14.063	4.989	No	0.727
AN-700	Minor	-----	99.51	2.817	14.064	4.993	Yes	0.701
AN-850	Minor	-----	98.71	2.817	14.069	4.994	Yes	0.701
AA-400	32.27	60.72	5.80	-----	-----	-----	No	-----
AA-550	9.75	23.23	66.11	2.817	14.062	4.992	Yes	0.698
AA-700	1.29	-----	98.71	2.817	14.068	4.994	Yes	0.693
AA-850	Minor	-----	98.64	2.818	14.091	5.000	Yes	0.734
NN-400	11.69	29.18	1.75	-----	-----	-----	No	0.808
NN-550	32.96	14.71	52.33	2.818	14.058	4.989	No	0.735
NN-700	2.16	1.54	96.31	2.816	14.075	4.998	Yes	0.654
NN-850	Minor	-----	99.59	2.816	14.076	4.998	Yes	0.707

When SEM photos (Figure 5.4) of the samples are investigated, it is seen that particle size is increased with temperature due to grain growth at higher temperatures.

Figure 5.5 reveals that the lowest particle size is achieved with the starting chemical CoA, however, the difference between particle size is not significant to decide the effect of starting chemicals on particle size. All samples in this figure were calcined at 850°C for 24 hours.

Bursting and melting were observed when the samples were checked during calcination. The effect of bursting on the samples can be seen in Figure 5.6 with the cavities between the bundles. This bursting is thought to be mainly due to NOx gas evolution and it is also less likely to be because of fast evaporation of the residual water (due to incomplete drying during freeze drying, maybe water is trapped inside a particle).

Having seen that single phase HT-$LiCoO_2$ can be produced at 700°C, an experiment with the calcination temperature between 550°C and 700°C, for example at 625°C was conducted. The freeze drying time is increased to 63 hours in that sample and the starting chemicals are chosen as Li-acetate and Co-nitrate because they show the worst drying performance when compared with other combinations. Even in that situation, no difference in the drying performance is observed. Moreover, the amount of layered $LiCoO_2$ is very low (60.53%) and the splitting of [006]-[012] and [108]-[110] peaks is hardly seen. Therefore we conclude that we must reach at least 700°C to have single phase HT-$LiCoO_2$.

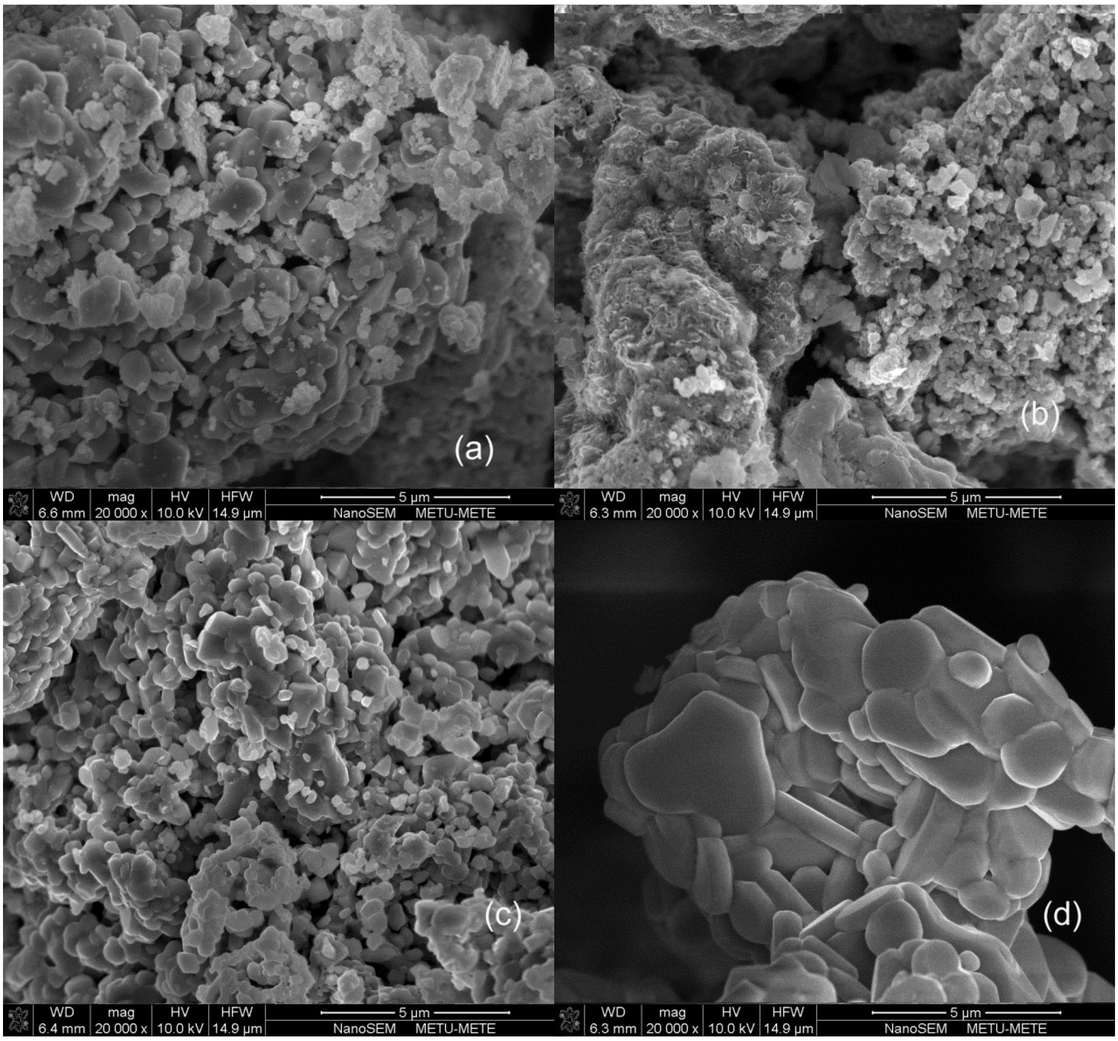

Figure 5.4. SEM photos of experiment having starting chemicals as LiA and CoN which calcined at a) 400°C, b) 550°C, c) 700°C d) 850°C.

Gupta and Manthiram [102] claimed that decreasing the cooling rate (1°C/min) after calcination is important for achieving ordered structure of layered $LiCoO_2$, in other words they saw that the ratio of [003]/[104] was increased with smaller cooling rates. Therefore, two samples which were calcined at 625°C and 850°C for 24 hours, were cooled at a rate of about 3°C/min. However, neither peak intensity nor ratio [003]/[104] was different than that of fast cooled samples.

The structural and morphological analysis of the results of starting chemicals did not show significant differences, therefore any combination could be chosen for doping studies.

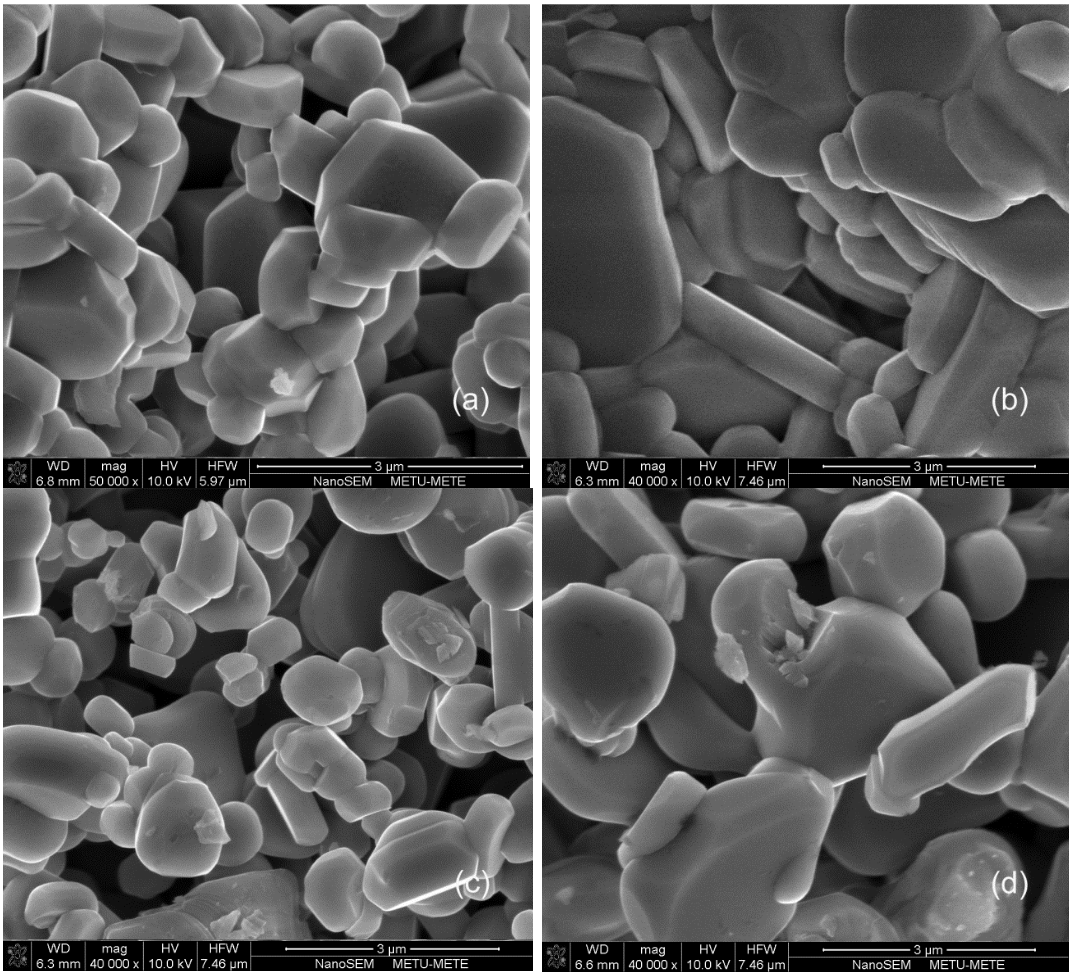

Figure 5.5. SEM photos of having a) LiN-CoA, b) LiA-CoN, c) LiA-CoA and d) LiN-CoN as starting chemicals.

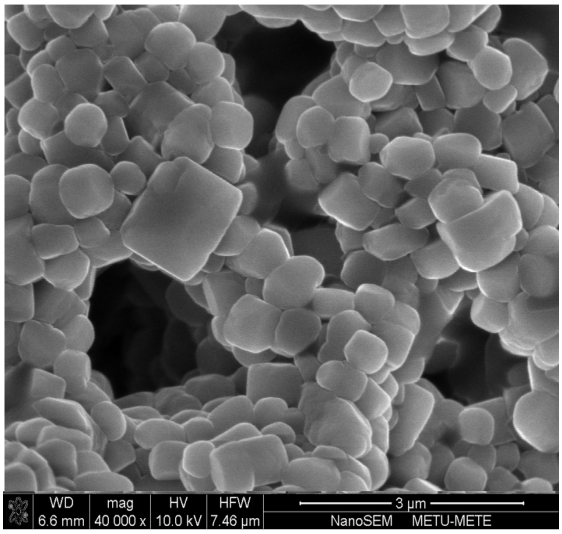

Figure 5.6. SEM photo of an experiment showing the cavities occurred during bursting.

5.2.2. Production of doped $LiCoO_2$

5.2.2.1 5 mole% doping by using LiA-CoN as starting chemicals

During doping experiments, same solution preparation steps and same freeze drying receipt were followed. Calcination was applied at 550°C, 700°C and 850°C. As at 400°C, there was no significant amount of layered $LiCoO_2$ in all samples, calcination was not applied at this temperature and the results of calcination at 550°C are not shown as they had very low content of HT-$LiCoO_2$. Moreover, in some samples the calcination was applied for less than 24 hours (1, 4 and 12 hours) but unfortunately there was no improvement in the content of HT-$LiCoO_{2,}$ therefore the results of these were not shown also. The alloying elements were added in such a way that Li:Co:M mole ratio (M=Cr, Mo, Mn, W) was 1.2:0.95:0.05. Therefore it was aimed to produce a material having a formula $LiCo_{0.95}M_{0.05}O_2$. Except Mn, every doping element has an impurity phase identified in XRD patterns. These impurity phases were Li_2CrO_4, a spinel phase containing Co and Mo (termed as CoMo spinel) and Li_4WO_5 for Cr, Mo and W doping, respectively.

From Table 5.2, the results of the doped samples can be seen as well as that of the undoped sample. Moreover, the position of oxygen (z) in the structure was calculated and discussed for these samples. It is seen that doping inversely affects the amount of HT-$LiCoO_2$ at 700°C. The sample calcined at 700°C without any dopant has more layered $LiCoO_2$ than that of any doped sample. When considering lattice parameter *c* which is an indicator for the incorporation of doping elements into the layered structure, it can be claimed that only Mn incorporates into the structure at both 700°C and 850°C. Although amount of layered $LiCoO_2$ calcined at 850°C is larger than that calcined at 700°C for all dopants, lattice parameter *c* increases in Mn and Cr containing sample with increasing temperature. However; lattice parameter *c* of Cr doped sample calcined at 850°C is not different than that of undoped sample, so it is hard to say that Cr is incorporated into the structure. For W and Mo doped samples, increasing the temperature result in increasing M containing impurity phase. For both samples, lattice parameter *c* decreases with temperature. At 700°C, incorporation into the structure can be thought but the content is not solely layered $LiCoO_2$. It is believed that at 700°C, all dopants except Cr are partially incorporated into the spinel structure. This structure is destroyed with temperature and at 850°C, Li, Co and dopants are liberated. Some Li is lost to the atmosphere, some goes to M containing impurity phase (Li_4WO_5) and some goes to layered structure. For Co, same situation exists; some goes to M containing impurity phase (CoMo spinel) and some goes to layered structure. Therefore Mo and W amounts to be doped into layered structure decrease. The soundness of this postulate can be checked with the comparison of amounts of Li_2CO_3 and Co_3O_4 in Mo and W doped samples. It is seen that amount of Li_2CO_3 is larger in Mo and W doped sample calcined at 850°C.

Table 5.2. The results of the doped samples.

Sample Name	Impurity phase (%)[a]	Spinel (%)	Layered (%)	Layered *a* (Å)	Layered *c* (Å)	*c/a*	z	[003]/ [104]
AN-700	-----	-----	99.51	2.817	14.064	4.993	0.2463	0.701
AN-850	-----	-----	98.71	2.817	14.069	4.994	0.2457	0.701
ANCr5-700	4.50	-----	93.45	2.817	14.058	4.990	0.2461	0.714
ANCr5-850	-----	-----	98.17	2.818	14.071	4.993	0.2463	0.702
ANMo5-700	minor	21.66	73.18	2.821	14.082	4.992	0.2456	0.767
ANMo5-850	2.58	-----	95.29	2.818	14.064	4.991	0.2448	0.854
ANMn5-700	-----	19.91	77.79	2.818	14.079	4.996	0.2517	0.737
ANMn5-850	-----	-----	99.16	2.817	14.096	5.004	0.2452	0.815
ANW5-700	minor	17.10	79.68	2.821	14.103	4.999	0.2458	0.791
ANW5-850	4.37	-----	94.33	2.817	14.062	4.992	0.2451	0.874

Note: The amount of phases do not add to 100%, Balance is mainly about Li_2CO_3 with about minor amounts of Co_3O_4 in some samples

[a] Li_2CrO_4, CoMo spinel and Li_4WO_5 for Cr, Mo and W doping, respectively.

SEM and EDX analyses are applied to the samples. SEM photos of the samples calcined at 700°C are given in Figure 5.7.

From Figure 5.7, it is seen that, with doping, particle size decreases. The differences in particle size are not significant for Mo, Mn and W dopants but it seems that it is smallest for W doped samples and largest for Cr doped samples. The shape of the particles is between hexagon and sphere. For illustrative purposes, Cr doped samples are shown to display the particle size differences at different temperatures. This can be seen from Figure 5.7b and Figure 5.7c, and particle size is larger for 850°C as expected.

EDX analyses were applied for all doped samples. For doping with Cr, the sample calcined at 700°C had Li_2CrO_4 as an impurity phase. The existence of this phase was confirmed by EDX with having a region containing higher amounts of Cr than that of other regions containing Cr content between 1 and 8 mole%. From these two observations, it was deduced that at 700°C, a significant amount of Cr could not be incorporated into the layered structure. However; this was not true for sample calcined at 850°C. The EDX analysis revealed that Cr content changed between 4 and 6 mole% which was the nearly same amount with the doping content, therefore it can be claimed that Cr was doped at least partially into the layered structure at higher temperatures.

When Mo, Mn and W doped samples were considered, Mo doped samples had Mo content of 2 and 4 mole% for both temperatures, Mn doped samples had Mn content of about 5 mole% for both temperatures, W doped samples had W content between 6 and 10 mole% for both temperatures. The changes of the dopant content in different regions were very low that uniform distribution of these dopants can be claimed. This could be attributed to the incorporation into the layered structure. This statement is more valid and incorporation amount is higher for Mn doped sample when compared to Mo and W doped samples.

With 5 mole% doping studies, it was inferred that 5 mole% was beyond the solubility limit for layered HT-$LiCoO_2$ except for Mn doping. Also, during the studies having LiA-CoN as starting chemicals, not only complete drying was achieved but also the melting and bursting of the powders into the furnace were seen. As a result, there occurred great loss in the final product in terms of mass. Mass balance showed that about 60% of Co and 75% of Li were lost on the average. This loss which was inherently not equal for all samples would affect the morphology and structure of the samples, undoubtedly. Although some precautions were taken for dispersion of powders into the furnace, no improvements could be seen. As a result it was decided not to use LiA-CoN as starting chemicals for future studies. Instead LiN and CoN were used as starting chemical due to the reason that bursting was not seen during preliminary experiments.

5.2.2.2 5 mole% doping by using LiN-CoN as starting chemicals

During these studies, calcination was again applied at 550°C for 4, 12 and 24 hours and at 700°C for 1, 4, 12 and 24 hours but single phase HT-$LiCoO_2$ could not be produced, hence results of these studies were not shown. At 850°C, calcination was applied for 1, 4, 12 and 24 hours and the results of these studies were given in Table 5.3 with the results of undoped sample.

From Table 5.3, it is seen that with increasing holding time, the amount of layered HT-$LiCoO_2$ is decreased. This encourages the claim that with high temperature and long-time calcination, the layered structure was decomposed due to the loss of Li. However; with undoped and Mn doped samples, this situation did not occur. Therefore, it is thought that undoped and Mn doped samples are more stable at higher temperatures than that of Cr, Mo and W doped samples. Increasing of lattice parameter *c* with holding time could be attributed to the increase in temperature as discussed in section 5.2.1.

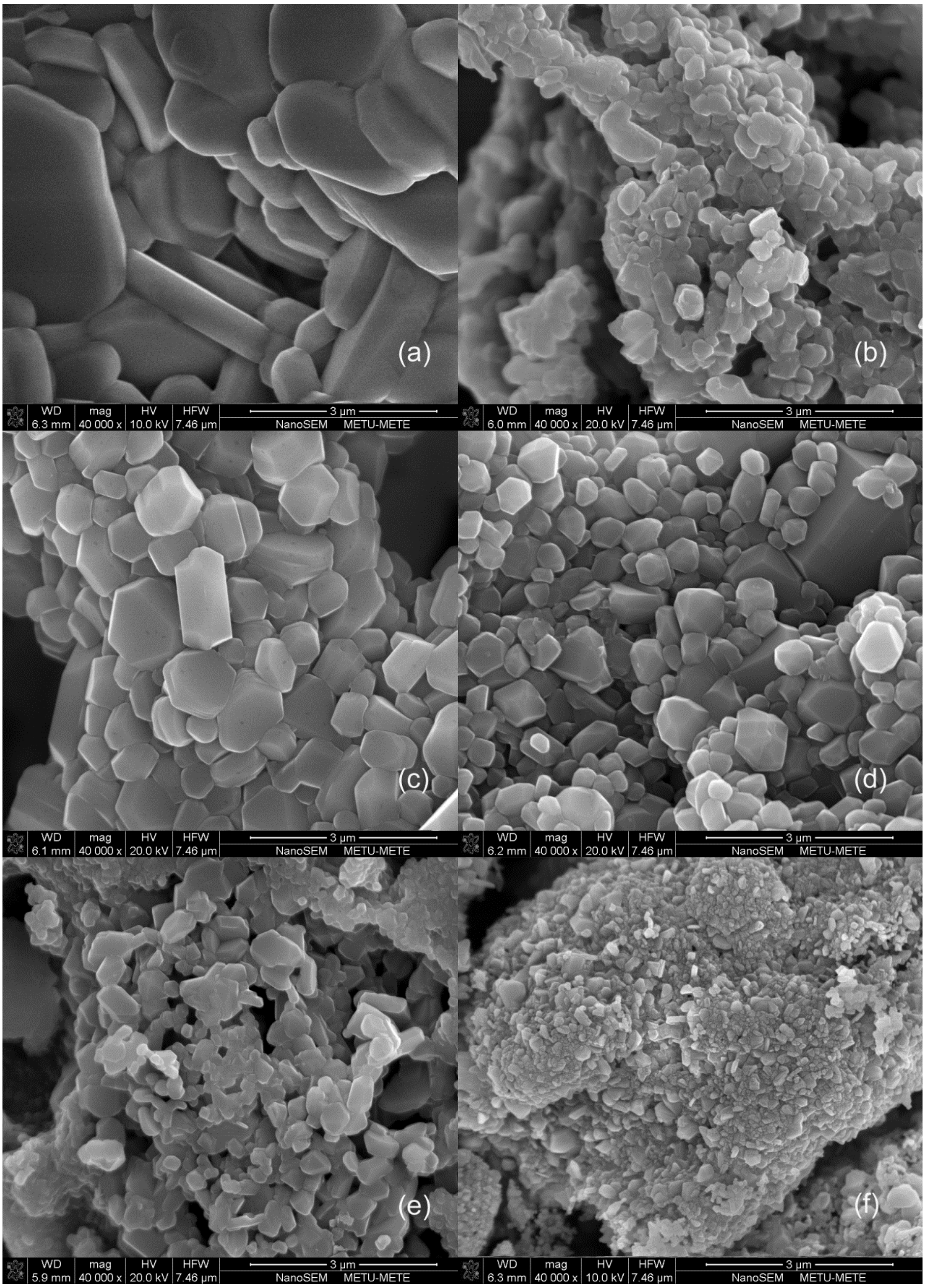

Figure 5.7. SEM photos of samples a) AN-850, b) ANCr5-700 c) ANCr5-850, d) ANMo5-850, e) ANMn5-850 f) ANW5-850.

Table 5.3. The results of the doped samples having LiN-CoN as starting chemicals.

Sample Name	Impurity phase (%)[a]	Spinel (%)	Layered (%)	*a* (Å)	*c* (Å)	*c/a*	z	[003]/ [104]
NN-700	-----	1.54	96.31	2.816	14.075	4.998	0.2473	0.654
NN-850	-----	-----	99.59	2.816	14.076	4.998	0.2453	0.707
NNCr5-850-1	1.43	-----	96.92	2.819	14.076	4.993	0.2455	0.834
NNCr5-850-4	Minor	-----	98.86	2.818	14.076	4.995	0.2447	0.877
NNCr5-850-12	-----	Minor	97.03	2.820	14.086	4.995	0.2451	0.859
NNCr5-850	-----	-----	92.61	2.819	14.083	4.996	0.466	0.822
NNMo5-850-1	1.89	-----	97.52	2.815	14.058	4.994	0.2457	0.848
NNMo5-850-4	2.18	-----	97.60	2.815	14.059	4.994	0.2454	0.900
NNMo5-850-12	1.92	-----	97.13	2.815	14.054	4.993	0.2449	0.894
NNMo5-850	2.23	-----	95.22	2.815	14.052	4.992	0.2451	0.849
NNMn5-850-1	-----	Minor	98.42	2.817	14.088	5.001	0.2463	0.768
NNMn5-850-4	-----	-----	97.71	2.819	14.092	4.999	0.2457	0.775
NNMn5-850-12	-----	Minor	98.12	2.818	14.099	5.003	0.2459	0.761
NNMn5-850	-----	-----	99.28	2.817	14.098	5.005	0.2452	0.790
NNW5-850-1	2.91	----	94.13	2.819	14.078	4.994	0.2457	0.868
NNW5-850-4	3.16	----	95.14	2.818	14.071	4.993	0.2454	0.902
NNW5-850-12	5.93	----	91.38	2.819	14.069	4.991	0.2459	0.907
NNW5-850	-----	----	88.86	2.819	14.085	4.996	0.2473	0.743

Note: The amount of phases does not add to 100%, Balance is mainly about Li_2CO_3 with about minor amounts of Co_3O_4 in some samples

[a] Li_2CrO_4, CoMo spinel and Li_4WO_5 for Cr, Mo and W doping, respectively.

When LiA-CoN and LiN-CoN studies were compared, the behaviour of impurity phases with increasing temperature resembled each other, meaning that increasing calcination temperature or increasing time at elevated temperatures resulted in higher amount of impurity phases for W and Mo doped samples and lower impurity phases for Cr doped sample. However; the ordering was better in LiN-CoN samples. With LiN-CoN samples, there was no dispersion to the furnace, so weight loss did not observed. It was an interesting result that Mn doped samples had lower [003]/[104] ratios than other doped samples.

When the incorporation of doped samples was considered, it could only be claimed that Mn was incorporated into the structure.

It was seen that with LiN-CoN starting chemicals, no significant improvement on the purity of HT-$LiCoO_2$ was achieved. It was again inferred that 5 mole% doping was too high to achieve a product forming a solid solution having the formula of $LiCo_{0.95}M_{0.05}O_2$. Therefore decreasing of the doping amount was considered and discussed in the next section.

Although SEM and EDX analyses were applied to LiN-CoN samples, the results were not shown here because of revealing similar photos and contents with LiA-CoN samples.

As it was discussed earlier, Gupta and Manthiram [102] related ordering with cooling rate. With decreasing cooling rate to 3°C/min, meaningful results could not be achieved. However; as Gupta and Manthiram [102] applied 1°C/min as the cooling rate, lower cooling rates were applied to the calcined samples and the results are discussed in next section.

5.2.2.3 Attempts to increase the ratio of [003]/[104]

For these studies, the samples that contain single phase layered $LiCoO_2$ were used. One of the samples used was produced by using LiA-CoA starting chemicals and calcined at 850°C for 24 hours (AA). This calcined sample was further treated in three different ways as follows;

a. 12 hours more calcining and fast cooled to room temperature (AA-a)
b. 16 hours more calcining and cooled with a rate of 1.3°C/min (AA-b)
c. Cooled at a rate of 2°C/min directly from 850°C (AA-c)

Moreover, LiN-CoN starting chemicals were also used for this purpose. This sample was also produced by calcining at 850°C for 24 hours (NN). This calcined sample was further treated in four different ways as follows;

a. 24 hours more calcining and fast cooled to room temperature (NN-a)
b. 24 hours more calcining and cooled at a rate of 2°C/min (NN-b)
c. Cooled at a rate of 2°C/min directly from 850°C (NN-c)
d. 2 hours more calcining and cooled at a rate of 1°C/min (NN-d)

The results are given in Table 5.4.

As it is seen from Table 5.4, there is no significant increase in the ratio of [003]/[104] even with longer calcination time or slower cooling rate. It is very interesting that *c/a* values are the highest for the ones that calcined at 850°C for 24 hours and cooled at room temperature.

Table 5.4. The results of the studies aiming to increase the ratio of [003]/[104].

Sample	I_{003} ($count^{1/2}$)	I_{104} ($count^{1/2}$)	[003]/[104]	c (Å)	a (Å)	c/a
AA	56.40	76.95	0.732	14.091	2.818	5.000
AA-a	77.14	98.11	0.786	14.059	2.814	4.996
AA-b	48.55	63.24	0.768	14.053	2.812	4.997
AA-c	90.76	108.07	0.840	14.075	2.816	4.999
NN	73.38	104.90	0.700	14.076	2.816	4.999
NN-a	103.94	115.19	0.902	14.071	2.817	4.995
NN-b	78.32	107.75	0.727	14.069	2.816	4.997
NN-c	101.27	120.69	0.839	14.068	2.817	4.994
NN-d	61.11	70.69	0.864	14.072	2.817	4.996

5.2.2.4 1 mole% doping by using LiN-CoN as starting chemicals

As LiN-CoN starting chemicals yielded better results than LiA-CoN samples, 1 mole% doping was applied to LiN-CoN starting chemicals. The doping elements used were Cr and W for this study. Calcination was applied at 700°C for 12 and 24 hours, and at 850°C for 1, 4, 12 and 24 hours. The results are compared with that of 5 mole% doped samples and are given in Table 5.5.

When Table 5.5 is examined, , samples containing 5 mole% dopants yielded worse results than samples containing 1 mole% doping almost at all temperatures and time. At higher alloying amounts, unidentified peaks are more likely to occur. Moreover, 2nd phases (Li_2CrO_4 and Li_4WO_5) are more likely to occur at higher alloying amounts. Lattice parameters *a* and *c* are larger for 5 mole% doping but *c/a* values do not show such a different behaviour. Also the amount of layered structure is always larger with 1 mole% doping than that of 5 mole% doping. For 1 mole% doping, about 750°C is enough for producing nearly single phase structure. It is easily concluded that doping with 1 mole% alloying yields better results than that of doping with 5 mole% doping. However, it is not easy to be sure for incorporation into the layered structure although 1 mole% doping seems to yield better results. Moreover, it is certain that increasing the amount of doping elements introduce more impurity phases (Li_2CO_3, Co_3O_4, 2nd phase etc.) to the structure as the solid solubility of HT-$LiCoO_2$ is exceeded.

For 1 mole% doping more calcination tests have been done which were at 750°C and 800°C for 4, 12 and 24 hours. Especially calcination at 750°C for 24 hours yielded satisfactory results in terms of the amount of layered structure, occurrence impurity phases.

After performing extensive work with acetate and nitrate samples, it was succeeded to produce solid solution of 1 mole% doped HT-$LiCoO_2$. However; using nitrate and acetate samples melting always occurred during calcination and bursting of the powders were occurred except for LiN-CoN samples. Bursting is undoubtedly very bad both for the process and furnace as most of the powders are lost. When melting occurs, the aim for applying freeze drying becomes unnecessary as formation of liquid phase causes the degradation of crystallinity of the samples. As a result of these two main reasons, using of acetates and nitrates were left and new starting chemicals were sought.

Table 5.5. Comparison of results of samples with 1 and 5 mole% Cr and W.

Sample Name	Impurity phase (%)	*a* (Å)	*c* (Å)	*c/a*	Layered (%)	[003]/[104]
NNCr1-700-12	minor	2.814	14.042	4.991	98.09	0.891
NNCr1-700	minor	2.814	14.033	4.987	96.64	0.870
NNCr1-850-1	----	2.816	14.059	4.993	99.47	0.874
NNCr1-850-4	minor	2.815	14.058	4.994	98.68	0.902
NNCr1-850-12	----	2.816	14.059	4.993	99.40	0.898
NNCr1-850	----	2.816	14.063	4.995	99.38	0.803
NNCr5-700-12	minor	2.819	14.073	4.992	94.32	0.914
NNCr5-700	----	2.822	14.082	4.990	84.47	0.935
NNCr5-850-1	1.43	2.819	14.076	4.993	96.92	0.834
NNCr5-850-4	minor	2.818	14.076	4.995	98.86	0.877
NNCr5-850-12	----	2.820	14.086	4.995	97.03	0.859
NNCr5-850	----	2.819	14.083	4.996	92.61	0.822
NNW1-700-12	----	2.816	14.064	4.994	96.01	0.894
NNW1-700	minor	2.818	14.058	4.989	94.76	0.847
NNW1-850-1	----	2.815	14.054	4.992	99.80	0.857
NNW1-850-4	2.13	2.815	14.060	4.994	92.34	0.907
NNW1-850-12	2.61	2.815	14.062	4.996	95.96	0.922
NNW1-850	----	2.816	14.064	4.994	99.61	0.872
NNW5-700-12	minor	2.820	14.060	4.986	77.69	0.824
NNW5-700	1.66	2.822	14.074	4.987	87.13	0.856
NNW5-850-1	2.91	2.819	14.078	4.994	94.13	0.868
NNW5-850-4	3.16	2.818	14.071	4.993	95.14	0.902
NNW5-850-12	5.93	2.819	14.069	4.991	91.38	0.907
NNW5-850	----	2.819	14.085	4.996	88.86	0.743

5.3. Preliminary Studies with Hydroxide Method

Chiang et al. [34] tried to produce $LiCoO_2$ by precipitating cobalt hydroxide, $Co(OH)_2$ (CoH). Precipitation was done during addition of CoN solution to solution of lithium hydroxide, (LiH). They washed the precipitate for getting rid of nitrate species by applying decantation with centrifuging, they repeated these processes for 4-5 times. After having rinsed the precipitate thoroughly, it was freeze dried and calcined. As this process contains no nitrate and acetate species, it is probable that melting and bursting will not occur. Therefore, it was decided to apply this process for the remaining period of the study. The flow chart of the hydroxide method was given in Figure 4.2.

5.3.1. Preliminary tests with hydroxide method

The results achieved with the preliminary tests are given in Table 5.6. It is seen that 750°C is enough for producing single phase layered structure with this method. Ordering is better for this method when compared with acetate-nitrate method. It is interesting that commercial $LiCoO_2$ also contains Li_2CO_3. The XRD patterns of the samples that are calcined at 750°C for 24 hours and the commercial $LiCoO_2$ do not show any difference. Figure 5.8 reveals this similarity. Table 5.6 shows the samples that are calcined for 24 hours at the indicated temperature. Cr doped samples have lower values of lattice parameter c indicating that Cr incorporation into the layered structure or Co-site cannot be achieved. Undoped sample has the lowest c values when compared with other doped samples. Undoped sample and commercial $LiCoO_2$ are very similar in their structural properties.

Table 5.6. Results of the alloying experiments with hydroxide method.

Sample	Impurity phase (%)	Li_2CO_3 (%)	Layered (%)	[003] /[104]	a (Å)	c (Å)	c/a
HH-850	-----	Minor	99.25	0.866	2.816	14.065	4.995
HHCr1-750	-----	Minor	99.85	0.916	2.816	14.061	4.993
HHCr1-850	Minor	1.72	97.42	1.015	2.817	14.063	4.992
HHMo1-750	-----	Minor	99.55	0.957	2.816	14.067	4.995
HHMo1-850	-----	-----	100.00	0.909	2.818	14.074	4.994
HHMn1-750	-----	Minor	99.76	0.895	2.816	14.072	4.997
HHMn1-850	-----	Minor	97.72	0.906	2.815	14.076	5.000
HHW1-750	-----	Minor	99.40	0.931	2.817	14.075	4.996
HHW1-850	-----	Minor	99.89	0.945	2.816	14.076	4.998
Commercial $LiCoO_2$	-----	Minor	99.74	0.917	2.818	14.064	4.991

5.3.2. Comparison of hydroxide and acetate-nitrate methods

During this thesis, the production of layered single phase HT-$LiCoO_2$ and doping of this structure were studied up to now. The studies are summarized as follows;

a. Production of undoped $LiCoO_2$ by using LiA-CoA-LiN and CoN as starting chemicals,

b. Doping of $LiCoO_2$ by M (Cr, Mo, Mn and W) elements with a ratio of Li:Co:M as 1.2:0.95:0.05 by using LiA-CoN,

c. Doping of $LiCoO_2$ by M with a ratio of Li:Co:M as 1.2:0.95:0.05 by using LiN-CoN,

d. Doping of $LiCoO_2$ by Cr and W with a ratio of Li:Co:M as 1.2:0.99:0.01 by using LiN-CoN,

e. Doping of $LiCoO_2$ by M with a ratio of Li:Co:M as 1.2:0.99:0.01 by using LiH-CoH.

After freeze dried these five sets of the experiments, the samples were calcined at temperatures ranging from 550°C to 850°C. The duration of the calcination was altered from 1-24 hours. Satisfactory results could be achieved after calcination at 550°C. However; relatively good results were achieved at higher temperatures. Although at elevated temperatures, less time was spent to produce almost single phase HT-$LiCoO_2$, calcination duration of 24 hours seemed to yield better results.

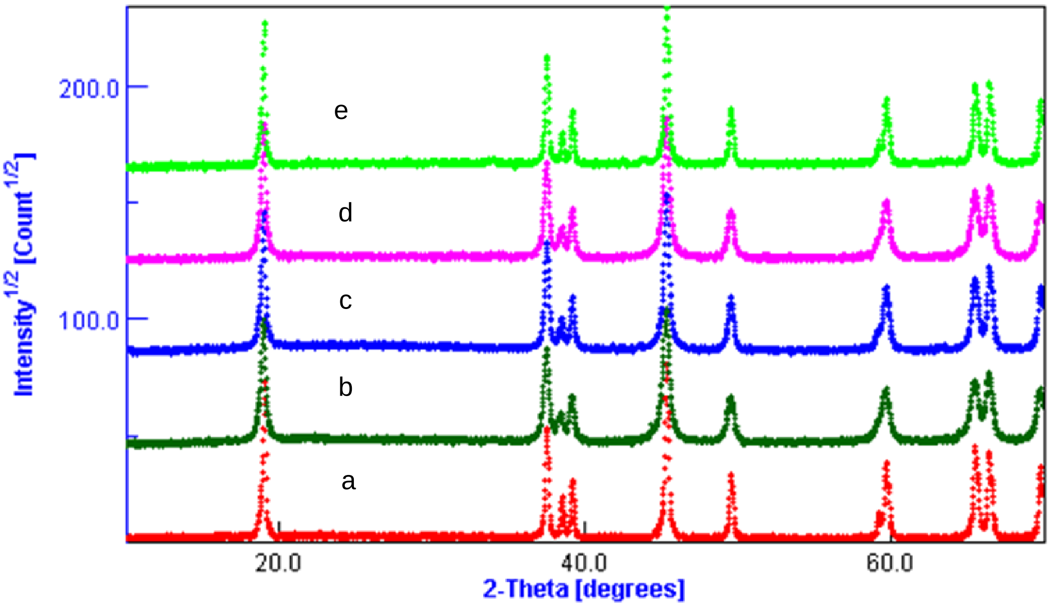

Figure 5.8. XRD patterns of doped samples (W-b, Mn-c, Mo-d, Cr-e) calcined at 750°C for 24 hours and commercially sold $LiCoO_2$ (a). The starting chemicals are LiH and CoH

5.3.2.1 Comparison of undoped experiments

Table 5.7 and Figure 5.9 reveal that the best results are obtained from the LiH-CoH starting chemicals. Although there are not significant differences for the amount of layered structure and *c/a* values, [003]/[004] ratio is highest for this sample except for the commercial one. SEM photographs reveal that hydroxide sample has the lowest particle size, in addition to that particle sizes are uniformly distributed. Also it is seen that using the hydroxide method has lower particle size than that of commercial $LiCoO_2$ which is believed to be produced at about 900°C.

Table 5.7. The results and comparison of undoped experiments.

Starting Chemicals (Li-Co)	*Calcination (T-t)* (°C-hr)	*c/a*	*[003]/[104]*	*Layered (%)*	*Code*
LiN – CoA	850 – 24	4.995	0.656	99.16	a
LiA – Co	850 – 24	4.994	0.701	98.71	b
LiA – CoA	850 – 24	5.000	0.734	98.64	c
LiN – CoN	850 – 24	4.998	0.707	99.59	d
LiH – CoH	850 – 24	4.995	0.866	99.40	e
Commercial $LiCoO_2$	----	4.991	0.917	99.74	f

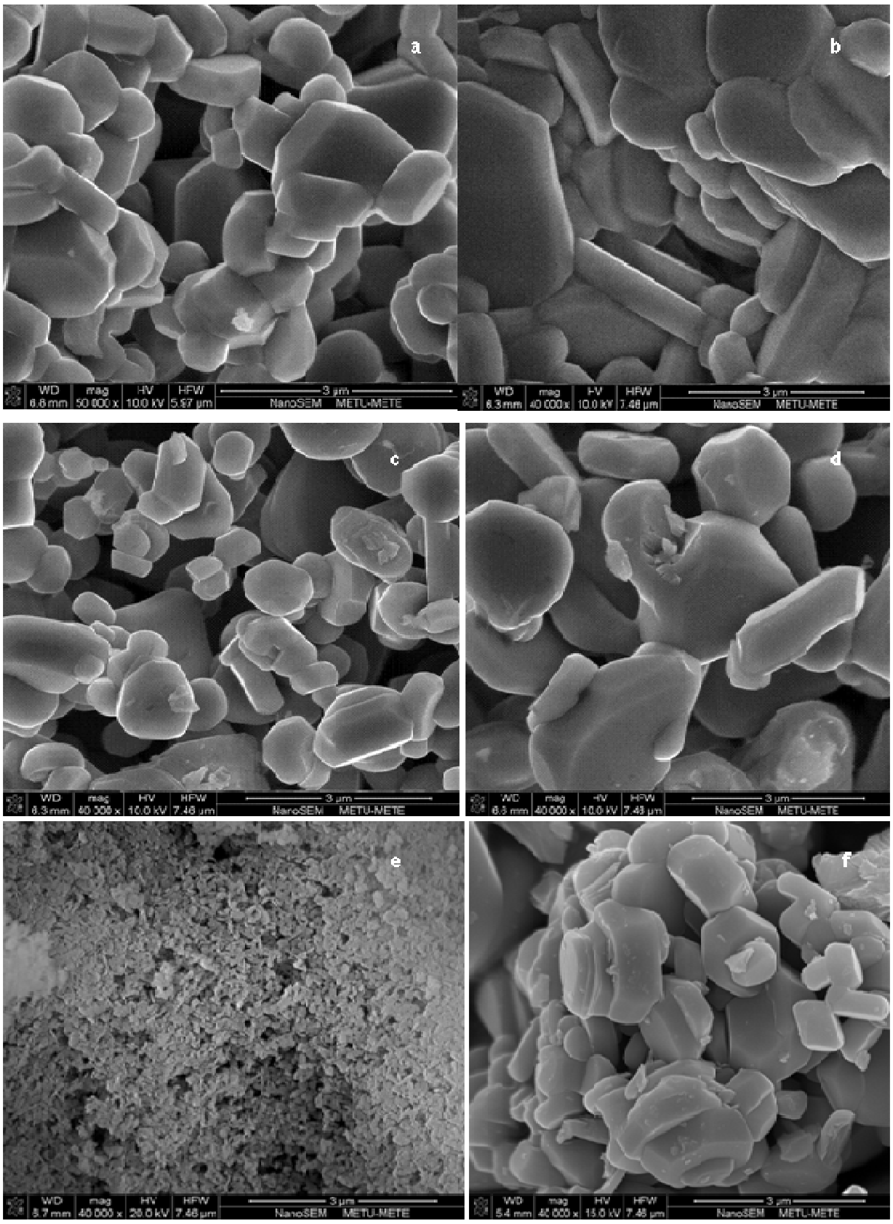

Figure 5.9. SEM photos of undoped samples, codes are given in Table 5.7.

5.3.2.2 Comparison of doped experiments

The results of the experiments with doped samples resembled with each other when the comparison was made between acetate-nitrate and hydroxide methods. For every doped element, hydroxide method yielded better results in ordering, single phase production of HT-$LiCoO_2$, particle size and incorporation of dopants into the structure. Therefore, only W doped samples are shown here which could be illustrative for other dopants as they show similar behaviour. The chemical and structural analyses of W doped samples can be seen in Table 5.8. Morphological properties are seen in Figure 5.10.

Table 5.8 and Figure 5.10 reveal interesting results. W doping depresses grain growth. With temperature the grains grow more. The particle size is the lowest and [003]/[104] ratio is the highest for the samples produced with hydroxide method. Increasing temperature causes secondary phases or unidentified peaks except for the hydroxide samples. Although 700°C is not enough for producing single phase structure, 750°C is enough for hydroxide samples. With 5 mole% W doping, single phase structure cannot be obtained.

Even though there are some minor differences in the results of other dopants, above discussion of comparison between acetate-nitrate and hydroxide methods are valid and same for them.

Table 5.8. The results and comparison of W doped experiments.

Start. Chem. (Li-Co) - W amount(%) - Code	Calcination (T-t) (°C-hr)	*c/a*	[003]/ [104]	Layered (%)	Li_4WO_5 (%)
LiA – CoN – 0 – a	850 – 24	4.994	0.701	98.71	----
LiN – CoN – 0 – b	850 – 24	4.998	0.707	99.59	----
LiH –CoH – 0 – c	850 – 24	4.995	0.866	99.40	----
LiA – CoN – 5 – d	700 – 24	5.000	0.791	79.68	Minor
LiA – CoN – 5 – e	850 – 24	4.992	0.874	94.33	4.37
LiN – CoN - 5 – f	850 – 12	4.991	0.907	91.38	5.93
LiN – CoN - 5 – g	850 – 24	4.996	0.743	88.86	----
LiN – CoN – 1 – h	750 – 24	4.995	0.869	99.79	----
LiN – CoN – 1 – i	850 – 12	4.996	0.922	95.96	2.61
LiN – CoN – 1 – j	850 – 24	4.994	0.872	99.61	----
LiH – CoH – 1 – k	750 – 24	4.996	0.931	99.40	----
LiH – CoH – 1 – l	850 – 24	4.998	0.945	99.89	----

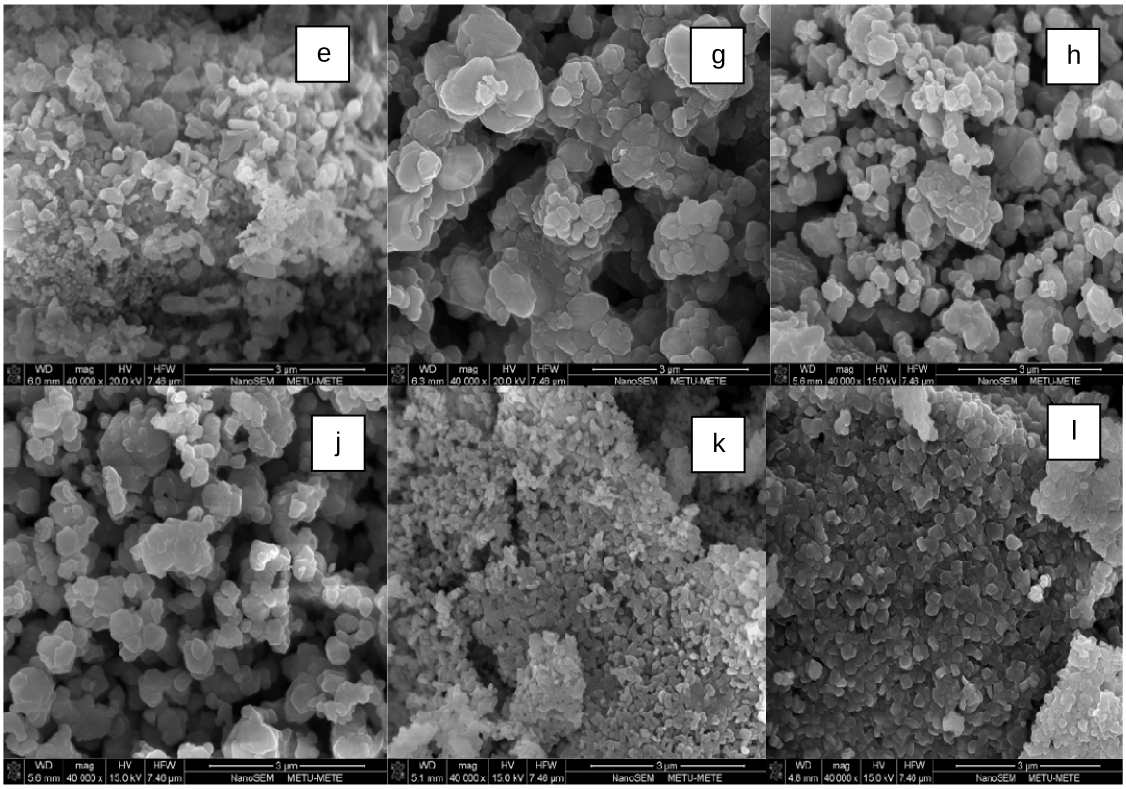

Figure 5.10. SEM photographs of W doped samples, codes are given in Table 5.8.

5.4. Comprehensive Studies with Hydroxide Method

With the experiences that were gained from the previous studies, it was decided not to apply calcination at lower temperatures such as 550°C and higher temperatures as 850°C. Instead calcination was applied at temperatures between 600°C and 750°C. With hydroxide method, the starting molarity of CoN is important as the amount of dopants and LiOH are determined accordingly. Therefore, it is decided to conduct the experiments with two different starting molarity of Co-nitrate solution, 0.1 and 0.3 M. The results will be discussed together.

5.4.1. Effect of pH

While the experiments were conducted with hydroxide methods, it was determined that close control of pH was needed during the precipitation of $Co(OH)_2$. pH value must be set around 10.7 and 10.8 for precipitating only $Co(OH)_2$ which can be understood from the pink color of $Co(OH)_2$. If pH is hold at higher values, then co-precitipation of another undesired CoO containing compound and $Co(OH)_2$ is observed. This lowers the amount of $Co(OH)_2$ which act as templates from which HT-$LiCoO_2$ is produced [34]. Production of Co containing compound during precipitation leads to formation of Co_3O_4 and Li_2CO_3 at higher temperatures (around 400°C). Eventually it is needed to eliminate both of these compounds during calcination for producing single phase HT-$LiCoO_2$.

5.4.2. Determination of the molarity of CoN

During the experiments, Li:Co:M ratio was again set as 1.2:0.99:0.01. Molarity of CoN was at values of 0.1M and 0.3M. After freeze drying for 48 hours, the precursors were calcined for 1, 4, 12 and 24 hours at 700°C and 750°C. For all doped samples, calcining for 1 and 4 hours at the indicated temperature did not yield single phase HT-$LiCoO_2$. Moreover calcining at 600°C for 24 hours did not yield good results. Therefore the data related with these calcination times and temperatures are not given. The other results are given in Table 5.9.

From Table 5.9, it is seen that, although 650°C seems enough for Mo doping, *c/a* value, especially lattice parameter *c* value is low when compared with other calcination parameters. Therefore, it is concluded that at least 700°C is needed for producing single phase HT-$LiCoO_2$ with [003]/[104] ratio being approximately 1 and *c/a* value being 4.99.

When the purity of HT-$LiCoO_2$ is considered, 0.1 M CoN and 0.3 M CoN do not yield different results. In addition to this, lattice parameters *c* and *a* as well as *c/a* ratio do not change. In contrast, it seems that [003]/[104] ratio depends on molarity of CoN as experiments beginning with 0.1M CoN yield higher [003]/[104] ratio. However; this ratio is higher than 1 for almost all doped samples. Moreover; when the comparison is made when calcination temperature is 750°C and time is 24 hours, the difference of this ratio gets smaller. The comparison of average [003]/[104] ratio of different molarities can be seen from Table 5.10. The average is found by using the ratio of [003]/[104] for doped samples at the indicated molarity, calcination time and temperature. The average for [003]/[104] ratio and lattice parameter *c* for doping elements are calculated by taking the averages of experiments in which calcination is applied at 700°C for 24 hours and at 750°C for 12 hours and 24 hours, separately.

From Figure 5.11, SEM photos of the doped samples produced with different molarities of CoN can be seen. Particle size and morphology did not change with the change of the molarity of CoN. In other words, the effect of molarity of CoN on particle size is very low. It is also seen that Cr containing samples have the largest particle size and the least homogeneously distributed particles. There is no large difference between the particle size of the other samples containing Mo, Mn and W. The particle size of layered $LiCoO_2$ containing Cr is between 500-600 nm, and that of layered $LiCoO_2$ containing other elements is between 200-300 nm. The shapes of the powders are more or less uniaxial.

When Table 5.10 is investigated, it is seen that no any dopants at a certain molarity show better results in terms of [003]/[104] ratio and lattice parameter *c*. For example, Cr doped samples have higher value of lattice parameter *c* but lower ratio of [003]/[104] for 0.3 M CoN. The behaviour is inversed for W doped samples and the difference between ratios of [003]/[104] becomes insignificant. Mn and Mo doped samples have higher lattice parameter *c* and [003]/[104] ratio for 0.1 M CoN. Although conducting experiments with CoN molarity of 0.1 M seem to yield better results, the difference from 0.3 M is not substantial. When the amount of starting chemicals is taken into consideration, continuing the experiments with using 0.3 M CoN seems better alternative. For example, if 0.1 M CoN is used, to achieve the stoichiometric formula for $LiCr_{0.01}Co_{0.99}O_2$, only 4.1 µg of CrO_3 must be weighed or 7.2 µg of AMoT must be weighed. These masses are so low that careful attention must be paid.

Table 5.9. The results with the hydroxide method with different CoN molarity.

	Sample code	Layered (%)	Li_2CO_3 (%)	*c* (Å)-*a*(Å)-*c/a*	V (Å)^3	[003]/ [104
0.3 M CoN solution	HHCr1-700-12	97.71	1.96	14.053-2.816-4.990	289.528	1.021
	HHCr1-700-24	99.64	Minor	14.060-2.817- 4.992	289.807	0.984
	HHCr1-750-12	96.31	2.26	14.058-2.816- 4.992	289.652	0.970
	HHCr1-750-24	99.58	Minor	14.062-2.817- 4.993	289.846	0.978
	HHMo1-700-12	98.68	1.18	14.067-2.818- 4.992	290.194	1.118
	HHMo1-700-24	99.44	Minor	14.070-2.818- 4.992	290.387	1.116
	HHMo1-750-12	99.55	Minor	14.068-2.818- 4.992	290.219	1.086
	HHMo1-750-24	99.65	Minor	14.065-2.817- 4.993	290.020	1.094
	HHMn1-700-12	99.06	Minor	14.067-2.818- 4.992	290.164	1.118
	HHMn1-700-24	99.75	0.25	14.073-2.819- 4.993	290.469	1.048
	HHMn1-750-4	99.52	Minor	14.065-2.818- 4.992	290.095	1.086
	HHMn1-750-12	99.79	Minor	14.068-2.817- 4.994	290.014	1.082
	HHMn1-750-24	99.79	Minor	14.069-2.817- 4.994	290.144	1.072
	HHW1-700-12	98.99	1.01	14.075-2.821- 4.990	290.912	1.043
	HHW1-700-24	99.39	Minor	14.069-2.818- 4.992	290.353	1.075
	HHW1-750-12	99.50	Minor	14.067-2.818- 4.992	290.177	1.028
	HHW1-750-24	99.61	Minor	14.069-2.819- 4.992	290.308	1.060
0.1 M CoN solution	HHCr1-650-24	97.53	2.07	14.059-2.819- 4.988	290.175	1.139
	HHCr1-700-12	99.46	Minor	14.059-2.818- 4.989	290.097	1.039
	HHCr1-700-24	99.64	Minor	14.057-2.817- 4.990	289.765	1.245
	HHCr1-750-12	99.50	Minor	14.057-2.817- 4.991	289.726	1.181
	HHCr1-750-24	98.95	Minor	14.058-2.817- 4.991	289.768	0.922
	HHMo1-650-24	99.18	Minor	14.061-2.819- 4.988	290.316	1.495
	HMo1-700-12	99.67	Minor	14.073-2.820- 4.991	290.699	1.208
	HHMo1-700-24	99.64	Minor	14.078-2.820- 4.992	290.903	1.410
	HHMo1-750-12	100.00	-----	14.075-2.820- 4.990	290.891	1.393
	HHMo1-750-24	99.85	Minor	14.071-2.819- 4.992	290.520	1.407
	HHMn1-650-24	98.58	1.42	14.068-2.819- 4.991	290.438	1.403
	HHMn1-700-12	99.70	Minor	14.072-2.819- 4.992	290.547	1.346
	HHMn1-700-24	99.75	Minor	14.069-2.818- 4.993	290.261	1.280
	HHMn1-750-12	99.85	Minor	14.069-2.818- 4.993	290.201	1.228
	HHMn1-750-24	99.84	Minor	14.074-2.819- 4.993	290.529	1.307
	HHW1-650-24	97.22	1.50	14.067-2.819- 4.989	290.526	0.984
	HHW1-700-12	99.35	Minor	14.070-2.819- 4.991	290.517	1.018
	HHW1-700-24	99.72	Minor	14.073-2.819- 4.992	290.578	0.999
	HHW1-750-12	99.67	Minor	14.071-2.818- 4.993	290.299	0.978
	HHW1-750-24	99.67	Minor	14.073-2.818- 4.994	290.403	1.004

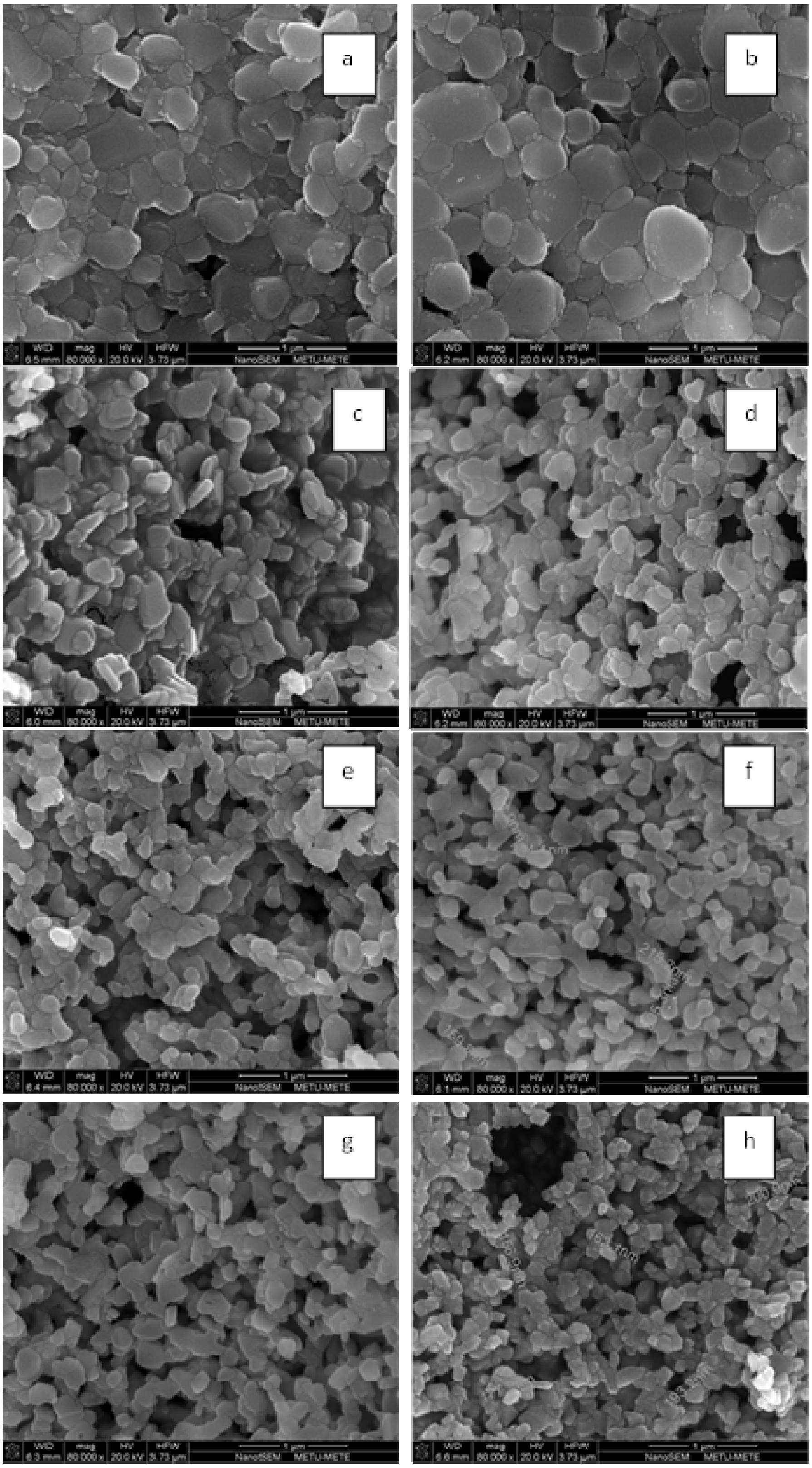

Figure 5.11. SEM photos of doped layered $LiCoO_2$, Cr (a-b), Mo (c-d), Mn (e-f), W (g-h), left column belongs to samples with 0.3 M CoN, right column with 0.1 M CoN.

Table 5.10. Averages of [003]/[104] ratio and lattice parameter *c* for doped samples having CoN molarity of 0.1 M and 0.3M.

Calcination Temperature and Time	Molarity of CoN (M)	Average of [003]/[104] ratio	*c* (Å)
700°C – 24 h.	0.3	1.056	14.0680
750°C – 12 h.	0.3	1.042	14.0651
750°C – 24h.	0.3	1.051	14.0664
700°C – 24 h.	0.1	1.234	14.0694
750°C – 12 h.	0.1	1.195	14.0677
750°C – 24h.	0.1	1.160	14.0690
Doping Element	Molarity of CoN (M)	Average of [003]/[104] ratio	*c* (Å)
Cr	0.3	0.977	14.0602
Cr	0.1	1.116	14.0571
Mo	0.3	1.099	14.0677
Mo	0.1	1.403	14.0748
Mn	0.3	1.067	14.0699
Mn	0.1	1.272	14.0705
W	0.3	1.054	14.0683
W	0.1	0.994	14.0725

During EDX analyses, it was intended to find a region and/or particle that contained higher amount of the alloying elements than the general. Therefore it was applied at the magnifications of x5.000, x40.000 and about x3.000.000. With this method, differences for the amount of Cr, Mo, Mn and W could not be found and their contents lied between 0.5 and 3 mole%. However; when EDX was applied to the sample that contained the highest amount of Li_2CrO_4 (coded as HHCr1-750-12 in Table 5.9 and produced with 0.1M CoN solution), there was a region/particle that contained 45 weight% Cr. Considering that Li_2CrO_4 contains 40 weight% Cr, it was believed that this particle is Li_2CrO_4 (Figure 5.12). So with this result, it is claimed that EDX yields nearly correct results for determining the incorporation of dopants into the layered structure.

After the experiments conducted for producing doped layered $LiCoO_2$, it is decided to use hydroxide method for further studies. Due to the experiences with freeze drying, the time of this process was lowered to 24 hours and no change was observed in the drying performance. Therefore, duration of freeze drying was lowered to 24 hours for the samples produced hereafter.

Although 1 mole% doping yielded satisfactory results with respect to purity of layered $LiCoO_2$, [003]/[104] ratio, splitting of [006]-[102] and [108]-[110] peaks and lattice parameters *c*,*a* and *c/a* values, it was thought that with more amount of doping, the discussion on the structure of layered $LiCoO_2$ could be made more explicitly. Therefore doping of 3 and 5 mole% with M (Cr, Mo, Mn and W) elements were also studied.

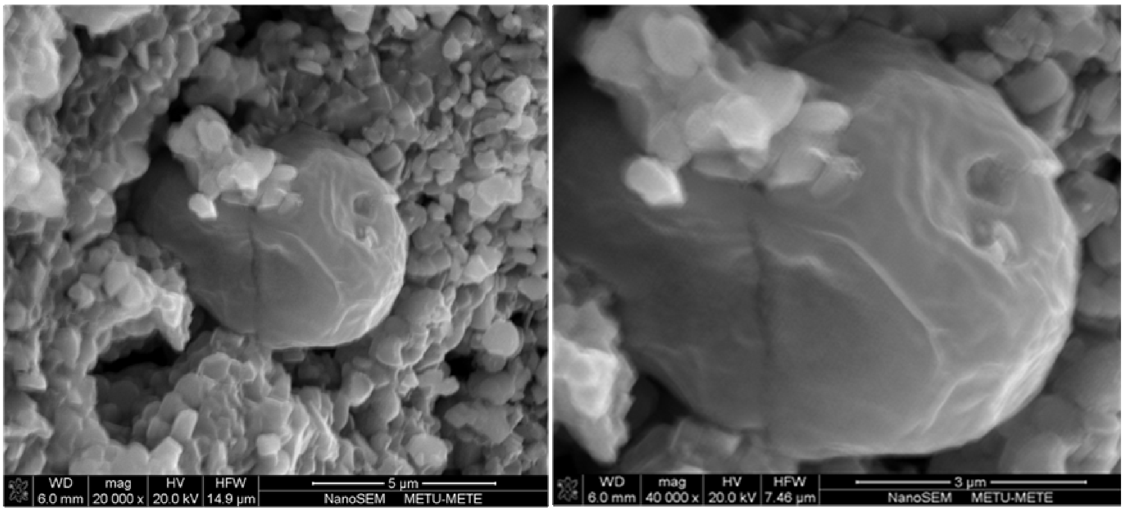

Figure 5.12. High Cr containing particle, left x20000 and right x40000 magnified.

5.4.3. Doping with Higher Amounts

With Mn doping, Mn containing impurity phase did not occur, so Mn was added with 10 mole% instead of Co. The studies were conducted by using 0.3 M of CoN solution. The freeze dried precursors were subject to calcination at 700°C and 750°C for 24 hours. From XRD patterns (Figure 5.13), it is seen that for doping contents of 5 mole%, secondary phases (M containing phase, Li_2CO_3, Co_3O_4, spinel $LiCoO_2$) were formed. The results of the Rietveld analyses are given in Table 5.11. The results belong to calcination at 750°C for 24 hours.

Table 5.11. The results of the studies with 3 and 5 mole% doping.

Sample	Layered (%)	*c* (Å)	*a* (Å)	*c/a*	I_{003}	I_{104}	[003]/[104]
HHCr1-750	99.58	14.0628	2.817	4.992	78.52	80.30	0.978
HHCr3-750	99.48	14.0671	2.819	4.990	76.38	80.27	0.952
HHCr5-750	83.76	14.0691	2.819	4.991	70.38	71.44	0.985
HHMo1-750	99.00	14.0761	2.820	4.992	53.50	48.92	1.094
HHMo3-750	93.35	14.0796	2.820	4.993	67.32	68.09	0.989
HHMo5-750	89.05	14.0742	2.820	4.991	67.85	68.27	0.994
HHMn1-750	99.04	14.0778	2.820	4.993	79.05	73.71	1.072
HHMn3-750	88.97	14.0877	2.821	4.994	59.54	63.58	0.936
HHMn5-750	95.18	14.0930	2.821	4.995	53.08	59.97	0.885
HHMn10-750	87.19	14.1078	2.825	4.995	49.73	59.84	0.831
HHW1-750	100.00	14.0783	2.821	4.991	71.25	67.21	1.060
HHW3-750	87.53	14.0894	2.823	4.991	52.36	56.67	0.924
HHW5-750	83.61	14.0983	2.824	4.992	48.51	52.89	0.917

From Table 5.11, it is clearly seen that, with doping amount lattice parameters *a*, *c* and *c/a* values for W and Mn doped samples increase. In contrast to these, ratios of [003]/[104] decrease. With these results, it can be claimed that W and Mn can be incorporated into the structure of layered $LiCoO_2$. Moreover, some of them should go to Li-site so that ratio of [003]/[104] decreases. It is also deduced that with increase in doping amount, crystallinity gets worse which is evidenced from the values of the intensities of [003] and [104] peaks, individually. For Mo and Cr, such a conclusion cannot be drawn, easily. Instead, it can be claimed that the solubility of layered $LiCoO_2$ for Mo is lower than 3 mole% as the purity of layered structure is lowered without significant change or uniform increase in lattice parameters *a*, *c* and *c/a* values like that of W and Mn doped samples. With Mo doping content increasing beyond 1 mole%, intensities of [003] and [104] peaks as well as [003]/[104] ratio do not change. The same discussion is valid for Cr doped samples but it is not as certain and obvious like Mo doped samples.

Regardless of the type of the doping element and the effect of the dopants on the structure, it is certain that doping with amounts higher than 3 mole% causes impurities.

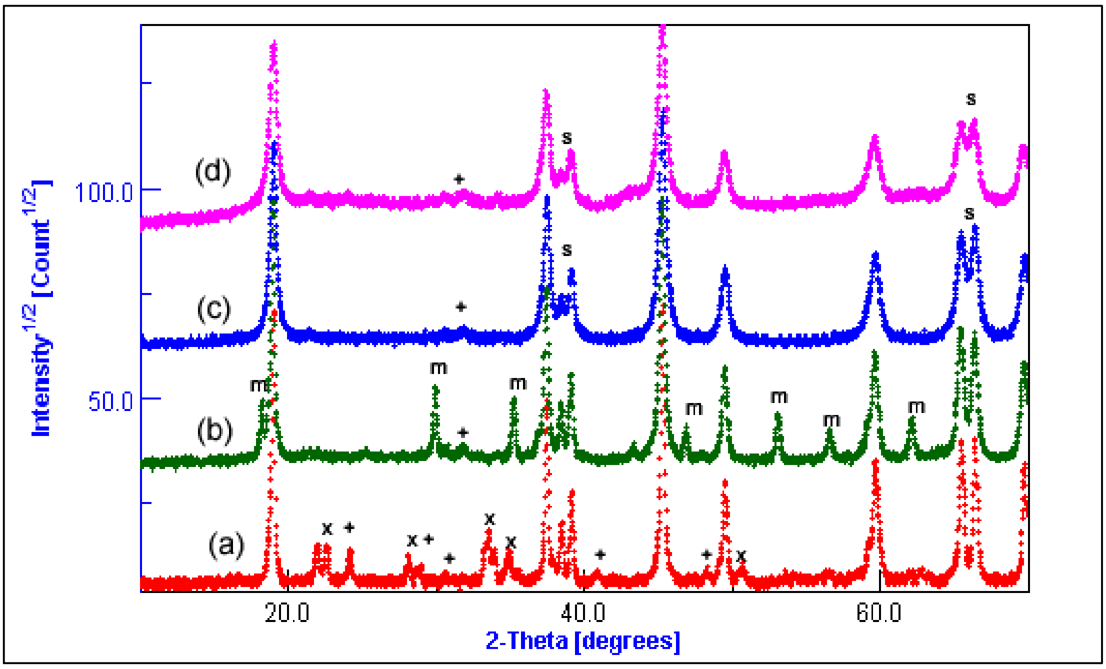

Figure 5.13. XRD Patterns of 5 mole% a) Cr, b) Mo, c) Mn, d) W doped samples calcined at 750°C for 24 hours.

From Figure 5.13, it is seen that, every doped sample has different impurities and HT-$LiCoO_2$ content. Cr doped sample contains Li_2CrO_4 (coded as “x”) and Li_2CO_3 (coded as “+”) whereas Mo doped sample contains a spinel phase having a general formula of CoMo (coded as “m”). Although, the only impurity seems to be Li_2CO_3 in Mn and W doped samples, uncompleted splitting of [006]-[102] peaks and [108]-[110] peaks as well as two bulges at about 2θ~19° (Figure 5.14) indicate the occurence of spinel LT-$LiCoO_2$ coded as "s" in Figure 5.13. Also [003] peaks of Mo and Cr doped samples are narrower than that of Mn and W doped samples. Figure 5.14 shows this difference for Cr and Mn doped samples.

The freeze dried precursors were subjected to calcination at 700°C for 24 hours. Unfortunately; the produced samples contained between 6 and 10 mole% of impurities mainly of Li_2CO_3. Therefore, another 24 hours of calcination at 700°C was carried out but impurities (Li_2CO_3) remained at levels of 5 and 10 mole% again. Having seen that 48 hours of calcination at 700°C was not enough for producing single phase HT-$LiCoO_2$, 14 hours of calcination at 750°C was applied, also. With this last process, although the amount of Li_2CO_3 lowered to about 4 mole%, it was still very high when compared with the previous experiments.

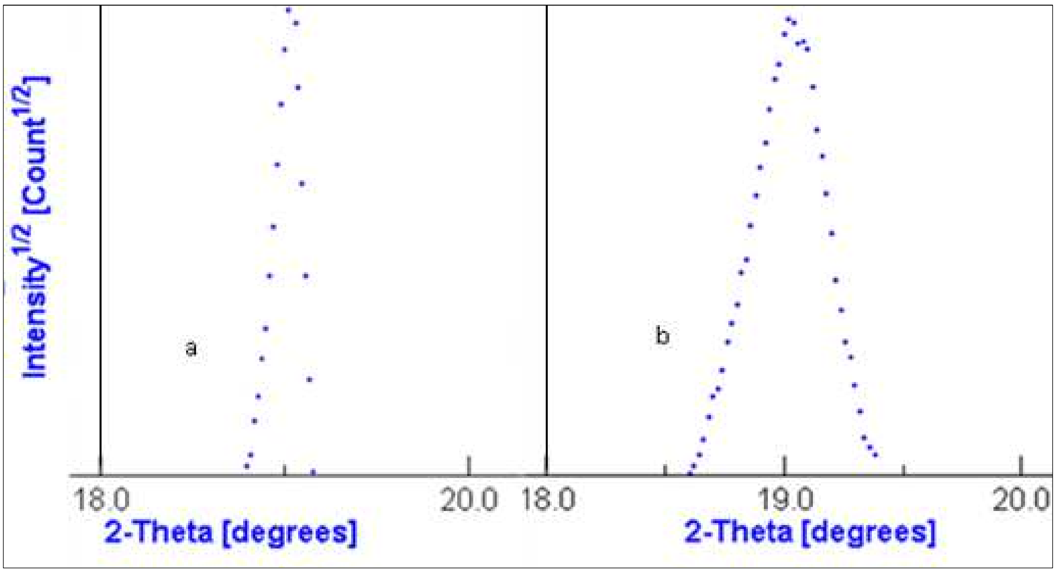

Figure 5.14. Position and appearance of [003] peaks for a) Cr, b) Mn doped samples.

5.4.4. Attempts to decrease impurity (Li_2CO_3) level

Whittingham [18] claimed that Li_2CO_3 in layered $LiCoO_2$ was useful for increasing safety of Li-ion batteries. Moreover, Nishi [103] intentionally used excess Li_2CO_3 in his study to develop a safety vent. He also insisted that residual Li_2CO_3 in the cathode material did not show any negative effect on the cycle life of the cells. However; as Li_2CO_3 forms according to below reaction [104];

$$LiCoO_2 + \frac{x}{2}CO_2 + \frac{x}{4} \Rightarrow Li_{1-x}CoO_2 + \frac{x}{2}Li_2CO_3 \qquad (5.1)$$

it is most likely that the capacity of HT-$LiCoO_2$ will be lowered as some Li will be lost as Li_2CO_3. Therefore, it was decided to do some revisions on the optimum parameters of the process. These revisions are;

a. Decreasing the Li:Co ratio from 1.2 to lower values
b. Discarding the application of pre-calcination (350°C for 2 hours).

For the “a” option, two different Li:Co ratio were used, 1.05 and 1.12. For the “b” option, two samples were produced with the same parameters but, one sample was calcined directly at 750°C for 24 hours and other sample was pre-calcined (350°C for 2 hours) before higher temperature calcination (750°C for 24 hours).

The results are listed in Table 5.12. From this table it is seen that the ratio of 1.2 for Li:Co is high so that Li_2CO_3 phase is formed even if pre-calcination is not applied. Although it is seen that Li_2CO_3 amount is 1.4 mole% for the “A” sample, the direct calcined of this sample does not contain Li_2CO_3. As the ratio of [003]/[104] which is an indication for the ordering of $LiCoO_2$ is higher for the lower ratios, it is better to use 1.05 as Li:Co ratio. Moreover, during the process after decanting of $Co(OH)_2$, no drying is applied. Therefore $Co(OH)_2$ is used as wet. It is certain that the water contain some Li ions as washing is applied with LiOH solution. Therefore, it seems that Li ions used more than it is needed for producing stoichiometric $LiCoO_2$. Hence, it is decided to use 1.05 as the ratio for Li:Co. As ratio of [003]/[104] is higher for all ratios of Li:Co in the pre-calcined sample, it is decided to pre-calcine the samples for further studies. However; in order to be more certain, a set of doping experiments with different dopant contents and Li:Co ratio were also applied. The samples were calcined at 750°C for 24 hours. The results are given in Table 5.13.

Table 5.12. The results of the experiments aiming to decrease the Li_2CO_3 content. A, B and C stands for the Li:Co ratios of 1.05, 1.12 and 1.20, respectively. “DC” suffix shows that the sample is directly calcined.

Sample	Layered (%)	Li_2CO_3 (%)	[003]/[104]	*c* (Å)	*a* (Å)	*c/a*
A	98.60	1.40	1.249	14.0677	2.820	4.989
A-DC	100.00	-----	1.001	14.0650	2.818	4.991
B	100.00	-----	1.058	14.0680	2.820	4.989
B-DC	100.00	-----	0.978	14.0666	2.818	4.992
C	99.13	0.87	1.084	14.0715	2.820	4.990
C-DC	98.67	1.33	0.971	14.0699	2.819	4.991

Table 5.13. The results of the doping experiments for decreasing the Li_2CO_3 content. A and C stands for Li:Co ratios of 1.05 and 1.2, respectively. W2 means there are 2 mole% W in the sample instead of Co.

Sample	Layered (%)	Li_2CO_3 (%)	[003]/[104]	*c* (Å)	*a* (Å)	*c/a*
A-W2	100.00	-----	1.060	14.0835	2.822	4.991
C-W2	91.74	7.44	0.912	14.0795	2.821	4.991
C-W1	92.89	6.75	1.005	14.0769	2.821	4.990

It is seen from Table 5.13 that, when Li:Co ratio is 1.05, the best results are achieved in terms of purity of layered $LiCoO_2$ and ordering characteristics. The significant change of lattice parameters shows that W is incorporated into the structure of layered $LiCoO_2$.

At the end of the studies for decreasing the Li_2CO_3 content, it is decided to use Li:Co ratio of 1.05 and apply pre-calcination in the experiments.

CHAPTER 6

ELECTROCHEMICAL CHARACTERIZATION

Samples for electrochemical characterization were produced using powders with below processing parameters:

- CoN molarity, 0.3 M
- Li:Co:M ratio, 1.05:0.99:0.01 and 1.05:0.98:0.02
- Freeze Drying Time, 24 hours
- Pre-Calcination; at 350°C for 2 hours
- Calcination; at 750°C for 24 hours

From Table 5.13, it was inferred that doping with 2 mole% was worth to study when Li:Co ratio is 1.05.

With these parameters, 10 samples were produced. These were listed in the 2nd column of Table 6.1 with their codes as undoped, Cr1, Cr2, Mo1, Mo2, Mn1, Mn2, W1, W2, W1Mn1. Hereafter these codes will be used.

Doctor Blade technique was used for preparing the cathode materials.

6.1. Structural Characterization

Figures 6.1-6.3 display the XRD patterns of 1 mole% doped samples, 2 mole% doped samples, as well as co-doping of W and Mn (W1Mn1).

From Table 6.1, the Rietveld results of these XRD patterns are seen. The codes in the second column of Table 6.1 will be used hereafter. From Table 6.1, it is obviously seen that layered single phase HT-$LiCoO_2$ can be produced. All samples have more or less ordered structure as [003]/[104] ratios are near 1. However; W1Mn1 have this ratio as 0.910. It is thought that this lower ratio is caused by occupation of Li-site by one of the doping elements, rather than Co-site. However; the lattice parameters for W1Mn1 are so high that significant occupation of Li-site cannot be proposed. C.Pan et al. [67] claimed that Cr might occur in Li-site due to their Nuclear Magnetic Resonance (NMR) studies. We saw similar behaviour with Cr doped samples so that Cr occupation of Li-site can be claimed.

In order to see whether an experimental difference and/or variation in Rietveld analyses are in question for the samples, we applied XRD to an impure undoped sample in different days. This sample was subjected to XRD for 6 times in 2 months. It was seen that the values of lattice parameter *c* were between 14.067±0.004 Å and [003]/[104] ratios were between 1.001±0.08. This value is lower than 1.2 which is the ratio to be achieved for perfect ordering according to [45]. Purity of layered $LiCoO_2$ was between 96.22±0.54 mole%.

When Figures 6.1, 6.2 and 6.3 are considered together, there are some minor differences in the samples which the detection limit for this difference is below than that of XRD and Rietveld analysis. The main visual difference of the samples is due to the completion of splitting of [006]-[012] and [108]-[110] peaks but the difference is not significant for detailed discussion.

Table 6.1. The results of the Rietveld analyses.

Doped Element and Amount	Code	Layered (%)	[003]/[104]	*c* (Å)	*a* (Å)	*c/a*
0 mole%	Undoped	100.00	1.005	14.063	2.818	4.990
1 mole% Cr	Cr1	100.00	0.949	14.059	2.818	4.989
2 mole% Cr	Cr2	100.00	1.080	14.058	2.817	4.990
1 mole% Mo	Mo1	100.00	1.024	14.067	2.819	4.990
2 mole% Mo	Mo2	100.00	1.192	14.070	2.819	4.991
1 mole% Mn	Mn1	100.00	1.015	14.070	2.818	4.993
2 mole% Mn	Mn2	100.00	0.978	14.074	2.819	4.993
1 mole% W	W1	100.00	1.048	14.070	2.819	4.991
2 mole% W	W2	100.00	1.047	14.074	2.820	4.991
1 mole% W and 1 mole% Mn	W1Mn1	100.00	0.910	14.071	2.819	4.991

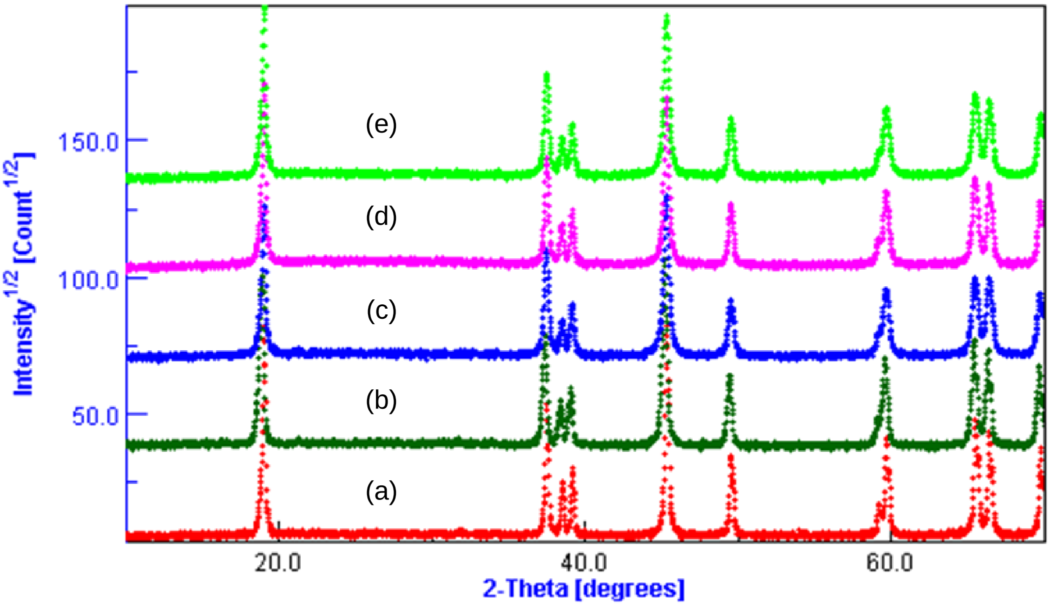

Figure 6.1. XRD Patterns of a) undoped, b) Cr1, c) Mo1, d) Mn1, e) W1.

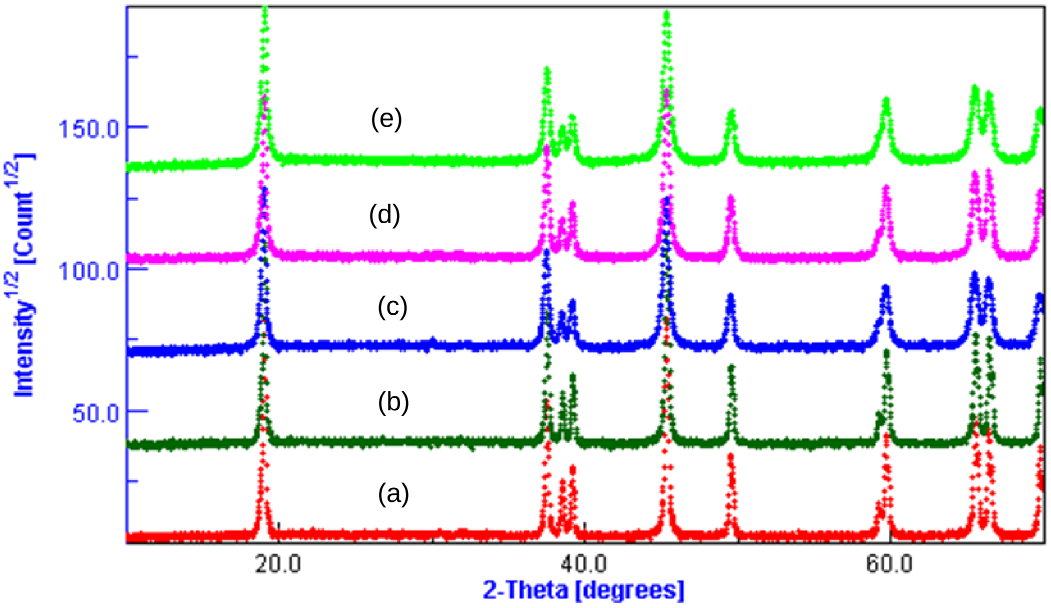

Figure 6.2. XRD Patterns of a) undoped, b) Cr2, c) Mo2, d) Mn2, e) W2.

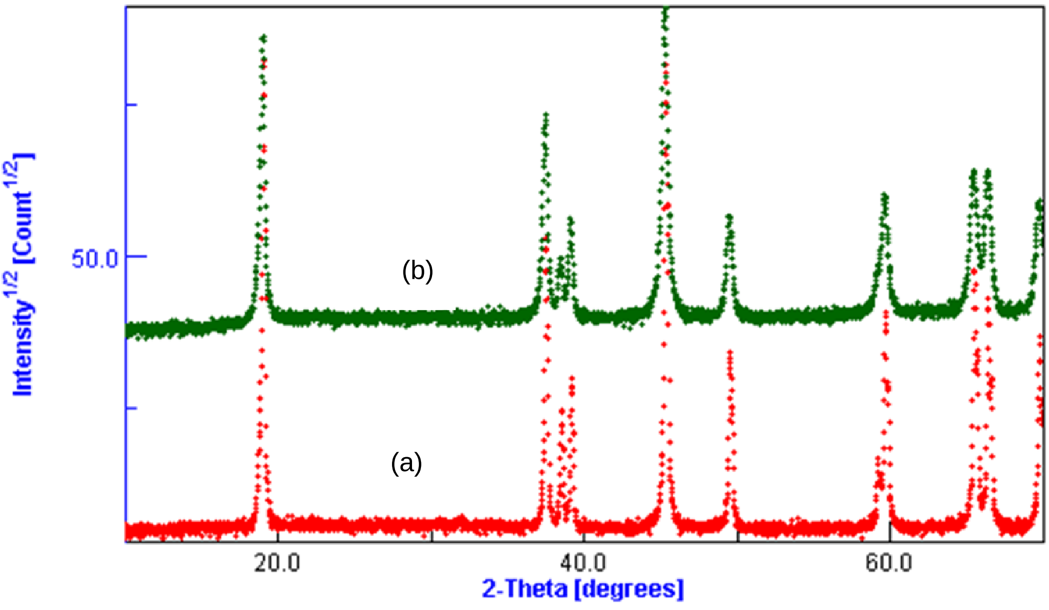

Figure 6.3. XRD patterns of a) undoped, b) W1Mn1.

6.2. Microstructure and Distribution of Dopants in the Structure

For determining the morphology and particle size distribution of samples, SEM photos were taken. Also, EDX analyses were applied for chemical analyses throughout the bulk samples.

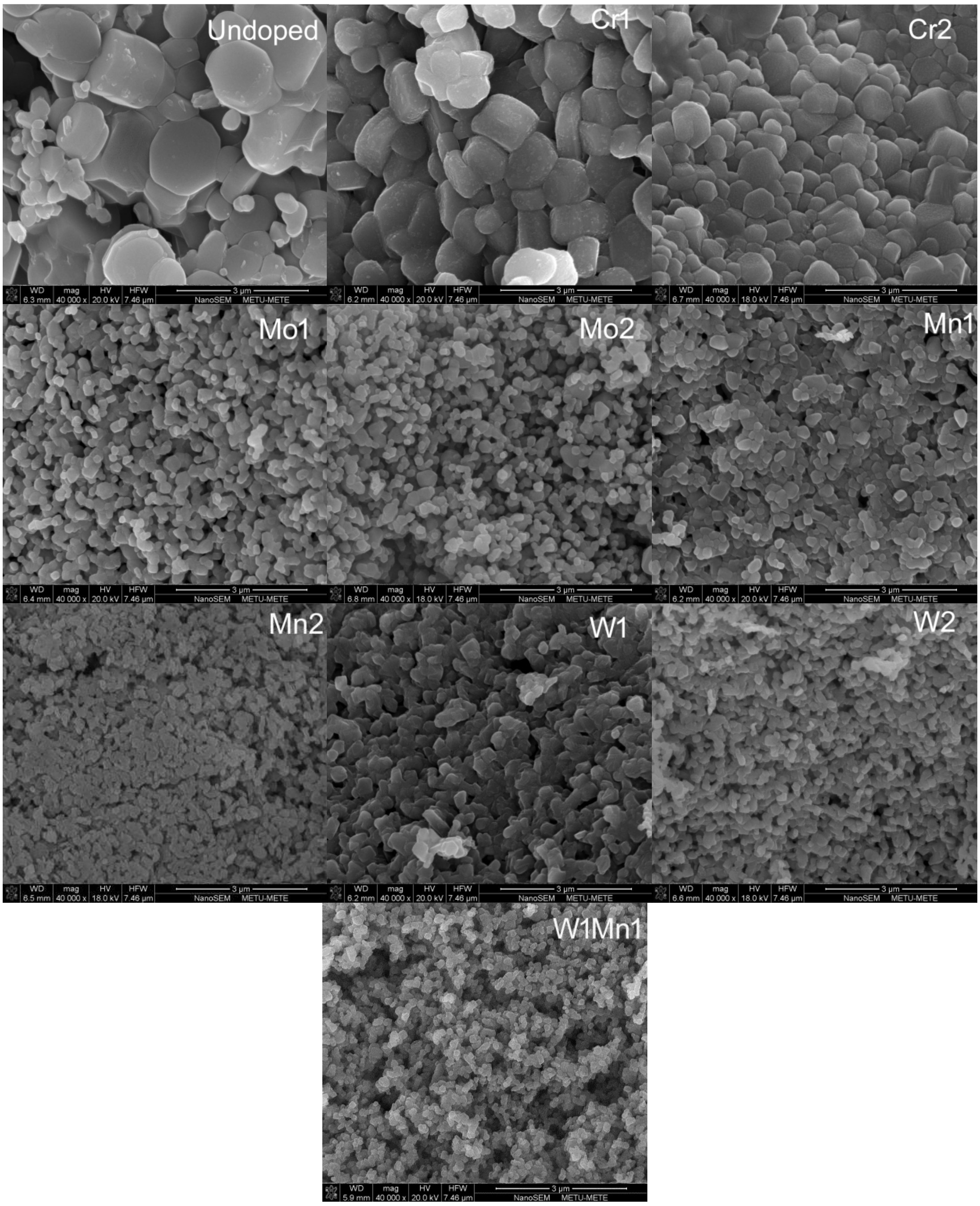

Figure 6.4. SEM photos of the doped samples.

From Figure 6.4, it is seen that particle sizes of undoped and Cr doped samples are larger than the others. Their particles sizes are in the vicinity of 600-1000 nm while the others have the particle sizes of about 200-500 nm. Also it is seen that the samples containing 1 mole% dopants have larger particle size than these of having 2 mole% dopants. W1Mn1 has nearly the same particle size with 2 mole% doping elements. It can be easily claimed that doping elements act as grain growth inhibitors. Although the shape of the powders is not uniform, it is seen that the shape is between hexagon and sphere.

EDX was applied to different regions in the samples. The doping content and EDX results are nearly same. Besides EDX, mapping is applied for all the materials in order to decide on the uniform distribution of Co and doping elements. The pictures taken during mapping are given in Figure 6.5. From mapping pictures, it is seen that the doping elements are uniformly distributed throughout the matrix phase, $LiCoO_2$. During mapping, the regions that contain different doped elements are tried to be used. For example, for 1 mole% Cr doping, a region that contains 1, 3 and 5 mole% Cr is used for mapping. If such a region cannot be found, mapping is applied at a region that seems different than the general appearance of the material. Only the mapping pictures of 2 mole% doped samples are given in Figure 6.5.

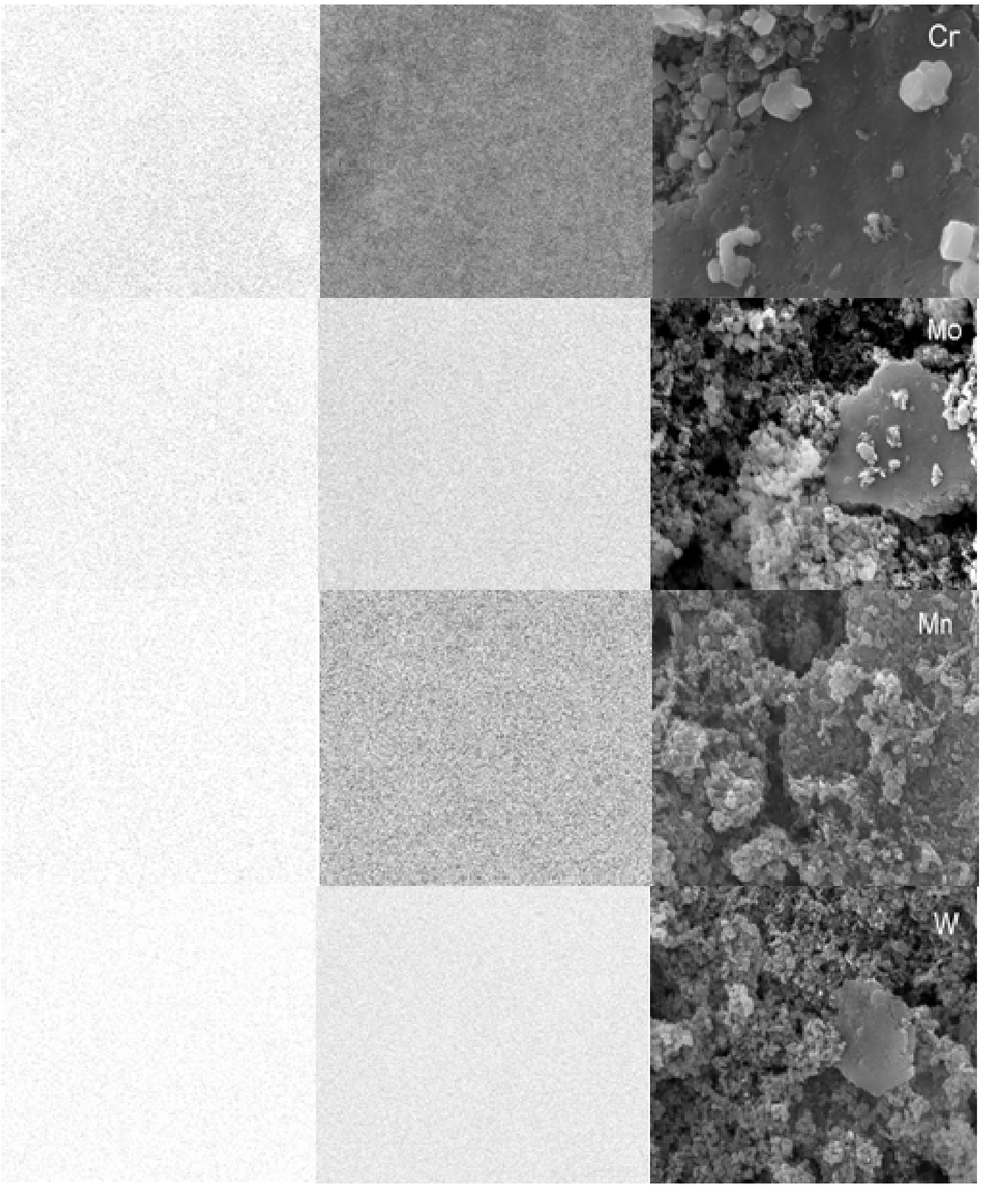

Figure 6.5. The mapping of 2 mole% doped samples, middle pictures belong to Co and left pictures belong to doped elements.

Mapping is also applied for the sample W1Mn1 and it is seen that W, Mn and Co is uniformly distributed throughout the matrix phase, $LiCoO_2$. The mapping of W1Mn1 is given in Figure 6.6.

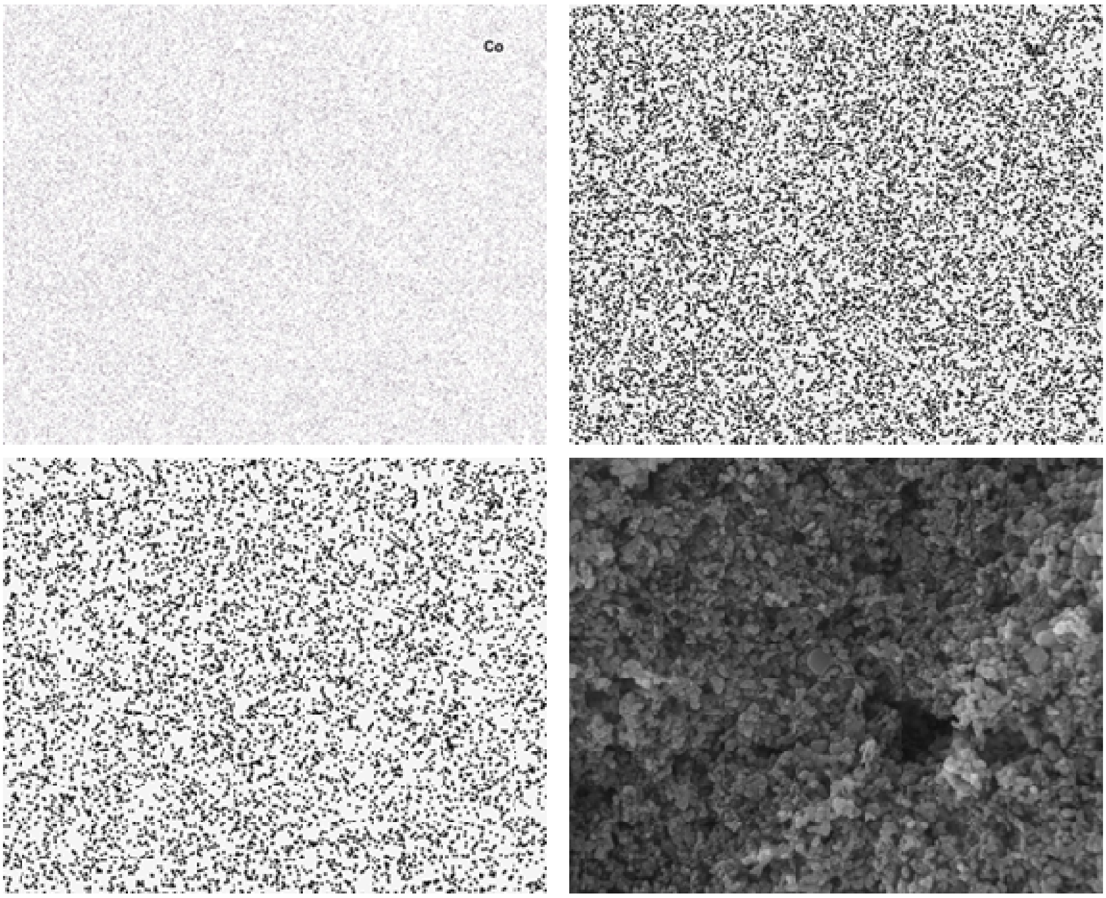

Figure 6.6. The mapping of W1Mn1, upper left is for Co, upper right is for Mn and lower left is for W as well as the photo (lower right) of the region.

In order to test the validity of mapping, a sample having high amount of second phase was used. For this purpose, a sample that had 1.43 weight % Li_2CrO_4 as an impurity phase was used. First the sample was thoroughly investigated in order to find a region having different appearance than the general appearance. After deciding for such a region, EDX was applied and Cr content was found about 16 mole% which was higher than the bulk Cr content. Therefore it was decided to apply mapping at this region. Figure 6.7 reveals the mapping and Table 6.2 gives the chemical analysis of the region.

As seen from figure 6.7, by mapping, regions containing different elemental distribution can be distinguished (the amount of Co is very low at the flat particle which is at the bottom of the picture or the amount of Cr at the flat particle is more than the other part of the region).

Therefore as uniform distribution of dopants is seen at other samples, we can conclude that doping elements are incorporated into structure of layered $LiCoO_2$.

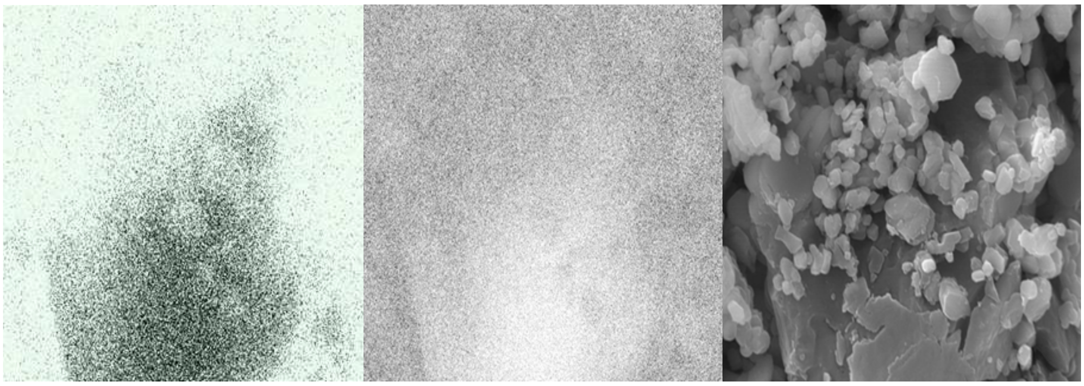

Figure 6.7. Mapping of sample having a region containing high Cr (left side) and Co (middle) as well as the photo (right) of the region.

Table 6.2. EDX results of the region mapped and depicted in Figure 6.7.

Element	Weight %	Mole %
CrK	14.53	16.16
CoK	85.47	83.84

6.3. Galvanostatic Charge-Discharge Tests

6.3.1. Discharge Capacities and Cycleability of Samples

After having decided that the doping elements were incorporated, electrochemical properties of the samples were determined.

The first technique used for this purpose was charge-discharge tests. The cycle test was conducted between 2.75-4.25 V. Two sets of tests were applied to the samples. In the first set, the charge rate was held at 0.3C (1C corresponds to 140 mAh/gr) and in the second set, the charge rate was held at 1C. For both sets, discharge rate was 0.3C, 0.75C, 1.5C and 3C for each 20 cycles. In the first set, last 5 cycles were reserved for charging and discharging with 0.3C. In the second set, 5 more cycles were applied for charging with 1C and discharging with 0.3C and finally, last 5 cycles were reserved for charging with 0.3C and discharging with 0.3C. To sum up, 85 cycles were applied in the first set, and 90 cycles were applied in the second set excluding the first charge-discharge cycle in which charge rate and discharge rate were 0.3C. The results of the charge-discharge tests of the first set (charge rate, 0.3C) for 1 mole% doped samples can be seen from Figure 6.8.

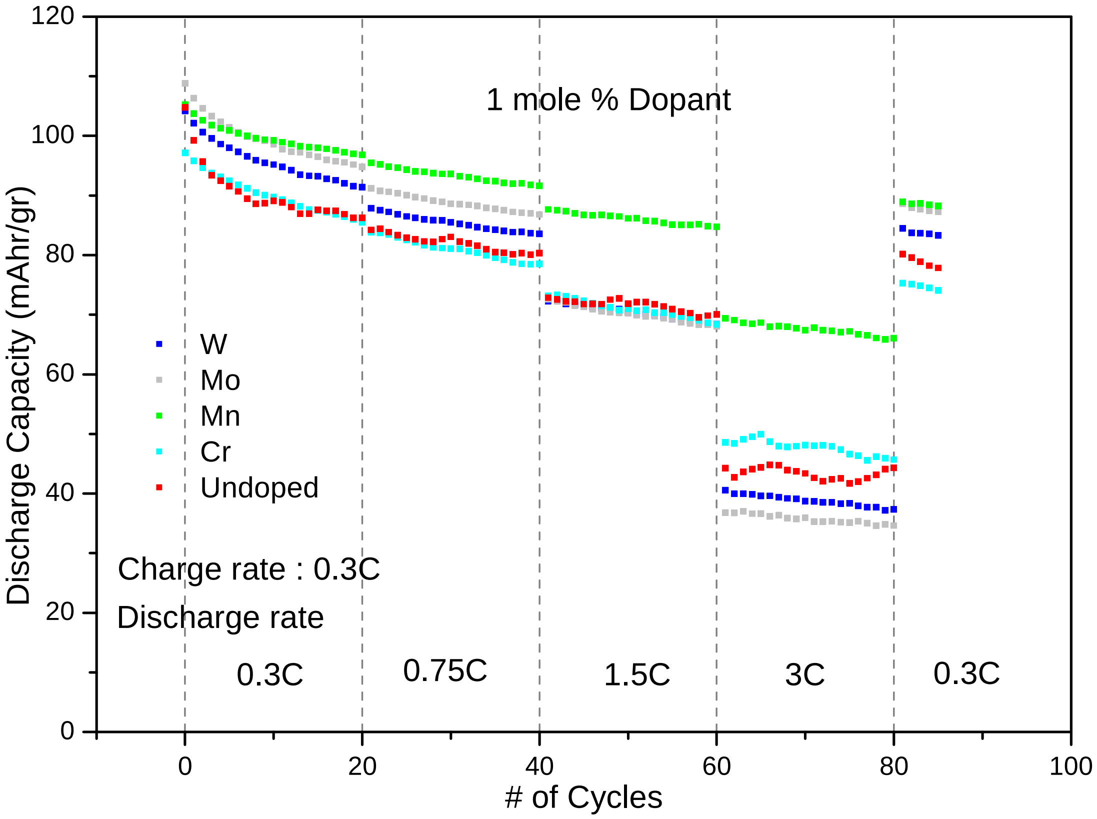

Figure 6.8. Charge-discharge curves of 1 mole% doped samples when charge rate is 0.3C.

Figure 6.8 reveals that Mn1 has the best cycling behaviour while Cr1 has the worst behaviour at the end of the full set. Increasing the discharge rate results in better performance with Mn1. Higher discharge rates make the performance of Mo1 worse, however, it can gain a significant amount of capacity when discharge rate is lowered. The first discharge capacity is almost same for all samples except Cr1. The value of this parameter for undoped, Cr1, Mo1, Mn1 and W1 is 104.8, 97.2, 108.8, 105.2 and 104.2 mAh/gr, respectively. At the end of the 81st cycle, undoped, Cr1, Mo1, Mn1 and W1 have capacity retention of 42.3, 47.0, 31.8, 62.8 and 35.8%, respectively. When these samples were charged one more time with 0.3C charge rate, it is seen that capacity retention increases for all samples. The capacity retention for undoped, Cr1, Mo1, Mn1 and W1 is 76.5, 77.5, 81.4, 84.5 and 81.1%, respectively. Therefore it can be claimed that, Mn doped sample shows the best charge-discharge behaviour in terms of cycleability and high rate capability. High rate capabilities of Mo1 and W1 are very low while both samples have sufficient capacities at moderate discharge rates (0.3C-0.75C). Although Cr1 shows good high rate capability, its capacity retention is the worst at the end of the whole cycle.

The results of the charge-discharge tests for 2 mole% doped samples are given in Figure 6.9 from which it is interestingly seen that Cr2 has the best high rate capability. It is also seen that this sample has the worst capacity gain at the end of the whole cycle. Excluding Cr2, undoped sample has the worst electrochemical behaviour. The first discharge capacity does not change significantly but this time undoped sample has the highest first discharge capacity. The value of this parameter for undoped, Cr2, Mo2, Mn2 and W2 is 104.8, 100.1, 100.6, 102.3 and 103.3 mAh/gr, respectively. At the end of the 81st cycle, undoped, Cr2, Mo2, Mn2 and W2 have capacity retention of 42.3, 57.1, 36.0, 31.2 and 30.4%, respectively. When these samples were charged one more time with 0.3C charge rate, it is seen that for all samples capacity retention increase. The capacity retention for undoped, Cr2, Mo2, Mn2 and W2 is 76.5, 71.3, 81.8, 80.5 and 82.4%, respectively. For 2 mole% doped sample, a general trend for all of the electrochemical properties cannot be reached. The first discharge capacity is better for undoped, high rate capability is the best for Cr2 and capacity retention is highest for W2 throughout the whole cycle. Although high rate capability of Cr2 is the best, capacity retention is the worst for this sample. This is very interesting result and the reason of this result is unknown.

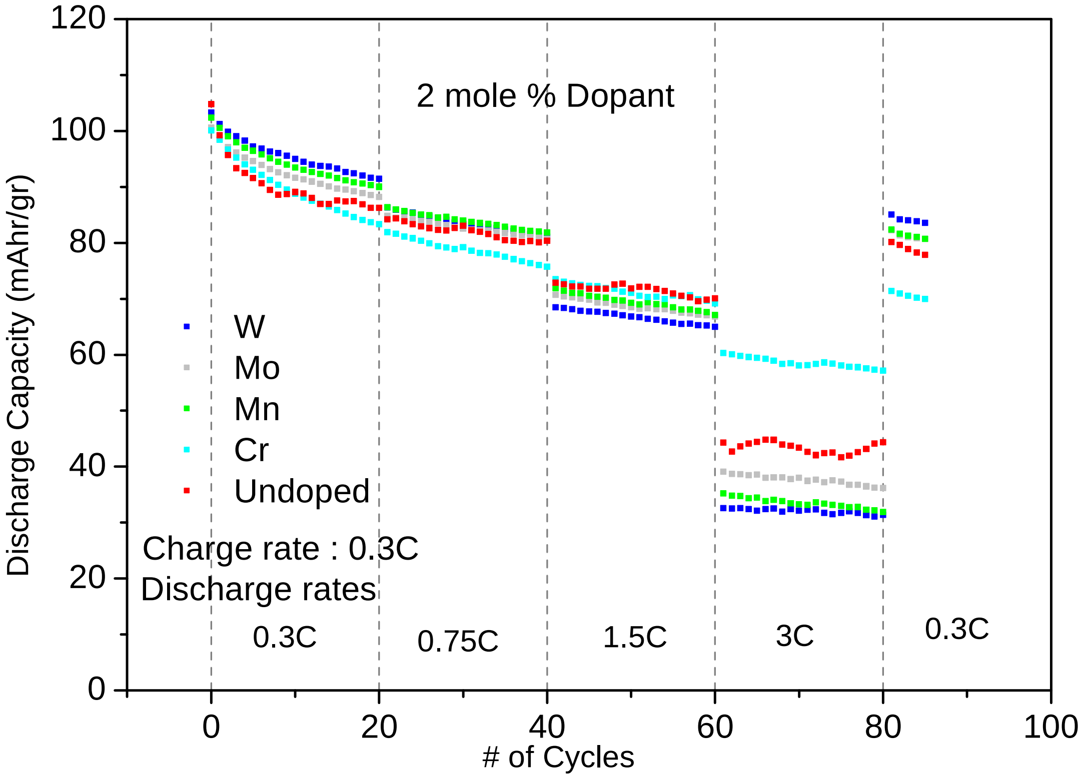

Figure 6.9. Charge-discharge curves 2 mole% doped samples when charge rate is 0.3C.

It is also deduced that doping with a content of 2 mole% gives worse electrochemical behaviour than 1 mole% doping. The results are displayed in Figure 6.10. Both of the doping content recovers well after discharged at higher rates. For Cr doped samples, Cr2 has better high rate capability, while cycleability is better for Cr1. All electrochemical performance of W1 and Mn1 is better than W2 and Mn2, respectively. For Mo doped samples, although Mo1 shows better electrochemical performance, Mo2 has slightly better high rate capability. Excluding high rate capability (discharge rate of 3C), Cr and Mo doped samples have almost same gap between the discharge results indicating that there is no much difference between 1 mole% and 2 mole% doping contents when cycleability is considered. However; for Mn and W doped samples, increasing discharge rate leads to gradual increase of the gap between 1 mole% and 2 mole% doping of these elements. The increase of gap for W doped samples is smaller than that of Mn doped samples.

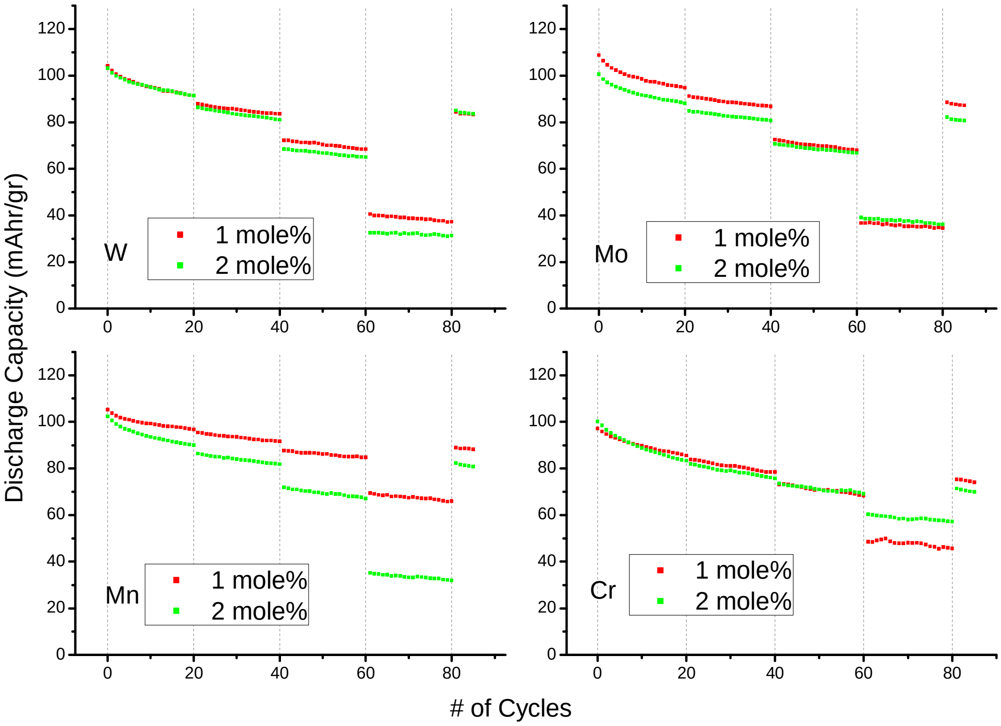

Figure 6.10. Charge-discharge behaviour of 1 mole% and 2 mole% doped samples when charge rate is 0.3C.

After completing the set having the charge rate of 0.3C, the second set in which charge rate was 1C was applied. Figure 6.11 reveals the results of 1 mole% doped sample when charge rate is 1C. The first cycle of this set contains charge and discharge rates of 0.3C.

From Figure 6.11, it is seen that Cr1 has the best cycling behaviour while W1 has the worst behaviour at the end of the cycles with charge rate of 1C. Recalling that the last 5 experiments were conducted with charge rate of 0.3C, it is again seen that Mo1 gains the capacity that is lost with higher discharge rates. After 81 cycles, while W1 retains about 35.8% of its first discharge capacity with lower charge rates (0.3C), it only retains 25.1% of the first discharge capacity with charge rate of 1C. Interestingly, this value is the worst among other doped samples. Mn1 shows similar behaviour, capacity retention of this sample when charge rate is 1C is nearly halved when compared with charge rate of 0.3C (37.7%

versus 62.8%). The comparison of capacity retentions towards different charge rates reveal same results for Mo1 (31.8% versus 29.1%). As usual, an exception is seen for Cr1 which is the only sample having higher capacity retention when charge rate is 1C (52.0% versus 47.0). The first discharge capacity does not change significantly but this time Mn1 has the highest first discharge capacity. The value of this parameter for undoped, Cr1, Mo1, Mn1 and W1 is 95.7, 89.7, 92.5, 98.5 and 89.2 mAh/gr, respectively. First discharge capacities of all samples are decreased with increasing charge rate. Mn1 has the highest capacity among 1 mole% doped samples. It is to be remembered that the first squares in figures showing the results of tests with 1C charge rate, belong to preliminary test which has charge and discharge rate of 0.3C for one cycle.

The comparison of doped samples with different charge rates can be seen schematically in Figure 6.12. From this figure, it is obviously seen that all samples show worse cycleability with higher charge rates as expected. Interestingly, Cr1 has better high rate capability with 1C charge rate and high rate capability of Mo1 seems independent of charge rate. Other samples show notable differences with increasing charge and discharge rates.

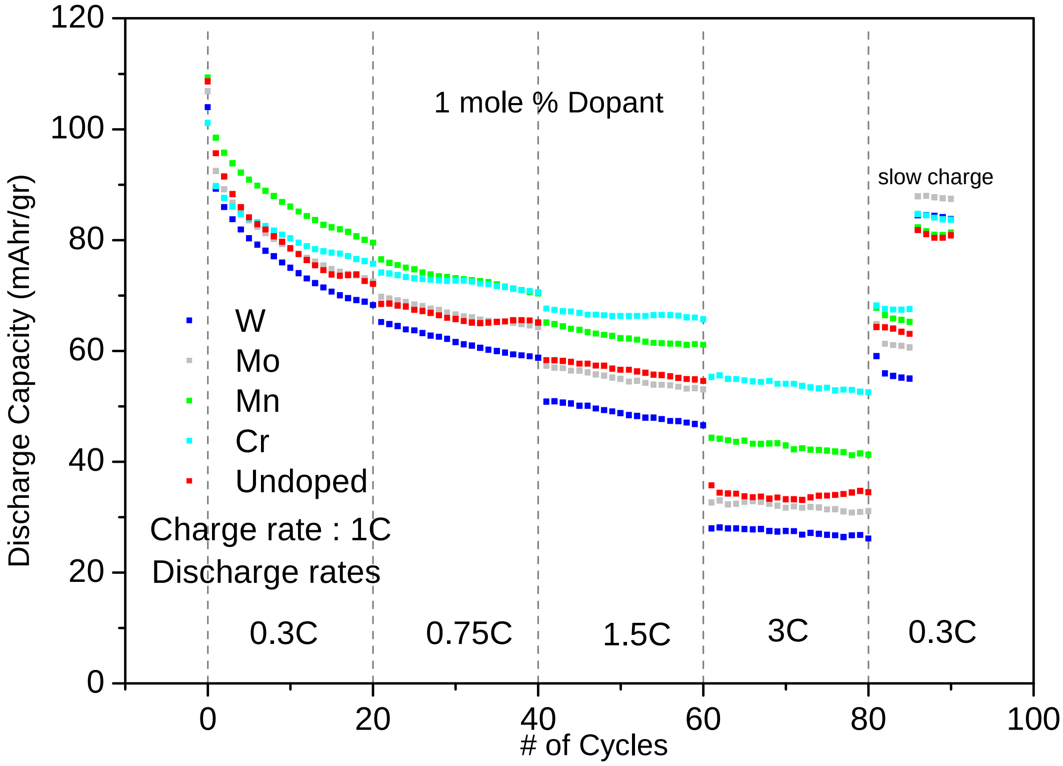

Figure 6.11. Charge-discharge curves of 1 mole% doped samples when charge rate is 1C.

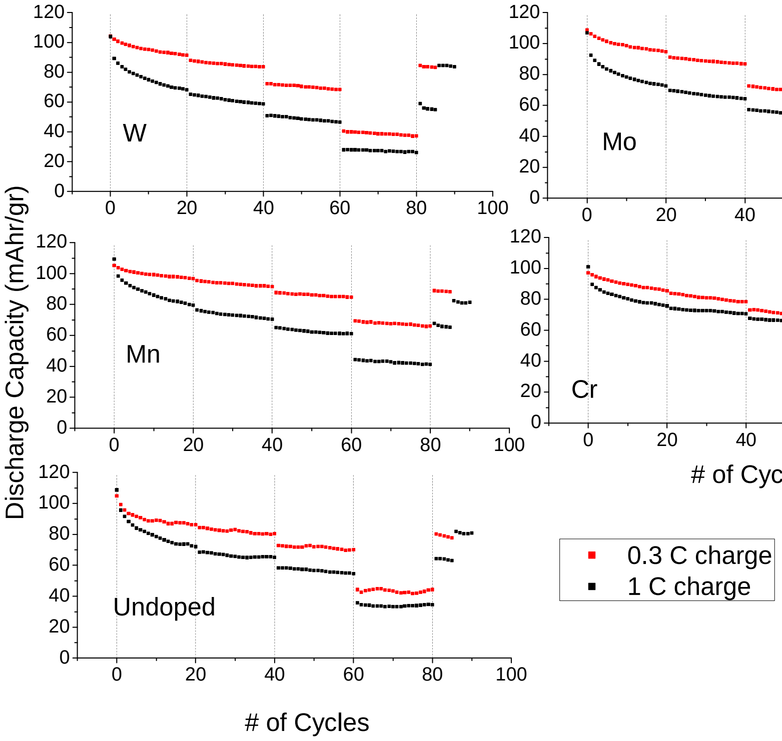

Figure 6.12. The results of the charge-discharge tests of 1 mole% doped samples with different charge rates.

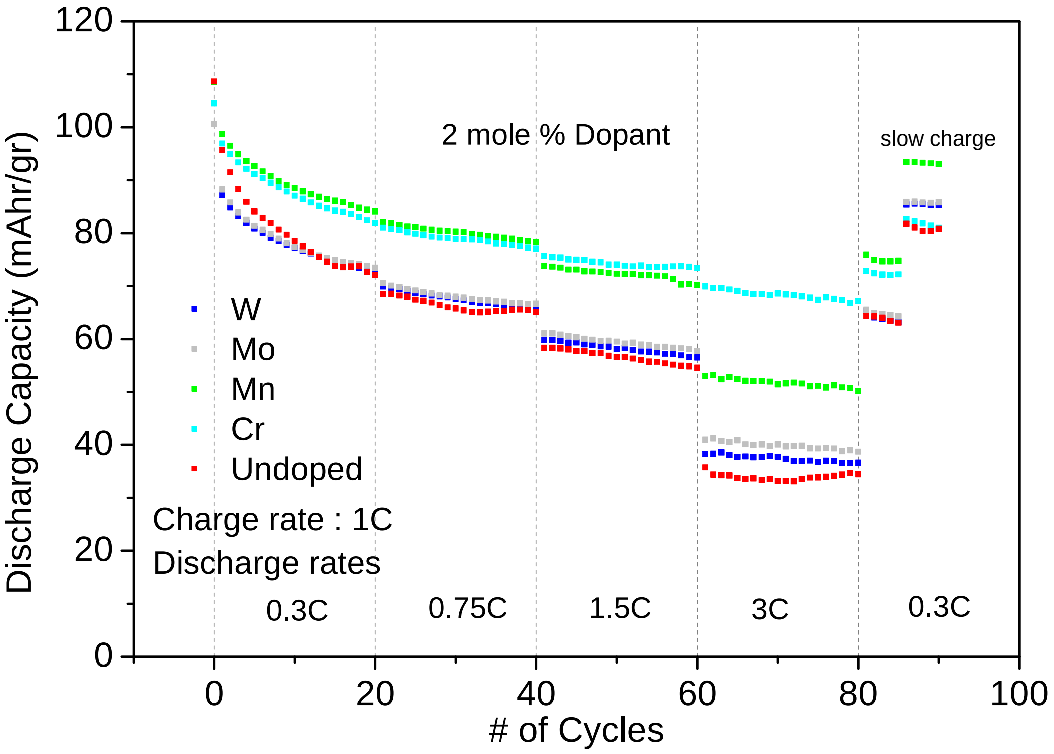

Figure 6.13. Charge-discharge curves of 2 mole% doped samples when charge rate is 1C.

From Figure 6.13, the results of the charge-discharge tests of 2 mole% doped samples when charge rate is 1C can be seen. From the results, it is seen that Cr2 shows the best behaviour which is similar to the experiments having charge rate of 0.3C. High rate capability of Cr2 is far better than that of other doped samples. At the end of the tests with charge rate of 1C, Mn2 has the best cycleability. When charge rate is lowered to 0.3C (last 5 cycles), the gap between Mn2 and other samples is increased. W, Mo and undoped have worse high rate capability but they can recover their capacity when discharge rate is 0.3C. The first discharge capacity is again highest for Mn containing sample (Mn2). The value of this parameter for undoped, Cr2, Mo2, Mn2 and W2 is 95.7, 96.9, 88.2, 98.7 and 87.2 mAh/gr, respectively. First discharge capacities are generally decreased with increasing doping content except Cr doped samples. This abnormal behaviour of Cr doped samples is also seen with charge rate of 0.3C.

When 2 mole% doped samples are compared towards the charge rates (Figure 6.14), it is seen that at low and moderate discharge rates (0.3C-0.75C-1.5C), charging with 0.3C yield better results for all samples. However; when high discharge rates are used (3C), the result is reversed that charging rates of 1C yield better results except undoped sample. For Mo doped samples, high rate capability seems independent from charge rate. Charge retention for Cr2 when charge rate is 0.3C is 57.1% and this value is increased to 64.3% when charge rate is 1C. At the charge rate of 0.3C, capacity retention values for Mo2, Mn2 and W2, are 36.0, 31.2 and 30.4%, respectively while these values are 38.5%, 46.2% and 36.4%, respectively at the charge rate of 1C. It is seen that the samples can be charged at higher rates without significant capacity loss. Figure 6.14 reveals the electrochemical behaviour difference of the samples between 0.3C and 1C charge rates.

From Figure 6.14, it is also seen that the loss in the first cycle is larger for charge rate of 1C, as expected.

When charge-discharge results for high charge rate (1C) are compared towards doping content, it is seen that for every discharge rate, 2 mole% doping yield better results. Figure 6.15 gives the charge-discharge tests with charge rate of 1C with different dopant contents. In experiments with charge rate of 1C, every sample shows better cycleability for 2 mole% doping contents. The gap between the discharge capacities increase with increase in discharge rates, however, similar differences are occurred for all samples, therefore it can be claimed that the cycleability of 2 mole% doped samples is better than that of 1 mole% doped samples. For first discharge capacities such an obvious conclusion cannot be drawn as capacities of 2 mole% doped samples are lower for all samples except Cr doped ones. High rate capability is better for 2 mole% doped samples.

Same procedure was followed for W1Mn1. The results of the charge-discharge tests of this sample are given in Figure 6.16 with the comparison of undoped, Mn1 and W1.

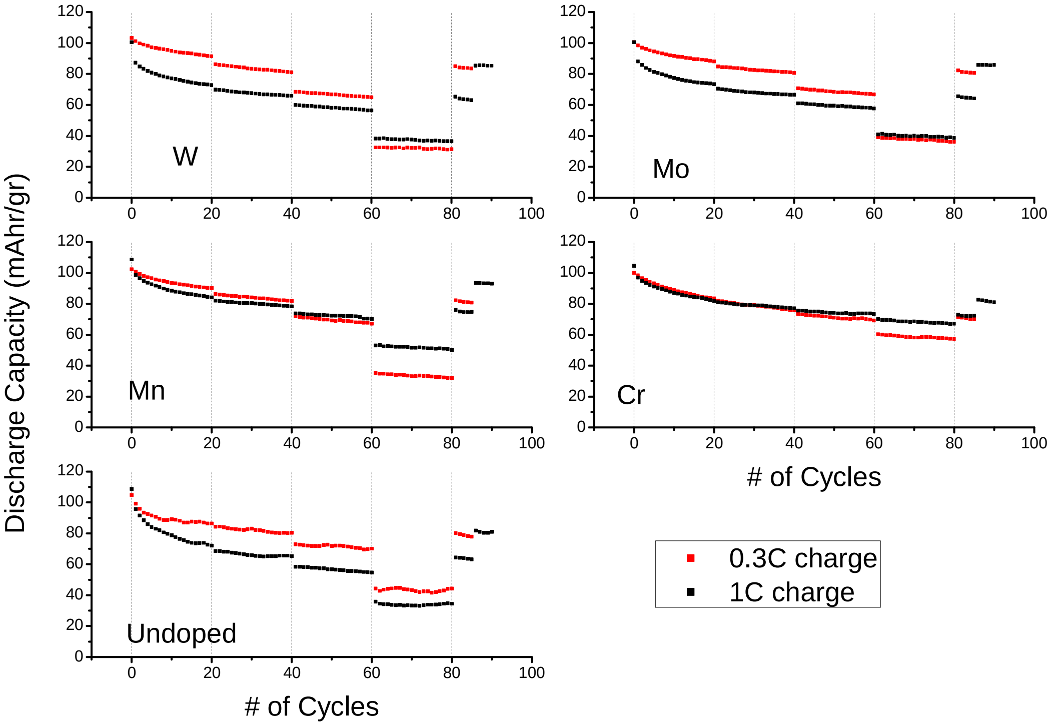

Figure 6.14. The results of the charge-discharge tests of 2 mole% doped samples with different charge rates.

From Figure 6.16, it is seen that W1Mn1 sample has the best electrochemical behaviour in terms of high rate capability and charge retention. The capacity of this sample is not so different than other samples. For 0.3C, it has only 3.3 mAh/g lower capacity than the sample having the highest capacity (Mo1, 108.8 mAh/g). For 1C, it has the largest discharge capacity with 99.2 mAh/g).

Table 6.3 summarizes all results of charge-discharge tests from which it is seen that W1Mn1 shows much better electrochemical behaviour than the others. When electrochemical behaviours are discussed, almost all electrochemical parameters are better for doped samples than that of undoped sample. When first discharge capacities are considered, 2 mole% doped samples have lower capacities than 1mole% doped samples indicating increase of Li-site occupation or inhomogeneous distribution of dopants in the structure. W1Mn1 has much higher rate capability than other samples. It also has very good cycleability. Mo doped samples can recover the capacity loss satisfactorily, but cannot have the best behaviour in any of the electrochemical parameters. To sum up, cycleability and high rate capability of undoped are increased with doping. When high rate capability is taken into account, it is seen that Cr doped samples have the best behaviour among the other doped samples so it is meaningful to compare high rate capability of W1Mn1, Cr1 and Cr2 samples. Figure 6.17 reveals this comparison and it is seen that high rate capability of W1Mn1 is better. Also, the capacity retention at the end of the full cycle is better for W1Mn1.

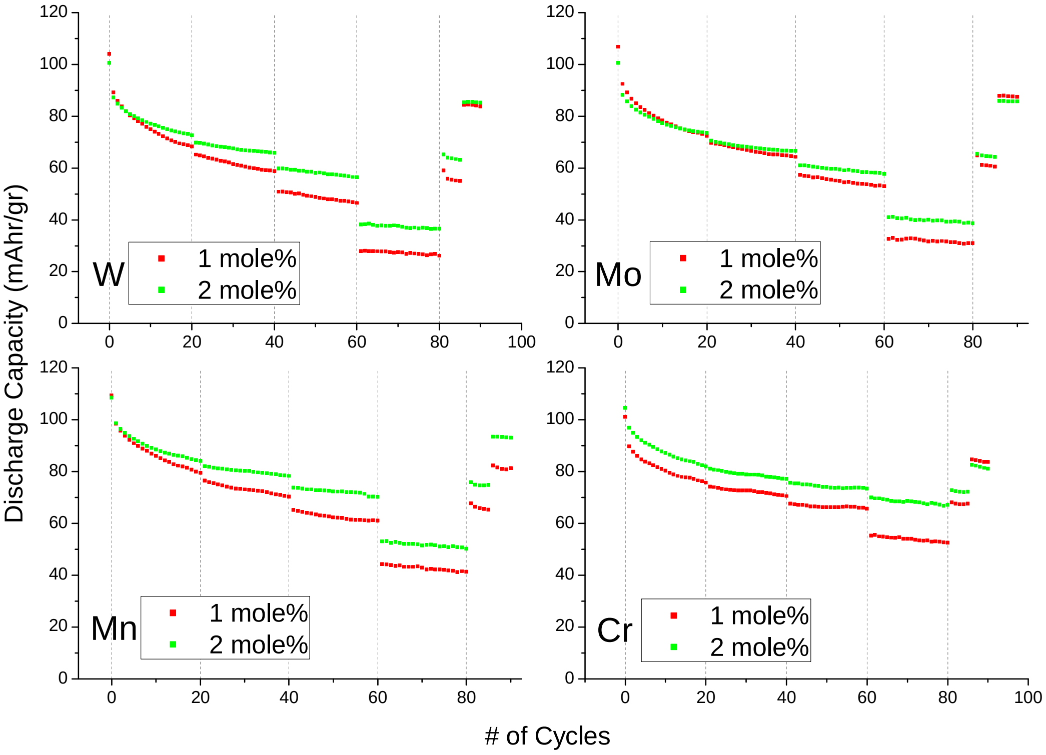

Figure 6.15. Charge-discharge of 1 and 2 mole% doped samples when charge rate is 1C.

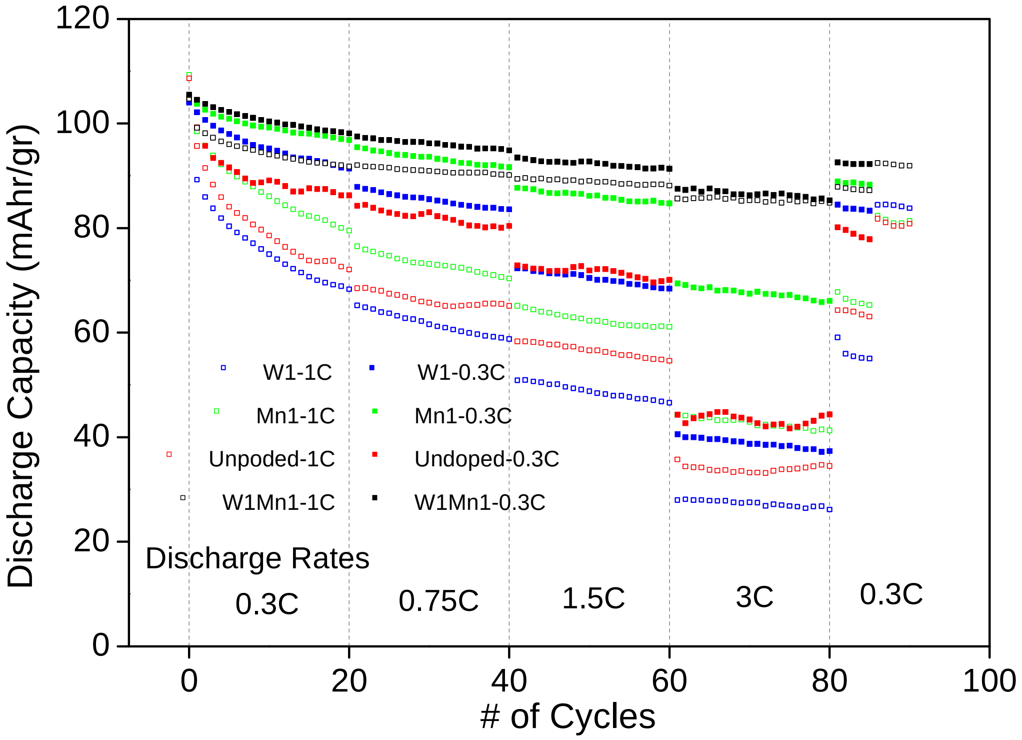

Figure 6.16. Comparison of charge-discharge tests of W1Mn1, undoped, Mn1 and W1.

Table 6.3. Summarizing the results of charge-discharge tests.

Sample	FDC Ch0.3	CR81 Ch0.3	CR82 Ch0.3	FDC Ch1	CR81 Ch1	CR82 Ch1	CR87 Ch1
Undoped	104.8	42.3	76.5	95.7	31.7	59.2	75.3
Cr1	97.2	47.0	77.5	89.7	52.0	67.4	83.8
Cr2	100.1	57.1	71.3	96.9	64.3	69.7	79.1
Mo1	**108.8**	31.8	81.4	92.5	29.1	60.7	82.3
Mo2	100.6	36.0	81.8	88.2	38.5	65.1	85.4
Mn1	105.2	62.8	84.5	98.5	37.7	62.0	75.3
Mn2	102.3	31.2	80.5	98.7	46.2	69.9	86.1
W1	104.2	35.8	81.1	89.2	25.1	56.8	81.2
W2	103.3	30.4	82.4	87.2	36.4	64.9	84.9
W1Mn1	105.5	**80.8**	**87.8**	**99.2**	**81.0**	**83.9**	**88.3**

LEGEND:

FDC Ch0.3 = First Discharge Capacity when charge rate is 0.3C (mAh/gr)
FDC Ch1 = First Discharge Capacity when charge rate is 1C (mAh/gr)
CR81 Ch0.3 = % Cap. retaining after 81 cy. (at the end of the cycle having the dis.rate as 3C) – Ch. Rate 0.3C
CR82 Ch0.3 = % Cap. retaining after 82 cy. (the first cycle having the dis. rate as 0.3C-last) – Ch. rate 0.3C
CR81 Ch1 = % Cap. retaining after 81 cy. (at the end of the cycle having the dis.rate as 3C) – Ch. rate 1C
CR82 Ch1 = % Cap. retaining after 82 cy. (the first cycle having the dis. rate as 0.3C-last) – Ch. rate 1C
CR87 Ch1 = % Cap. retaining at the beginning of the 87th cycle when Ch. rate 0.3C and Dis. rate 0.3C – Ch.rate 1C for 86 cycles

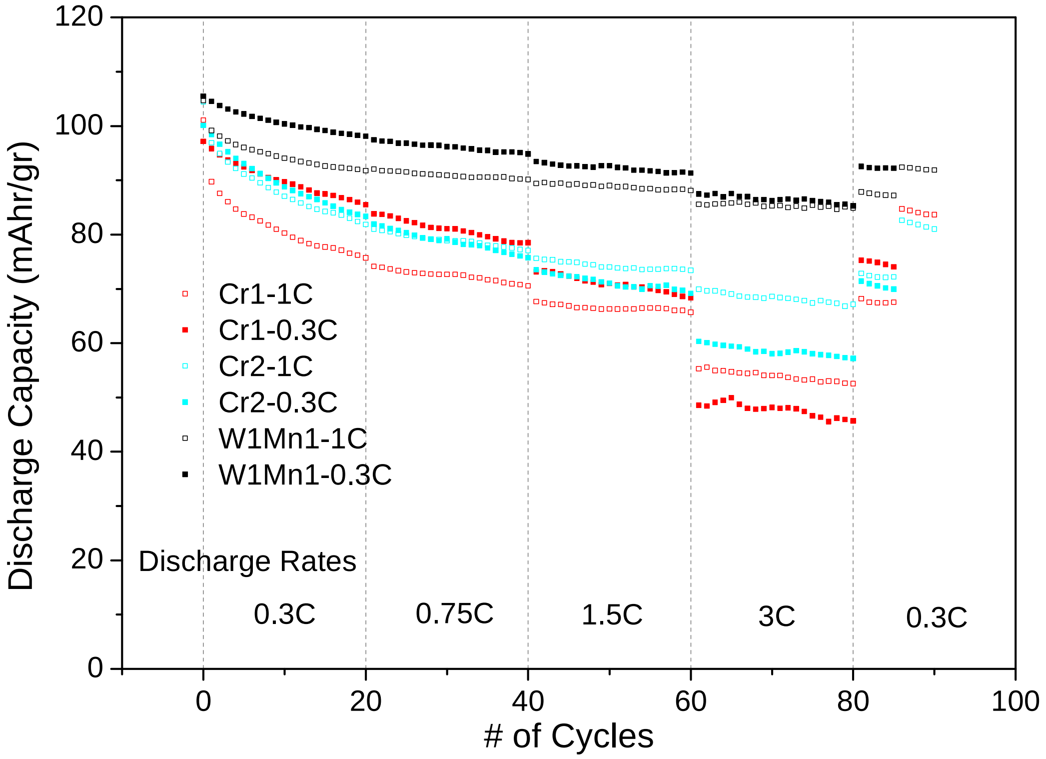

Figure 6.17. Comparison of charge-discharge tests of W1Mn1,Cr1 and Cr2.

6.3.2. Voltage profiles and energies of samples

Voltage profiles of the samples at a certain cycle were plotted. At every discrete step of charge-discharge tests, the voltage profile at the 5th cycle is plotted. Table 6.4 summarizes the voltage values at the middle of the profiles.

From Table 6.4, it is seen that W1Mn1 also shows the highest voltage value. Considering that the capacity of W1Mn1 is relatively high, it can be claimed that W1Mn1 is the highest energy containing sample among undoped and other doped samples.

For voltage profiles, there is no significant difference between the doped samples, but undoped sample shows the worst behaviour for every voltage profile. The voltage profile of W1Mn1 does not change with charge and discharge rates The gap between W1Mn1 and other samples is increased with the fastest discharge rate, 3C as evidenced from Figure 6.20i and 6.20j.

Apart from numerical values, the best cycleability of W1Mn1 can be visually seen from Figures 6.18 and 6.19. As expected, with increasing discharge rate, shift of voltage profiles to lower voltages and discharge capacities are seen. However; this shift is minimal for W1Mn1 for both charge rates (0.3C and 1C). Although discharge capacities are lowered with 1C charge rate than that of 0.3C charge rate, it is seen that with increasing discharge rate, the gap between voltage profiles of W1Mn1 does not change for 1C and 0.3C charge rates. This is an important indication of the high rate capability of W1Mn1.

When W1Mn1 is excluded from the discussion, it is seen that the differences between undoped sample and other doped samples are not significant. When doping contents are compared, for charge rate of 0.3C, Mo and W doped samples show no difference. Cr2 has better profile than that of Cr1. In contrast to that, Mn1 has better profile. When the comparison is made for charge rate of 1C, similar behaviour is seen for all samples except Mn. For 1C charge rate, Mn2 has better profile than Mn1 especially for higher discharge rates.

From Figure 6.20, voltage profiles of W1Mn1, undoped and samples doped with 1and 2 mole% are seen at various charge and discharge rates. The profiles are plotted during discharge. They belong to the 5th cycle of the tests. Extreme rates (Figure 6.20i and 6.20j; charge rate is 1C, discharge rate is 3C) are chosen in order to see cycleability at highest charge-discharge rates (harsh condition). Eight more plots with various charge and discharge rates including the mildest condition where charge rate is 0.3C and discharge rate is 0.3C (column 2 in Table 6.4, Figure 6.20a and 6.20b) are drawn. Although the voltage profile of W1Mn1 is one of the best for the samples at different charge and discharge rates, the best profile of W1Mn1 can be easily seen in plots having charge and discharge rates as 1C and 3C, respectively. Regarding that voltage profiles are related with the chemistry of materials, it may be claimed that co-doping of W and Mn alters the chemistry of undoped towards higher voltage profile.

These results indicate that W1Mn1 is the best sample to be used as cathode material in Li-ion batteries among the samples studied in this thesis with regard to cycleability, high rate capability and voltage profiles. Considering that the discharge capacities are nearly same for all samples, highest voltage profile at high charge-discharge of W1Mn1 lets this sample to be used in applications requiring high energy and fast kinetics.

Table 6.4. Some numerical values of voltage at the middle of profiles of the samples.

Sample	V5 (V) 0.3-0.3i	V5 (V) 0.3-3	V5 (V) 0.3-0.3s	V5 (V) 1-0.3i	V5 (V) 1-3	V5 (V) 1-0.3s	V5 (V) 1-0.33-0.3s
Undoped	3.70	3.00	3.65	3.70	2.94	3.59	3.62
Cr1	3.79	3.10	3.69	3.75	3.21	3.70	3.75
Cr2	**3.83**	3.28	3.75	3.79	3.47	3.79	3.82
Mo1	3.73	3.13	3.65	3.71	3.07	3.61	3.69
Mo2	3.75	3.03	3.65	3.73	3.11	3.64	3.74
Mn1	3.80	3.28	3.75	3.75	3.11	3.65	3.72
Mn2	3.77	3.01	3.68	3.74	3.21	3.69	3.74
W1	3.75	3.10	3.67	3.70	3.03	3.56	3.68
W2	3.72	3.01	3.64	3.71	3.06	3.62	3.71
W1Mn1	3.81	**3.62**	**3.79**	**3.80**	**3.65**	**3.81**	**3.83**

LEGEND:

V5 0.3-0.3i = Voltage values at the 5th cycle when charge and dis. rate is 0.3C (first 0.3C dis. rate)
V5 0.3-3 = Voltage values at the 5th cycle when charge rate 0.3C and dis. rate is 3C
V5 0.3-0.3s = Voltage values at the 5th cycle when charge and dis. rate is 0.3C (last 0.3C dis. rate)
V5 1-0.3i = Voltage values at the 5th cycle when charge rate 1C and dis. rate is 0.3C (first 0.3C dis.rate)
V5 1-3 = Voltage values at the 5th cycle when charge rate 1C and dis. rate is 3C
V5 1-0.3s = Voltage values at the 5th cycle when charge rate 1C and dis. rate is 0.3C (last 0.3C dis. rate)
V5 1-0.3-0.3s = Voltage values at the 5th cy. when ch. rate 0.3C and dis. rate is 0.3C (after 85 cy. with ch. rate 1C)

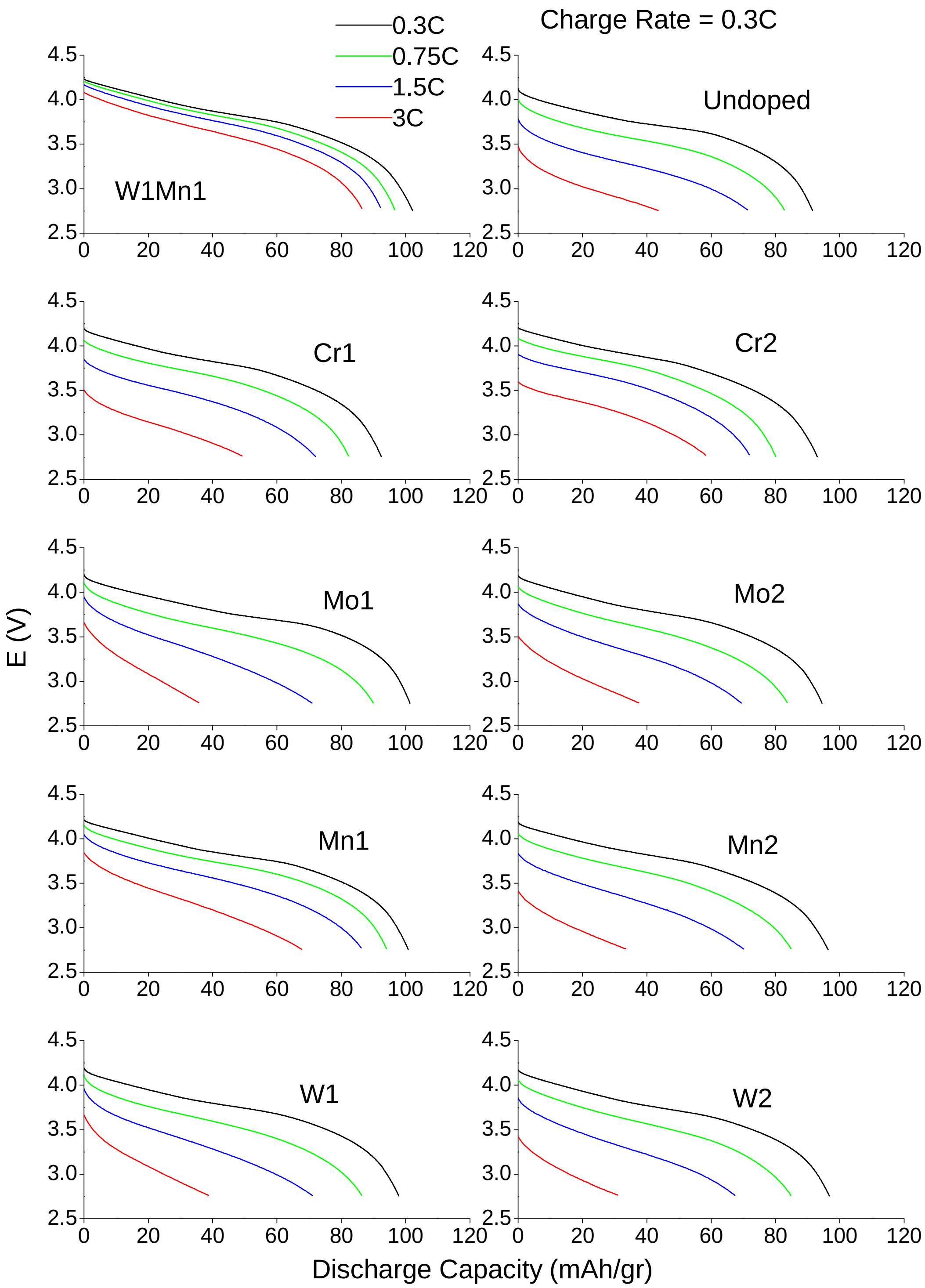

Figure 6.18. Voltage profiles of the samples charged at 0.3C and discharged at given C rates.

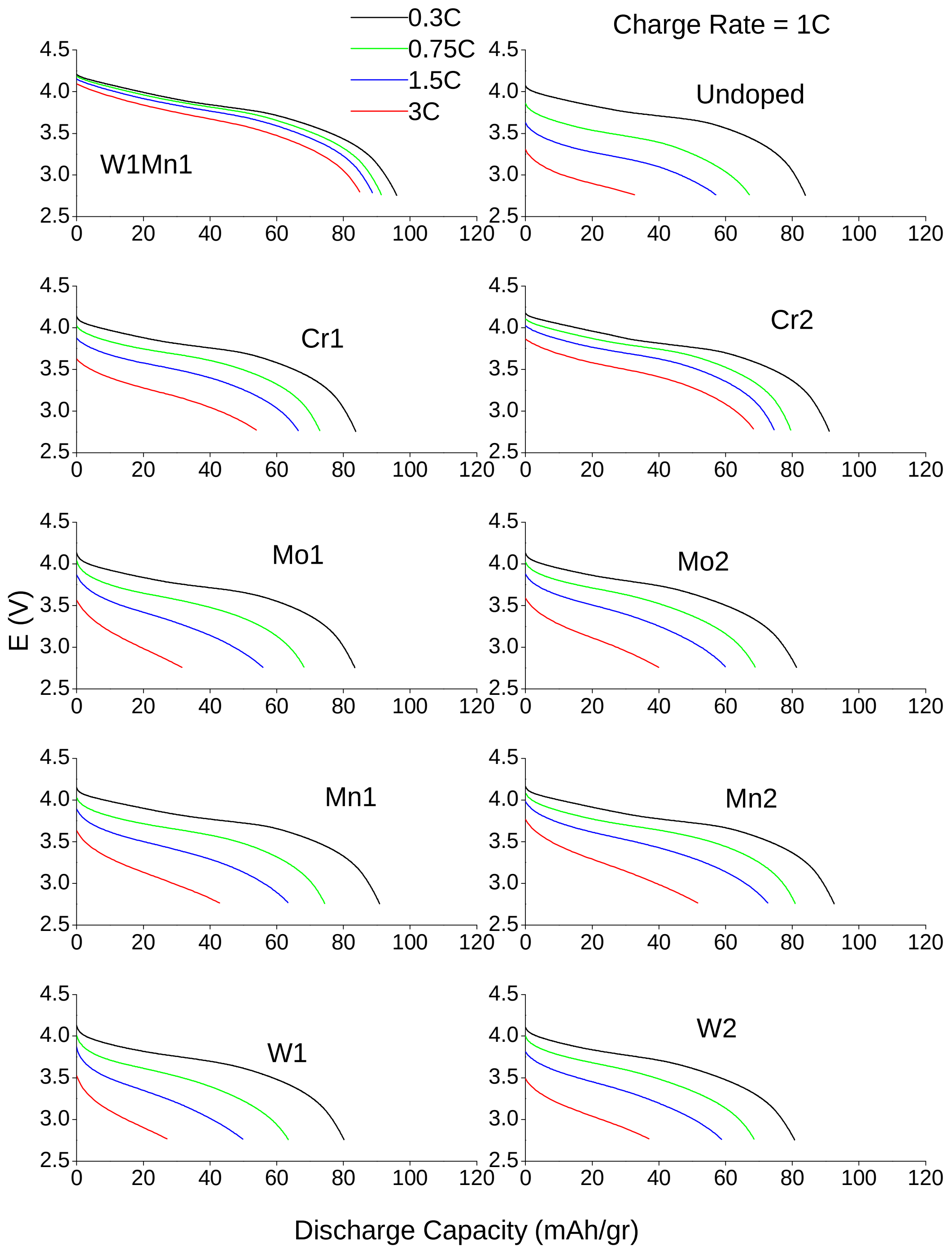

Figure 6.19. Voltage profiles of the samples charged at 1C and discharged at given C rates.

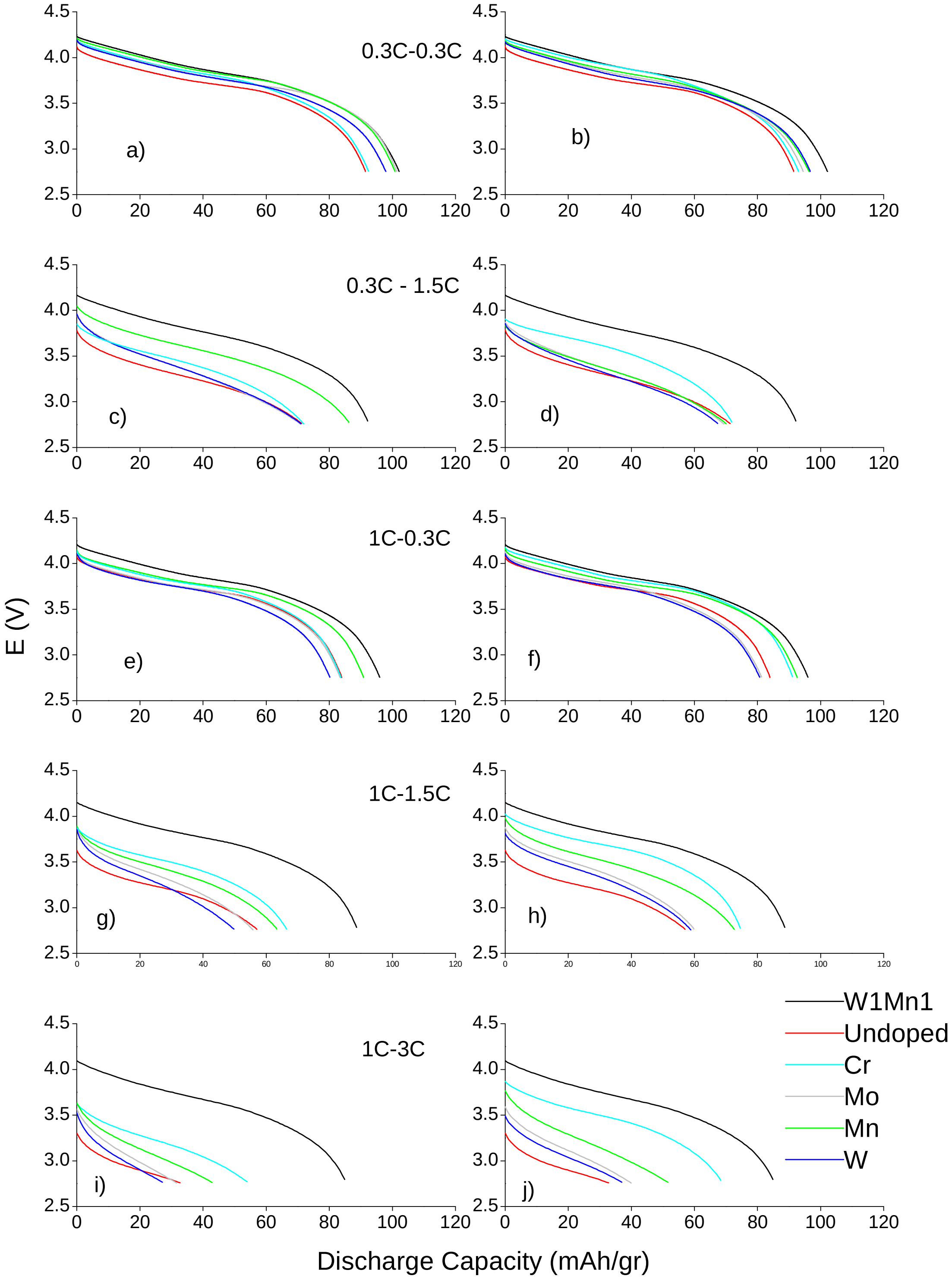

Figure 6.20. Voltage profiles of all samples, left plots belong to 1 mole% dopants and right plots belong to 2 mole% dopants; a) and b) charged and discharged at 0.3C, c) and d) charged at 0.3C, discharged at 1.5C, e) and f) charged at 1C, discharged at 0.3C, g) and h) charged at 1C, discharged at 1.5C, i) and j) charged at 1C, discharged at 3C

6.4. Cyclic Voltammetry (CV)

6.4.1. Reversibility, Kinetics and Diffusion Coefficients of Samples

Cyclic Voltammetry was applied to the samples, Undoped, Cr1, Cr2, Mo1, Mo2, Mn1, Mn2, W1, W2 and W1Mn1. It was applied with three different scan rates, 0.02 mV/s, 0.05 mV/s and 0.08 mV/s between 3-4.5V. At each scan rate first two cycles were recorded.

During the estimation of the ratio peak currents, both methods indicated in section 3.2 was used. The classical ratio is shown by simply i_{pa}/i_{pc} and the ratio found by extrapolating the baseline for cathodic scan is shown by Ext. i_{pa}/i_{pc} in Table 6.5.

From Table 6.5, the numerical values of the CVs of the 2nd cycle with scan rate 0.02 mV/s can be seen. Peak current ratios estimated from classical and extrapolation methods do not give different results when comparison of these ratios is in question rather than that of individual values. Therefore, it is decided to continue by taking the classical estimation of ratios into account. Table 6.5 reveals very important results such as reversibility is the highest for W1Mn1 with ΔE value 0.069mV which is nearly equal to the theoretical value of reversible process (ΔE ~0.059 mV for one electron transfer). Moreover the value of i_{pa}/i_{pc} for W1Mn1 is nearest to 1 when compared with other samples.

Table 6.5. The numerical values of CVs of samples during 2nd cycle with v=0.02 mV/s.

Sample	E_{pa} (V)	E_{pc} (V)	ΔE (V)	i_{pa} (mA)	i_{pc} (mA)	i_{pa}/i_{pc}	Ext. i_{pa}/i_{pc}
Undoped	4.037	3.807	0.230	0.78	0.62	1.258	1.829
Cr1	4.030	3.811	0.219	0.73	0.63	1.159	1.825
Cr2	3.990	3.836	0.154	0.72	0.66	1.091	1.452
Mo1	4.017	3.829	0.188	0.58	0.50	1.160	1.933
Mo2	3.999	3.833	0.166	0.60	0.52	1.154	1.796
Mn1	4.093	3.817	0.276	0.43	0.38	1.132	2.945
Mn2	4.002	3.838	0.164	0.51	0.47	1.085	1.841
W1	4.025	3.821	0.204	0.57	0.52	1.096	1.939
W2	4.025	3.818	0.207	0.37	0.35	1.057	1.814
W1Mn1	3.938	3.869	0.069	0.48	0.47	1.021	1.371

When shapes of CVs with different scan rates (Figure 6.21 and Figure 6.22) are considered, the sharpest and narrowest shape belongs to W1Mn1. These results indicate that the reversibility of W1Mn1 is the best among other samples.

CVs shown in Figure 6.21 and 6.22 belong to the second cycles. From these figures, results of CVs of all 10 samples can be seen with regard to scan rates. It is seen that the sharpest cathodic and anodic peaks belong to W1Mn1. This indicates faster intercalation/deintercalation kinetics which is also evidenced from charge-discharge tests. CVs of undoped, Cr1 and Cr2 resemble with each other. It is seen that with increase in doping content except W doped sample, the peaks get sharper meaning that faster intercalation/deintercalation occur [105]. With CVs, it is seen that reversibility increases with doping. From Table 6.6 and Table 6.7, the numerical values of anodic and cathodic currents and voltages are given for all scan rates. From these tables, slopes of current vs. scan rate and voltage vs. scan rate graphics for anodic and cathodic scans can also be seen. Diffusion coefficients were estimated by Randles-Sevcik equation (refer to section 3.2, equation 3.1) with;

Table 6.6. Data of anodic i (deintercalation) and E of CVs with ν of 0.02, 0.05 and 0.08 mV/s.

Sample	ν = 0.02 mV/s		ν = 0.05 mV/s		ν = 0.08 mV/s		Slope i-ν	Slope E-ν	D (cm^2/s) x10^{-9}
	i (mA)	E (V)	i (mA)	E (V)	i (mA)	E (V)			
Undoped	0.78	4.037	1.34	4.182	1.76	4.291	0.218	1.786	2.7
Cr1	0.73	4.030	1.23	4.156	1.65	4.278	0.204	1.732	2.3
Cr2	0.72	3.990	1.19	4.078	1.57	4.169	0.189	1.247	2.0
Mo1	0.58	4.017	0.98	4.125	1.30	4.220	0.160	1.421	1.4
Mo2	0.60	3.999	0.97	4.082	1.24	4.144	0.142	1.020	1.1
Mn1	0.43	4.093	0.72	4.312	0.97	4.496	0.120	2.825	0.8
Mn2	0.51	4.002	0.90	4.101	1.22	4.175	0.157	1.217	1.4
W1	0.57	4.025	0.96	4.136	1.28	4.242	0.157	1.516	1.4
W2	0.37	4.025	0.58	4.124	0.75	4.204	0.084	1.256	0.4
W1Mn1	0.48	3.938	0.74	3.967	1.04	3.985	0.123	0.332	0.9

Table 6.7. Data of cathodic i (intercalation) and E of CVs with ν of 0.02, 0.05 and 0.08 mV/s.

Sample	ν = 0.02 mV/s		ν = 0.05 mV/s		ν = 0.08 mV/s		Slope i- ν	Slope E- ν	D (cm^2/s) x10^{-9}
	i (mA)	E (V)	i (mA)	E (V)	i (mA)	E (V)			
Undoped	0.62	3.807	0.84	3.721	1.03	3.641	0.091	-1.160	0.5
Cr1	0.63	3.811	0.85	3.720	1.03	3.628	0.089	-1.276	0.4
Cr2	0.66	3.836	0.87	3.772	1.01	3.708	0.078	-0.932	0.3
Mo1	0.50	3.829	0.78	3.768	0.99	3.710	0.109	-0.831	0.7
Mo2	0.52	3.833	0.80	3.769	1.01	3.723	0.109	-0.666	0.7
Mn1	0.38	3.817	0.53	3.728	0.60	3.609	0.050	-1.439	0.1
Mn2	0.47	3.838	0.74	3.781	0.96	3.738	0.109	-0.703	0.7
W1	0.52	3.821	0.80	3.749	1.00	3.693	0.107	-0.899	0.6
W2	0.35	3.818	0.52	3.740	0.64	3.671	0.065	-1.029	0.2
W1Mn1	0.47	3.869	0.71	3.842	0.78	3.809	0.070	-0.416	0.3

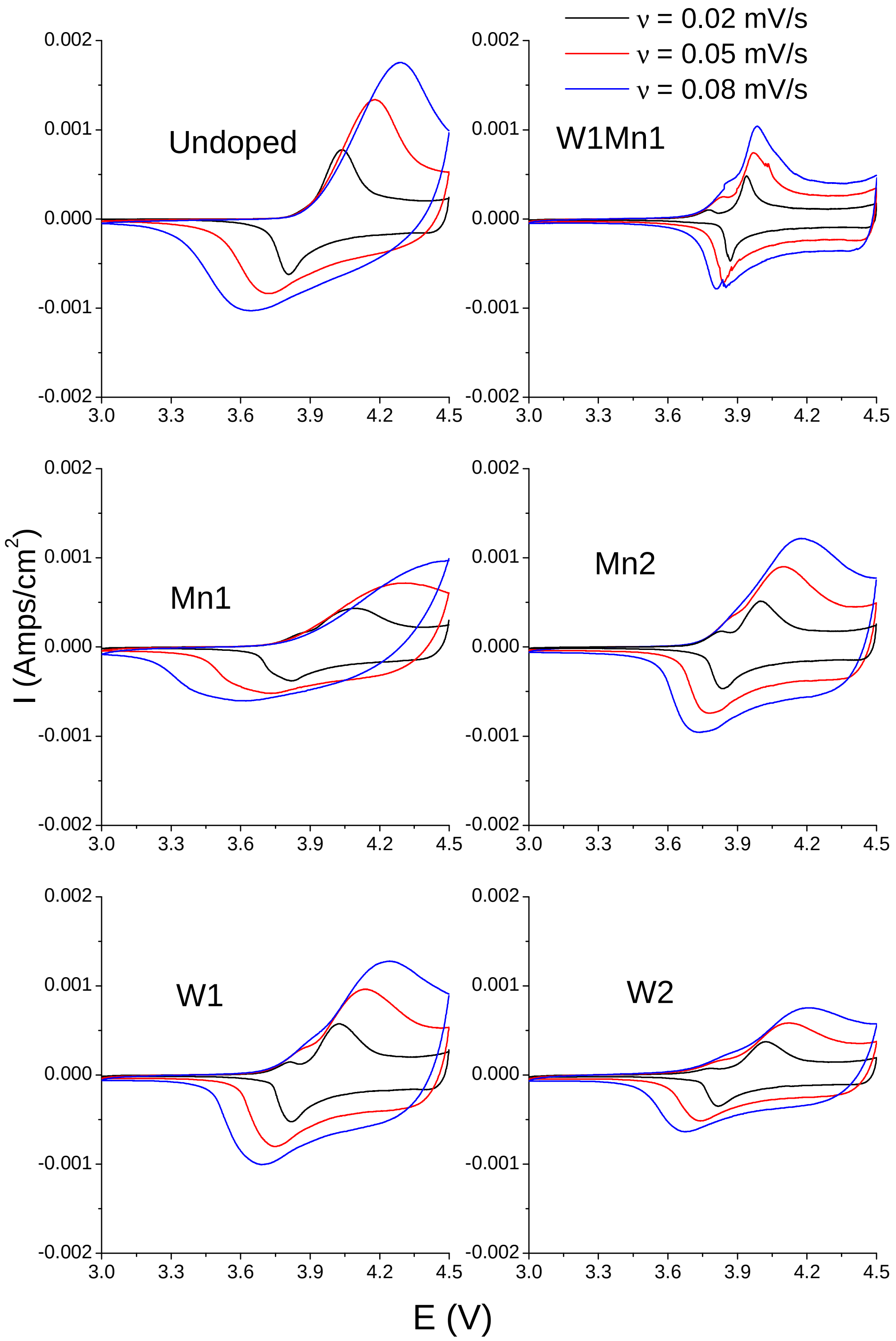

Figure 6.21. CVs of undoped, W1Mn1, Mn1, Mn2, W1 and W2 with ν of 0.02 mV/s, 0.05mV/s and 0.08 mV/s.

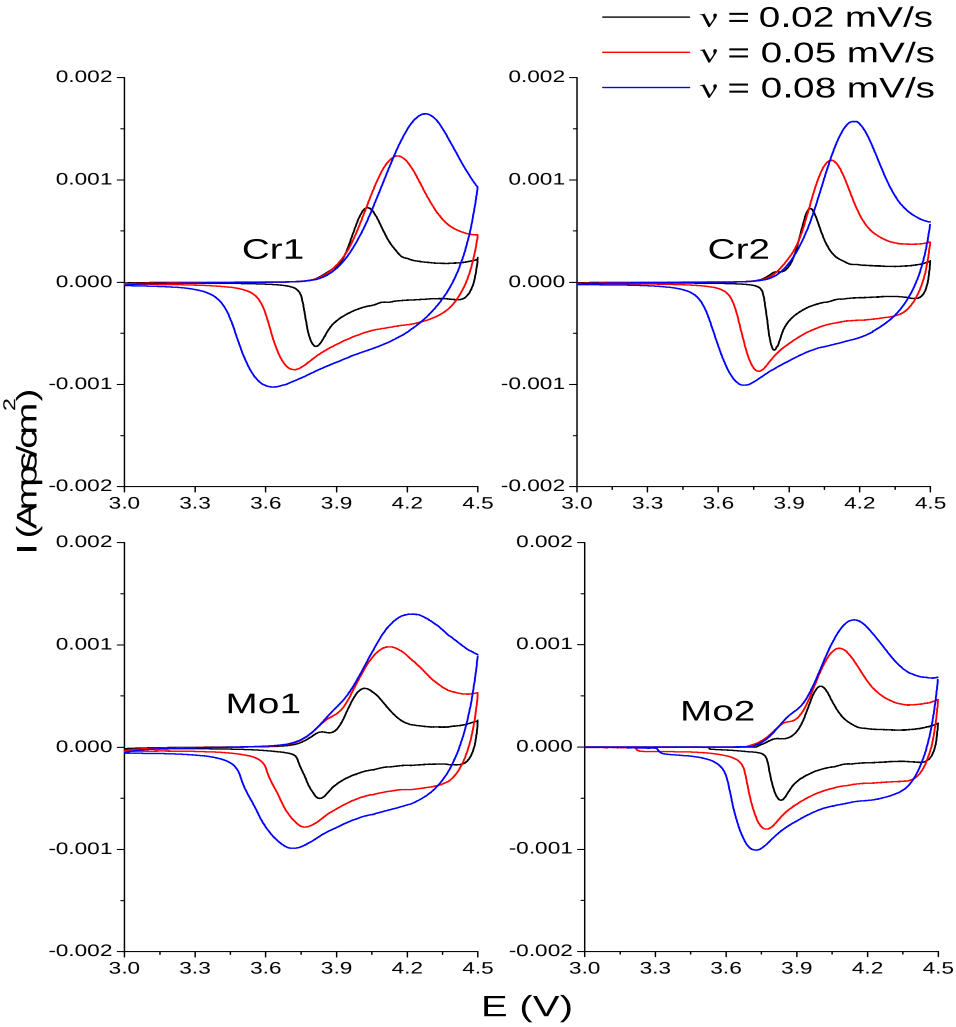

Figure 6.22. CVs of Cr1, Cr2, Mo1, Mo2 with ν of a)0.02 b)0.05 c)0.08 mV/s.

From Table 6.6 and Table 6.7, it is seen that diffusion coefficient values are not responsible for better kinetics of W1Mn1 because although it has higher values than that of most samples, the largest values are for undoped sample and Mn2 for anodic and cathodic scans, respectively. Mn1 has the smallest diffusion coefficient for cathodic scan and W2 has the smallest diffusion coefficient for anodic scan. The values of diffusion coefficients for the samples are in accordance with the results obtained by Waki et al. [61] by using CV. They estimated diffusion coefficient of undoped sample as $2.6\text{x}10^{-8}$ cm^2/s and 20 mole% Mn doped sample as $6.4\text{x}10^{-8}$ cm^2/s. These values are bit higher than the values estimated in this study. It is believed that this is due to the higher cation mixing in this study. In addition to that they estimated surface area and used it in their calculations, whereas geometric area was used in this study. Apart from CV, different methods were applied for estimating diffusion coefficients. The diffusion coefficients estimated in this study are consistent with the diffusion coefficients estimated by Mizushima et. al [106] ($5\text{x}10^{-9}$ cm^2/s for Li_xCoO_2,

$0.2 \leq x \leq 0.8$, estimated by galvanostatic method) and Choi and Pyun [107] (10^{-8} to 10^{-9} cm^2/s for Li_xCoO_2, $0.5 \leq x \leq 0.7$, estimated by galvanostatic intermittent titration technique, GITT).

From Table 6.6, during anodic scan (de-intercalation), the diffusion coefficient of undoped is the largest among the other samples. Although, lattice parameter *c* of undoped is smallest, highest diffusion coefficient can be attributed to the lower degree of cation mixing for this sample which can be evidenced from lack of high voltage peaks during CV (Figures 6.26 to 6.30). Moreover; Li-gap which is discussed in detail in Chapter 7 is comparably higher than other samples.

When i vs. scan rate plots of these samples are drawn (Figure 6.23), it is seen that the gap between anodic and cathodic scans is the smallest for W2. The gap between anodic and cathodic scans is large for Cr and undoped sample.

However, when slopes of voltage vs. scan rates are considered, it is seen that, the smallest slopes for both anodic and cathodic scans belong to W1Mn1 with values of 0.332 and 0.412, respectively. This is an indication that W1Mn1 is much more stable when deviation from equilibrium potential is considered. In other words, polarization resistance of W1Mn1 is lower hence it is better high energy cathode material when compared with other samples in this thesis. Voltage vs. scan rate plots of W1Mn1 when compared with undoped, Cr2, Mn1, W1, W2 and Mo2 for both anodic and cathodic directions are given in Figure 6.24. From this figure, the gap between anodic and cathodic scans were enlarged less with W1Mn1 when compared with other samples. Similar behaviours were observed for other samples also.

From CV data, it is inferred that difference in intercalation and deintercalation rates is the lowest for W1Mn1. Moreover, reversibility properties are best for this sample. This is due to the lower polarization resistance of W1Mn1.

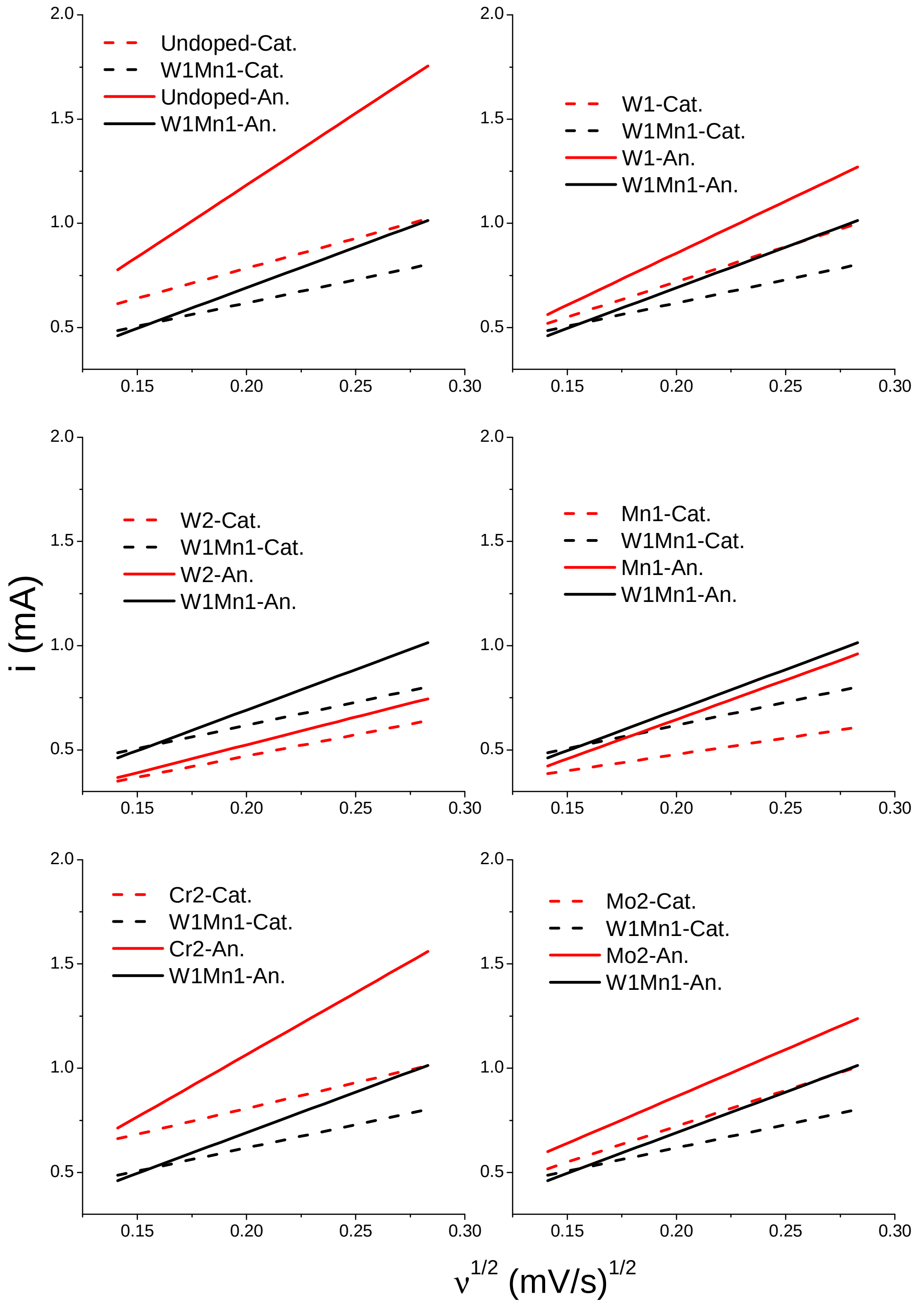

Figure 6.23. Anodic and cathodic current vs. $\nu^{1/2}$ plots of W1Mn1 and other samples.

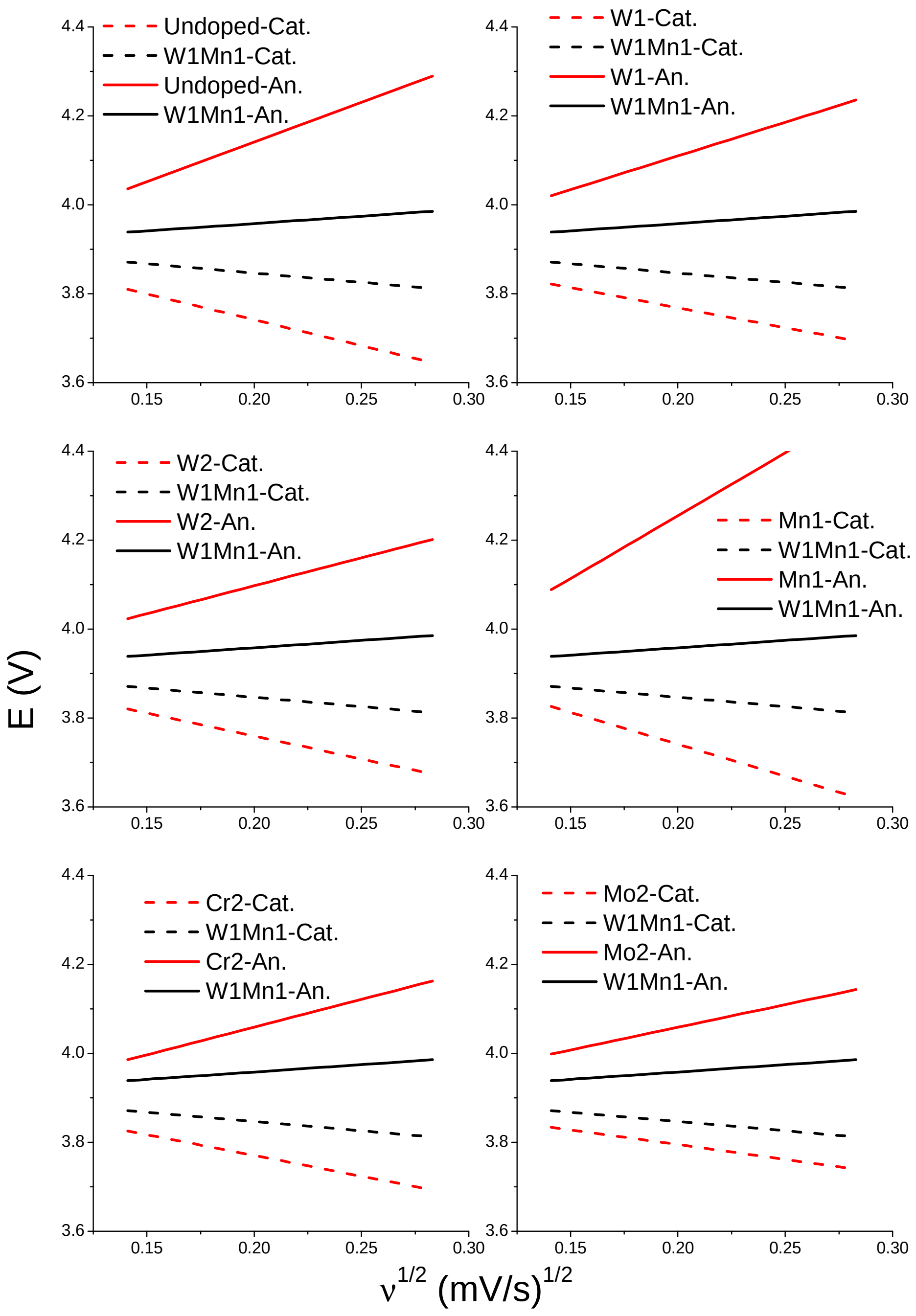

Figure 6.24. E vs. $\nu^{1/2}$ plots of W1Mn1 and other samples.

6.4.2. High Voltage and Impurity Peaks of CVs

It is known that cathodes containing layered $LiCoO_2$ undergo hexagonal-monoclinic-hexagonal phase transition at above 4.1 V. The change of lattice parameters and these transitions were studied by Reimers and Dahn [108]. They proposed a phase diagram which is given in Figure 6.25 with change of the lattice parameters during the phase transitions. According to them, between $0.93<x\leq1$, hexagonal to hexagonal phase transition begins and transition is completed when $x=0.75$. Between $0.55\leq x<0.75$, single phase occurs. Deintercalation of Li beyond 0.55 results in hexagonal to monoclinic transition. However; doping [109] or coating of $LiCoO_2$ [110] may depress these transitions or may make them to be seen more clearly as observed by Gopukumar et al. [73].

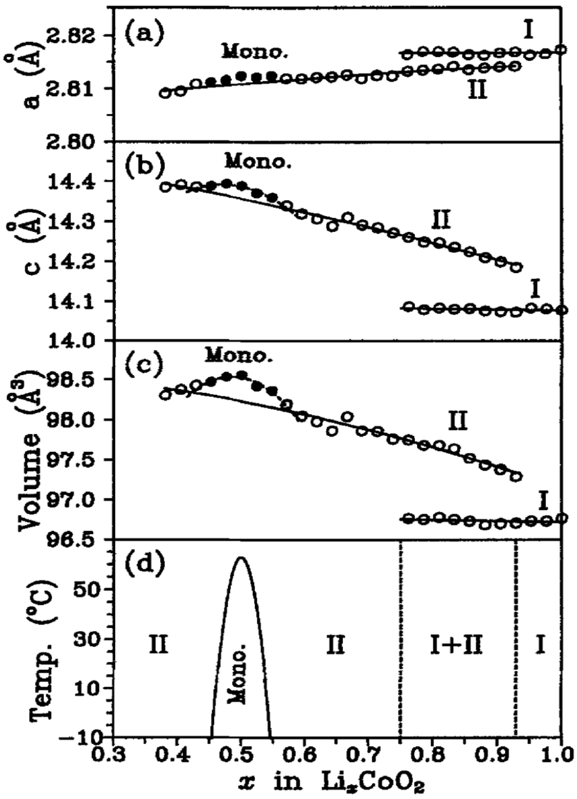

Figure 6.25. Phase transitions and lattice parameters change of Li_xCoO_2 with x [108].

From Figures 6.21 and 6.22, it is also seen that scan rates of 0.05 mV/s and 0.08 mV/s are high for determining peaks belonging to phase transitions. For determining phase transitions and phase impurities, Fey et al. [110] proposed slow scan rate and investigation of first cycle in order to be able to observe these peaks. Therefore, CVs having the scan rates of 0.02 mV/s for the first cycle are investigated in detail for high voltage peak occurrence. Figure 6.26 through 6.30 show the CVs of first cycles which have scan rates of 0.02 mV/s. In each figure CV of undoped sample is given for comparison. Moreover, in each figure the high voltage region (4.00-4.25 V) is enlarged in order to better visualize the peaks and an inlet is displayed for this region. Also as there occurs a single peak during anodic scan at about 3.8 V, this region is enlarged and is shown at the left bottom of each figure.

From Figures 6.26-6.30, it is seen that there occurs single peak at voltages of about 3.8 V during anodic scan. This peak was also observed by Huang et al. [111]. They observed this peak at their samples fired at 300°C and 600°C. XRD patterns revealed an impurity phase of Li_2CO_3 at 300°C in their study. Although this impurity peak was disappeared at 600°C in the XRD pattern, they still observed a minor peak at about 3.8 V during anodic scan in CV. They thought that with temperature, the ordering and purity of layered $LiCoO_2$ was increased Yoon and Kim [112] attributed this peak to occurrence of LT-$LiCoO_2$. As it is determined from [003]/[104] ratio that there occurs cation mixing in the samples, formation of LT-$LiCoO_2$ can be validated. From XRD, this phase cannot be identified as the content of it is low and diffraction patterns are similar with HT-$LiCoO_2$. Moreover; Kavan and Gratzel [113] claimed that CV is a better method for identifying minor peaks. Therefore, these peaks can be attributed to very low amount of Li_2Co_3 or LT-$LiCoO_2$ in the samples. All doped samples have this minor peak at about 3.8 V except undoped. When ICP analyses are consulted (Table 7.1), it is seen that undoped has the least Li content (except W1Mn1) and this sample does not contain any minor peaks in CV.

Gopukumar et al. [73], Madhavi et al. [114] and Huang et al. [111] claimed that having minor peaks at high voltages (> 4 V) might be ascribed to inhomogeneous distribution of elements in $LiCoO_2$ matrix. Results of CV in this study are in agreement with these studies. Plots of CVs of doped samples show negligible differences with each other. So it can be claimed that the differences in structural, ordering and impurities of the samples in this study is so low that, they are not dominant to explain the differences in electrochemical behaviours.

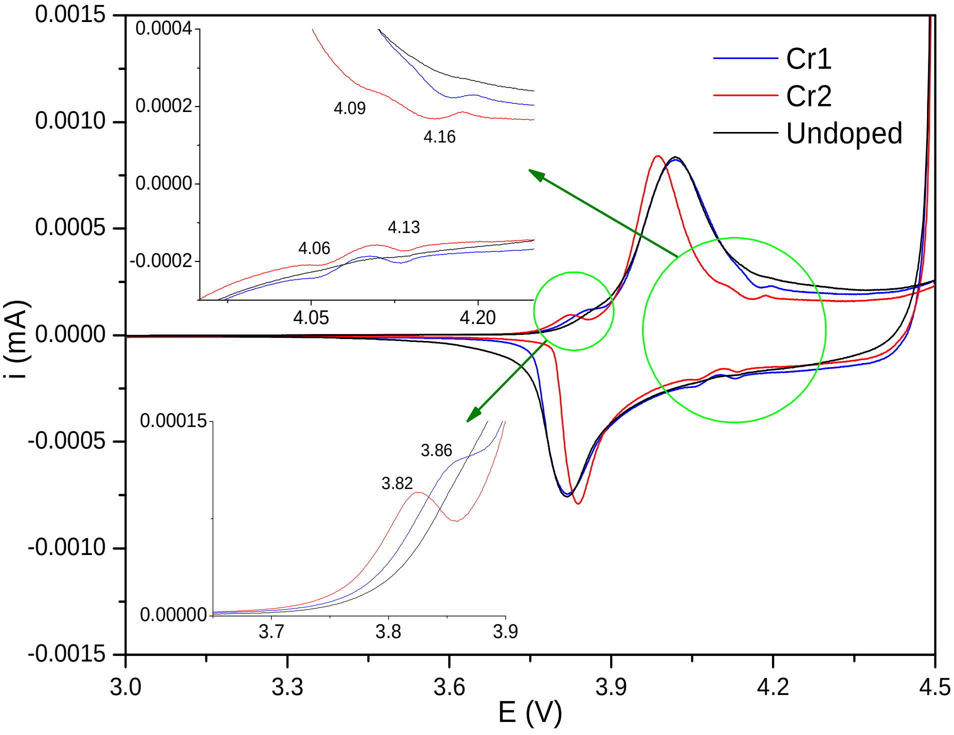

Figure 6.26. CVs of Cr1, Cr2 and undoped samples with scan rates of ν = 0.02mV/s.

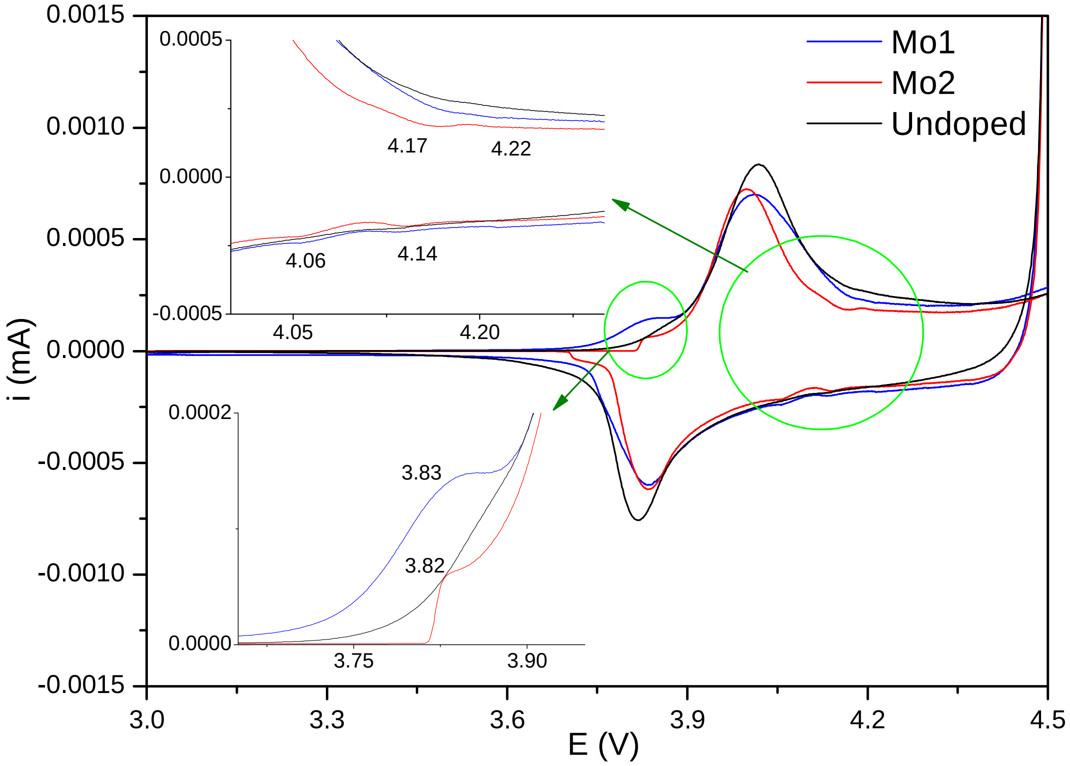

Figure 6.27. CVs of Mo1, Mo2 and undoped samples with scan rates of ν = 0.02mV/s.

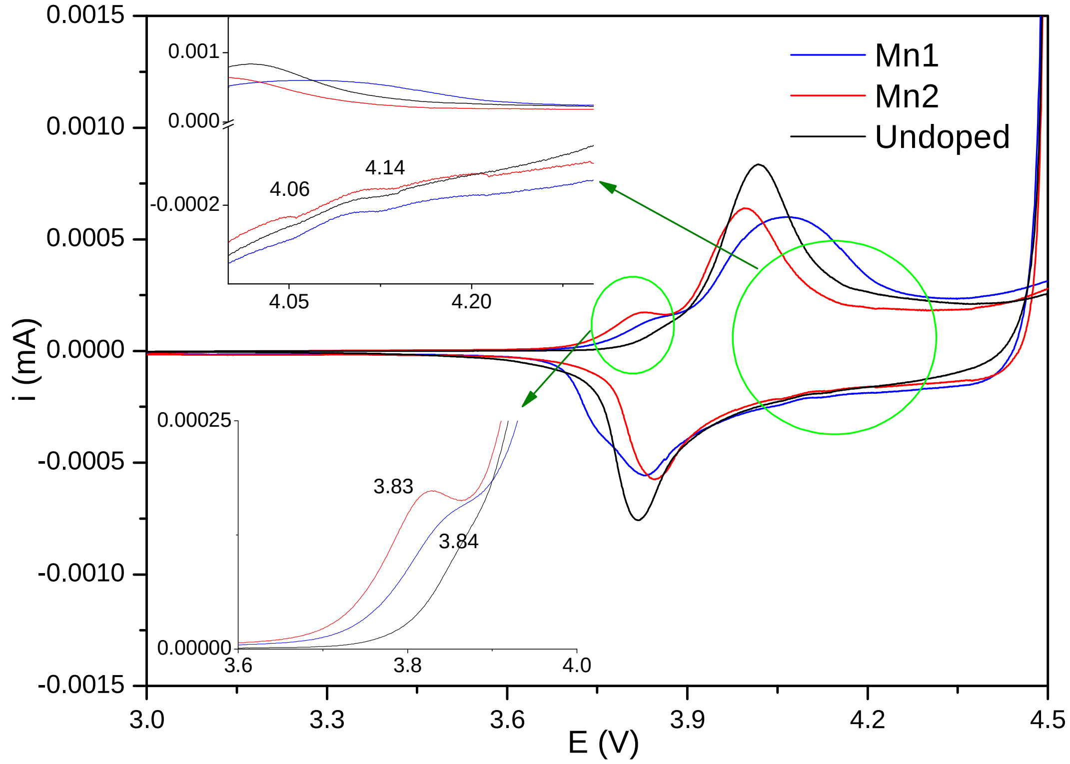

Figure 6.28. CVs of Mn1, Mn2 and undoped samples with scan rates of ν = 0.02mV/s.

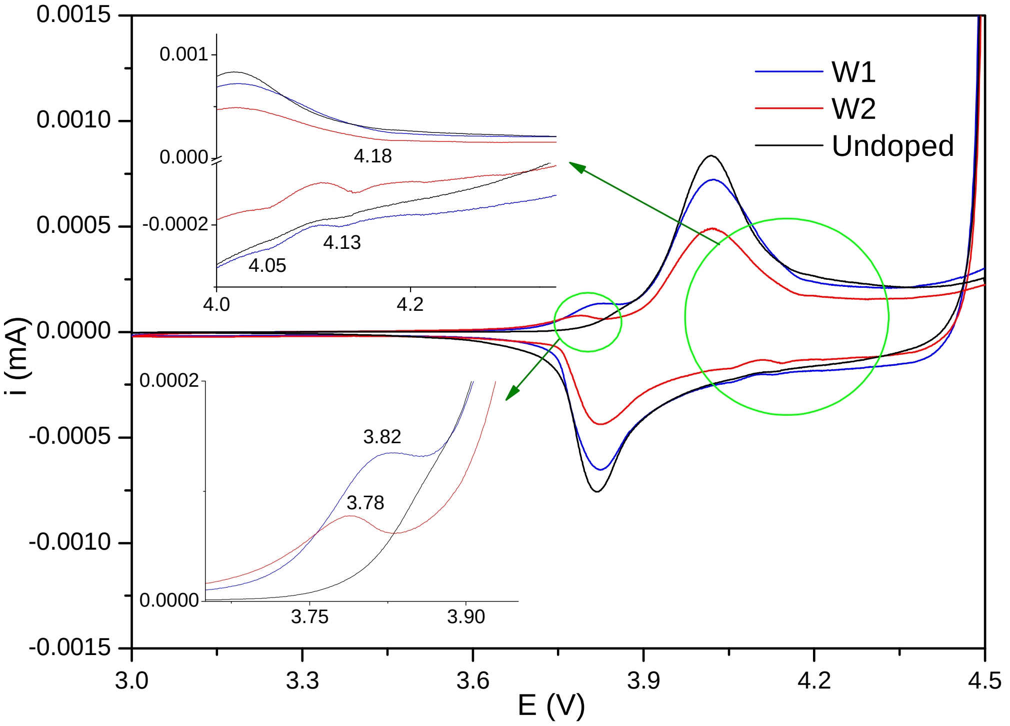

Figure 6.29. CVs of W1, W2 and undoped samples with scan rates of ν = 0.02mV/s.

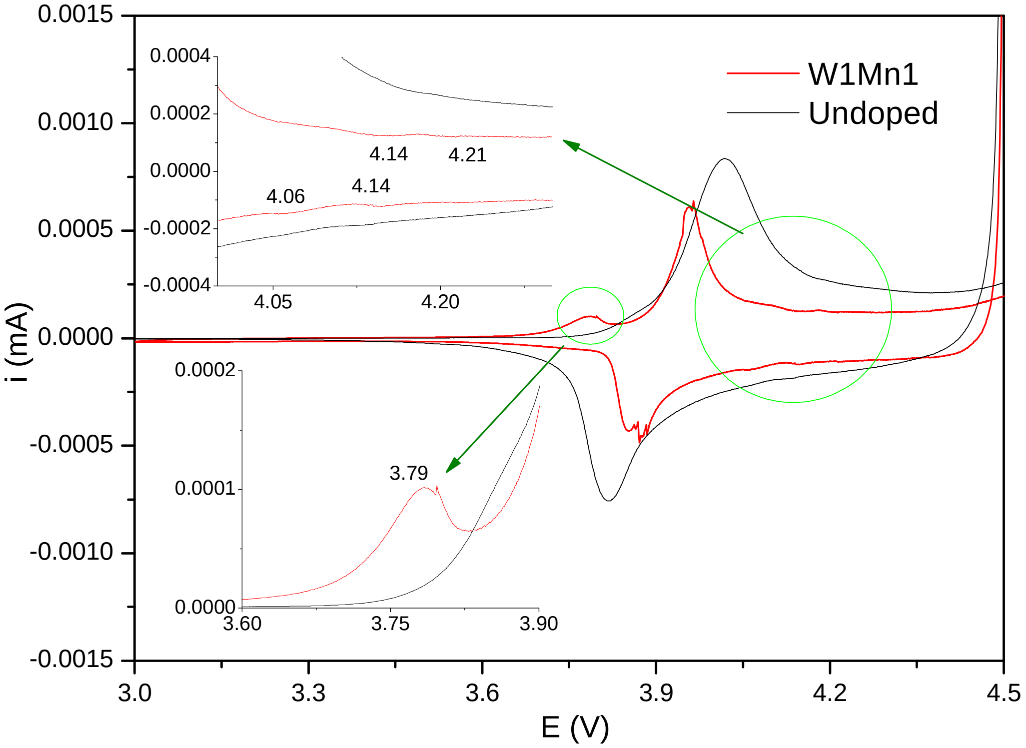

Figure 6.30. CVs of W1Mn1 and undoped samples with scan rates of ν = 0.02mV/s.

6.5. Electrochemical Impedance Spectroscopy (EIS)

In the previous section it was determined that the better electrochemical properties of W1Mn1 were resulted from lower polarization resistance of this sample rather than structural property and chemical content of this sample. In order to validate this statement, EIS was applied to all samples. The results of EIS for all samples are given from Figures 6.31 to 6.35.

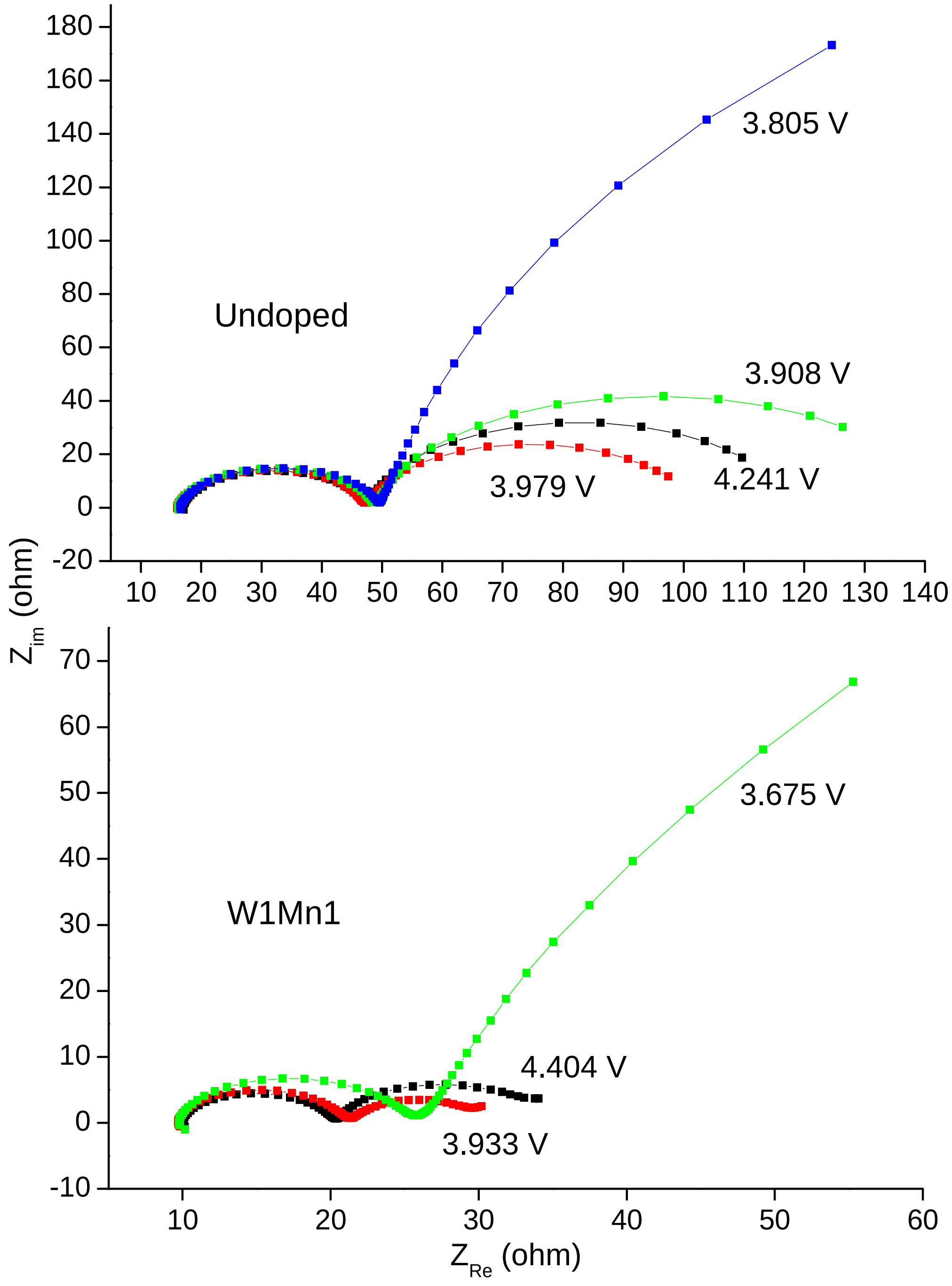

Figure 6.31. Nyquist plots of undoped and W1Mn1 with OCV values near each plot.

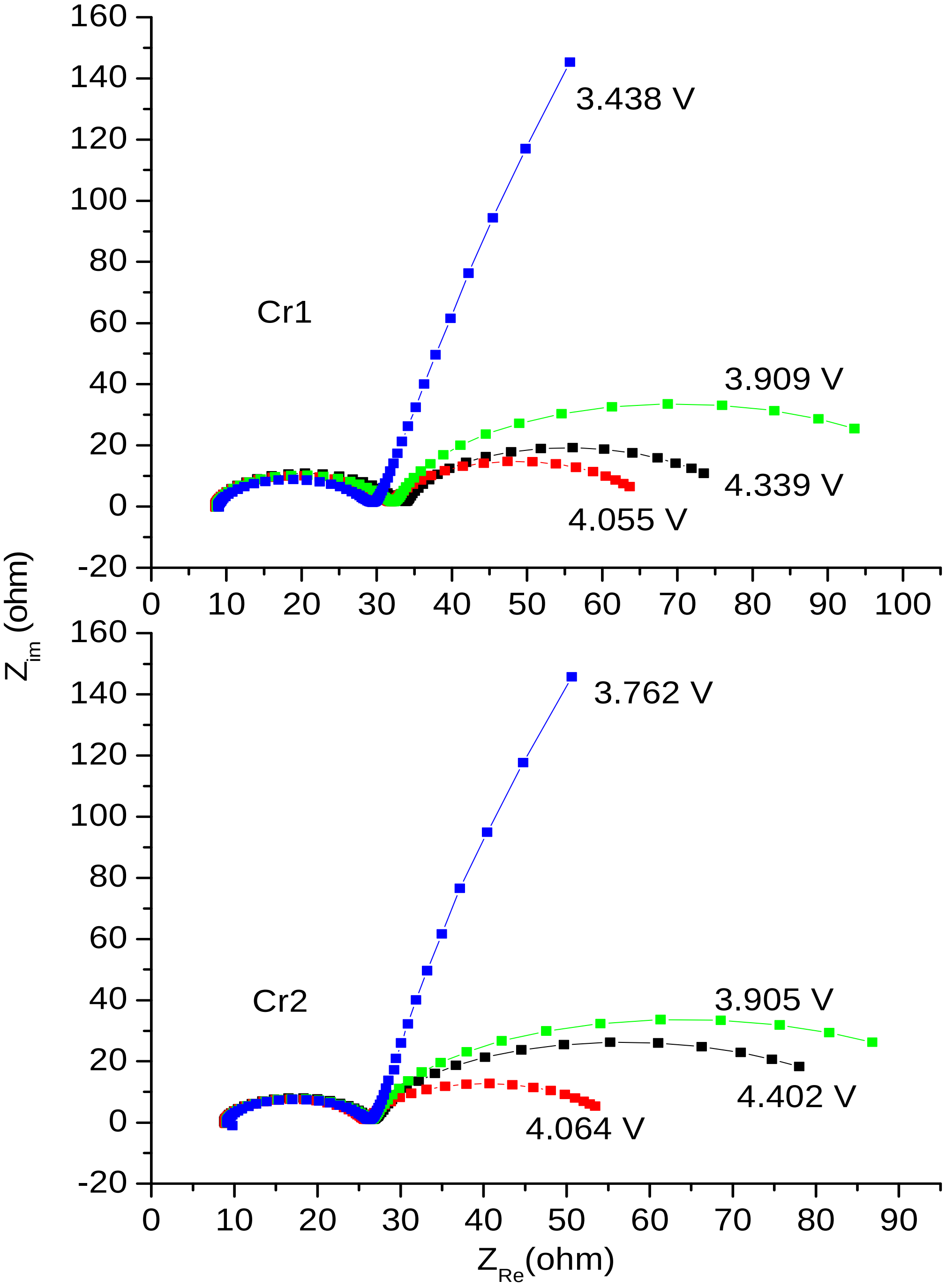

Figure 6.32. Nyquist plots of Cr1 and Cr2 with OCV values near each plot.

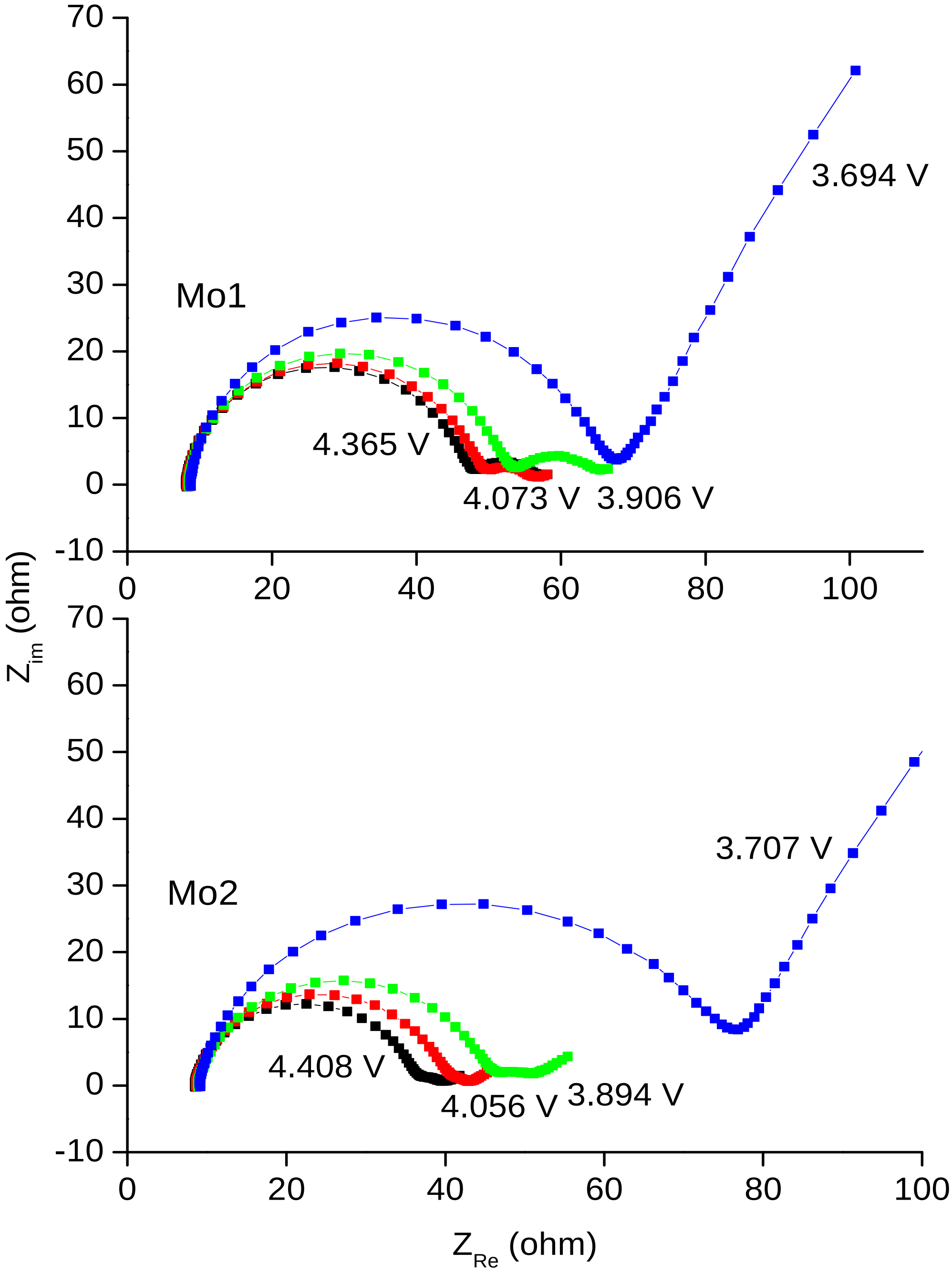

Figure 6.33. Nyquist plots of Mo1 and Mo2 with OCV values near each plot.

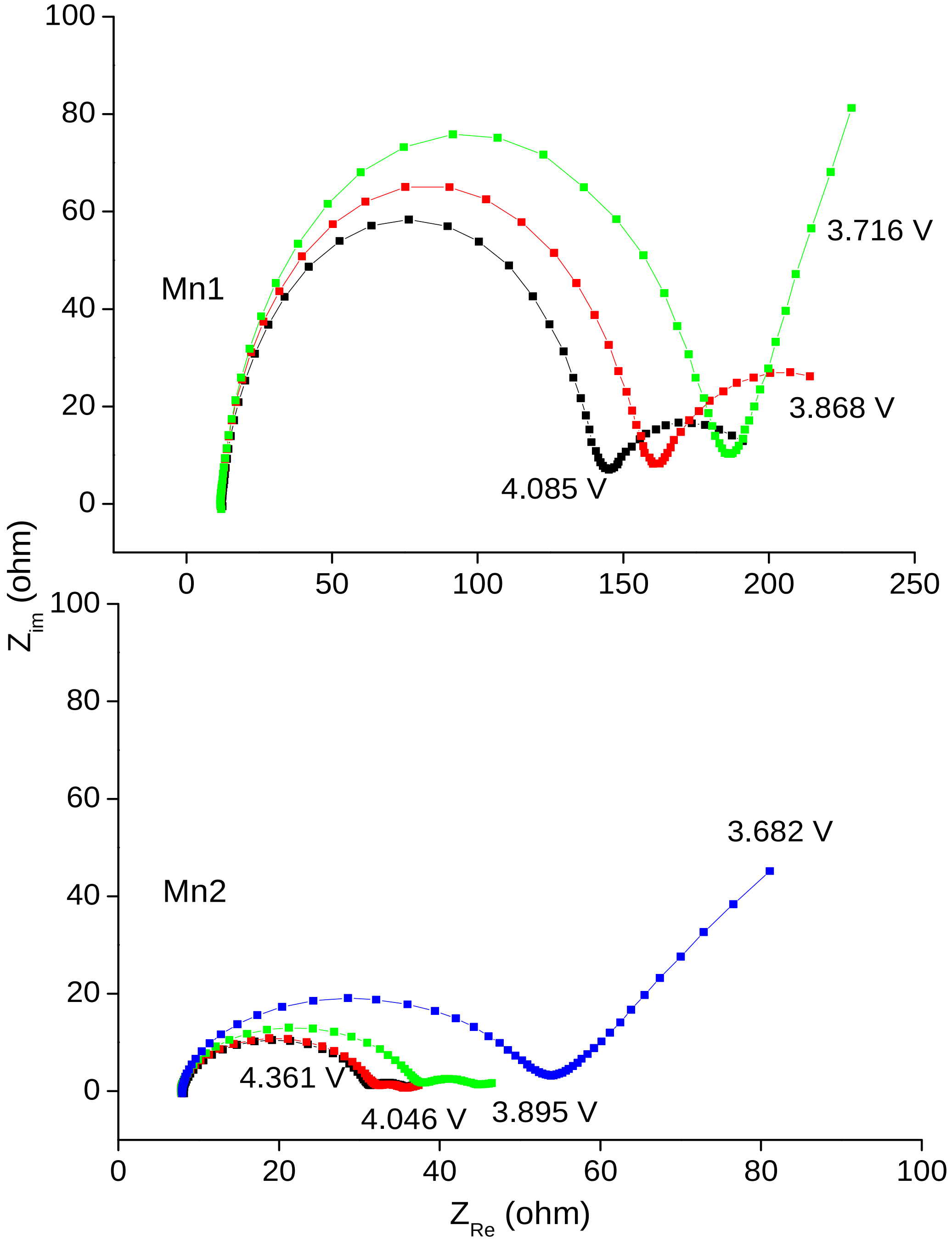

Figure 6.34. Nyquist plots of Mn1 and Mn2 with OCV values near each plot.

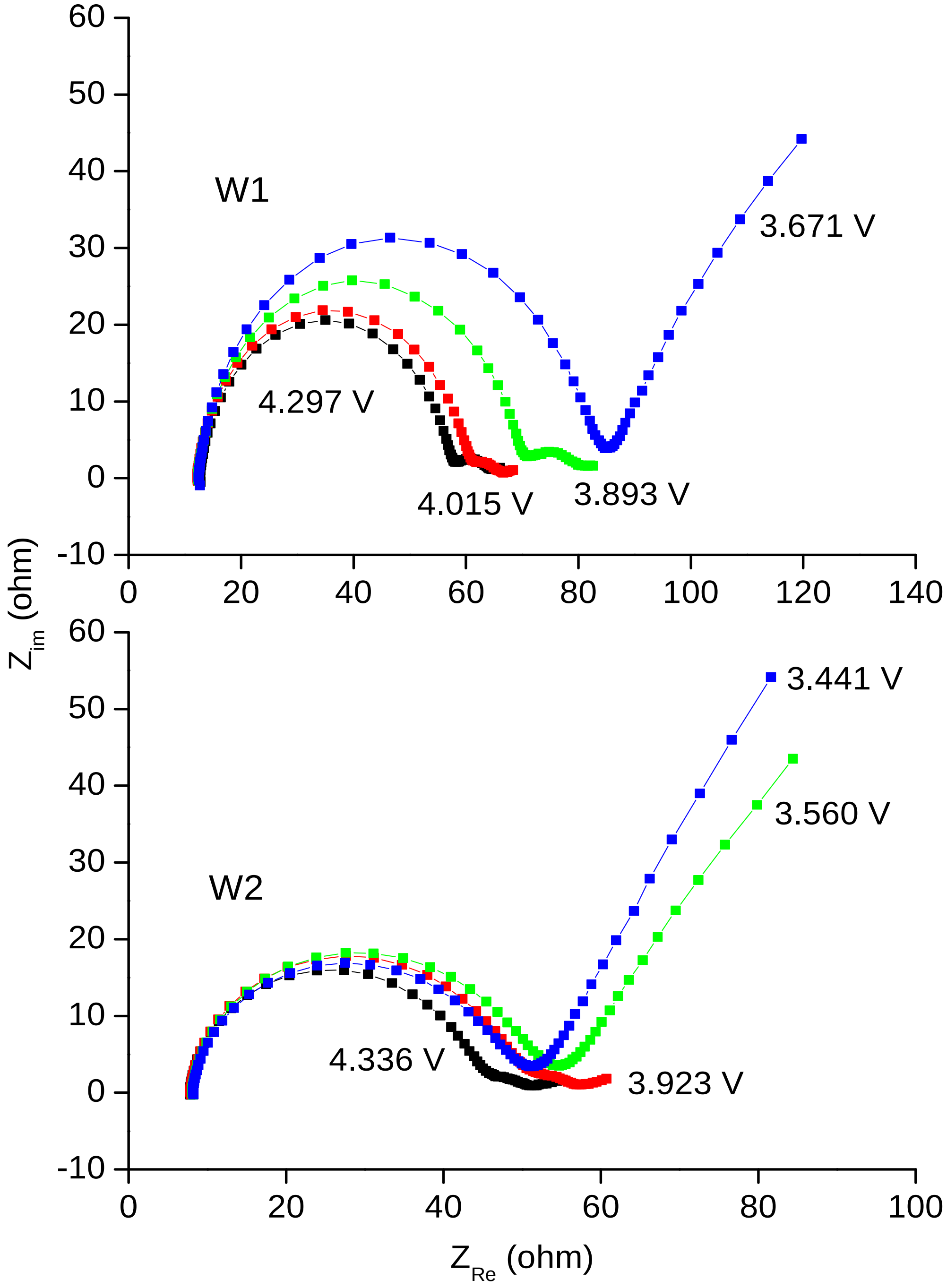

Figure 6.35. Nyquist plots of W1 and W2 with OCV values near each plot.

EIS results were fitted to three models that were discussed in detail in Chapter 3 (refer to Figure 3.14) by using ZsimpWin commercial software [115]. These models were surface layer model (SL), adatom model (AD) and modified adatom model (mAD). For illustration purposes, an experimental data as well as the fit data are given in Figure 6.36 for Mo1.

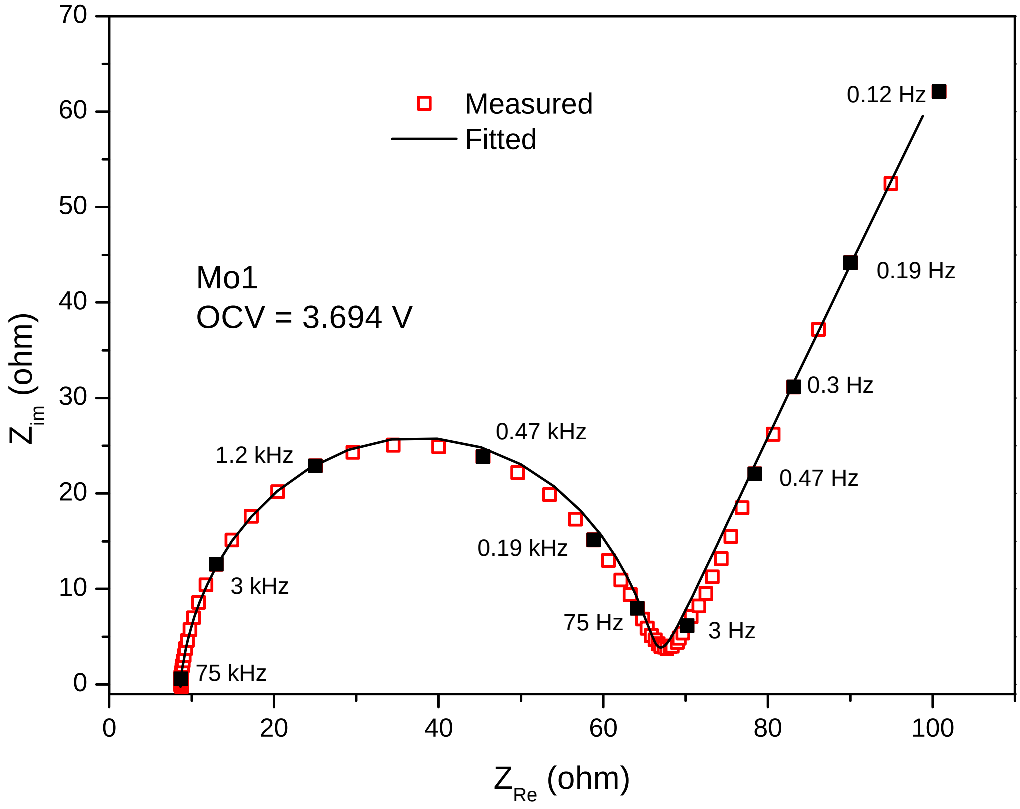

Figure 6.36. Experimental and fit data of Mo1. Frequency values are black squares.

The three models were fitted to the EIS results by using the same method as illustrated in Figure 6.36. Their χ^2 (chi-squared distribution) were estimated for every OCVs in order to decide for the best fitted model. From Table 6.8, the values χ^2 can be seen for these models.

As it is seen from Table 6.8, the lowest values for all samples and open circuit voltages were belong to the surface layer (SL) model. Therefore the study will discuss the results of EIS by taking SL model into account. In this model, according to Levi et al. [94] semi-circle belonging to surface layer impedance is potential independent. In this study this independency can be seen from Figures 6.31 to 6.35 and 6.37. Moreover; they claimed that [94], rough calculations of capacitance of this film yielded values around 10^{-6} F which is the case in this study as evidenced from Table 6.9 and Figure 6.39. They related charge transfer to slow Li^+ ion interfacial transfer between surface film and $LiCoO_2$ particle in the cathode and they claimed dependency of this resistance to potential [94]. This is again the case observed in this study as seen from Figures 6.31 to 6.35 and 6.38.

The numerical values of resistances for surface film and charge transfer for SL model given in Table 6.9. Surface film capacitances in Table 6.9 were estimated by using the formulas given in Chapter 3 as equations 3.14 and 3.15. Both equations were used for all samples and it was seen that there was only minor differences such as 1 μF in capacitance values. For this reason, only results of equation 3.15 are given in Table 6.9.

Table 6.8. The values χ^2 with different models and OCVs.

Sample	Model	**χ^2 at various OCVs**			
Undoped	OCV, V	3.805	3.908	3.979	4.241
	SL	**4,418E-05**	**4,943E-05**	**3,464E-05**	**3,286E-05**
	AD	3,943E-04	4,242E-04	4,098E-04	3,759E-04
	mAD	5,434E-04	4,660E-04	4,098E-04	3,759E-04
Cr1	OCV, V	3.438	3.909	4.055	4.339
	SL	**1,937E-04**	**1,351E-04**	**1,180E-04**	**1,370E-04**
	AD	1,049E-03	8,760E-04	8,873E-04	9,357E-04
	mAD	5,101E-02	6,966E-04	8,873E-04	9,300E-04
Cr2	OCV, V	3.762	3.905	4.064	4.402
	SL	**3,050E-04**	**1,019E-04**	**7,263E-05**	**2,238E-04**
	AD	7,284E-04	4,562E-04	3,650E-04	4,383E-04
	mAD	4,339E-04	3,165E-04	3,647E-04	3,758E-04
Mo1	OCV, V	3.694	3.906	4.073	4.365
	SL	**1,805E-04**	**7,506E-05**	**7,051E-05**	**6,242E-05**
	AD	1,263E-03	4,911E-04	2,818E-04	4,038E-04
	mAD	1,561E-03	-----	-----	-----
Mo2	OCV, V	3.707	3.894	4.056	4.408
	SL	**7,172E-05**	**9,236E-05**	**7,376E-05**	**6,456E-05**
	AD	2,890E-04	4,301E-04	2,027E-04	2,286E-04
	mAD	3,421E-03	4,321E-04	2,029E-04	2,295E-04
Mn1	OCV, V	3.716	3.868	-----	4.085
	SL	**1,596E-05**	**1,412E-05**	-----	**2,039E-05**
	AD	-----	-----	-----	-----
	mAD	-----	-----	-----	1,413E-03
Mn2	OCV, V	3.682	3.895	4.046	4.361
	SL	**3,184E-04**	**9,593E-05**	**7,324E-05**	**4,335E-05**
	AD	1,416E-03	2,978E-04	1,703E-04	1,893E-04
	mAD	1,495E-03	2,979E-04	2,038E-04	1,893E-04
W1	OCV, V	3.671	3.893	4.015	4.297
	SL	**1,153E-05**	**8,603E-05**	**6,732E-05**	**4,711E-05**
	AD	4,501E-04	4,246E-04	2,495E-04	2,683E-04
	mAD	4,653E-04	4,246E-04	2,496E-04	2,683E-04
W2	OCV, V	3.441	3.560	3.923	4.336
	SL	**4,086E-04**	**2,345E-04**	**2,125E-04**	**1,750E-04**
	AD	2,104E-03	8,243E-04	2,986E-04	2,606E-04
	mAD	2,715E-03	8,375E-04	2,992E-04	2,068E-04
W1Mn1	OCV, V	3.657	3.933	-----	4.404
	SL	**2,012E-04**	**5,166E-05**	**-----**	**4,627E-05**
	AD	5,360E-04	2,900E-04	-----	2,744E-04
	mAD	8,698E-04	2,943E-04	-----	2,911E-04

Table 6.9. Surface film resistance and capacitances as well as charge transfer resistances of the samples for all OCVs.

Values for surface film resistances (R_{sf})				
Sample	*Resistances (ohm) - OCV Values (V)*			
Undoped	33.12 – 3.805	32.63 – 3.908	31.19 – 3.979	30.49 – 4.241
Cr1	20.62 – 3.438	23.48 – 3.909	23.17 – 4.055	24.89 – 4.339
Cr2	17.20 – 3.762	17.46 – 3.905	16.95 – 4.064	17.86 – 4.402
Mo1	57.43 – 3.694	43.42 – 3.906	39.63 – 4.073	38.57 – 4.365
Mo2	65.84 – 3.707	34.24 – 3.894	29.41 – 4.056	26.24 – 4.408
Mn1	170.40 – 3.716	145.8 – 3.868	-----	129.80 – 4.085
Mn2	44.13 – 3.682	28.29 – 3.895	23.21 – 4.046	22.61 – 4.361
W1	70.98 – 3.671	56.99 – 3.893	47.45 – 4.015	44.48 – 4.297
W2	41.37 – 3.441	47.15 – 3.560	39.12 – 3.923	34.85 - 4.336
W1Mn1	16.03 – 3.675	11.48 – 3.933	-----	10.35 – 4.404
Values for surface film capacitances (C_{sf})				
Sample	*Capacitances (μF) - OCV Values (V)*			
Undoped	3.05 – 3.805	3.11 – 3.908	3.10 – 3.979	3.04 – 4.241
Cr1	3.43 – 3.438	3.50 – 3.909	3.55 – 4.055	3.58 – 4.339
Cr2	3.45 – 3.762	3.43 – 3.905	3.42 – 4.064	3.51 – 4.402
Mo1	4.19 – 3.694	4.10 – 3.906	4.09 – 4.073	4.12 – 4.365
Mo2	2.87 – 3.707	3.83 – 3.894	3.89 – 4.056	3.85 – 4.408
Mn1	4.32 – 3.716	4.28 – 3.868	-----	4.19 – 4.085
Mn2	4.31 – 3.682	4.01 – 3.895	3.90 – 4.046	3.83 – 4.361
W1	3.98 – 3.671	3.89 – 3.893	3.87 – 4.015	3.81 – 4.297
W2	4.57 – 3.441	4.48 – 3.560	4.42 – 3.923	4.35 – 4.336
W1Mn1	3.90 – 3.675	3.72 – 3.933	-----	3.68 – 4.404
Values for charge transfer resistances (R_{ct})				
Sample	*Resistances (ohm) - OCV Values (V)*			
Undoped	715 – 3.805	93.20 – 3.908	54.28 – 3.979	69.50 – 4.241
Cr1	6468 – 3.438	75.71 – 3.909	34.26 – 4.055	44.80 – 4.339
Cr2	4437 – 3.762	75.40 – 3.905	29.26 – 4.064	60.42 – 4.402
Mo1	3867 – 3.694	15.21 – 3.906	9.94 – 4.073	11.50 – 4.365
Mo2	570 – 3.707	12.95 – 3.894	5.835 – 4.056	0.0011 – 4.408
Mn1	1846 – 3.716	79.89 – 3.868	-----	52.49 – 4.085
Mn2	2.86×10^{5} – 3.682	10.85 – 3.895	5.5 – 4.046	5.24 – 4.361
W1	248.7 – 3.671	12.74 – 3.893	8.247 – 4.015	8.476 – 4.297
W2	1.79×10^{17} – 3.441	43.72 – 3.560	11.97 – 3.923	10.28 – 4.336
W1Mn1	541 – 3.675	8.671 – 3.933	-----	13.55 – 4.404

Table 6.9 reveals numerically that surface film resistance of W1Mn1 has the lowest value for fully discharged condition (OCV of 3.675 V). This may be an indication that the electrochemical superiority of this sample may originate from modification of surface which makes the sample having higher ionic conduction.

Electrolyte resistance (R_{el}) is included in Surface Layer model, but the values of this parameter are not shown as they do not change significantly with the samples. It was seen that the values of R_{el} were between is 12.34±4.63 ohm. This is an expected result as same electrolyte solution is used in all cells.

Resistances of surface film and charge transfer as well as capacitance of surface film versus OCV plots can be seen from Figures 6.37 to 6.39. When Figure 6.37 is examined, it is seen that all impedance values are decreased with OCV values except that of Cr1 and W2. Minor increase in resistances is seen for these samples. For W1Mn1, the R_{sf} change with OCV values are very small (from 16.03 ohm to 10.35 ohm) indicating that the surface film formed during synthesis is stable upon lithium deintercalation. Besides this, W and/or Mn ions make the surface film more conductive. Same situation can be claimed for Cr2. The resistance of this sample does not change with Li deintercalation which reveals that surface film is stable during cycling processes.

Similar plots are drawn for charge transfer resistances (Figure 6.38, extreme values of W2, Mn2 and Mo2 are excluded in the plot). With OCV Values, significant change of R_{ct} is observed. This is expected since Levi et al. [94] claimed the dependency of this resistance to potential. The similarity of plots of R_{sf} and R_{ct} versus OCV is explained by Zhao et al. [116]. They claimed that formation of channels for Li-ion transfer was completed during the first charge-discharge cycle. Although the results of Zhao et al. [116] and this study show some consistencies, the decrease of R_{ct} with OCV values is much steeper in this study. Moreover; Nobili et al. [105] claimed that if R_{ct} did not change with OCV values, then rate-determining step of electrode reactions did not involve classical charge transfer instead this step could be ascribed to Li+ ion desolvation step. They [105] claimed that the overall mechanism was analogous to adatom model (AD model) in this case. As the experiments in this study did not fit well to this model, it may be assumed that sharp decrease of R_{ct} with OCV values is due to the charge-transfer of electrons being the rate determining step. Zhuang et al. [97] claim that with symmetry factor of 0.5, R_{ct} shows a rapid increase when $x<0.5$ (x is the insertion level of Li to host material) and rapid decrease when $x>0.5$. As relatively rapid increases are seen for all samples, it is believed at the lowest OCV, the insertion level of Li is lower than 0.5.

Figures 6.37, 6.38 and 6.39 display the change of R_{sf}, R_{ct} and C_{sf} with OCV values, respectively.

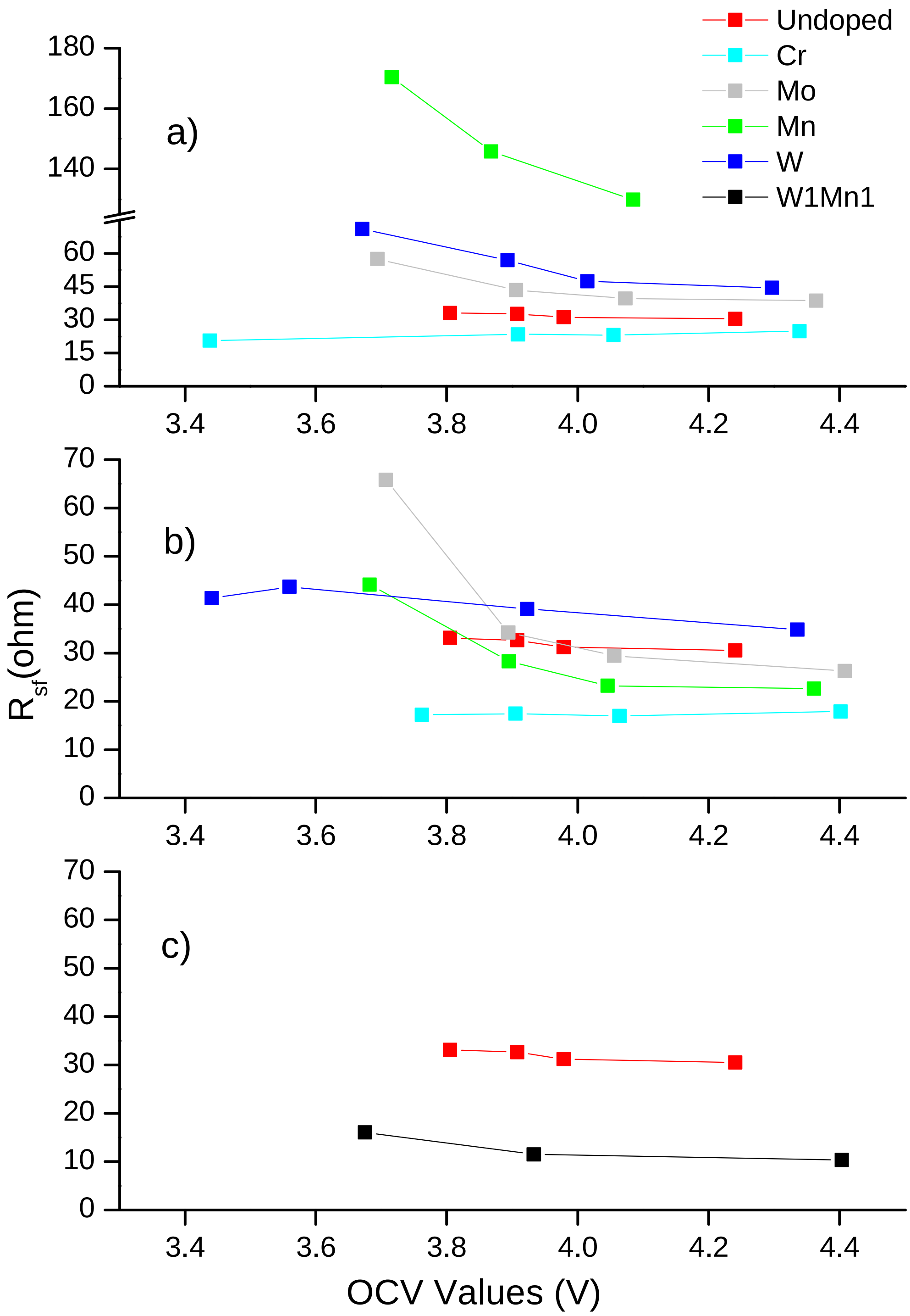

Figure 6.37 Surface film resistances of doped samples compared with undoped sample, a) Cr1, Mo1, Mn1, W1, b) Cr2, Mo2, Mn2, W2, c) W1Mn1.

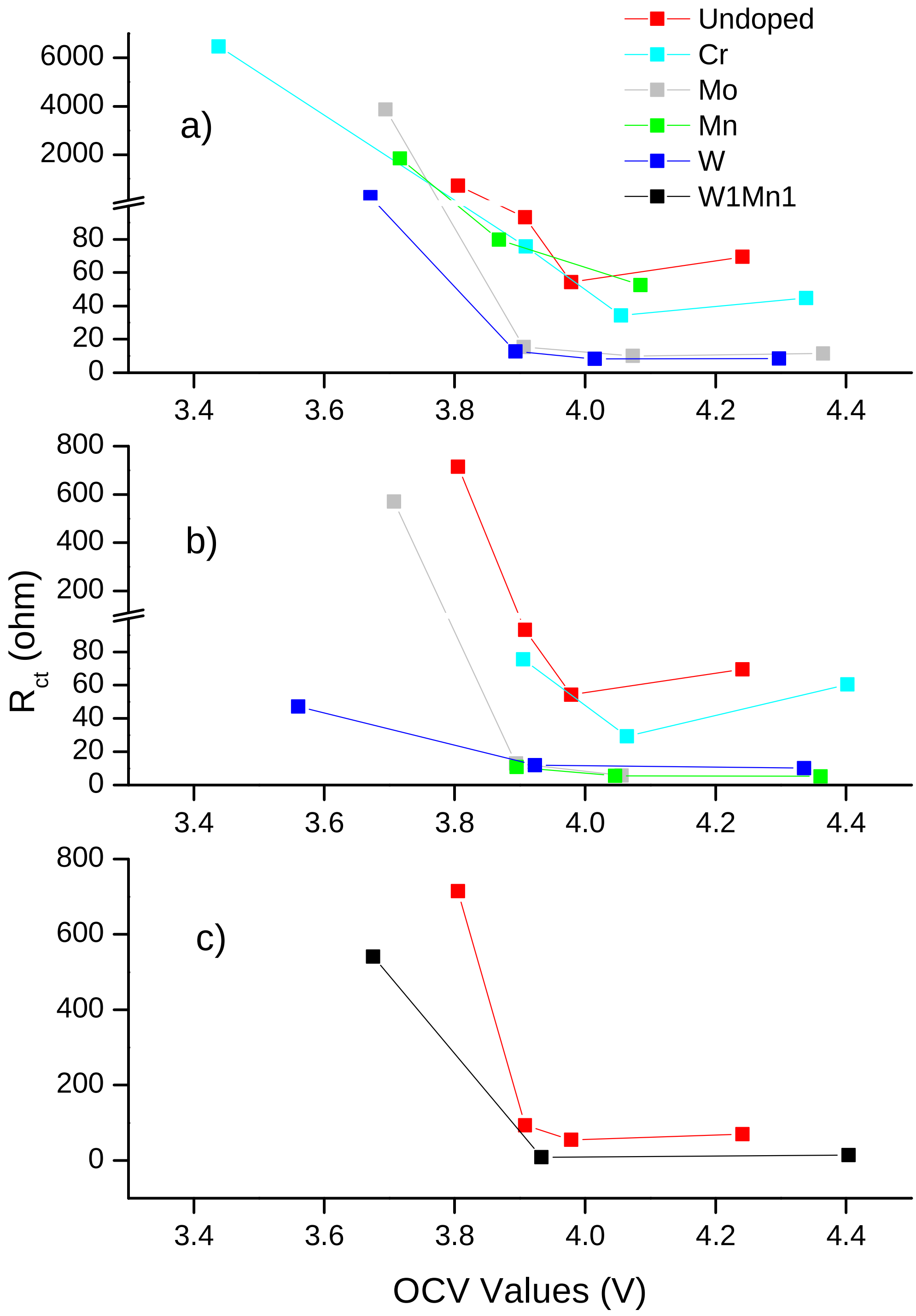

Figure 6.38. Charge transfer resistances of doped samples compared with undoped sample, a) Cr1, Mo1, Mn1, W1, b) Cr2, Mo2, Mn2, W2, c) W1Mn1.

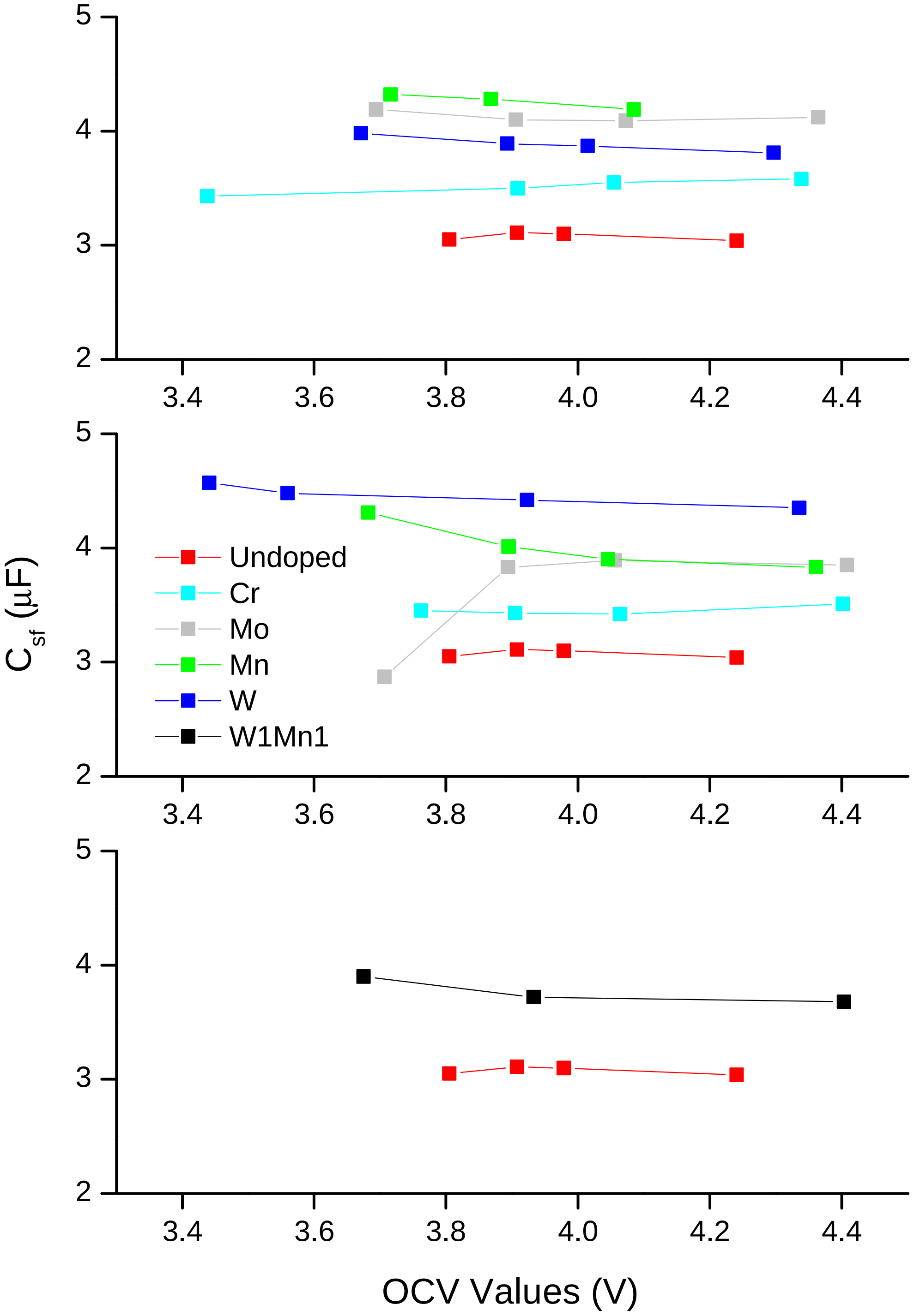

Figure 6.39. Surface film capacitances of doped samples compared with undoped sample, a) Cr1, Mo1, Mn1, W1, b) Cr2, Mo2, Mn2, W2, c) W1Mn1.

Surface film capacitances do not change significantly with OCV values, however a significant increase in capacitance values with the beginning of Li-deintercalation are seen with Mo2 which remains constant for further de-intercalation. Undoped, Cr and Mo doped samples show some minor deviations from steady decrease of capacitances with OCV values.

From capacitance versus OCV plots, it is seen that Cr doped samples and undoped sample have the smallest capacitance values. The reason for this behaviour may be attributed to two different parameters of these samples. It is known that capacitance is directly proportional with surface area of samples and inversely proportional with the thickness of surface film (as surface film is under investigation) according to equation 6.1.

$$C = \varepsilon \frac{A}{l} \tag{6.1}$$

where;
ε is permittivity of surface film, A is surface area of samples and, l is thickness of the surface film.

Therefore; two parameters responsible for lower capacitances of Cr doped and undoped samples may be higher particle size (low surface area) or high surface film thickness as also stated by Zhuang et al. [97].

Undoped and W1Mn1 were aged at discharged state in air tight cells for about 1 month. EIS data was again taken from these samples and plots of fresh (EIS data taken just after cell preparation) and aged samples were seen from Figure 6.40. It is seen that surface film formed on W1Mn1 is very stable and do not grow. The surface film resistance value (R_{sf}) remains nearly constant for about 1 month. However; for undoped, an increase in resistance value for solid-electrolyte interface is observed revealing that the film is growing with passage of time. Zhuang et al. [97] gives the formula of the rate of change of the thickness of surface film as in equation 6.2.

$$\frac{dl}{dt} = (\frac{1}{2}k)^{1/2} t^{-1/2} \tag{6.2}$$

where;
k is proportionality constant and t is time.

Zhuang et. al [97] claims that increasing thickness of surface film is causing the consumption of Li irreversibly. Therefore, the total Li loss during cycling is due to the increase of surface film thickness. From Figure 6.40, it is seen that surface film on W1Mn1 does not grow or rate of increase of thickness of surface film is very low. This stable surface film prevents the irreversible Li loss hence the material becomes stable.

Interestingly charge transfer resistance (R_{ct}) drops in W1Mn1 after aging.

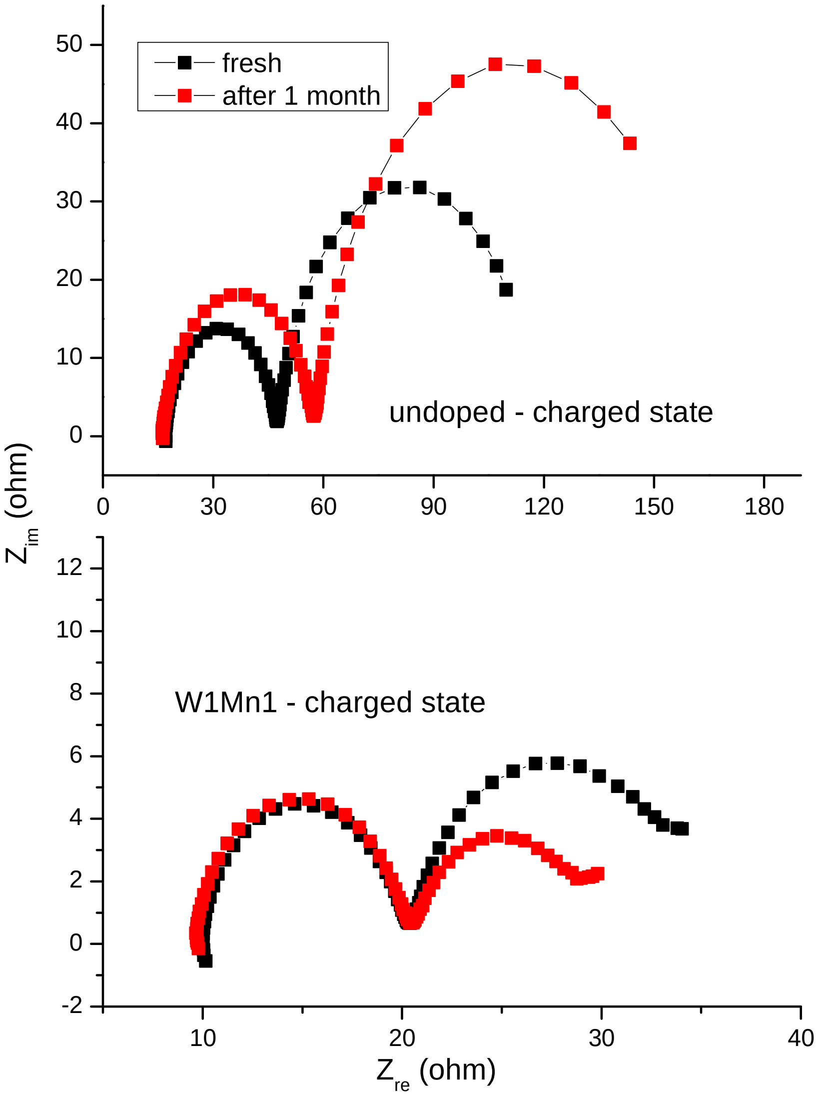

Figure 6.40. The change of impedances of undoped and W1Mn1 with time.

CHAPTER 7

DISCUSSION OF THE RESULTS

Throughout this study, 10 samples were produced and structural, microstructural and electrochemical characterization techniques were applied to these samples. W1Mn1 yields the best results when requirement for high energy cathode material is taken into account.

In order to explain the reason for electrochemical superiority of W1Mn1, firstly, the structural parameters are revised. Rietveld analyses of the samples showed that solid solution of $LiCo_{1-x-y}M_xN_yO_2$ could be produced. Therefore, Rietveld analyses were repeated by introducing only layered $LiCoO_2$ to the MAUD Programme [98] and XRD patterns were fitted by refining site occupations (Li and Co sites) and oxygen positions. Many studies in the literature explain the electrochemical performance increase by referring it to the increase in lattice parameter *c*. Increase of lattice parameter *c* results in wider gap for Li diffusion so that Li ions can more easily intercalate or deintercalate throughout the matrix. However; this approach excludes the change of position of oxygen atoms with doping. Without taking oxygen position (z) into account it is not possible to claim faster diffusion only by looking for lattice parameter *c*. For this argument, a new term called Li-gap (depicted in Figure 7.1) is introduced and it is calculated by below equation:

$$\mathrm{Li-gap} = \left[\frac{2}{3} - (2 \times z)\right] \times c \qquad (7.1)$$

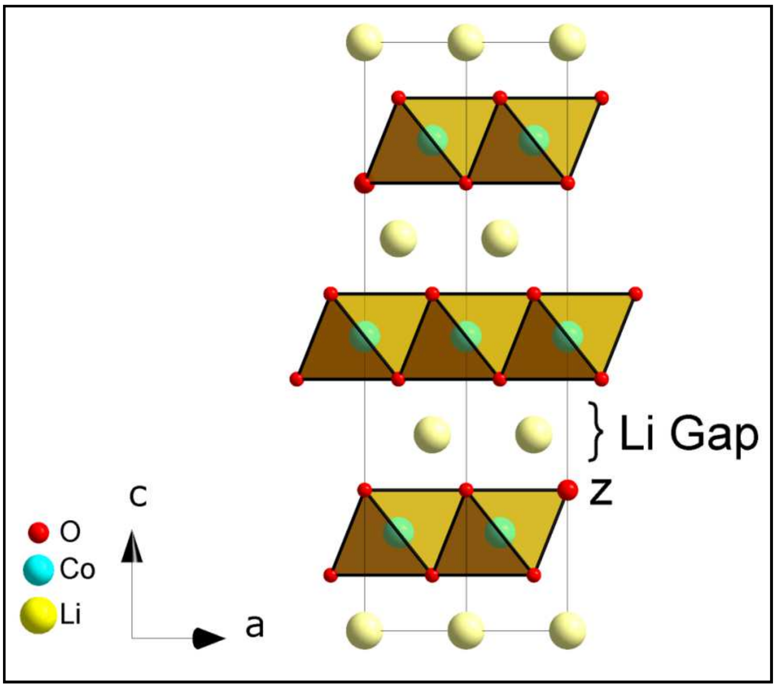

Figure 7.1. Schematic illustration of Li-gap in $LiCoO_2$ structure.

Table 7.1 is extended version of Table 6.1 in which lattice parameter *c*, oxygen position, Li-gap, diffusion coefficient during intercalation and formulas estimated by the results of ICP analysis can be seen. Although GSAS software [100] was also used for this purpose, more meaningful results were achieved with MAUD programme [98].

Table 7.1. Results of ICP and Rietveld analyses with refining site occupation and oxygen position (z). $D_{int.}$ stands for diffusion coefficient of Li during intercalation.

Sample	*c* (Å)	z	Li-gap (Å)	$D_{int.}$ $(cm^2/s) \times 10^{-9}$	Formulas based on ICP Result (Co is added to 1)
Undoped	14.063	0.2415	2.5840	0.5	$Li_{1.015}Co$
W1Mn1	14.071	0.2451	2.4825	0.4	$Li_{0.985}CoMn_{0.011}W_{0.0092}$
W1	14.070	0.2418	2.5763	0.3	$Li_{1.074}CoW_{0.0098}$
W2	14.074	0.2413	2.5903	0.7	$Li_{1.078}CoW_{0.0183}$
Mn1	14.070	0.2418	2.5759	0.7	$Li_{1.040}CoMn_{0.01}$
Mn2	14.074	0.2422	2.5664	0.1	$Li_{1.075}CoMn_{0.0198}$
Cr1	14.059	0.2421	2.5666	0.7	$Li_{1.043}CoCr_{0.0086}$
Cr2	14.058	0.2401	2.6209	0.6	$Li_{1.068}CoCr_{0.017}$
Mo1	14.067	0.2420	2.5688	0.2	$Li_{1.054}CoMo_{0.01}$
Mo2	14.070	0.2419	2.5736	0.3	$Li_{1.070}CoMo_{0.02}$

Increase in lattice parameter *c* is due to the differences in ionic radii. Shannon [117] estimated the ionic radii for the elements with different oxidation states. The radii of the elements used in this study are given in Table 7.2 with spin state, coordination number and oxidation states. Only the ionic radii with coordination number of 6 are given in Table 7.2.

Cobalt in layered HT-$LiCoO_2$ is at low spin state with oxidation state of 3+. The ionic radius of this ion is 0.545 Å. The ionic radii of Cr, Mo and Mn with oxidation state of 3+ are 0.615 Å, 0.690 Å and 0.580 Å, respectively. W does not have oxidation state of 3+. Ionic radius of W with oxidation state 4+ is 0.660 Å. The increase in lattice parameter *c* for Mo, Mn, W and W1Mn1 can be explained by higher ionic radii of these elements than Co^{3+}. It is strange that although Cr^{3+} has higher ionic radius than Co^{3+}, lattice parameters *c* of Cr1 and Cr2 are smaller than undoped. The most relevant explanation for this abnormal result is that Cr ions occupy some of Li sites. Pan et al. [67] found some fingerprints of Cr ions in Li-site by Li-MAS NMR study. As ionic radius of Li^+ is much higher than that of Cr^{3+}, shrinkage in lattice parameter *c* can be seen. This hypothesis can be corroborated by the lower first discharge capacity of Cr1 (97.2 mAh/g) than undoped (104.8 mAh/g). Cr2 still has lower lattice parameter *c* than undoped and the capacity of this sample is still lower than undoped. Therefore it can be claimed that Li sites are partly occupied by Cr atoms. Moreover, for Cr2, a formation of surface film with lower resistivity can be questioned by looking at higher rates of charge and discharge as well as capacity retention values (cycling property) in Tables 6.3 as well as Figures 6.9 and 6.13.

Table 7.2. Ionic radii of elements used in this study [117].

Element	Coordination Number	Spin State	Oxidation State	Ionic Radius (Å)
Li	6	-----	1+	0.760
Co	6	Low Spin	2+	0.650
		Low Spin	3+	0.545
		High Spin	4+	0.530
Cr	6	-----	2+	0.730
		-----	3+	0.615
		-----	4+	0.550
		-----	5+	0.490
		-----	6+	0.440
Mo	6	-----	3+	0.690
		-----	4+	0.650
		-----	5+	0.610
		-----	6+	0.590
Mn	6	Low Spin	2+	0.670
		High Spin	2+	0.830
		Low Spin	3+	0.580
		High Spin	3+	0.645
		-----	4+	0.530
		------	7+	0.460
W	6	-----	4+	0.660
		-----	5+	0.620
		-----	6+	0.600

When ICP results are discussed, it is seen that every sample except W1Mn1 has higher lithium content than the stoichiometric amount. This is an expected result as Li:Co ratio was chosen as 1.05:1 at the beginning of the experiments. The smallest Li:Co ratio belong to undoped with a value of 1.015. For all other doped elements, Li:Co ratios are higher for doping with 2 mole% than doping with 1 mole%. This is also expected as Li:Co:M ratio is chosen as 1.05:0.99:0.01 for 1 mole% doping and 1.05:0.98:0.02 for 2 mole% doping. Inherently, theoretical Li:Co ratio for doping with 1 mole% is 1.061 while this ratio is 1.071 for doping with 2 mole%. As content of phases other than HT-$LiCoO_2$ (most probably Li_2CO_3 or LT-$LiCoO_2$) was very low in the samples, overstoichiometry of Li is preserved. With this ratio in order to have charge neutrality, Co^{3+} ions should reduce to Co^{2+} ions. As Co^{2+} ions act as charge compensators [73], this assumption is valid. It is certain that occurrence of Co^{2+} ions at the surface retards formation of Co^{4+} ions during charge-discharge tests. One mechanism for decreasing of the cycle life is dissolution of Co^{4+} ions into the electrolyte due to the deintercalation of Li ions from host matrix $LiCoO_2$. During deintercalation, $LiCoO_2$ transforms into Li_xCoO_2 (x<1) and Co^{3+} oxidizes to Co^{4+}. Therefore the dissolution of Co^{4+} ions will be delayed and the cycle life can be improved for doped samples. This hypothesis is validated by the charge retention values in Table 6.3.

As it is seen that [003]/[104] ratio is lower than 1.2 for all samples and there occurs some minor peaks in CV for all doped samples, perfect ordering of elements in the structure cannot be claimed.

Above discussion is valid for all samples except W1Mn1. For W1Mn1, first of all, the findings of low diffusion coefficient of W1Mn1 from CV results are proved by the lowest value of Li-gap for W1Mn1. So it is certain that electrochemical superiority of W1Mn1 does not solely arise from lattice parameters increase and higher number of Co^{2+} ions. It is known that the increase of electrochemical property of this sample is due to its low surface film resistivity (section 6.5) and lower polarization resistance (section 6.4). It is believed that lower particle size of this sample (section 6.2) may not be regarded for explaining electrochemical performance as diffusion coefficient is not pointing out such a deduction. From ICP results, it is seen that only W1Mn1 has Li:Co ratio lower than 1. Therefore in order to see if oxidation state of Co in W1Mn1 is different than that of other samples, X-ray photoelectron spectroscopy spectra (XPS) for C, O, Li, Co, Mn and W were collected for W1, Mn1, undoped and W1Mn1. XPS spectra of O, Co, Mn and W can be seen in Figure 7.2.

From Figure 7.2, it is seen that especially for W1 and W1Mn1, there is one more peak for C and O spectra indicating that there is an impurity phase, most probably Li_2CO_3 in this sample. This argument is supported by Madhavi et al. [114] and Moses et al. [118] who claimed that extra O peak at 531.2 eV belonged to Li_2CO_3. Same situation exists for C peak. There occurs extra peak at 289.5 eV which matches that of C peak for Li_2CO_3 according to XPS database of National Institute of Standards and Technology (NIST) [119] and Khassin et al. [120].

For Li spectra; the peak at 59.8 eV coincides with that of Co 3p and the peak at 53.7 eV belongs to that of Li1s for $LiCoO_2$ [118].

For Co spectra, it seems that, $2p_{3/2}$ and $2p_{1/2}$ peaks are shifted towards higher binding energies and satellite peak is observed at binding energies of ~789 eV for all samples. However; the intensity of satellite peaks for W1Mn1 is highest and that of undoped is smallest. Moreover, the shift is largest for W1Mn1 and lowest for undoped. Peak shift and satellite peaks are an indication of occurrence of ions having oxidation state of 2+ according to Moses et al. [118], Prabakar et al. [121] and Tan et al. [122].

For Mn and W spectra, NIST is referred [119]. For W1Mn1, the peaks of Mn appeared at 641.8 eV ($Mn2p_{3/2}$) and 651.6 eV ($Mn2p_{1/2}$) and that of W appeared at 34.8 eV and 36.9 eV for $W4f_{7/2}$ and $W4f_{5/2}$, respectively. For Mn1, peaks of $Mn2p_{3/2}$ and $Mn2p_{1/2}$ were at 642.5 eV and 654.1 eV, respectively. For W1, peaks of $W4f_{7/2}$ and $W4f_{5/2}$ appeared at 34.9 eV and 37.1 eV.

According to [119], Mn peaks for Mn1 were in the vicinity of that of MnO_2 therefore some atoms of Mn have state of 4+. However; as ionic radius of Mn^{4+} is smaller than Co^{3+}, than expansion in lattice parameter *c* cannot be expected if all Mn atoms are in 4+ state. Ozawa et al. [123] indicated that lower binding energies and asymmetric spectra are legends of occurrence of Mn^{3+}. For Mn1, same arguments are valid. Mn peaks for W1Mn1 were best fitted with Mn compounds having Mn at the oxidation state of 2+. As a consequence, it can be claimed that Mn oxidation state in Mn1 is larger than that of W1Mn1.

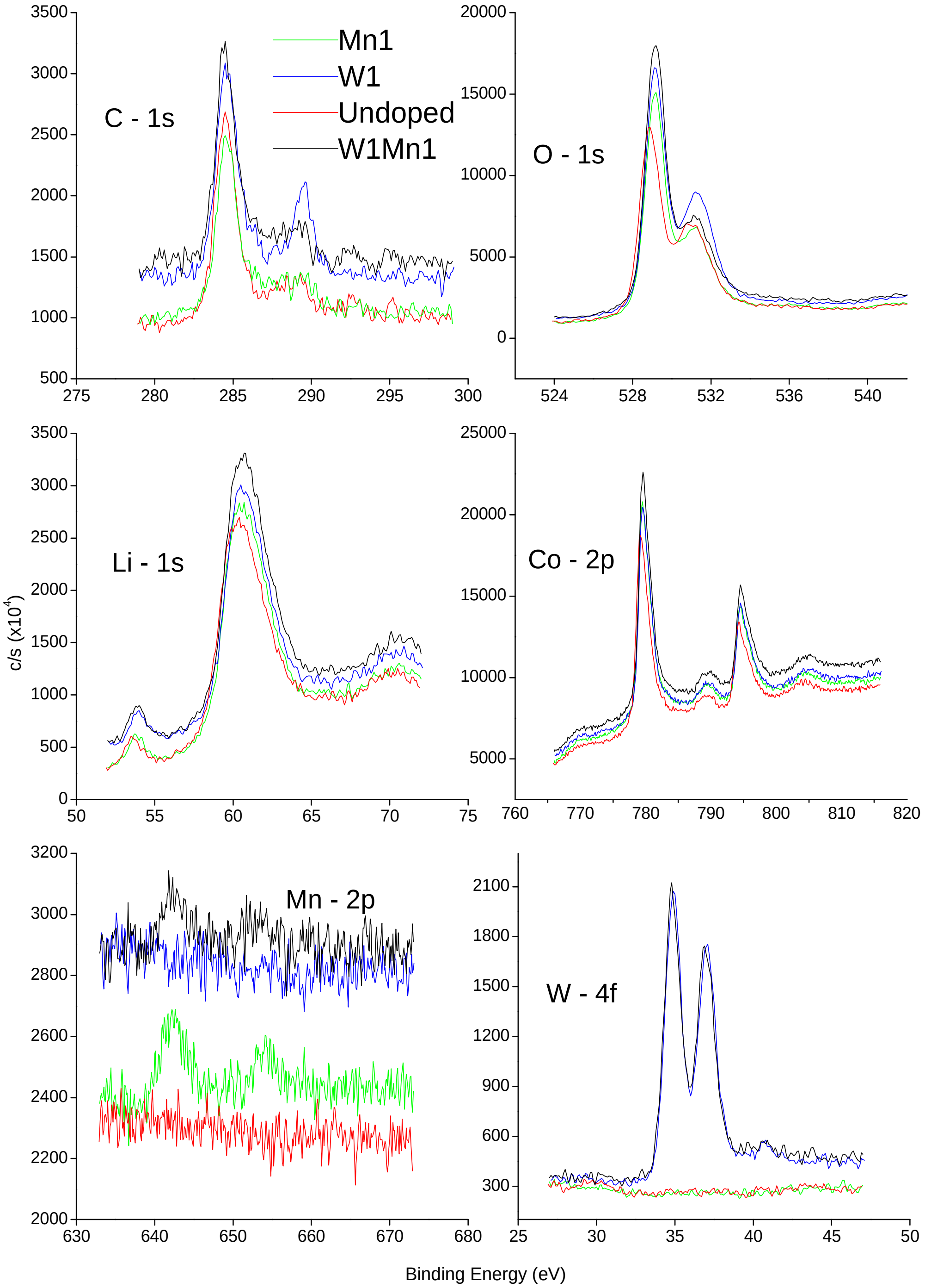

Figure 7.2. XPS spectra of undoped, Mn1, W1 and W1Mn1.

W peaks for W1 and W1Mn1 do no show significant differences and these peaks do not show any shoulder indicating that all W atoms were in the same oxidation state [121, 124]. Moreover; the peak values are in the vicinity of 6+ state according to [119].

From XPS spectra, it is seen that the content of Co^{2+} in W1Mn1 is not so different than that of other samples. Low ratio of [003]/[104] of W1Mn1 reveals that ordering in this sample is worse than other samples. Li sites are occupied by some of W or Mn ions which can be seen from lower lattice parameter c of W1Mn1 when compared with Mn2 and W2. The differences in first discharge capacities of W1Mn1 and other samples are so low that they are caused by experimental variations both during synthesis and ICP analysis. Therefore it is proposed that surface property of W1Mn1 is different than that of other doped samples. In order to see if there occurs surface modification of W1Mn1 in the presence of Mn and/or W, XPS at different depths was applied to this sample for determining if there are any differences for Mn and W content at the surface and in the bulk of the sample. The results can be seen in Figure 7.3. The sample was sputtered with Ar at energy of 3000 eV for 5 minutes. This process is repeated two times. From Figure 7.3, it is seen that surface chemistry is different as it is clearly seen that W content at the surface is much higher than the content in the bulk. The bulk content of W does not change with depth so it is clear that W accumulates on the surface for W1Mn1. Moreover, O shows different spectra at the surface which belong to Li_2CO_3 impurity as stated earlier [114, 118].

With all these results and discussions, it is deduced that better electrochemical performance of W1Mn1 is more related with surface rather than bulk diffusion or structural parameters.

In order to see the case in W only doped sample, another XPS was applied to W1. Exactly the same XPS procedure was applied as in W1Mn1. The results are given in Figure 7.4.

From Figures 7.3 and 7.4, it is seen that W and O are distributed similarly for W1Mn1 and W1. Both samples have similar W related surface chemistry and spectra for W and O are shifted for both samples at the surface. Besides satellite structures, as stated before, shift in XPS is another indication of different oxidation states. More specifically, according to Andersson [104], shift of binding energies is due to changes in chemical environment and oxidation state of a certain atom. It is believed that this situation is occurring in W1 and W1Mn1 so that shifts of O and W peaks are observed.

In spite of similarities in XPS spectra of W1Mn1 and W1 they show significantly different electrochemical performance. Therefore, the electrochemical superiority of W1Mn1 over W1 can be attributed to the role of Mn which distributed uniformly throughout the bulk.

Next few paragraphs are reserved for explaining the structural and electrochemical behaviour of W1Mn1 in this study.

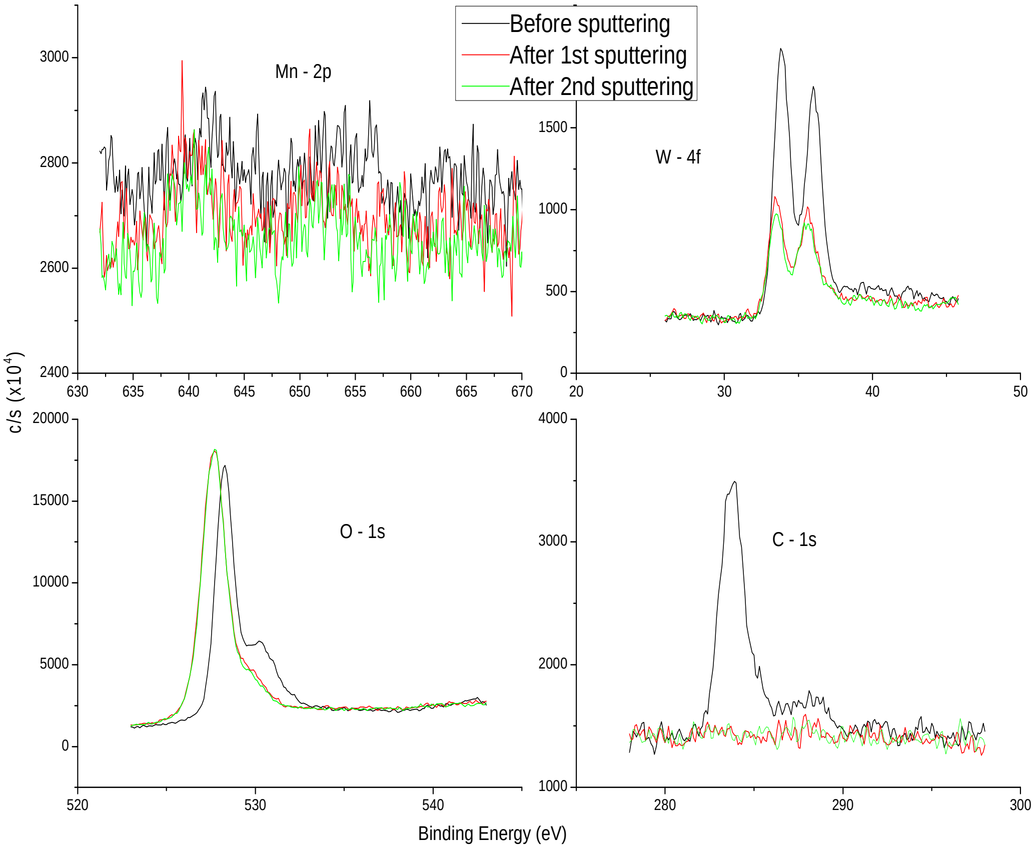

Figure 7.3. XPS spectra of W1Mn1, before sputter (on the surface), after first sputter and after second sputter (deeper depth than first sputter).

First of all, it is seen from [003]/[104] ratio that the ordering of W1Mn1 is lowest among all samples. Disordering of W1Mn1 is also seen from high voltage peaks obtained during CV. Increase of lattice parameter *c* with respect to undoped sample shows that W and Mn are incorporated into the structure of W1Mn1. However; some of these elements occupy Li-sites which can be seen from relatively low first discharge capacity. Also this sample contains minor amount of Li_2CO_3 as an impurity phase. These are responsible for lower ordering of this sample. Moreover; Li-gap is the smallest which leads to low diffusion coefficient. The data of Li-gap and diffusion coefficients yield consistent values.

Reversibility is satisfactorily high for this sample which can be proved from peak potential differences between anodic and cathodic scans (ΔE). The value of 0.069 V for this parameter is near to 0.059 V which is the value for full reversibility. Reversibility of this sample can also be determined from charge-discharge tests.

High rate capability of this sample is comparatively high that it retains about 84% of initial capacity after 85 cycles with 1 C charge rate.

Reversibility and high rate capability of this sample are not due to increase of diffusion coefficients. This is evidenced by lowest value of Li-gap and lowest value of diffusion coefficient. Moreover, increase of electrochemical performance does not depend to structural parameters which are lattice parameter *c* and ordering as depicted by [003]/[104] ratio. Beyond these parameters, electrochemical superiority is due to the surface character which has low resistance. This character cannot only be attributed to the presence of W rich layer at the surface unless Mn is present. This surface character modifies solid-electrolyte interface, makes it more conductive and stable. Moreover, dissolution of Co^{4+} which is responsible for degradation of the cathode material during cycling is prevented as a result of this behaviour.

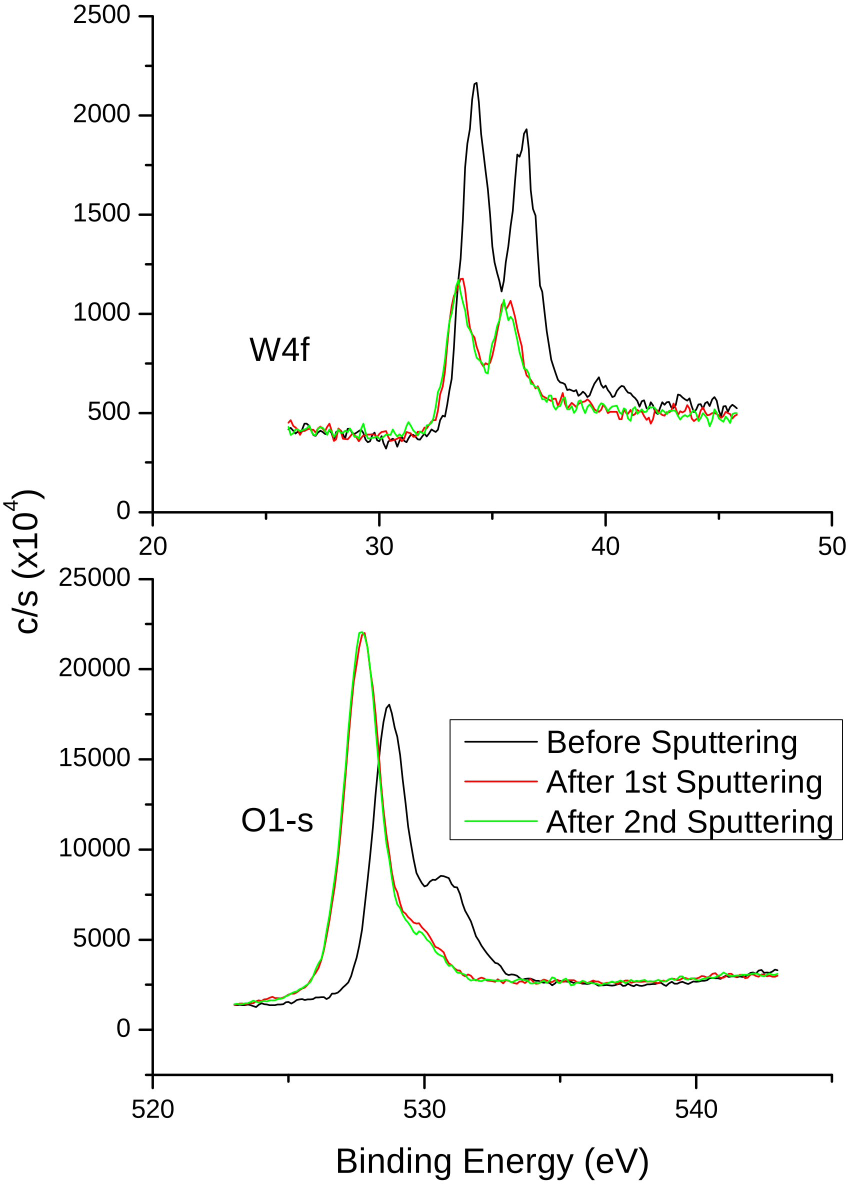

Figure 7.4. W4f and O1s peaks of W1.

Table 7.3 is a summary of data obtained for W1Mn1 in this study by comparing with undoped.

Table 7.3. The data obtained after structural and electrochemical characterization of W1Mn1 and undoped.

Parameter	Data of W1Mn1	Data of Undoped
[003]/[104] ratio	0.910, smallest of all samples	1.005
Lattice parameter *c*, (Å)	14.071	14.063
c/a	4.991	4.990
Li gap, (Å)	2.4825	2.5840
Particle size, nm	~ 200	~ 1000
First Discharge Capacity charged at 0.3C, mAh/g	105.5	104.8
First Discharge Capacity charged at 1C, mAh/g	99.2	95.7
Capacity retention after 82 cycles charged at 0.3C, %	87.8, largest of all samples	76.5
Capacity retention after 82 cycles charged at 1C, %	83.9, largest of all samples	59.2
ΔE between anodic and cathodic peak potentials during CV (V)	0.069, smallest of all samples	0.230
Deintercalation Diffusion Coefficient (cm^2/s) x 10^{-9}	0.9	2.7, largest of all samples
Slope of E vs. $\nu^{1/2}$ (during deintercalation)	0.332, smallest of all samples	1.786
High peak voltages during CV indicating inhomogeneous distribution of doped elements	at 4.14 and 4.21V during anodic at 4.06 and 4.14 V during cathodic scans	No high voltage peaks
Low peak voltage during CV indicating presence of Li_2CO_3	at 3.79 V during anodic scan	No low voltage peak
Surface film resistance at discharged state, ohm	16.03, smallest of all samples	33.12
Surface film resistance at charged state, ohm	10.35, smallest of all samples	30.49
Capacitance at discharged state, μF	3.90	3.05
Capacitance at charged state, μF	3.68	3.04, smallest of all samples
Charge transfer resistance at discharged state, ohm	541	715
Charge transfer resistance at charged state, ohm	13.55	69.5, largest of all samples
Aged surface film resistance with respect to fresh sample	Unchanged	Increased
Aged charge transfer resistance with respect to fresh sample	Decreased	Increased

CHAPTER 8

CONCLUSION

In this study, it is aimed to produce a cathode material with higher energy content. Two different production methods which both incorporate freeze drying and calcination processes are applied. The acetate-nitrate method did not yield satisfactory result as the close control of calcination process is difficult. With hydroxide method, layered and single phase $LiCoO_2$ can be produced.

During solution preparation and $Co(OH)_2$ synthesizing, it is observed that close control of pH value is needed. It must be hold at a value in the vicinity of 10.75. Increase of pH beyond this value causes another Co-containing phase (most probably Co_3O_4) to precipitate. This is undesired as decomposition Co_3O_4 requires elevated temperatures and Li_2CO_3 is formed with free Li which otherwise form $LiCoO_2$ by reacting and exchanging ion with $Co(OH)_2$. Formation of Li_2CO_3 and Co_3O_4 lead to conventional synthesis of $LiCoO_2$ which higher temperatures must be reached for production of single phase $LiCoO_2$. This is contradicting with the aim of applying freeze drying.

After extensive experiments, it is seen that Li:Co ratio is an important parameter for achieving single phase HT-$LiCoO_2$. Increasing of this ratio gives rise to impurity phases such as Li_2CO_3 and M containing phases. Moreover; excess Li occupy Co sites which results in low ordering of the samples evidenced from [003]/[104] ratio. Freeze drying of 24 hours is enough for effective drying of the samples. Calcinations at temperatures of about 700-750°C for 12-24 hours are needed for producing ordered and single phase undoped and doped HT-$LiCoO_2$. Applying pre-calcination at 350°C for 2 hours yield more ordered structures.

Doped element containing phases as well as Li_2CO_3 and Co_3O_4 are formed when the doping content is beyond 2 mole%. Nearly all doped elements show better high rate capability and cycleability than undoped sample. Undoped sample has the largest particle size.

Cycleability, polarization behaviour and rate capability of W1Mn1 is the best among other samples. The reason for this lies in the fact that surface of W1Mn1 becomes ionically conductive. It is seen that W1Mn1 can be used in batteries where high charge-discharge rates are needed. Moreover; as other electrochemical properties of this sample is very good, it can be a good candidate for replacing commercial $LiCoO_2$ based cathode materials.

The increase of electrochemical performance of W1Mn1 is not related with diffusion coefficient.

Although individual doping of W and Mn generally yields good electrochemical performance, simultaneous doping of these samples results in significant increase in high rate capability and cycleability.

Many studies in literature take the increase of lattice parameter *c* into account for explaining better electrochemical performance of doped HT-$LiCoO_2$. However; with this study, it is shown that this explanation is lacking as it does not regard the position of oxygen in the lattice. A new term Li-gap is introduced in this study which is estimated by a formula having both lattice parameter *c* and oxygen position z. Electrochemical performance is related with this term. It is seen that although increase of lattice parameter *c* is seen for almost all samples, electrochemical behaviour is not directly related with this increase. Moreover; Li-gap may not solely responsible for explanation of electrochemical behaviour.

Increase of ordering results in increase of electrochemical behaviour. During this study numerical values for ordering are estimated and there seems no difference between the ordering of the samples as all have [003]/[104] ratios in the vicinity of 1. However; it is generally observed that with doping, ordering decreases since they inhomogeneously distributed throughout the structure lowering the ordering of the structures. This is especially valid for W1Mn1 which is the best sample among the other samples in this study. Eventually it can be claimed that ordering change in this study does not mainly responsible for electrochemical performances.

To conclude it is seen that surface chemistries are very important for producing electrochemically superior cathode materials.

REFERENCES

[1] B.G.Pollet and J. I.Staffell, *Electrochimica Acta,* vol. 84, p. 235, 2012.

[2] M.Werber, M.Fischer and P.V.Schwartz, *Energy Policy,* vol. 37, p. 2465, 2009.

[3] S.Unnasch and L.Browning, “Fuel Cycle Energy Conversion Efficiency Analysis,” California Energy Commission, California, USA, 2000.

[4] M.Fischer, M.Werber and P.V.Schwartz, *Energy Policy,* vol. 37, p. 2639, 2009.

[5] H.Kawamoto, “Science & Technology Trends Quarterly Review No.36,” 2010.

[6] C.X.Zu and H.Li, *Energy & Environmental Science,* vol. 4, p. 2614, 2011.

[7] D.Hill and N.Mjos, “Adding Value to High Energy Density Batteries, Position Paper-12,” DNV, 2012.

[8] D. Linden and T. B. Reddy, Handbook of Batteries, 3rd ed., McGraw Hill, 2001, pp. 1.3-1.7 and p.35.5.

[9] *Rechargeable Batteries Applications Handbook,* USA: Butterworth-Heinemann, 1998.

[10] G. Pistoia, Batteries for Portable Devices, Elsevier, 2005, p. 33.

[11] N. Kularatna, Power Electronics Design Handbook, 2nd ed., Butterworth-Heinemann, 1998, p. 142.

[12] J.T.Vaughey, L. Fransson, H. Swinger, K. Edström and M. Thackeray, *Journal of Power Sources,* vols. 119 - 121, p. 64, 2003.

[13] W. A. v. Schalkwijk and B. Scrosati, Advances in Li-ion Batteries, Kluwer Academic Publishers, 2002, p. 79.

[14] G. Pistoia, Batteries for Portable Devices, Elsevier, 2005, p. 114.

[15] K.Ozawa, *Solid State Ionics,* vol. 69, p. 212, 1994.

[16] R.E.Franklin, *Proceedings of the Royal Society A,* vol. 209, p. 196, 1951.

[17] C.A.Vincent and B.Scrosati, Modern Batteries, 2nd ed., Elsevier, 1997, pp. 217-219.

[18] M.S.Whittingham, *Chemical Reviews,* vol. 104, p. 1471, 2004.

[19] J.W.Fergus, *Journal of Power Sources,* vol. 195, p. 939, 2010.

[20] H.Kawai, M. Nagata, H. Tukamoto and A. West, *Journal of Power Sources,* vols. 81-82, p. 67, 1999.

[21] R.J.Gummow and M. Thackeray, *Materials Research Bulletin,* vol. 27, p. 327, 1992.

[22] R.J.Gummow, D.C.Liles, M.M.Thackeray and W.I.F.David, *Materials Research Bulletin,* vol. 28, p. 1177, 1993.

[23] R.B.Ellestad and B. Babbitt.Patent US2545424, 1951.

[24] W.D.Johnston, R. Heikes and D. Sestrich, *Journal of Physics and Chemistry of Solids,* vol. 7, p. 1, 1958.

[25] K.Mizushima, P. Jones, P. Wiseman and J. Goodenough, *Materials Research Bulletin,* vol. 15, p. 783, 1980.

[26] E.Antolini, *Solid State Ionics,* vol. 170, p. 159, 2004.

[27] S.G.Kang, S. Kang, K. Ryu and S. Chang, *Solid State Ionics,* vol. 120, p. 155, 1999.

[28] W.T.Jeong and K. Lee, *Journal of Power Sources,* vol. 104, p. 195, 2002.

[29] A.Burukhin, O. Brylev, P. Hany and B. Churagulov, *Solid State Ionics,* vol. 151, p. 259, 2002.

[30] Y.Li, C. Wan, Y. Wu, C. Jiang and Y. Zhu, *Journal of Power Sources,* vol. 85, p. 294, 2000.

[31] E.I.Santiago, A. Andrade, C. Santosc and L. Bulhoes, *Solid State Ionics,* vol. 158, p. 91, 2003.

[32] H.Yan, X. Huang, Z. Lu, H. Huang, R. Xue and L. Chen, *Journal of Power Sources,* vol. 68, p. 530, 1997.

[33] K.Y.Choi, K. Kim and Y. Yang, *Journal of Materials Processing Technology,* vol. 171, p. 118, 2006.

[34] Y.M.Chiang, Y. Jang, H. Wang, B. Huang, D. Sadoway and P. Ye, *Journal of the Electrochemical Society,* vol. 145, p. 887, 1998.

[35] O.A.Brylev, O. Shlyakhtin, T. Kulova, A. Skundin and Y. Tretyakov, *Solid State Ionics,* vol. 456, p. 291, 2003.

[36] C.Delmas, C. Fouassier and B. Hagenmuller, *Physica B+C,* vol. 99, p. 81, 1980.

[37] J.W.Choi, unpublished Ph.D. Thesis submitted to "The University of Texas at Austin", Texas, USA, 2006.

[38] C.D.W.Jones, E. Rossen and J. Dahn, *Solid State Ionics,* vol. 68, p. 65, 1994.

[39] A.Honders, J. der Kinderen, A. van Heeren, J. de Wit and G. Broers, *Solid State Ionics,* vol. 15, p. 265, 1985.

[40] O.A.Shlyakhtin, S. Choi, S. Yoon and Y. Oh, *Electrochimica Acta,* vol. 50, p. 505, 2004.

[41] K.Kanamura, A. Goto, R. Ho, T. Umegaki, K. Toyoshima, K. Okada, Y. Hakuta, T. Adschiri and K. Arai, *Electrochemical and Solid State Letters,* vol. 3, p. 256, 2000.

[42] A.K.Arof, *Journal of Alloys and Compounds,* vol. 449, p. 288, 2008.

[43] E.D.Jeong, M. Won and Y. Shim, *Journal of Power Sources,* vol. 70, p. 70, 1998.

[44] W.T.Jeong and K. Lee, *Journal of Power Sources,* vol. 104, p. 195, 2002.

[45] M.Sathiya, A. Prakash, K. Ramesha and A. Shukla, *Materials,* vol. 2, p. 857, 2009.

[46] D.Larcher, M. Palacin, G. Amatucci and J. Tarascon, *Journal of the Electrochemical Society,* vol. 144, p. 408, 1997.

[47] S.Venkatraman, V.Subramanian, S.G.Kumar, N.G.Renganathan and N.Muniyandi, *Electrochemistry Communications,* vol. 2, p. 18, 2000.

[48] G.Ceder, Y.M.Chiang, D.R.Sadoway, M.K.Aydınol, Y.I.Jang and B.Huang, *Nature,* vol. 392, p. 694, 1998.

[49] M.K.Aydınol, A.F.Kohan, G.Ceder, K.Cho and J.Joannopoulos, *Physical Review B,* vol. 56, p. 1354, 1997.

[50] Y.I.Jang, B.Huang, H.Wang, G.R.Maskaly, G.Ceder, D.R.Sadoway, Y.M.Chiang, H.Liu and H.Tamura, *Journal of Power Sources,* vols. 81-82, p. 589, 1999.

[51] H.Huang, G.V.S.Rao and B.W.R.Chowdari, *Journal of Power Sources, v*ols. 81-82, p. 690, 1999.

[52] C.Julien, M.A.C.Lopez, M.Lemal and S.Ziolkiewicz, *Materials Sceince and Engineering B,* vol. 95, p. 9, 2002.

[53] S.T.Myung, N.Kumagai, S.Komaba, H.Chung, *Solid State Ionics,* vol.139, p.47, 2001.

[54] M.N.Khan and J.Bashir, *Materials Research Bulletin,* vol. 41, p. 1589, 2006.

[55] A.Kinoshita, K.Yanagida, A.Yanai, Y.Kida, A.Funahashi, T.Nohma and I.Yonezu, *Journal of Power Sources,* vol. 102, p. 283, 2001.

[56] C.Delmas and I.Saadoune, *Solid State Ionics,* vols. 53-56, p. 370, 1992.

[57] C.Julien, *Solid State Ionics,* vol. 157, p. 57, 2003.

[58] R.Alcantara, P.Lavela, J.L.Tirado, R.Stoyanova and E.Zhecheva, *Journal of the Electrochemical Society,* vol. 145, p. 730, 1998.

[59] R.Stoyanova, E.Zhecheva and L.Zarkova, *Solid State Ionics,* vol. 73, p. 233, 1994.

[60] K.Numata and S.Yamanaka, *Solid State Ionics,* vol. 118, p. 117, 1999.

[61] S.Waki, K.Dokko, T.Itoh, M.Nishizawa, T.Abe and I.Uchida, *Journal of Solid State Electrochemistry,* vol. 4, p. 204, 2000.

[62] M.Zou, M:Yoshio, S.Gopukumar and J.I.Yamaki, *Chemistry of Materials,* vol. 15, p. 4699, 2003.

[63] Y.Lu, M.Wei, L.Yang and C.Li, *Journal of Solid State Chemistry,* vol. 180, p. 1775, 2007.

[64] Y.Zheng, X.Huang, J.Dai, Z.Zhu and J.Xie, *Ceramics International,* vol. 37, p. 2913, 2011.

[65] N.Yabuuchi, K.Yamamoto, K.Yoshii, I.Nakai, T.Nishizawa, A.Omaru, T.Toyooka and S.Komaba, *Journal of the Electrochemical Society,* vol. 160, p. A39, 2013.

[66] S.Madhavi, G.V.S.Rao, B.V.R.Chowdari and S.F.Y.Li, *Electrochimica Acta,* vol. 48, p. 219, 2002.

[67] C.Pan, Y.J.Lee, B.Amundsen and C.P.Grey, *Chemistry of Materials,* vol. 14, p. 2289, 2002.

[68] M.Zou, M.Yoshio, S.Gopukumar and J.I.Yamaki, *Chemistry of Materials,* vol. 17, p. 1284, 2005.

[69] S.A.Needham, G.X.Wang, H.K.Liu, V.A.Drozd and R.S.Liu, *Journal of Power Sources,* vol. 174, p. 828, 2007.

[70] H.Tukamoto and A.R.West, *Journal of the Electrochemical Society,* vol. 144, p. 3164, 1997.

[71] Y.Jin, P.Lin and C.H.Chen, *Solid State Ionics,* vol. 177, p. 317, 2006.

[72] H.S.Kim, T.K.Ko, B.Ki.Na, W.I.Cho and B.W.Chao, *Journal of Power Sources,* vol. 138, p. 232, 2004.

[73] S.Gopukumar, Y.Jeong and K.B.Kim, *Solid State Ionics,* vol. 159, p. 223, 2003.

[74] V.Palomares, A.Goni, I. Muro, I. Meatza, M.Bengoechea, O.Miguel and T.Rojo, *Journal of Power Sources,* vol. 171, p. 879, 2007.

[75] V.Koleva, E.Zhecheva and R.Stoyanova, *Journal of Alloys and Compounds,* vol. 476, p. 950, 2009.

[76] J.J.Xu and J.Yang, *Electrochemistry Communications,* vol. 5, p. 230, 2003.

[77] H.Schlörb, M.Bungs and W.Plieth, *Electrochimica Acta,* vol. 42, p. 2619, 1997.

[78] F.Franks, *European Journal of Pharmaceutics and Biopharmaceutics,* vol. 45, p. 221, 1998.

[79] A.A.Baresi, R.Pisano, D.Fissore, V.Rasetto, S.A.Velardi, A.Vallan, M.Parvis and M.Galan, *Chemical Engineering and Processing,* vol. 48, p. 408, 2009.

[80] Y.D.Tretyakov and O.A.Shlyakhtin, *Journal of Materials Chemistry,* vol. 9, p. 19, 1999.

[81] B.Lee and S.Komarneni, Chemical Processing of Ceramics, 2nd ed., Taylor & Francis Group, 2005, pp. 77-137.

[82] R.G.Compton and C.E.Banks, Understanding Voltammetry, 2nd ed. ed., London: Imperial College Press, 2011, pp. 107-109.

[83] R.Nicholson, *Analytical Chemistry,* vol. 37, p. 1351, 1965.

[84] "Gamry Instruments, Inc-Application Note Rev.1.0," 9 March 2010. [Online]. Available: www.gamry.com. [Accessed 2013 February 2013].

[85] U.Retter and H.Lohse, "Electrochemical Impedance Spectroscopy," in *Electroanalytical Methods-Guide to Experiments and Applications, Editor: F.Scholz,* Berlin, Springer-Verlag, 2005, pp. 149-166.

[86] S. Krause, "Impedance Methods," in *Encyclopedia of Electrochemistry, Volume 3, Editors: A.J.Bard, M.Stratmann, P.R.Unwin* , Wiley-VCH, 2003, pp. 196-230.

[87] M.Risa, H.Yukinori, I.Masako, I.Koji and S.Daisuke, *NEC Technical Journal,* vol. 5, p. 52, 2010.

[88] A.J.Bard and L.R.Faulkner, in *Electrochemical Methods Fundamentals and Applications,* New York, John Wiley & Sons, Inc., 2001, pp. 98-102 and 368-416.

[89] V.F.Lvovich, Impedance Spectroscopy - Applications to Electrochemical and Dielectric Phenomena, New Jersey: John Wiley & Sons, Inc., 2012, pp. 37-47.

[90] D.Andre, M.Meiler, K.Steiner, H.Walz, T.S.Guth and D.U.Sauer, *Journal of Power Sources,* vol. 196, p. 5349, 2011.

[91] C.H.Hsu and F.Mansfeld, *Corrosion,* vol. 57, p. 747, 2001.

[92] G.J.Brug, A. v. Eeden, M.S.Rehbach and J.Sluyters, *Journal of Electroanalytical Chemistry,* vol. 176, p. 275, 1984.

[93] P.G.Bruce and M.Y.Saidi, *Journal of Electroanalytical Chemistry,* vol. 105, p. 93, 1992.

[94] M.D.Levi, G.Salitra, B.Markovsky, H.Teller, D.Aurbach, U.Heider and L.Heider, *Journal of the Electrochemical Society,* vol. 146, p. 1279, 1999.

[95] Y.Zhang and C.Y.Wang, *Journal of the Electrochemical Society,* vol. 156, p. A527, 2009.

[96] Y.M.Choi, S.I.Pyun, J.S.Bae and S.I.Moon, *Journal of Power Sources,* vol. 56, p. 25, 1995.

[97] Q.C.Zhuang, X.Y.Qiu, S.D.Xu, Y.H.Qiang and S.G.Sun, "Diagnosis of Electrochemical Impedance Spectroscopy in Lithium-Ion Batteries," in *Lithium Ion Batteries - New Developments*, Rijeka, Croatia, Intech, 2012.

[98] L.Lutterotti, S.Matthies and H.R.Wenk, *International Union of Crystallography CPD Newsletters,* vol. 21, p. 14, 1999 - Version 2.33 (2011).

[99] H.J.Orman and P.J.Wiseman, *Acta Crystallographica,* vol. C40, p. 12, 1984.

[100] A.C.Larson and R. Dreele, "General Structure Analysis System (GSAS)," Los Alamos National Laboratory Report LAUR 86-748, 1994.

[101] B.Riley, *US 4567031,* 1986.

[102] R.Gupta and A.Manthiram, *Journal of Solid State Chemistry,* vol. 121, p. 483, 1996.

[103] Y.Nishi, in Lithium Ion Batteries, Eds. M.Wakihara and O.Yamamoto, Tokyo: Kodansha Ltd. and Wiley-VCH, 1998, p. 181.

[104] A.Andersson, "Surface Phenomena in Li-ion Batteries", Ph.D Thesis submitted to Uppsala University, Uppsala, Sweden, 2001.

[105] F.Nobili, F.Croce, R.Tossici, I.Meschini, P.Reale and R.Marassi, *Journal of Power Sources,* vol. 197, p. 276, 2012.

[106] K.Mizushima, P.C.Jones, P.J.Wiseman and J.B.Goodenough, *Solid State Ionics,* Vols. 3-4, p. 171, 1981.

[107] Y.M.Choi and S.I.Pyun, *Solid State Ionics,* vol. 109, p. 159, 1998.

[108] J.N.Reimers and J.R.Dahn, *Journal of Electrochemical Society,* vol. 139, p. 2091, 1992.

[109] P.Ghosh, S.Mahanty and R.N.Basu, *Electrochimica Acta,* vol. 54, p. 1654, 2009.

[110] G.T.K.Fey, J.G.Chen and T.P.Kumar, *Journal of Applied Electrochemistry,* vol. 35, p. 177, 2005.

[111] B.Huang, Y.I.Jang, Y.M.Chiang and D.R.Sadoway, *Journal of Applied Electrochemistry,* vol. 28, p. 1365, 1998.

[112] W.S.Yoon and K.B.Kim, *Journal of Power Sources* , vols. 81-82, p. 517, 1999.

[113] L.Kanav and M.Gratzel, *Electrochemical Solid State Letters,* vol. 5, p. A39, 2002.

[114] S.Madhavi, G.V.S.Rao, B.V.R.Chowdari and S.F.Y.Li, *Journal of the Electrochemical Society,* vol. 148, p. A1279, 2001.

[115] B.Yeum, "ZsimpWin Electrochemical Impedance Modeling Software, version 3.22," EChem Software, Ann Arbor, 2007.

[116] J.Zhao, L.Wang, X.He, C.Wan and C.Jiang, *International Journal of Electrochemical Science,* vol. 5, p. 478, 2010.

[117] R.D.Shannon, *Acta Crystallographica Section A: Foundations of Crystallography,* vol. A32, p. 751, 1976.

[118] A.W.Moses, H.G.G.Flores, J.G.Kim and M.A.Langell, *Applied Surface Science,* vol. 253, p. 4782, 2007.

[119] A.V.Naumkin, A.K.Vaas, S.W.Gaarenstroom and C.J.Powell, "NIST X-ray Photoelectron Spectroscopy Database (Version 4.1)," 15 September 2012. [Online]. Available: http://srdata.nist.gov/xps/. [Accessed 3 May 2013].

[120] A.A.Khassin, T.M.Yurieva, V.V.Kaichev, V.I.Bukhtiyarov, A.A.Budneva, E.A.Paukshtis and V.N.Parmon, *Journal of Molecular Catalysis A: Chemical,* vol. 175, p. 189, 2001.

[121] S.J.R.Prabakar, S.C.Han, S.P.Singh, D.K.Lee, K.S.Sohn and M.Pyo, *Journal of Power Sources,* vol. 209, p. 57, 2012.

[122] B.J.Tan, K.J.Klabunde and P.M.A.Sherwood, *Journal of American Chemical Society,* vol. 113, p. 855, 1991.

[123] K.Ozawa, Y.Nakao, T.Mochiku, L. Z.Cheng, H.Iwai, Y.Tsuchiya, H.Fujii and N.Igawa, *Journal of the Electrochemical Society,* vol. 159, p. A300, 2012.

[124] H.Qi, C.Wang and J.Liu, *Advanced Materials,* vol. 15, p. 411, 2003.

CURRICULUM VITAE

PERSONAL INFORMATION

Surname, Name	: Büyükburç, Atıl
Nationality	: Turkish (TC)
Date and Place of Birth	: 5 August 1976, Ankara
Marital Status	: Married
Phone	: +90 533 350 42 53
Fax	: +90 312 428 09 33
Email	: atilbuyukburc@gmail.com

EDUCATION

Degree	Institution	Year of Graduation
MS	METU Industrial Engineering	2003
BS	METU Metallurgical and Materials Engineering	1999
High School	TED Ankara College, Ankara	1994

WORK EXPERIENCE

Year	Place	Enrollment
2007-Present	TÜBİTAK	Scientific Programs Chief Expert
2006-2007	Anadolu University	Teaching Assistant
2000-2006	Eti Mine Works G.M.	Engineer
1998-2000	AKAT Eng. Co.	Engineer
1998 August	AKAT Eng. Co.	Intern Engineering Student
1997 August	Erkunt Industry	Intern Engineering Student

FOREIGN LANGUAGES

Advanced English, German Beginner

PUBLICATIONS

1. Büyükburç A., Köksal G. “An Attempt to Minimize the Cost of Extracting Lithium from Boron Clays Through Robust Process Design” Clays and Clay Minerals, 53 (3), 301-309, (2005)

2. Büyükburç A., Maraşlıoğlu D., Bilici U., Köksal G. “Extraction of Lithium from Boron Clays by Using Natural and Waste Materials and Statistical Modeling to Achieve Cost Reduction” Minerals Engineering, 19 (5) 515-517 (2006)

3. Mergen A., Bilen M., Büyükburç A., Gündüz M. “Kinetics of Leaching of Boehmetic Bauxite of Konya-Turkey with Hydrochloric Acid” Silicate Industriels, 67 (7-8), 75-80, (2002)

HOBBIES

Playing chess, reading historical books**,** playing basketball and soccer, collecting playing cards and book separators